DRAFT

AFRL-SR-BL-TR-98-

0261

REPORT DOCUMENTATION PAGE

1. AGENCY USE ONLY (Leave blank)	2. REPORT DATE	3. REPORT TYPE AND DATES COVERED
	November 1997	Final Report, April 1994-July 1997

4. TITLE AND SUBTITLE

NON-HALOGENATED FIRE EXTINGUISHANTS

5. FUNDING NUMBERS

F49620-94-1-0241

2303/DS

61102F

6. AUTHOR(S)

G. Dana Brabson, Roger A. Patterson,
Robert E. Tapscott, and Edward A. Walters

7. PERFORMING ORGANIZATION NAME(S) AND ADDRESS(ES)

New Mexico Engineering Research Institute
The University of New Mexico
Albuquerque, New Mexico 87106-4339

8. PERFORMING ORGANIZATION REPORT NUMBER

NMERI 97/35/32060

9. SPONSORING/MONITORING AGENCY NAME(S) AND ADDRESS(ES)

Air Force Office of Scientific Research
110 Duncan Avenue
Bolling Air Force Base, DC 20332-8080

10. SPONSORING/MONITORING AGENCY REPORT NUMBER

XXX

11 SUPPLEMENTARY NOTES

12a. DISTRIBUTION/AVAILABILITY STATEMENT

Unlimited

12b.

13. ABSTRACT (Maximum 200 words)

The production of halon fire extinguishing agents, which are widely used throughout the Air Force, is banned in the U.S. by international agreement, and no environmentally acceptable replacement equivalent to existing halons in toxicity and effectiveness has been identified. It is desired to identify mechanisms by which extinguishants inhibit and extinguish fires to provide a basis for selection of new agents. This project investigated catalytic reactions that remove key species (such as hydrogen) from the flame, and compared and contrasted the roles of heat absorption and heterogeneous reactions in flame inhibition. Flame speed (an indicator of the degree of inhibition) was earlier proven to equate to the amount of heat removed from a burner. Equipment was designed and built to generate particles, to measure the heat extracted from a set of burners (named Sapphire) under atmospheric and sub-atmospheric conditions, and to identify species in the various regions of the flame. Halons and other halogenated fire extinguishing agents, phosphorus-nitrogen compounds, and iron-containing compounds were tested. Correlations were made between the heat extracted and (1) the extinguishment of the flame and (2) the fuel/air ratio. A flame-molecular beam-mass spectrometer (Sapphire 2) proved to be effective for studying inhibition chemistry. Inhibition by iron compounds was demonstrated, and recommendations for future work were made.

14. SUBJECT TERMS	15. NUMBER OF PAGES
Halon, aerosol, flame inhibition, flame/fire extinguishment, molecular beam-mass spectrometer, iron pentacarbonyl.	16. PRICE CODE

17. SECURITY CLASSIFICATION OF REPORT	18. SECURITY CLASSIFICATION OF THIS PAGE	19. SECURITY CLASSIFICATION OF ABSTRACT	20. LIMITATION OF ABSTRACT
UNCLASSIFIED	Unclassified	Unclassified	Unclassified

DRAFT

PREFACE

This report was prepared by the Center for Global Environmental Technologies (CGET) Division, New Mexico Engineering Research Institute (NMERI), The University of New Mexico, Albuquerque, New Mexico, for the Air Force Office of Scientific Research, Bolling Air Force Base, DC under Air Force Contract F49620-94-1-0241, NMERI Number 8-32060.

The Start Date was 8 April 1994, and the End Date was 7 July 1997. The AFOSR Project Officers were Dr. Fred Hedberg and Dr. Walter Kozumbo, and the NMERI Principal Investigators were Robert E. Tapscott and Edward A. Walters.

(The reverse of this page is intentionally blank.)

DRAFT

ACKNOWLEDGMENTS

Many people made vitally important contributions to this work.

1. Rob Loomis was the student "on the ground floor," and designed significant parts of the flame-molecular beam-mass spectrometer.

2. Justin Schiro was a Research Experiences for Undergraduates (REU) student sponsored by the NSF. It was his idea to measure the heat extracted by the burner as a function of the fuel/oxidizer equivalence ratio, and he performed the first experiment.

3. Chris Spencer perfected the experiments in which the heat extracted by the burner was measured as a function of the fuel/oxidizer equivalence ratio, and performed the important experiments with agents having fuel character.

4. Helen Johnson was our second Research Experiences for Undergraduates (REU) student sponsored by the NSF. Her principal work was the measurement of flame speed as a function of heat extracted by the burner, but she also contributed to the acquisition of infrared spectra of post combustion products.

5. Carrie Weitz joined the team for a short while to study the infrared spectra of post-combustion product. She also performed the experiments in which alternate fuels were substituted for methane.

6. Tony Gennuso was our third Research Experiences for Undergraduates (REU) student sponsored by the NSF. He acquired the low-pressure flame molecular-beam mass spectrometric data for flames seeded with iron pentacarbonyl.

7. Patrick Owen helped build the low-pressure flame molecular-beam mass spectrometer, did many of the initial check-out experiments, and also measured the total energy emitted by the flames as a function of the fuel/oxidizer equivalence ratio.

8. Tamara Goodman worked very hard on laboratory-scale Class A fires, made some definitive measurements of flame speed as a function of fuel/oxidizer equivalence ratio, and determined the effective molar extinction coefficient of iron pentacarbonyl in our apparatus.

9. Dongmei Ye became our local expert on counterflow diffusion flames, and discovered the conditions under which two separate luminous zones were observed, an orange zone due to the initial formation of FeO, and the well known blue-green reaction zone due to luminescence by CH and C_2.

In addition, the authors especially appreciate the efforts of Hoshang Shahvar, who designed and built the driver for the pulsed nozzle, and of Lew Hartswick, who waved the magic wand over our electronic equipment when it quit working.

And finally, the authors gratefully acknowledge the many and fruitful technical discussions with Jacob Kaizerman, Everett Heinonen, Ted Moore, and Dr. Douglas Mather.

EXECUTIVE SUMMARY

A. OBJECTIVE

The overall objective of this research was to elucidate the mechanisms by which dry chemical fire extinguishing agents inhibit and extinguish fires, and thereby provide a scientific basis for selection and/or synthesis of new agents that equal or surpass the halons in effectiveness while not introducing deleterious halogen atom-containing compounds into the stratosphere. Metal-containing compounds in particular were to be investigated.

B. BACKGROUND

Under the Montreal Protocol, an international treaty enacted in 1987 and amended in 1990, 1992, and 1995, the production of the fire and explosion protection agents Halon 1211 and Halon 1301 was phased out in the United States at the end of 1993. Many operational U.S. Air Force aircraft have installed Halon 1301 fire suppression systems, both for engine nacelles and for enclosed spaces, and halon is discharged in some circumstances other than inflight fires (fuel tanks in the F-16 are routinely inerted with Halon 1301 on entry into combat, for example). To date, no environmentally acceptable Halon substitute that is equivalent to the existing Halons in toxicity and specific effectiveness has been identified. Replacements are all less effective than the present Halons in most scenarios and have some adverse global environmental impact (ozone depletion or global warming). While currently available stocks of Halons could last well into the next century in the absence of combat, combat sorties would rapidly deplete these stocks.

Recent work has identified several potential non-halocarbon and low-atmospheric-lifetime halocarbon substitutes for halon fire extinguishants; these include phosphorous compounds, metal compounds, and silicon compounds. Tropodegradable halocarbons, which contain features that assure short atmospheric lifetimes, also exhibit high promise. The work reported here focused primarily on the metal compounds because of considerable evidence that some metals inhibit fires by catalytically recombining flame radicals, in much the same manner as bromine atoms introduced into flames by Halon 1301 catalytically recombine hydrogen atoms.

C. SCOPE

Five tasks were included in the overall effort.

Task 1: To search the literature with particular emphasis on the homogeneous and heterogeneous catalytic reactions that remove key species (such as H atoms) from flames.

Task 2: To experimentally investigate (1) the important species generated when solid extinguishants are introduced into a flame, (2) the interactions of these species with the principal radicals normally found in flames, and (3) the fates of all of these species as a function of the amount of extinguishant added to the flame.

Task 3: To experimentally and theoretically analyze the role of heat absorption in the extinguishment of a flame.

Task 4: To experimentally assess the role of heterogeneous reactions at the surfaces of solids and/or aerosol particles.

Task 5: To develop new concepts in fire extinguishment based on the results of the preceding four tasks.

D. METHODOLOGY

The exploration of flame chemistry can be subdivided into two areas of work, one of which may be called the study of macroscopic properties, and the other may be described as the examination of microscopic properties. The present work contains elements of both, and significant results were obtained on both fronts.

Study of Macroscopic Properties: In macroscopic studies, one begins with a flame and examines the effect of adding candidate extinguishing agents on macroscopic observables which are indicative of inhibition and/or extinguishment.

Examination of Microscopic Properties: To understand the chemistry underlying the observed macroscopic properties, one examines the processes at the atomic and molecular levels. In some instances, one may use a flame as the primary source of atomic and molecular species.

In other cases, it is useful to generate the specific species of interest by other techniques. A flame was selected as the source for the present work.

E. APPROACH

1. Study of Macroscopic Properties

The methane-oxygen flame was selected for the study of macroscopic properties, and most of the effort was devoted to a study of the degree of inhibition as a function of the amount of candidate extinguishing agent added to the flame. The choice of a methane-oxygen flame was based on several considerations. First, this flame is reasonably representative of the more complex hydrocarbon-air flames, such as *n*-heptane-air. Second, the methane-oxygen flame is the simplest, the most thoroughly studied, and the most well understood of the hydrocarbon-oxygen flames. Third, since the methane-oxygen flame is the flame of choice for the examination of microscopic properties (see below), it was desired to use the same flame for the study of the macroscopic properties so that comparison of results might be facilitated.

Of the many macroscopic observables related to the degree of inhibition of the flame, the heat extracted by the burner was selected for this work. This method has a long-standing historical precedent, is non-intrusive, and proved to provide unexpectedly valuable insights into the mechanisms of inhibition. It is based on the observation by Botha and Spalding in 1954 that the heat extracted from a flame by a cooled burner is directly (linearly) related to the flame speed, and hence to the ability of the flame to propagate through the unburned gases; at extinguishment, the flame speed has dropped to zero. In these experiments, a heat-exchange fluid was circulated through a cooling loop on the periphery of the burner, and the amount of heat carried off in the heat-exchange fluid was measured as a function both of the amount of extinguishing agent added to the flame and of the stoichiometry (fuel/oxygen equivalence ratio) of the flame.

Many different compounds were studied by this technique. As a baseline, and to validate this technique as a method for distinguishing the thermal/physical inhibition mechanism from the catalytic/chemical inhibition mechanism, several well-known extinguishing agents were studied first. Then attention was given to a variety of metal-containing compounds, with the

primary emphasis being on iron-containing compounds. In conjunction with this work, effective methods were developed for introducing both slightly volatile metal compounds (using effusion cell methods) and metal salts (as aqueous aerosols) into atmospheric and subatmospheric flames.

2. Examination of Microscopic Properties

Flame-molecular beam-mass spectrometry was selected as the technique for examination of the microscopic properties. This technique also has historical precedent, and was the method used by Biordi and coworkers to examine the inhibition of methane-oxygen flames by Halon 1301 ($CBrF_3$) and related compounds in the 1970s. In this technique, the atomic and molecular species are directly sampled by probing a low-pressure methane-oxygen flame with a quartz nozzle; a mass spectrometer is used to identify and quantify the various species present in the flame. The molecular beam created by this sampling technique contains all of the species, both stable and transient, normally present in the flame, and the distribution of species in the beam is representative of the species in the flame. In a typical experiment, the sampling nozzle is moved incrementally from a location in the initiation zone (near the surface of the burner), through the reaction zone (luminous zone), and into the recombination zone. This procedure permits detailed examination of the chemistry, at the atomic and molecular level, throughout the flame, and allows one to examine the effect on this chemistry of adding extinguishing agents to the flame. For the work described here, a new instrument, based on proven principles and precedents, was constructed and placed in service. The primary emphasis of early experiments with this instrument was the examination of the effect of iron (using iron pentacarbonyl as a convenient source) on the flame.

F. RESULTS

1. Measurements of the Heat Extracted by the Burner

Two types of experiments were performed. In one, the heat extracted by the burner was measured as a function of the amount of extinguishing agent added to the premixed gases. In the other, the heat extracted by the burner was measured as a function of the

fuel/oxygen equivalence ratio (ϕ). Since the two types of experiments yielded different and complementary results, the results of each are briefly summarized.

a. Heat Extracted *vs.* Flow Rate Experiments

Experiments in which the heat extracted by the burner was measured as a function of the amount of agent added to the flame proved to provide important insights into the mechanisms of inhibition. Three uniquely different behaviors were observed and assigned to characteristics of the inhibiting agents.

Very steep initial slope. Compounds such as $CBrF_3$ and CH_3Br, which are known to catalytically recombine flame radicals, were found to yield Heat Extracted *vs.* Flow Rate curves with very steep initial slopes. The remaining data formed a straight line, with a negative slope, which intercepted the x-axis (within experimental uncertainty) at the point at which flameout was actually observed.

Lesser initial (or even positive) slope. Some compounds were found to promote fuel-lean flames. These compounds, such as C_2HF_5, included one or more hydrogen atoms. In fuel-rich flames, these compounds were found to yield linear Heat Extracted *vs.* Flow Rate curves with negative slopes. Here again, the intercepts with the x-axis were, within experimental uncertainty, the same as the points at which flameout was observed. In fuel-lean flames (and to a lesser extent in flames near ϕ=1.0), the initial slopes of the Heat Extracted *vs.* Flow Rate curves were less than the final slopes; in some cases, the initial slopes were positive, indicating that the compound combined with the excess oxygen in these fuel-lean flames to increase the total amount of heat in the flame. Compounds in this group had the additional characteristic that they shifted the effective fuel/oxygen equivalence ratio. A plot of heat extracted by the burner as a function of ϕ (see below) resulted in a curve with a maximum at a value of ϕ<1.0, thus implying that an oxygen-rich flame was the most difficult for a compound in this group to extinguish.

Constant slope. The last group of compounds exhibited linear curves throughout the entire range of amount of agent added; this was true for all flames, regardless of the fuel/oxygen equivalence ratio. Compounds in this group included the typical thermal agents

such as Ar and N_2. However, this group also included other compounds in which an additional linear inhibition mechanism was operative. Perhaps the most important example is the scavenging mechanism, in which one atom generated by reaction of the agent molecule reacts with and permanently removes a flame radical. As in the other two cases, the intercepts with the x-axis were, within experimental uncertainty, the same as the points at which flameout was observed.

The value of the Heat Extracted *vs.* Flow Rate data was not limited to an assessment of the significance of the shape of the curve. Additional information was provided by the slope of the curve. Since the slope of the Heat Extracted curve had units of energy/volume of agent (cal/cc), the slope of the curve was a measure of the effectiveness of the agent in removing energy from the flame (energy that, otherwise, would have been extracted by the burner).

b. Heat Extracted *vs.* Fuel/Oxygen Equivalence Ratio Experiments

Experiments in which the heat extracted by the burner was studied as a function of ϕ, the fuel/oxygen equivalence ratio, complemented the experiments in which the measurements were made as a function of the amount of agent added to the flame. Moreover, since the uninhibited flame was compared with the inhibited flame at each data point in the Heat Extracted *vs.* Fuel/Oxygen Equivalence Ratio experiment, this experiment also yielded a direct measure of the extinguishment effectiveness of the agent at each value of ϕ. The following two distinguishable types of behavior were observed:

Similar extinguishment effectiveness at all values of ϕ. Thermal agents such as N_2 displayed this behavior; however, this behavior was not limited to thermal agents. Thus, for example, the extinguishment effectiveness curve for Halon 1301 ($CBrF_3$) was nearly as flat as those for the purely thermal agents.

Minimum extinguishment effectiveness for fuel-lean flames. In sharp contrast, some agents yielded extinguishment effectiveness curves with distinct minima for fuel-lean flames. Particularly noteworthy in this regard were the agents with "fuel-content."

Curiously, iron pentacarbonyl ($Fe(CO)_5$), which is not believed to have "fuel character," displayed the same behavior.

2. Aerosol Generation and Delivery Techniques

Two techniques were explored and used successfully for generating aerosols and delivering them into the premixed flames studied in this work. In the first technique, an ultrasonic driver was used to generate very fine aerosols of aqueous solutions of inorganic metal compounds. As generated, the aerosols had large fractions of water. In some experiments, these aerosols were used as generated. In other experiments, a drying stage was added to remove nearly all of the water. Both atmospheric and subatmospheric pressure flames (down to 30 torr) were seeded with aerosols generated by this system. Spectroscopic data were collected for these flames, and some inhibition data were obtained as well. The principal drawback of this system was the fact that it was not designed for continuous replenishment of the solution. Consequently, the performance changed steadily over relatively short time spans. This fact made it difficult to make quantitative estimates of the extinguishment effectiveness of samples introduced by this technique. It is noted in passing that the Meker-type burner heads, selected and developed for this project, were particularly well suited for introduction of aerosols into the flames.

The second technique for generation and delivery of aerosols capitalized on the well-known technology for introducing fuel aerosols into internal combustion engines. Using a commercial pulsed fuel injector valve, aerosols of pressurized agents were introduced into a cup-burner system at atmospheric pressure, and it was shown that results could be obtained that were comparable to those of more conventional cup-burner experiments. Although only a few exploratory experiments were conducted, it appears that this system also has the potential for introducing aerosols of aqueous solutions of inorganic metal compounds into flames.

3. Possible Synergistic Effects

The two types of Heat Extracted experiments perfected in the present work are uniquely suited for the exploration of possible synergistic effects that might be expected when two agents with differing extinguishing mechanisms are used in concert. It should be possible to determine not only the overall effectiveness of the combined agent, but also to find out whether

the two agents truly act in synergism or whether one mechanism tends to dominate the other. While only one experiment was conducted with the primary goal of studying potential synergism, the results were definitive, raised important questions, and clearly demonstrated that the Heat Extracted experiments can indeed provide valuable insights into the question of possible synergistic effects.

4. The Flame-Molecular Beam-Mass Spectrometer Experiment

Experiments with $Fe(CO)_5$-doped flames yielded immediate results. In these experiments, the flame was profiled along the centerline, beginning in the initiation zone and ending in the recombination zone. The most dramatic effect occurred near the interface between the reaction zone and the recombination zone. Here, significant decreases in the concentrations of stable products (H_2O and CO_2) were observed along with large increases in the concentrations of reactants (CH_4 and O_2). In essence, seeding with $Fe(CO)_5$ caused a downstream shift of the flame chemistry. This observation is particularly noteworthy when compared with the results of similar experiments conducted by Biordi and coworkers with $CBrF_3$. In the $CBrF_3$ experiments, precisely the same sort of downstream shift of the flame chemistry was observed.

Attempts to observe iron-containing species (FeO, FeOH, and $Fe(OH)_2$) directly did not meet with success. While the mass to charge ratio (m/e)=17 (OH^+) peak was measured, experiments were not performed that would have differentiated between OH radicals generated by the flame and OH^+ ions due to fragmentation of H_2O; the latter was the principal contributor to the observed peak.

5. The Heterogeneous-Homogeneous Question

Heterogeneous systems were encountered throughout this work. On the one hand, agents were introduced as aerosols, while on the other hand, particulates were generated in the studies of iron-containing compounds. The results to date suggest that the aerosols are completely vaporized early in the flame. A few experiments were conducted with an instrument (based on Fraunhofer scattering) designed to confirm these preliminary results. Unfortunately, the experiments were not sufficiently reproducible, and definitive results could not be obtained.

The particulates generated in studies of flames seeded with iron-containing compounds, presumably aggregates of iron oxide molecules, were observed visually but not characterized further. However, the brightness and spectra distribution of the luminosity of these particles strongly suggest that the chemistry occurring on the surfaces of these particulates is important to the inhibition of the flame.

6. Other Metal-Containing Compounds

Work with other metal-containing compounds was restricted to the examination of the effects of aerosols of aqueous solutions of these compounds. Only alkali metals were examined, and the work was very preliminary in nature. While the alkali metals are known to be very effective flame modifiers, evidence from the literature suggests that transition metals and other metals with two or more easily accessible oxidation states are even more effective.

G. CONCLUSIONS

1. Measurement of the Heat Extracted by the Burner

The Heat Extracted experiments provided exceptionally valuable insights into the mechanisms of inhibition and extinguishment. The Heat Extracted from the premixed flame by the cooled burner was found to be an excellent measure of the degree of inhibition by the candidate extinguishing agent. Moreover, the shapes of the Heat Extracted curves yielded information beyond the measure of degree of inhibition. As a consequence, the Heat Extracted experiment has taken its proper place, along with other measures of inhibition, as a powerful tool in the arsenal of techniques for characterizing the mechanisms of flame inhibition and extinguishment. Uniquely characteristic Heat Extracted curves may be expected for several different classes of compounds.

2. Aerosol Generation and Delivery Techniques

Especially in view of the fact that the majority of the most interesting metal containing metal compounds have very small or negligible vapor pressures, the successes with the two aerosol generating techniques are viewed as being important. Moreover, it appears that the difficulties encountered in the present work can be rectified and are not inherent limitations

in the application of these techniques to future experiments. In the case of the ultrasonic aerosol generator, a modification that features continuous injection of fresh solution appears to offer considerable promise. As far as the pulsed valve (modified fuel injector) system is concerned, the potential appears unlimited, and the fact that the candidate agent is introduced in closely spaced pulses (rather than continuously) does not appear to be a problem with the possible exception of systems with high vapor pressure solvents.

3. Possible Synergistic Effects

Although one cannot yet draw definitive conclusions regarding the magnitude of possible synergistic effects, the potential of using the Heat Extracted technique as a method of studying these effects is well established.

4. The Flame-Molecular Beam-Mass Spectrometer Experiment

The flame-molecular beam-mass spectrometer experiments, although still in their infancy, have already made major contributions to the understanding of the mechanism of inhibition by iron-containing compounds. Moreover, major improvements in the capabilities of this instrument can be achieved with only minor changes to the hardware. These improvements would not only improve the quality of the data but also enable the study of key transient species that cannot now be observed. Even in its present configuration, the instrument is capable of evaluating the effects of metal-containing compounds other than $Fe(CO)_5$, including aqueous aerosols of inorganic materials such as iron nitrate and iron oxalate.

5. The Heterogeneous-Homogeneous Question

It is clear that important chemistry occurs on the surfaces of the easily visible particulates that characterize flames seeded with iron-containing compounds. While, it is presumed that this same chemistry occurs on the precursors to these visible particles (that is to say, on the particles too small to be seen visually), there is no information at present as to the relationship between particle size and the characteristic chemistry. This fact makes it very difficult to unravel the questions that relate to the relative importance of heterogeneous and

homogeneous mechanisms. Given the exceptional performance of iron-containing compounds as flame modifiers, these questions have great importance.

6. Other Metal-Containing Compounds

Although the experiments with other metal-containing compounds have been confined mainly to an examination of their spectroscopic properties, it is now appropriate to consider introducing these compounds into the flame-molecular beam-mass spectrometer. The flame-molecular beam-mass spectrometer now makes possible the resolution of questions such as whether the availability of multiple oxidation states is crucial to the extraordinary effectiveness of iron-containing compounds.

H. RECOMMENDATIONS

1. Measurement of the Heat Extracted by the Burner

It is suggested that the Heat Extracted be systematically compared and contrasted with the well-established techniques.

2. Aerosol Generation and Delivery Techniques

Both the pulsed valve and the ultrasonic aerosol generator should be pursued. Work with the pulsed valve should focus mainly on delivery of metal-containing compounds dissolved in solvents with relatively low volatilities, including, but not limited to, water. Efforts with the ultrasonic aerosol generator should be directed toward achieving higher and steadier delivery rates.

3. Possible Synergistic Effects

The study of possible synergistic effects should be explored vigorously. This study will both answer important questions as to the potential of synergism and provide additional detailed information on the "internal synergistic" contributions of the thermal and catalytic mechanisms available in a single agent.

4. The Flame-Molecular Beam-Mass Spectrometer Experiment

Immediate upgrades to the instrument should be implemented. With the upgraded instrument, the concentrations of key transient species, including the OH radical, should be measured and correlated with the behavior of stable species (which have already been examined with this instrument). The work should then be extended to the study of entrained aqueous aerosols of iron-containing compounds, and the results of these experiments should be compared and contrasted with the results obtained with $Fe(CO)_5$.

5. The Heterogeneous-Homogeneous Question

The question of whether the dominant mechanism of inhibition by metal-containing compounds is homogeneous or heterogeneous should be resolved. The iron-containing compounds seem to be quite suitable for an initial exploration of this question. However, it may be necessary to examine other compounds (with different propensities for forming aerosols) in order that a satisfactory answer to this question may be found.

6. Other Metal-Containing Compounds

Studies of metal-containing compounds (in addition to iron-containing compounds) should be initiated with the flame-molecular beam-mass spectrometer, and perhaps with other instruments (such as the Fraunhofer photometer) as well. These studies should focus on key mechanistic questions such as the unknown role of the availability of multiple oxidation states, the propensity to form particulates, and so forth. Manganese compounds are very high on the list of compounds that should be included in this work.

DRAFT

TABLE OF CONTENTS

TABLE OF CONTENTS (CONTINUED)

TABLE OF CONTENTS (CONTINUED)

TABLE OF CONTENTS (CONTINUED)

TABLE OF CONTENTS (CONTINUED)

TABLE OF CONTENTS (CONTINUED)

TABLE OF CONTENTS (CONTINUED)

TABLE OF CONTENTS (CONCLUDED)

LIST OF FIGURES

LIST OF FIGURES (CONTINUED)

LIST OF FIGURES (CONTINUED)

LIST OF FIGURES (CONTINUED)

LIST OF FIGURES (CONTINUED)

LIST OF FIGURES (CONTINUED)

LIST OF FIGURES (CONCLUDED)

DRAFT

LIST OF TABLES

LIST OF ABBREVIATIONS

AAWG	Advanced Agent Working Group
AC	alternating current
AFOSR	Air Force Office of Scientific Research
ARA	Applied Research Associates
CAS	Chemical Abstracts Service (American Chemical Society)
CGET	Center for Global Environmental Technologies
DC	direct current
EG	ethylene glycol
FC	(per)fluorocarbon
FEE	fractional extinguishment effectiveness
FIC	fluoroiodocarbon
FMBMS	Flame Molecular Beam Mass Spectrometer
FTIR	Fourier Transform Infrared
GC	Gas Chromatograph
GC/MS	Gas Chromatography/Mass Spectrometry
HCFC	hydrochlorofluorocarbon
HFC	hydrofluorocarbon
HFCTP	hexafluorocyclotriphosphazene
ID	inside diameter
LED	light-emitting diode
m/e	mass to charge ratio (in mass spectrometer)
MS	mass spectrometer
MW	molecular weight
N2 (N_2)	gaseous nitrogen
NMERI	New Mexico Engineering Research Institute
OD	outside diameter
ODP	ozone depletion potential
PFC	perfluorocarbon
PFPCTP	hexakis(2,2,3,3,3-pentafluoropropoxy)cyclotriphosphazene
PMT	photomultiplier tube
PN	phosphorus-nitrogen (compound)
rms	root mean square
SS	stainless steel
TC	thermocouple
TFECTP	hexakis(2,2,2-trifluoroethoxy)cyclotriphosphazene
USAF	United States Air Force
UV	ultraviolet

LIST OF UNITS AND SYMBOLS

A	absorbance
AC	alternating current
b	optical path length (cm) in an optical absorbance experiment
C	concentration (moles/liter)
cal	calorie
cm	centimeter
cm^{-1}	wave number (reciprocal centimeter)
c_p	heat capacity at constant pressure
DC	direct current
ft	foot
g	gram
ΔH^0	standard change in enthalpy (@298.15 K and 1 atm)
Hz	Hertz
J	Joule
K	Kelvin
kHz	kilohertz
kJ	kilojoule
Kohm	kilo-ohm (1000 ohms)
kPa	kilopascal
kV	kilovolt
L	liter
lb	pound
m	meter
mg	milligram
mL	milliliter
mV	millivolt
mol	mole
n	number of moles
P	pressure
P_o	pressure of a pure material

LIST OF UNITS AND SYMBOLS (CONCLUDED)

ppm	parts per million
psi	pounds per square inch
Q	heat
R	gas constant
s	second(s)
T	temperature
V	volume
v	volts
VAC	volts, alternating current
VDC	volt, direct current
V_0	burning velocity of the uninhibited flame
ΔH_v	heat of vaporization
δV	change in burning velocity
ε	molar absorptivity (in optical absorbance experiments)
μg	microgram
ϕ	fuel/oxidizer equivalence ratio
X	mole fraction
•	denotes a free radical, e.g., •OH, the hydroxyl free radical
[•OH]	square brakets denote the concentration of the species, e.g., the concentration of the •OH radical

(The reverse of this page is intentionally blank.)

DRAFT

SECTION I
INTRODUCTION

A. OBJECTIVE

The overall objective of this research was to elucidate the mechanisms by which dry chemical fire extinguishing agents inhibit and extinguish fires, and thereby provide a scientific basis for selection and/or synthesis of new agents that equal or surpass the halons in effectiveness while not introducing deleterious halogen atom-containing compounds into the stratosphere.

B. BACKGROUND

Under the Montreal Protocol, an international treaty enacted in 1987 and amended in 1990, 1992, and 1995, the production of the fire and explosion protection agents Halon 1211 and Halon 1301 was phased out in the United States at the end of 1993. To date, no environmentally acceptable halon substitute equivalent to the existing halons in toxicity and specific effectiveness has been identified.

Halocarbons as replacements for halons have been well studied, and it is unlikely that new, highly effective, halon replacements will be identified among the typical non-iodinated haloalkanes. The hydrochlorofluorocarbons (HCFC), perfluorocarbons (PFC or FC), and hydrofluorocarbons (HFC) are all less effective than the present halons in most scenarios. Moreover, all of these have some adverse global environmental impact (ozone depletion or global warming). PFCs and HCFCs are already subject to some restrictions, and such restrictions may eventually extend to HFCs. The single partial success among the candidate halocarbon replacements are the iodides, in particular, trifluoromethyl iodide (CF_3I), which is as effective as Halon 1301. However, the toxicity of the iodides restricts their use to selected applications. There is, therefore, an increasing incentive to examine compounds other than the typical haloalkanes.

The importance of this work to the U.S. Air Force (USAF) stems from the fact that many operational aircraft have installed Halon 1301 fire suppression systems, both for engine nacelles and for enclosed spaces. Moreover, Halon 1301 is discharged in some circumstances other than inflight fires; the fuel tanks in the F-16 are routinely inerted with Halon 1301 on entry into combat, for example. While currently available stocks of halons could last well into the next century in the absence of combat, combat sorties would rapidly deplete these stocks. Thus, one can forecast an increasing need (over an uncertain time line) for new extinguishing agents that do not compromise the weight and volume constraints of currently operational systems.

Recent work has identified several potential non-halocarbon and low-atmospheric-lifetime halocarbon substitutes for halon fire extinguishants. Work by the Advanced Agent Working Group (AAWG), which includes USAF and U.S. Army participation, has shown that the most promising non-halocarbon compounds are phosphorous compounds, metal compounds, and silicon compounds. The AAWG work (which emphasizes chemical options for total-flood Halon 1301 applications) and USAF work also show that tropodegradable halocarbons, which contain features that assure short atmospheric lifetimes, exhibit high promise. The work reported here focused primarily on the metal compounds. The principal reason was this: there is considerable evidence in the literature that at least some metals inhibit fires by catalytically recombining flame radicals, much in the same manner as bromine atoms introduced into flames by Halon 1301 catalytically recombine hydrogen atoms. It was, therefore, anticipated that it might be possible to match, or perhaps even exceed, the specific effectiveness of the halons (on a weight and volume basis) without incurring the environmental penalties attributable to the halons.

The historical motivation for experimenting with metal-containing compounds (such as $NaHCO_3$) was the thought that these compounds could be useful vehicles for introducing CO_2 at the sources of fires; however, it was quickly discovered that these compounds were unexpectedly effective extinguishing agents, and it was suspected that the metal was playing an important role in the extinguishment process. This proved to be the case. Today, dry chemical fire extinguishing systems are well established. Moreover, due in large part to the success of these metal-containing compounds, considerable effort has been devoted both to an investigation of the

mechanisms by which metals are involved in flame chemistry, and to a search for even more effective metal-containing compounds. To date, the fire suppression/inhibition properties of well over 100 metal-containing compounds, involving 33 or more different metals, have been studied (a review is provided in Reference 1).

It is now well established that both physical and chemical processes contribute to the extinguishing effectiveness observed for metal-containing compounds. Physical, or thermal, mechanisms are characteristic of all compounds. All compounds absorb energy from high temperature environments by virtue of their intrinsic heat capacities, and many absorb additional energy through phase transitions (such as vaporization) and/or transformations (such as decomposition).

At the same time, it is also well established that many metals and/or their compounds catalyze the recombination of flame radicals (especially H atoms and OH radicals), thereby upsetting the flame chemistry and contributing to extinguishment.

It has been shown that the extinguishing effectiveness of many metal-containing compounds can be correlated quantitatively with their thermal mechanisms and that, even though catalytic processes may also be operative, it is unnecessary to invoke these catalytic processes to account quantitatively for the effectiveness of these compounds. The metals for which this is true include both the alkali (Group IA) and alkaline earth (Group IIA) metals.

At the same time, some metal-containing compounds are so effective (especially when only very small amounts of the compounds have been introduced into the flame) that their behavior cannot be accounted for in terms of thermal mechanisms alone. It is this subset of extraordinarily effective metal-containing compounds that appears to offer potential for next-generation extinguishing agents. Perhaps the most thoroughly studied compounds in this subset are tetraethyl lead and iron pentacarbonyl. The former has been studied principally in relation to its influence on preignition knock in internal combustion engines, while the latter has been studied mainly from the vantage point of its flame extinguishing properties.

In the present work, studies of iron-containing compounds and of other metal-containing compounds have been extended. New insights have been developed which suggest that metal-containing compounds should indeed be considered for roles as next generation fire extinguishing agents, and directions for further work have been clearly delineated.

C. SCOPE

Five tasks are included in the overall effort.

Task 1: To search the literature with particular emphasis on the homogeneous and heterogeneous catalytic reactions that remove key species (such as H atoms) from flames.

Task 2: To experimentally investigate (1) the important species generated when solid extinguishants are introduced into a flame, (2) the interactions of these species with the key species normally found in flames, and (3) the fates of all of these species as a function of the amount of extinguishant added to the flame.

Task 3: To experimentally and theoretically analyze the role of heat absorption in the extinguishment of a flame.

Task 4: To experimentally assess the role of heterogeneous reactions at the surfaces of solids and/or aerosol particles.

Task 5: To develop new concepts in fire extinguishment based on the results for the preceding four tasks.

D. APPROACH

In many respects, the approach adopted in the present work paralleled that of Biordi and co-workers in their investigation of Halon 1301 ($CBrF_3$) at the U. S. Bureau of Mines in the 1970s (Reference 2). It will be recalled that Biordi et al., used a flame-molecular beam-mass spectrometer to measure the concentrations of the principal species in low-pressure methane-oxygen flames, and to explore the effect of adding small concentrations of $CBrF_3$ to these flames.

Much of the definitive information regarding the mechanism of inhibition of flames by $CBrF_3$ was the result of these studies.

Following a thorough review and analysis of the literature, a flame-molecular beam-mass spectrometer, dubbed the Sapphire 2 instrument, was designed, constructed, and placed into service. The principal components of the Sapphire 2 instrument (described in detail in Section II) were a low-pressure flat-flame premixed methane-oxygen-argon burner, and a medium resolution quadrupole mass spectrometer. A quartz probe inserted in the flame extracted a molecular beam, which, after passing though a differentially pumped chamber, entered the ionization region of the mass spectrometer.

The design of the Sapphire 2 instrument departed from that of the Biordi instrument in two important respects. First, a Meker burner was selected so that aerosols could be introduced into the flame with the premixed gases, and an ultrasonic aerosol generator capable of operating at subatmospheric pressures was designed as a source of the aerosols. Second, a non-intrusive diagnostic technique, based on a measurement of the heat extracted by the burner, was developed for determining the degree of extinguishment by the compound being studied. Although the development of this diagnostic technique was of secondary importance, it yielded such valuable insights into the mechanisms of flame inhibition that additional effort was devoted to its exploitation.

Several metals were studied. The initial focus was on metals known from the literature to have significant effects on flames. These included potassium, sodium, and iron. The first iron compound studied was iron nitrate, introduced as an aerosol. This work was then complemented by studies with iron pentacarbonyl; this latter compound was selected for its ease of introduction into typical flames, realizing that it is far too poisonous to be considered seriously as an extinguishing agent. At the same time, a series of slightly volatile iron complexes was prepared and introduced into typical flames.

Finally, the results of the experimental work were analyzed in the context of the available literature to yield recommendations as to the next steps to be taken.

SECTION II
EXPERIMENTAL INSTRUMENTATION AND PROTOCOLS

A. INTRODUCTION

From the first day of this project, it was the objective of the team to construct a flame-molecular beam-mass spectrometer, with which to explore the homogeneous and heterogeneous catalytic reactions by which effective flame inhibitors perturb the number densities of flame radicals (especially H atoms and OH molecules). This instrument was called Sapphire 2, and is described in Section II.D. However, as work on Sapphire 2 progressed, many other experiments related to the development and performance of Sapphire 2 were also done. In this regard, early experiments were performed to study the technology associated with the introduction of aerosols into a low-pressure flame. To this end, an ultrasonic aerosol generator, adapted for use with low-pressure flames, was developed and tested; this device is described in Section II.E. The ultrasonic nebulizer was checked out at atmospheric pressure, and then used to introduce aerosols into low-pressure flames. The low-pressure flame chamber built for these latter experiments was called Sapphire 1 and is described in Section II.C. Ultimately, the Sapphire 1 instrument served as much more than a test bed for the ultrasonic aerosol generator.

In parallel with the development of the ultrasonic aerosol generator, it was important to explore a non-intrusive technique (suitable for use in the low-pressure environment) for measuring the degree of inhibition of the flame. The technique selected was the measurement of the heat extracted from the flame by the burner. Initial experiments in the Sapphire 1 instrument were very successful and suggested that this technique could shed important light on extinguishment mechanisms. Accordingly, a series of burners was designed for operation at atmospheric pressure, and significant contributions were made. These burners were designated the "Sapphire 0" burners, to distinguish them from the two low-pressure burner systems. The Sapphire 0 burners are described next, and Sections III and IV discuss the work at atmospheric pressure with these burners.

B. SAPPHIRE 0—ATMOSPHERIC PRESSURE BURNERS

The term "Sapphire 0" was assigned to a set of burners and experiments at atmospheric pressure. A prototypical atmospheric burner, Sapphire 0-4, is illustrated by Figure 1. For this burner, the head was removed from a commercially available laboratory Meker burner. Cooling coils were added by silver-soldering 3/16-in OD copper tubing to the periphery of the burner.

The heat extracted from the flame by the burner was carried off by ethylene glycol (EG), circulated at a measured flow rate by a gear pump (MicroPump, Model 185-000). The primary factor in the selection of this particular gear pump for this application was constancy of flow rate. Irregularities in the flow (pulses, short-term and long-term variances) were directly reflected in the Heat Extracted data. The increase in temperature of the EG was measured by a pair of chromel-alumel thermocouples located in the cooling loop just below the points of attachment of the loop to the burner rim. The two thermocouples were electrically connected ("back-to-back") such that the difference in temperature between the EG entering the cooling loop and that leaving the cooling loop was measured; the absolute temperature of the EG was not measured (Figure 2). However, the temperature of the ethylene glycol entering the cooling loop was held constant at 23 °C (73 °F) by a constant temperature bath (Forma Temp. Jr. Model 2095).

The voltage generated by the pair of thermocouples was continuously recorded on a strip-chart recorder (1 mV full scale). In a typical experiment, 200-500 cal/minute were removed from the burner by the EG. The EG flow rate was selected such that the temperature rise in the coolant was about 10 °C (18 °F), corresponding to a 0.4 mV deflection of the pen on the strip chart recorder.

In early experiments, water was used as a coolant. However, with water as a coolant, frequent small steps in the Δt (difference of temperature) signal were observed, most likely caused by the formation and collapse of bubbles in the water in the cooling loop around the burner rim.

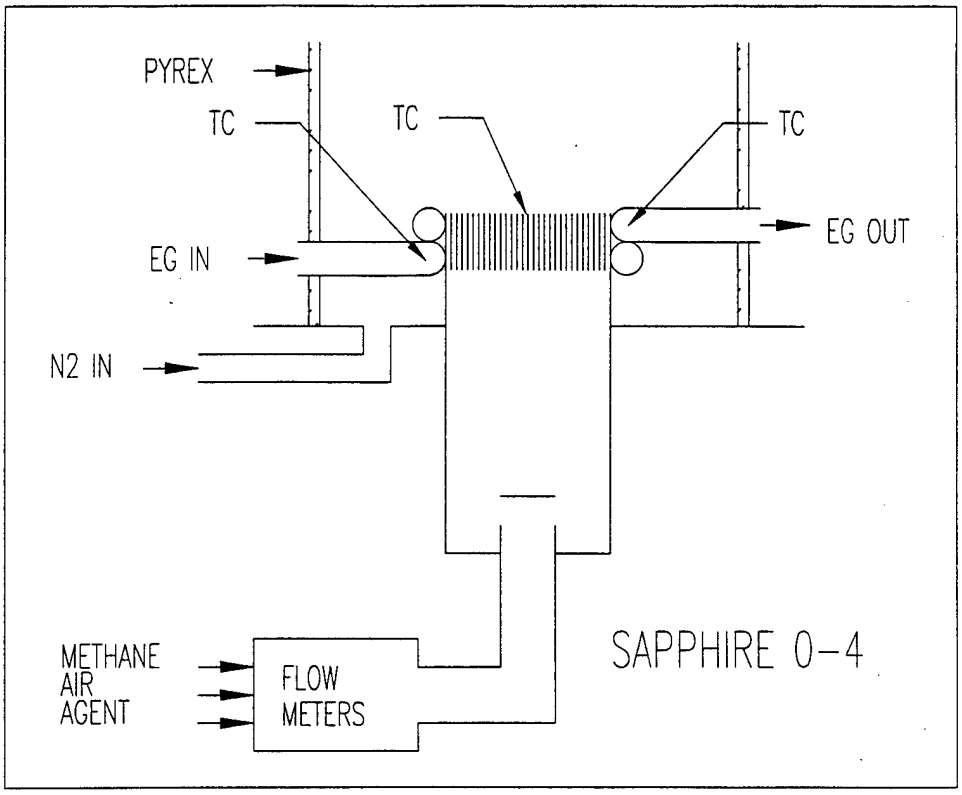

Figure 1. The Sapphire 0-4 Atmospheric-Pressure Burner.

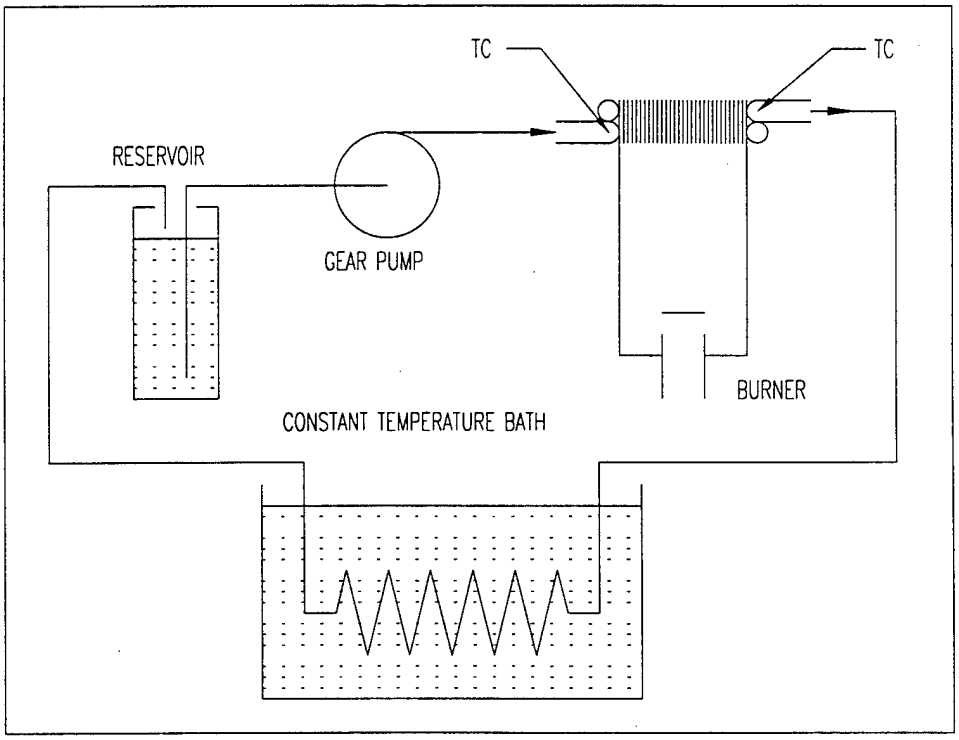

Figure 2. Block Diagram of the Ethylene Glycol Circulating System.

The flame holder in the Meker burner consisted of a square array of metal strips, 3/8 in (0.95 cm) wide and 0.040 in (0.10 cm) thick, spaced on 0.10 in (0.25 cm) centers. A chromel-alumel thermocouple, spot welded to the center of the grid, permitted continuous measurement of the temperature at the center of the burner. This feature proved to be particularly useful. Because the heat transfer through the flame holder was not instantaneous, the temperature at the center of the burner was higher than the temperature at the rim of the burner. Moreover, the temperature at the center of the burner could be directly related to the heat extracted by the burner, and hence to the heat generated by the flame.

The active flame area of the Meker burner, immediately above the flame holder, was 1.44 in^2 (9.32 cm^2); the flame holder was 64 percent open. The selection of a Meker burner (as opposed to a sintered frit burner) was dictated by the desire to permit direct introduction of aerosols. The modified Meker burner head was sealed to a 1 and 1/8-in (2.88-cm) OD mixing tube. The bottom of the mixing tube was soldered to a disk through which a 3/8-in (0.95-cm) OD tube was used to introduce the premixed gases. The top end of the 3/8-in (0.95-cm) gas delivery tube was closed with a silver-soldered disk, and two 1/4-in (0.64-cm) delivery ports were drilled on opposite sides of the tube. This simple arrangement prevented a core of premixed gases from impinging directly on the flame holder and achieved even distribution of the premixed gases across the diameter of the burner head.

To minimize interference by the external atmosphere, minimize recirculation of burned gases, and provide a draft-free environment for the flame, the flame was operated in a borosilicate glass envelope with a co-axial sheath of nitrogen gas. The linear flow rate of the sheath gas was about 2.8 in/s (7 cm/s). For comparison, the linear velocity of the room-temperature premixed gases at the surface of the burner was about 2.6 in/s (6.6 cm/s).

Although propane and butane were used for a few experiments, the vast majority of the data was obtained with methane as the fuel. Air (either house air, or oxygen and nitrogen mixed in the ratio of 21 percent O_2, and 89 percent N_2) was the oxidant of choice for most of the experiments. Gaseous inhibiting agents were premixed with the methane and air. Less volatile inhibiting agents and aerosols were entrained in the premixed fuel-oxidizer stream just before

entry into the burner. The flow rates of the individual gases were measured with variable area flow meters (rotameters, Omega). The rotameters were calibrated for each gas using Digital Flow Meters (Fisher Scientific Model 650 or Humonics Model 730), and the calibration was checked after each experiment. In all cases, the rotameters were configured with the needle valves downstream of the variable area tubes. In this configuration, the actual flow rate indicated by the rotameter was essentially independent of downsteam pressure variations. It was possible to change the flow rate of one gas without affecting the actual flow rate of the other gases. (In this configuration, the actual flow rate *did* depend on the upstream pressure of the gas, and care was taken to assure constant and reproducible pressures at the inlets to the rotameters.)

In typical atmospheric pressure experiments, the total flow rate in the uninhibited flame was approximately 3700 cc/min (at about 630 torr, the prevailing atmospheric pressure in Albuquerque), and the corresponding linear velocity of the premixed gases at the surface of the burner was about 2.4 in/s (6 cm/s). Following each change in experimental variables, a delay of 6 minutes was allowed for thermal equilibration of the burner; the exponential approach to equilibrium was easily observed on the strip chart recorder, and the limiting value (achieved at the end of the 6-minute interval) was recorded. The temperature at the center of the burner ranged from about 300 °C (572 °F) for uninhibited flames to near room temperature just prior to extinguishment.

In each experiment, the data recorded included (1) the differential voltage generated by the two thermocouples in the EG coolant loop, (2) the temperature at the center of the burner, (3) the flow rates of all the reactants and diluent, and (4) the flow rate of the EG. The heat extracted by the burner was calculated from the heat capacity and flow rate of the EG, and the temperature rise in the EG during its transit around the periphery of the burner head.

Two types of experiments were conducted; typical results for both types of experiments are included in later sections of this report.

Heat Extracted *vs.* Flow Rate Experiments. The flow rate of extinguishing agent was changed while all other flow rates were held constant; beginning with an uninhibited flame, the inhibitor was added incrementally until flameout was achieved.

Heat Extracted *vs.* Fuel/Oxidizer Equivalence Ratio Experiments. The flow rate of methane was changed (thus changing the fuel/oxidizer equivalence ratio, ϕ) while all other flow rates (including that of the inhibitor) were held constant; the Fuel/Oxidizer Equivalence ratio was scanned incrementally from the lean inflammability limit to the rich inflammability limit. The fuel/oxidizer equivalence ratio, ϕ, is defined such that ϕ=1.000 for a stoichiometric flame; thus, for methane-oxygen flames, $\phi = 2 \times$ [volume flow rate of methane]/[volume flow rate of oxygen].

The Sapphire 0-7 burner (Figure 3) was designed especially for the study of inhibiting agents with low volatilities. These agents were introduced from a heated cell, and the entire burner was wrapped with Nichrome resistance wire and heated to prevent condensation of the agent in the burner. Two other features of the Sapphire 0-7 burner are worthy of note; the applications of these features will be described later. The first was the provision for infrared spectroscopy of post-combustion gases. Openings were provided near the top of the borosilicate glass "chimney" (about 8.7 in [22 cm] above the surface of the burner). A Fourier Transform Infrared (FTIR) Spectrophotometer with external optics was located so that the optical axis passed through the post-combustion gases. A wire mesh screen placed over the top of the "chimney" prevented external air currents from disturbing the test environment; IR-transparent windows in the openings in the borosilicate glass "chimney" were not required. Very satisfactory data were obtained with this very simple arrangement.

A second feature of the Sapphire 0-7 burner was a provision for optical absorption photometry of the pre-combustion gases. This feature was incorporated for the study of iron(III) acetylaetonates and related compounds, which are quite highly colored. The concentrations of these inhibiting agents in the premixed gases were quantitatively estimated from measures of the absorbance of visible radiation in the absorption bands of these compounds. Results of these determinations are described in Section III.

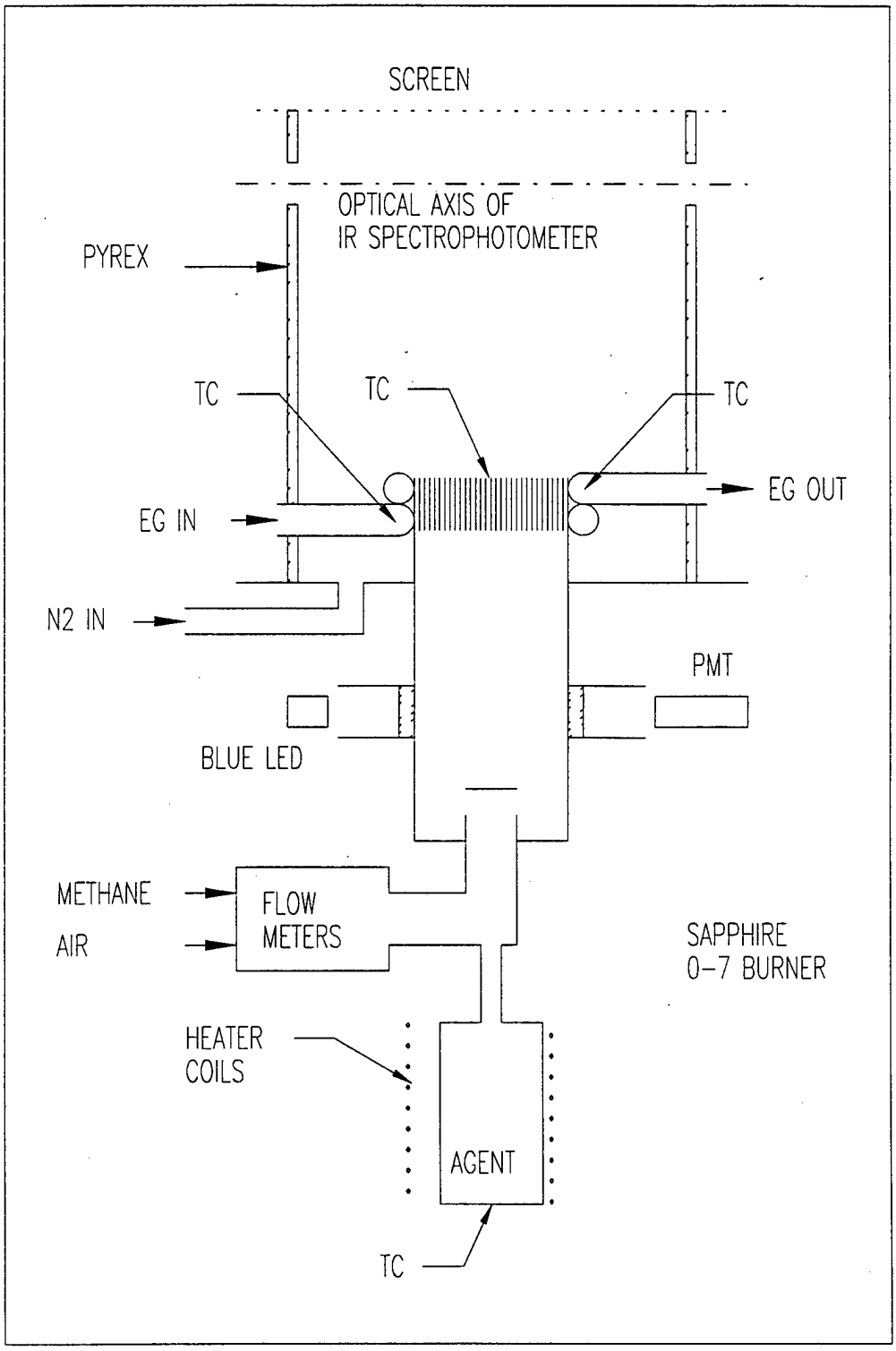

Figure 3. The Sapphire 0-7 Atmospheric-Pressure Burner.

C. SAPPHIRE 1—LOW-PRESSURE FLAME CHAMBER

The Sapphire 1 low-pressure flame chamber is illustrated by Figure 4. This chamber was initially constructed to serve as a testbed for the low-pressure burners and for the ultrasonic aerosol generator. Two different burners were used in this instrument. The first, Sapphire 1-1, was a sintered bronze burner (Newmet Krebsoge, Inc., Terrytown, CT). The burner was made by sintering bronze powder at 871 °C (1600 °F) in a 1.50-in (3.81-cm) ID copper tube; the depth of the sintered bronze flame holder was 5/8 in (1.59 cm). One-quarter inch (0.64 cm) OD copper tubing was soft-soldered to the periphery of the burner. This burner yielded excellent flat flames. For experiments at 30 torr, even with agents such as $CBrF_3$ (Halon 1301) that generated corrosive combustion products, the liftoff of the flame was sufficient to prevent appreciable degradation of the bronze frit. Unfortunately, this was not true of higher pressure experiments, and corrosion of the frit eventually destroyed the flow field and forced removal of this burner from service.

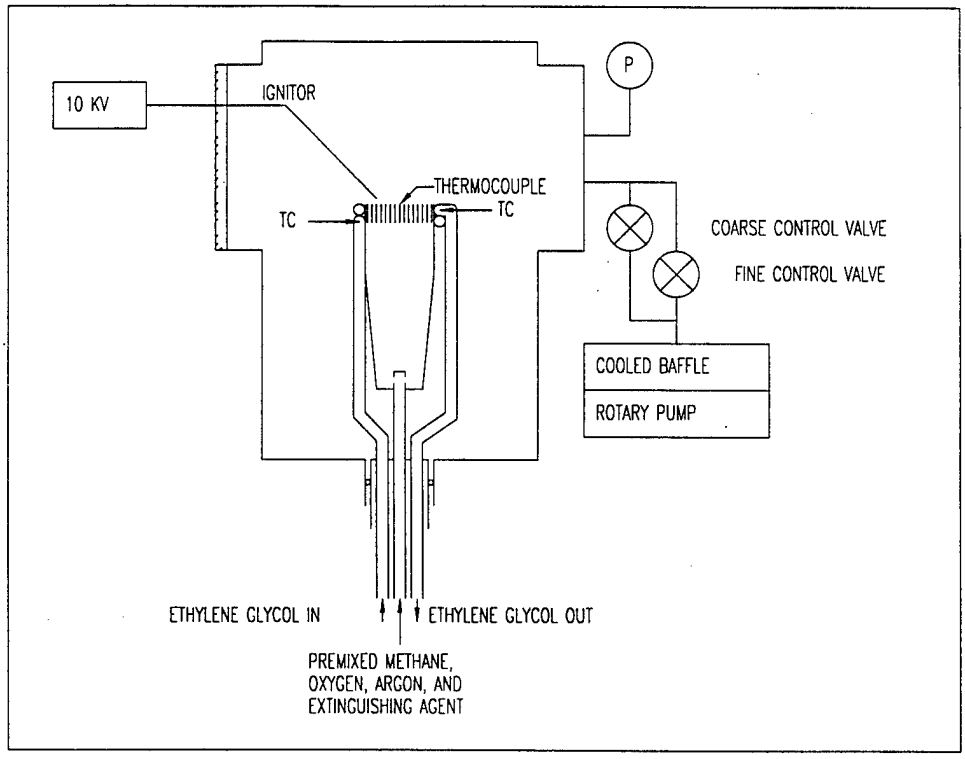

Figure 4. Block Diagram of the Sapphire 1 Instrument.

The second burner used in the Sapphire 1 instrument (Sapphire 1-2) was essentially identical to burner Sapphire 0-4, described in Section II.B. No provisions were made for shrouding either the Sapphire 1-1 burner or the Sapphire 1-2 burner with inert gas. The chamber window was poly(methylmethacrylate), since glass windows were quickly etched by the combustion products of some of the extinguishing agents.

The methane, oxygen, argon diluent, and extinguishing agent were metered individually with variable area flow meters, in exactly the same manner as described for the Sapphire 0 experiments. Typical flow rates (measured at the prevailing atmospheric pressure of 630 torr) were the following: CH_4, 332 cc/min; O_2, 566 cc/min; and Ar, 778 cc/min. Almost all of the Sapphire 1 experiments were conducted with fuel-rich flames, fuel/oxygen equivalence ratio, $\phi = 1.17$.

The pressure was controlled by a throttled, high-capacity mechanical pump (Scientific Instruments PS-1500). For experiments under steady flame conditions, it was satisfactory to throttle the pump with two valves, a large valve to set the approximate pumping speed, and a small valve for fine control. The pressure in the chamber was monitored with a Buordon gauge (Wallace-Tiernan).

D. SAPPHIRE 2—FLAME-MOLECULAR BEAM-MASS SPECTROMETER

The Sapphire 2 flame-molecular beam-mass spectrometer instrument is illustrated by Figure 5. The principal components were a flat-flame, premixed burner located in a low-pressure flame chamber, and a medium-resolution, quadrupole mass spectrometer.

The Sapphire 1-2 burner was moved from the Sapphire 1 instrument to the Sapphire 2 instrument upon completion of experiments in the former instrument. No provisions were made for shrouding the Sapphire 1-2 burner with inert gas. The Sapphire 1-2 burner was located on the centerline of the flame chamber and of the quartz sampling nozzle; no provisions were made for radial sampling of the flame. The burner was translated in the vertical (z) direction by an external, threaded screw mechanism. Once the absolute distance from the surface of the burner to the tip of the sampling nozzle had been determined for a particular setting of the positioning

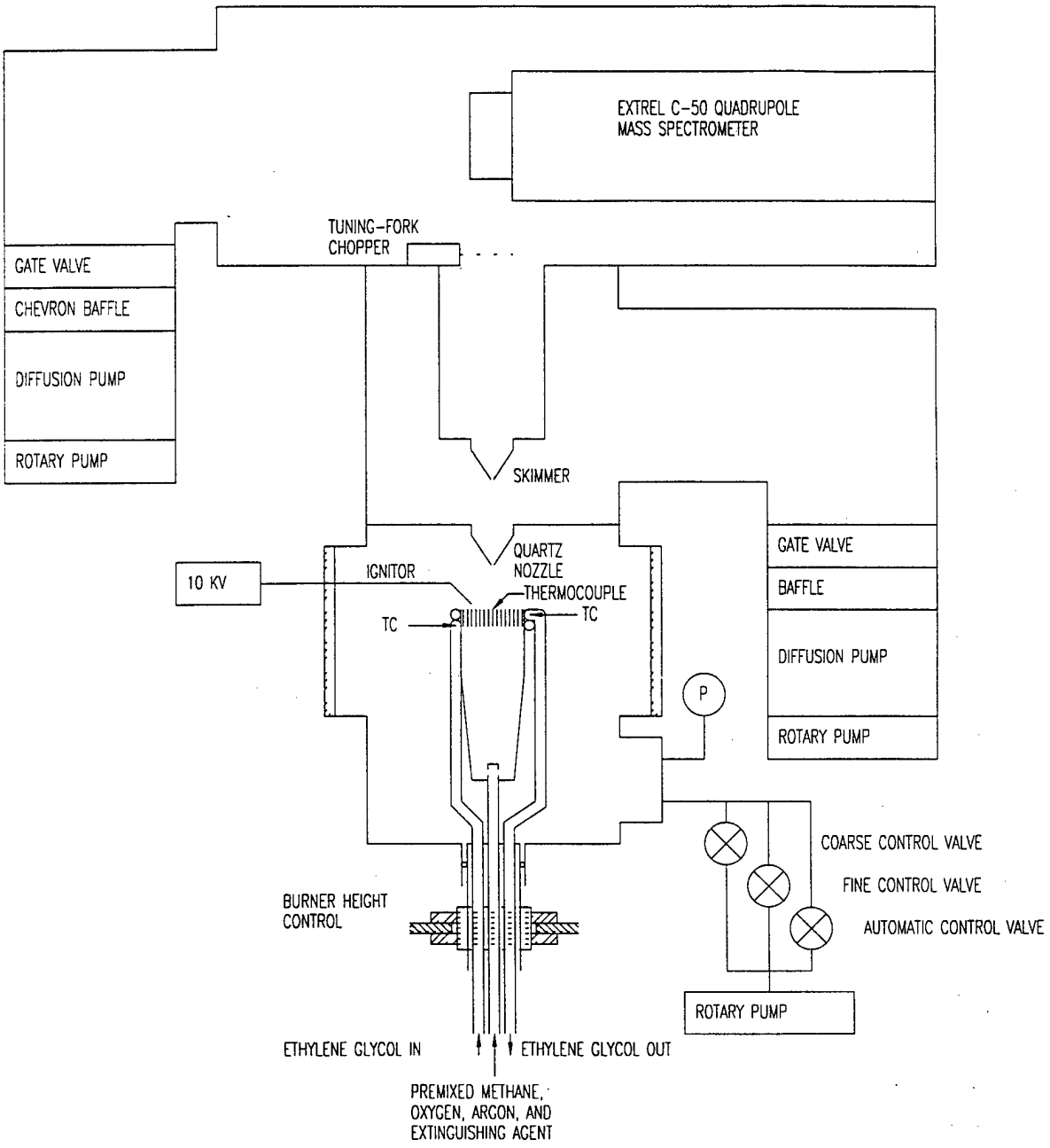

Figure 5. Block Diagram of the Sapphire 2 Instrument.

mechanism, accurate and reproducible positioning of the burner was possible to an accuracy and precision of ±0.004 in (±0.1 mm).

The methane, oxygen, and argon diluent were metered individually with variable area flow meters, in exactly the same manner as described for the Sapphire 0 experiments. For experiments with $Fe(CO)_5$ as the inhibiting agent, a separate stream of argon was saturated with $Fe(CO)_5$ vapor using a bubbler, and a small fraction of this stream was metered into the premixed combustion gases with a needle valve.

The low pressure in the flame chamber was achieved by a throttled, high-capacity mechanical pump (Scientific Instruments PS-1500). For early experiments in which tight control of the pressure was not essential, the two-valve arrangement used for the Sapphire 1 experiments was adopted, and the pressure was monitored with a Buordon gauge (Wallace-Tiernan). However, for experiments in which frequent changes were made in the flame conditions, an automated control system was essential; this system is illustrated by Figure 6. The heart of this system was a Vacuum Process Controller (Granville-Phillips Model 303); the output from the Model 303 Controller drove the solenoid valve. As illustrated by Figure 6, the solenoid valve was located in parallel with two manually-controlled valves. The manually controlled valves

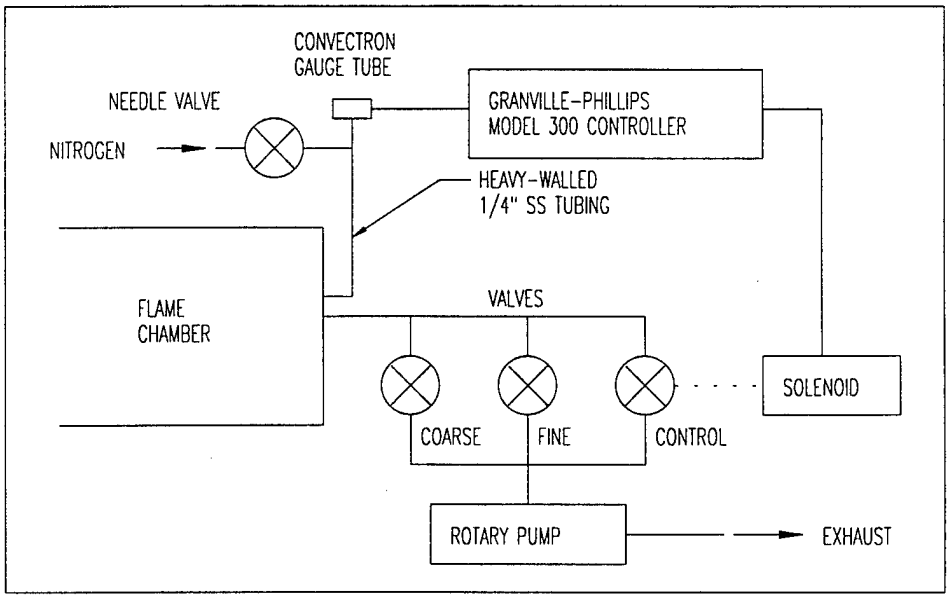

Figure 6. Block Diagram of the Pressure Control System for the Sapphire 2 Instrument.

were used to set the pressure in the flame chamber at a value somewhat above the desired value, and the solenoid valve provided additional pumping speed as required to maintain the system at the set point. The pressure sensing element was a Convectron gauge (Granville-Phillips). Because the sensing element in the Convectron gauge tube responds to thermal transport by the sensed gas, the response of this gauge is a strong function of the composition of the sensed gas; the key to successful operation of this system was provision of a small flow of nitrogen near the Convectron gauge tube. This arrangement assured that, regardless of the composition of the gases in the flame chamber, the response of the Convectron gauge was proportional to the true pressure in the chamber. In typical operation, the pressure in the chamber was held to ±1 percent of the total pressure. This degree of control proved to be adequate to prevent any discernible changes in the amplitudes of observed signals as a function of variations of pressure in the flame chamber. Tighter control was possible, but was not required.

The flame chamber was separated from the differential pressure chamber by a water-cooled copper plate. The flame was sampled with a quartz nozzle mounted in the center of the copper plate with an O-ring-sealed compression plate. The sampling nozzle was drawn to a fine point from 21-mm (0.83-in) OD, 18-mm (0.71-in) ID quartz tubing. Fine emery paper was used to grind the tip of the nozzle until breakthrough was observed visually with an eye piece. Continued grinding then allowed the orifice to be made to the desired diameter, in this case, 125 microns (1.25×10^{-4} m). The angle of the nozzle was about 50 degrees, and the distance from the tip of the nozzle to the copper plate was 0.75 in (19 mm).

The flame chamber had 4-in diameter windows to permit observation of the flame. A variety of optical diagnostic techniques could also be used. One-quarter inch (0.64-cm) OD copper tubing, soldered to the outside of the flame chamber, prevented appreciable warming of the chamber. Indeed, during operation of the flame, water was observed to condense on the inside of the chamber at locations cooled by the copper tubing on the outside. Condensation also occurred on the copper plate. Because the flame impinged directly on the copper plate, the gases exhausted from the chamber did not appreciably raise the temperature of the pipe leading to the exhaust pump, and no additional hardware was needed to cool the exhaust gases.

The differential pressure chamber was pumped by a 6-in diffusion pump (Varian VHS-6) with Dow Corning DC-704 diffusion pump oil. The length of the beam path between the tip of the nozzle and the tip of the skimmer was 1.9 in (4.8 cm). The diameter of the orifice in the skimmer (which defined the molecular beam entering the analyzer chamber) was 250 microns. The performance of the Sapphire 2 instrument was directly related to the background pressure in the differential pressure chamber. As the pressure in the differential pressure chamber rose, the mean free path decreased, and the probability increased that a molecule in the beam would be "bumped" out of the beam.

To establish a performance baseline for the Sapphire 2 instrument, argon was used as a test gas, and the following data were recorded as a function of argon pressure in the flame chamber: differential pressure chamber pressure, analyzer chamber pressure, size of the Ar^+ ion signal (at mass to charge ratio m/e=40), and noise level on the m/e=40 signal. The results are presented in Figures 7 and 8. (Note: The data presented in these figures were acquired before installation of the water-cooled baffle above the diffusion pump for the differential pressure chamber.) As expected, both the pressure in the differential pressure chamber and the pressure in the analyzer chamber were linear functions of the pressure of the argon test gas in the flame chamber. The behavior of the signal generated by the Lock-In Amplifier (Princeton Applied Research JB-5), as a function of the pressure of the test gas, clearly demonstrated that the beam was significantly perturbed by molecules in the background gas in the differential pressure chamber. Thus, there was an optimum argon pressure, above which the increase in the differential pressure chamber pressure resulted in a net degradation of the molecular beam intensity in the analyzer chamber. It was not expected that the root mean square (rms) noise on the signal would be inversely related to the signal size. Nevertheless, this was observed, and it accounts for the dramatic increase in signal-to-noise ratio with decreasing argon pressure (Figure 8). It was disappointing to discover that the optimum pressure of the argon in the flame chamber was so low, i.e., about 2 torr.

The clear implication was that, for the actual pumping speed of the differential pressure chamber pumping system, a smaller nozzle orifice diameter should have been selected. Indeed, it was discovered that some of the best data accumulated with the Sapphire 2 instrument were

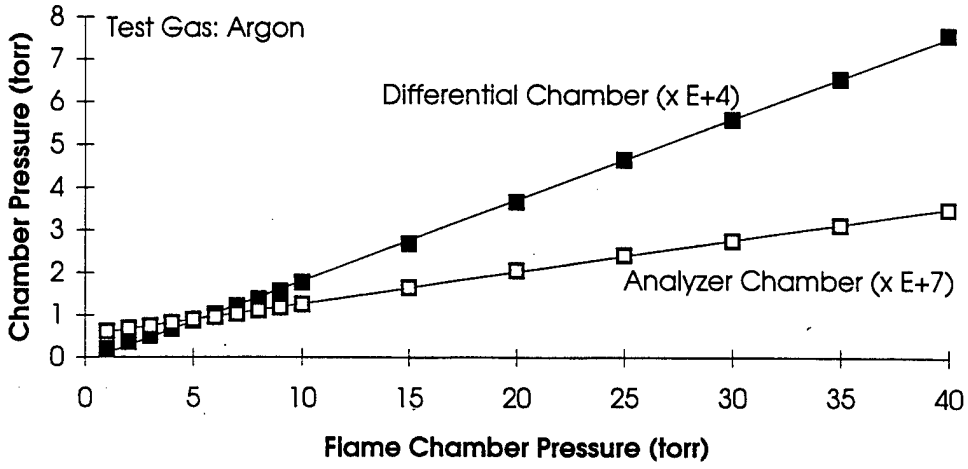

Figure 7. Performance Data for the Sapphire 2 Instrument. Pressures in the differential pressure and analyzer chambers as a function of the argon pressure in the flame chamber.

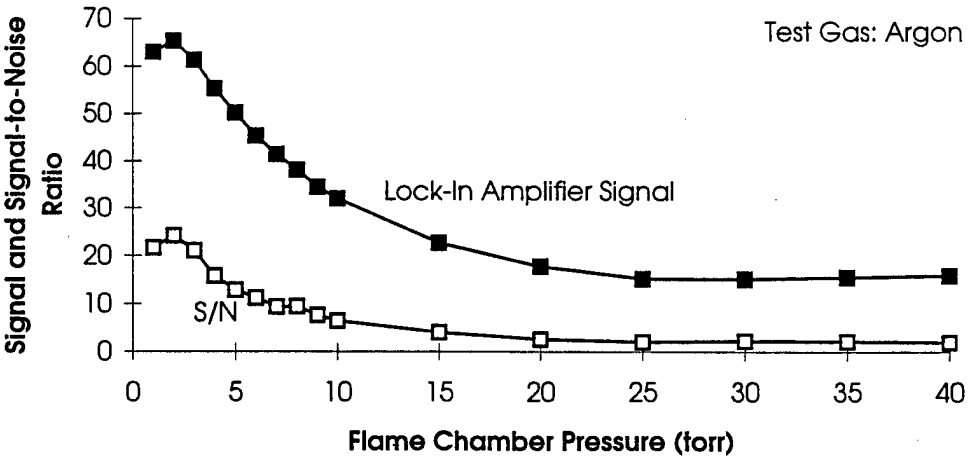

Figure 8. Performance Data for the Sapphire 2 Instrument: Signal and Signal-to-Noise Ratio. The lock-in amplifier signal represents data for the Ar^+ ion (@ m/e=40).

obtained with a partially blocked nozzle. Evidence for this partially blocked condition was readily obtained from an examination of the record of differential pressure chamber ionization gauge pressures, recorded during the course of the experiments.

The molecular beam traversed a distance of 12.2 in (31 cm) from the tip of the quartz sampling nozzle to the entrance of the ionization region in the Extrel C-50 Mass Spectrometer. The principal axis of the mass spectrometer (horizontal) was at a right angle with respect to the molecular beam (vertical). This geometry was selected so that neutral species would exit on the far side of the ionization region. No provisions were made for a liquid nitrogen cooled beam stop, but this feature could be added easily. It is believed that the instrumental background would be significantly reduced by addition of this feature.

The analyzer chamber was pumped by a 6-in oil diffusion pump (NRC) with Dow Corning DC-704 diffusion pump oil. A chevron baffle located above the diffusion pump normally was not cooled. Background pressures (without cooling the baffle) were less than 5×10^{-8} torr. Typical pressures as a function of pressure in the flame chamber are included in Figure 7.

The molecular beam was modulated with a 400-Hz tuning fork chopper (American Time Products), located 0.4 in (1 cm) below the entrance into the ionizing region of the mass spectrometer and driven by an oscillator (American Time Products Model CA-5A). Alignment of the nozzle, skimmer, chopper, and mass spectrometer was facilitated by replacing the burner with a HeNe laser located on the centerline of the burner mounting flange. When all components were properly aligned, the bright laser spot was observed (through conveniently located windows) on the top of the analyzer chamber. Over many months of operation, no drift in the alignment was observed.

The Extrel C-50 Mass Spectrometer was interfaced both with a Mass Spectrometer/RGA Interface (Vacuum Technologies, Inc. [VTI] AEROSCAN-1600), and with a Lock-In Amplifier (Princeton Applied Research JB-5). The VTI system was installed as recommended by the manufacturer, and the AEROSCAN software was installed on a personal computer with a 386

microprocessor. Both DOS and Windows software packages were available; the DOS software proved to be the more satisfactory. Spectra were recorded and stored on 3½-in floppy discs, and processed off-line using Quattro Pro (Borland). For phase sensitive detection of the 400 Hz-modulated beam, the signal from the AC OUT BNC connector on the C-50 was first processed with a 10-kHz bandwidth limiter (using the design recommended by Extrel) and then fed directly to the signal channel of the JB-5. The reference signal for the JB-5 was derived from the electronic driver for the 400-Hz chopper. The output from the JB-5 was passed through a simple DC voltage compensator circuit (6 VDC) to set the baseline voltage at 0 V, and then to a strip chart recorder.

It is useful to note that, if the Extrel C-50 was switched from the COMPUTER mode to the INTERNAL mode while the VTI AEROSCAN-1600 was on-line, the AEROSCAN system continued to acquire and display the analog data. In this configuration, the mass signal (generated internally and displayed on the monitor by the VTI software) was not transmitted to the Extrel C-50. This configuration was particularly advantageous in the search for very small contributors to the mass spectrum. With the Extrel C-50 in the SINGLE MASS mode, data were collected over a period of 100 seconds or more, and then stored on a floppy disc for off-line statistical analysis.

One of the important questions that must be asked about a molecular beam sampling system such as that described here is this: To what degree does the sampling probe disturb the flame? Two pieces of experimental evidence suggest that the flame was indeed perturbed. The first piece of evidence came from the observed temperatures at the center of the burner. Experiments were usually begun with the burner at a distance of 0.78 in (2 cm) or more below the tip of the quartz sampling nozzle; as the experiment progressed, the burner was incrementally raised toward the nozzle. The temperature at the center of the burner was observed to fall with each incremental decrease in the distance between the burner surface and the tip of the nozzle, an effect that became increasingly evident as the distance was reduced to smaller and smaller values. Typical data for uninhibited flames represent data collected for the temperature at the center of the burner as a function of the location of the quartz sampling nozzle with respect to the surface of the burner (Table 1).

TABLE 1. TEMPERATURE VERSUS NOZZLE LOCATION.

Distance, tip of nozzle to burner surface, mm	Temperature at burner center, °C
20.5	241
18.4	240
16.3	240
14.2	238
12.1	237
10.0	233
7.9	228
5.7	214
4.7	197
3.6	180
2.6	164
1.5	153
1.1	148

Additional evidence of perturbation of the flame came from visual observation of flames inhibited with iron pentacarbonyl ($Fe(CO)_5$). The inhibited flame in these experiments was a distinct yellow; however, in the vicinity of the quartz nozzle, and extending about 0.08 in (2 mm) into the flame from the nozzle, the color was slightly (but distinctly) different.

E. LOW-PRESSURE ULTRASONIC AEROSOL GENERATOR

Figure 9 illustrates the principal features of the ultrasonic aerosol generator. The key component was the commercially available ultrasonic crystal assembly (American Piezo Ceramics, Inc.). The assembly used in this work was similar to the units installed in ultrasonic humidifiers designed for home use. The complete nebulizer assembly (with electronics) was mounted directly on the bottom of the chamber designed by the author; the silastic seal was provided by the manufacturer. Four connections were made: Two leads were connected to a 48-VAC supply, while the other two leads were connected to a 10 Kohm potentiometer (to control the intensity of the ultrasonic vibration). [WARNING: The AC power leads must not be

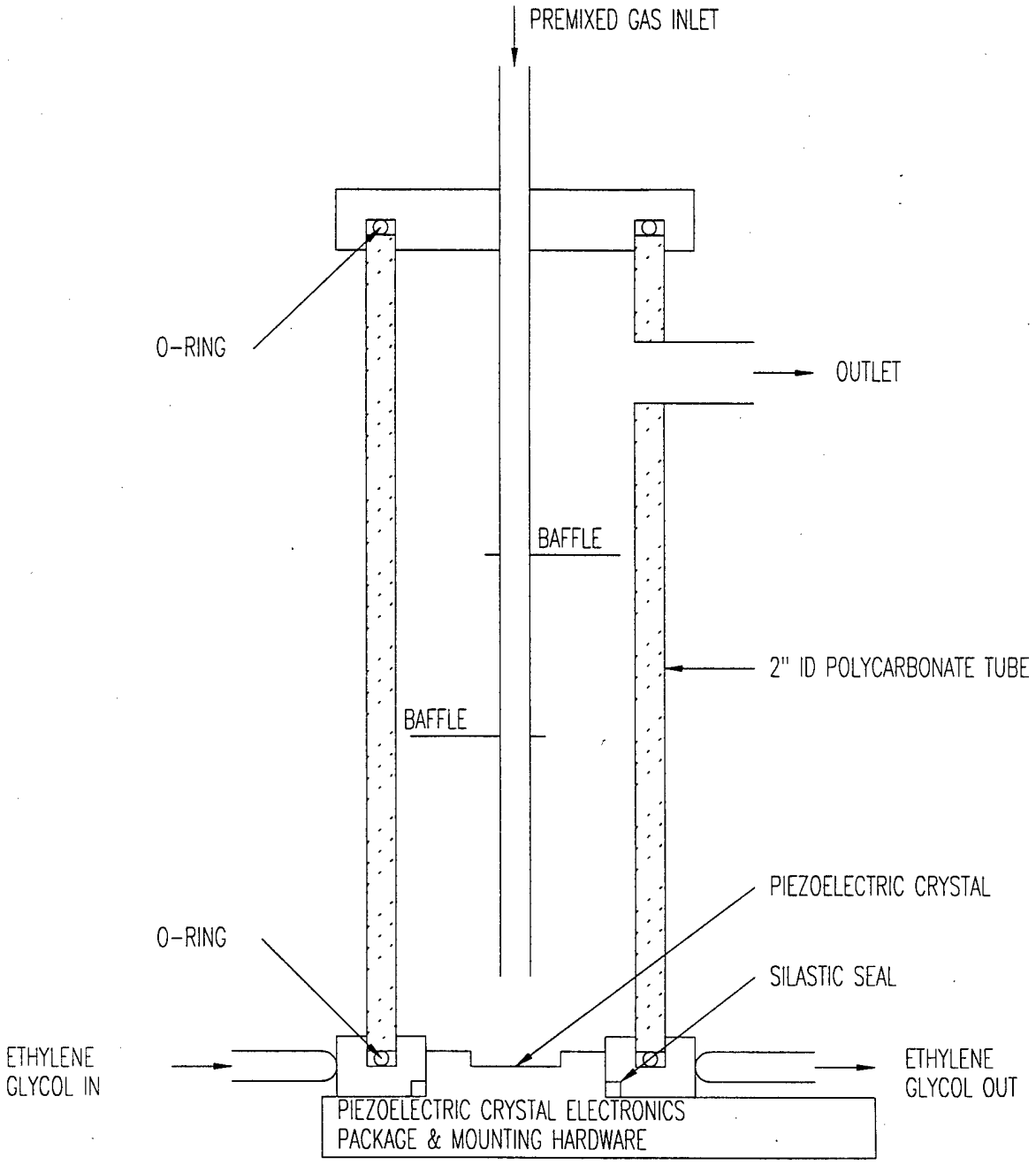

Figure 9. Ultrasonic Aerosol Generator.

connected to a grounded power supply such as an autotransformer; both power leads must float with respect to case ground. An isolation transformer was used by the author to achieve this design requirement.]

The ultrasonic aerosol generator was used both for atmospheric pressure experiments (with the Sapphire 0 burners) and for reduced pressure experiments (with the Sapphire 1 instrument). In all experiments, the premixed fuel-oxidizer-diluent stream was introduced into the nebulizer chamber through a 1/4-in (0.64-cm) OD tube, the end of which was about 0.8 in (2 cm) above the surface of the pool of liquid. For experiments with wet aerosols, the output from the chamber was introduced directly into the bottom of the burner.

The configuration for experiments with dry aerosols is shown in Figure 10. In these experiments, the wet aerosol was passed first through a 19-in (48-cm) long, 0.4-in (10-mm) OD borosilicate glass tube heated to 140 °C (284 °F), and then through an 12 in (30 cm) long, 0.4-in (10-mm) OD borosilicate glass chemical condenser cooled with chilled water. Condensed water was collected in the cold finger (immersed in an ice-water bath), located between the hot tube and the condenser.

Experiments with Sapphire 1 presented an interesting problem. If the condenser had been connected directly to the burner, the pressure in the nebulizer and condenser would have been only slightly above 30 torr, and a significant fraction of the vaporized water would have passed into the flame instead of being condensed and removed from the gas stream. This difficulty was solved by the simple expedient of inserting a 0.040-in (1-mm) flat-plate orifice between the top of the condenser and the bottom of the burner. In typical experiments with a total flow rate of about 1700 cc/min (measured at prevailing atmospheric pressure, 630 torr), the pressure in the aerosol generating system was about 300 torr, while the pressure in the flame chamber was 30 torr. In spite of this restriction in the flow path, very little of the aerosol was found to have "precipitated" upstream or downstream of the orifice.

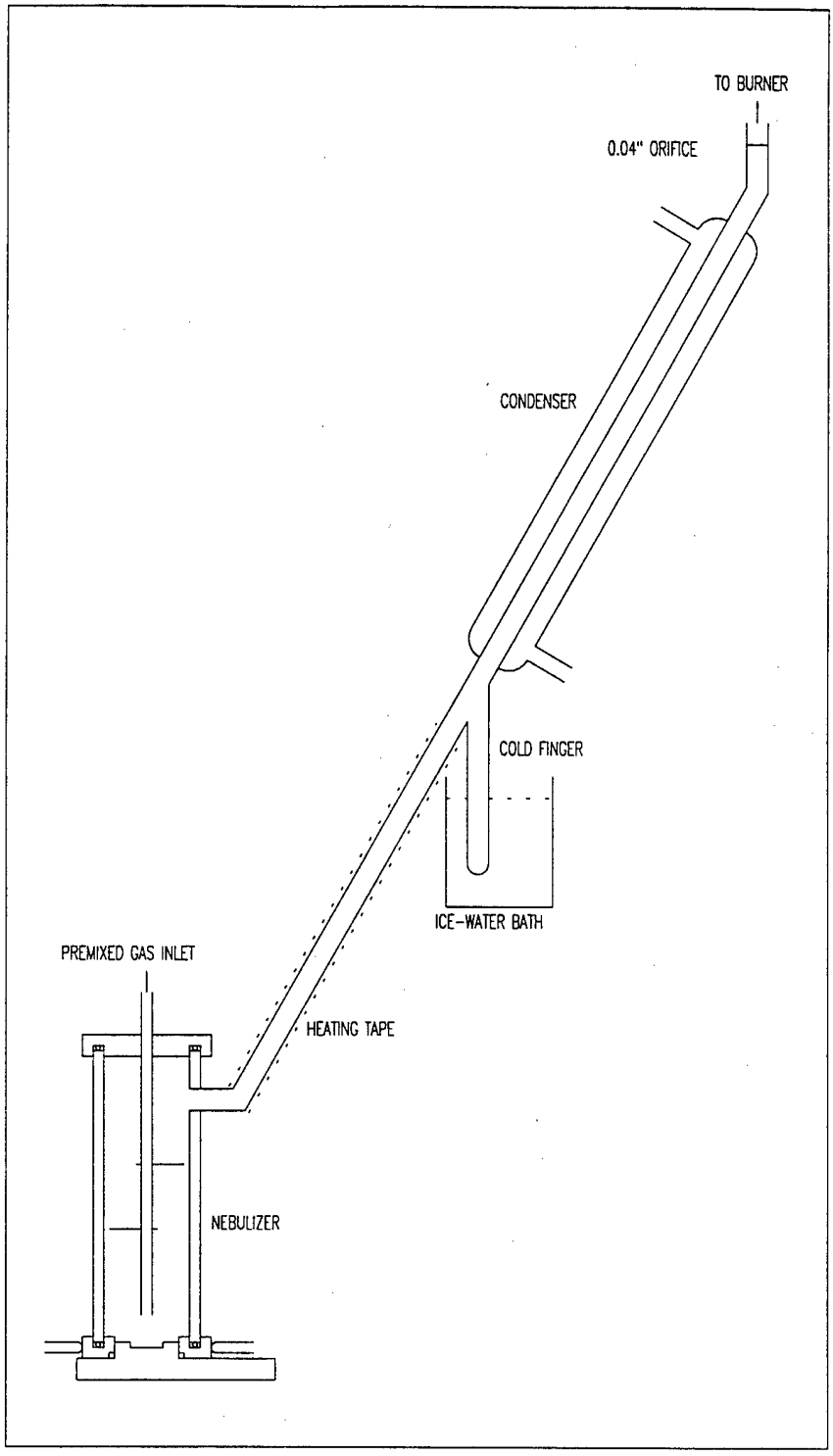

Figure 10. Ultrasonic Aerosol Generator System for Dry Aerosols.

F. DIRECT INJECTION OF LOW-BOILING LIQUIDS

1. Introduction

From a practical point of view, some extinguishing agents can be dispersed only as gases. However, many other agents, with lower vapor pressures, can be dispersed as mists or fine aerosols. HCFC-22 ($HCClF_2$) is such a material. This compound has a boiling point of -0.75 °C (-41.35 °F), a vapor pressure at 25 °C (77 °F) of 1040 kPa (151 psig), and a heat of vaporization of 55.81 cal/g (Reference 3). Because of its physical properties, it was possible to introduce this compound either as a gas (by taking it off the top of the cylinder), or as a liquid (by metering the pressurized liquid into the premixed gas stream). It was of interest to discover whether there would be a noticeable difference in the Heat Extracted experiments between the two alternate techniques of introducing the agent into the gas stream.

However, the interest in aerosols far exceeds this limited scope. Many materials have vapor pressures less than 101.3 kPa (14.7 psig) at room temperature and might be interesting as extinguishing agents if they could be introduced as aerosols. Not the least of these are water, and aqueous and non-aqueous solutions of metal-containing compounds.

2. Continuous Expansion Experiments

In the continuous expansion experiments, HCFC-22, pressurized to 1400 kPa (200 psig) with N_2, was fed by a small-diameter flexible tube to a small metering valve, located in a T in the premixed gas line, immediately below a Sapphire 0 burner. As soon as the high pressure liquid passed through the metering valve, some of it flash-vaporized and ejected small liquid particles into the premixed gas stream. These aerosol particles continued to vaporize as they were swept into the burner. It is not known whether any aerosol particles remained as the premixed gases passed through the flame holder in the burner. However, when the system was allowed to eject HCFC-22 into quiescent laboratory air, some aerosol particles were observed as far as 8 in (20 cm) from the metering valve.

There was one practical problem with this arrangement. As expected, the flash vaporization cooled the metering valve; at higher flow rates, the valve became chilled to the point that condensed liquid tended to obstruct the orifice, and the flow rate became unsteady. An

attempt to heat the valve proved to be of limited utility. Nevertheless, some useful data were acquired.

3. Pulsed-Valve Experiments

To gain experience with a pulsed valve, a used Volkswagen fuel injector valve was "acquired" and an electrical circuit was designed for controlling the pulse rate and duration. Figure 11 shows the circuit diagram for the driver for this valve. Since this type of valve has no provisions for driving it closed, the driver circuit was comparatively simple. The two knobs of the control panel determined the duration of the open signal (ON TIME) and the length of the interval (OFF TIME) between removal of the open signal and the application of the next open signal. The minimum open time was determined by the force constant of the spring and the mass of the moving element. A rough experimental estimate of this minimum pulse duration placed the value at about 5 ms. The pulse rate was variable from less than 1 Hz to about 100 Hz.

To examine the suitability of a pulsed valve for extinguishment experiments, a "cup-burner" type of experiment was designed. Figure 12 is a sketch of the experimental configuration. The pulsed valve was placed at the bottom of a mixing chamber, with the expectation that some mixing would occur as the aerosol-premixed gas mixture approached the flame, and that a nearly uniform (time-invariant) composition would pass by the flame.

In the experiment, a 100-cc high-pressure stainless steel cylinder was filled with liquid HCFC-22 at its room temperature vapor pressure. The steel cylinder, mounted in a support stand, was placed on the pan of an electronic balance (±0.001 g). The flexible 1/8-in (0.32-cm) OD delivery tube from the bottom of the steel cylinder to the pulsed valve was about 18 inches (46 cm) long and was arranged so that very little force was applied to the balance by the tube. This arrangement proved to be very satisfactory and permitted the HCFC-22 to be delivered at reasonable and easily measured flow rates.

The NMERI Standard Cup-burner was used (Reference 4). The inside diameter of the borosilicate glass mixing tube was 1.97 in (50 mm), and the outside diameter of the flame cup was 0.51 in (13 mm). The oxidant (air), was metered through a variable-area flow meter, and introduced into the mixing chamber at the bottom of a bed of glass beads. The level of the

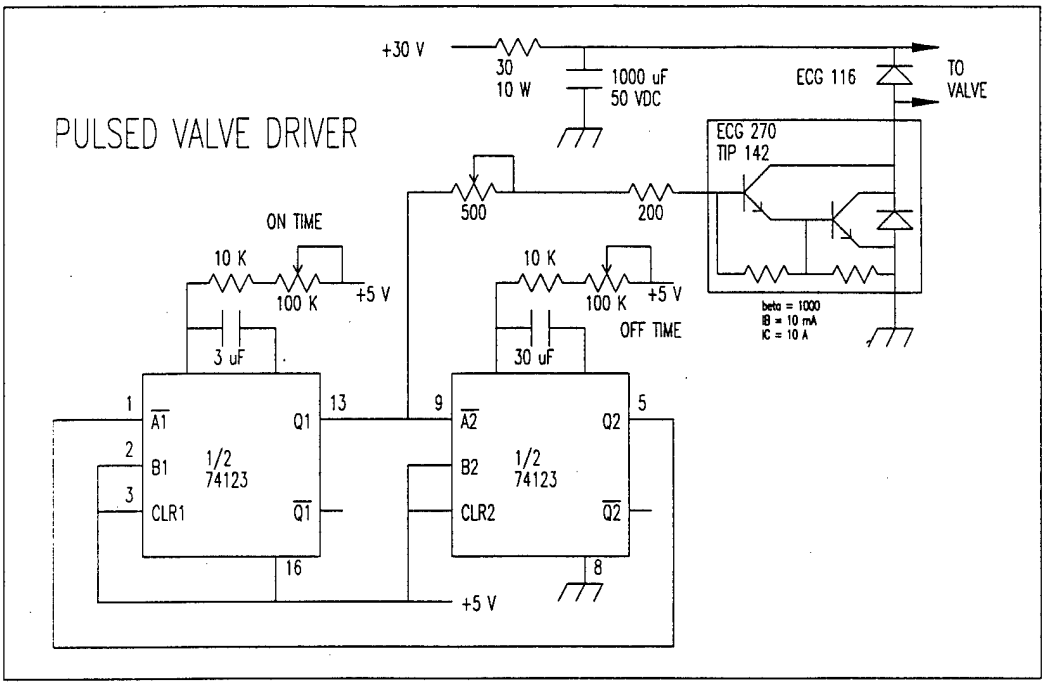

Figure 11. Pulsed-Valve Driver Schematic.

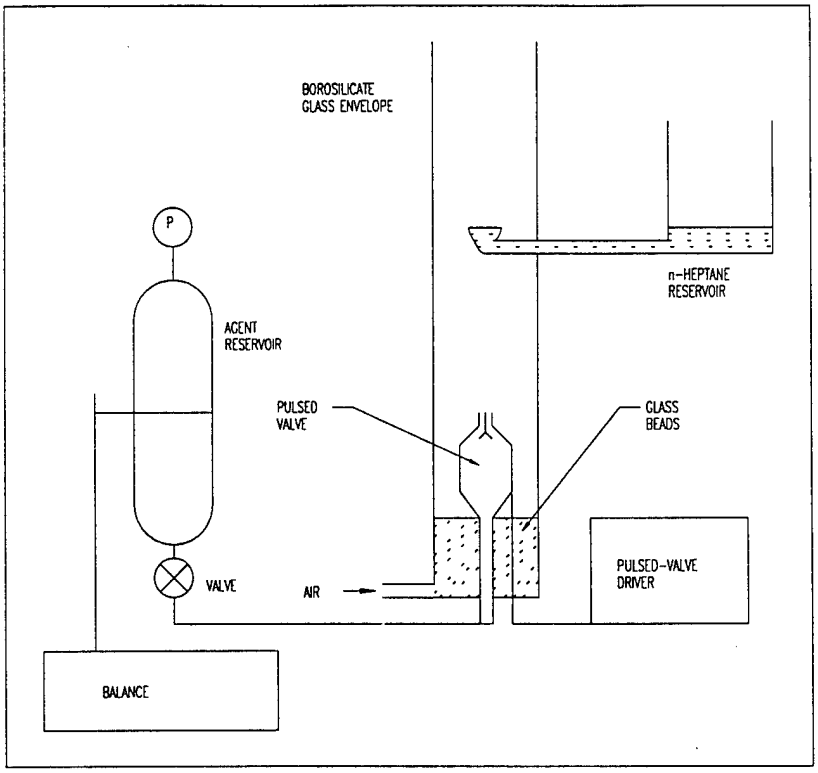

Figure 12. Block Diagram of the Pulsed-Valve Cup-Burner Experiment.

n-heptane fuel was maintained at the lip of the cup by controlling the height of the reservoir. In typical experiments, the flow rate of air was 7 L/min, which corresponds to a linear flow rate of about 6 cm/sec.

In the experiments, the pulse rate was started at 1 Hz and increased until the flame was extinguished. It was found that the pulsed valve could be operated for extended periods of time at constant delivery rates, without any difficulties associated with freezing and/or clogging. However, the flash evaporation of the HCFC-22 was so rapid that a pressure pulse was generated each time a burst of HCFC-22 was introduced into the chamber. This pressure pulse propagated at the speed of sound and disturbed the flame long before the HCFC-22 in the flow reached the flame. The magnitude of the disturbance depended on the distance of the valve from the cup. The relationship was not simple, and it was possible to locate the valve at a position such that a node in the pressure pattern was located at the flame. Thus, by selecting a suitable distance from the valve to the cup, the effect of the pressure pulse was minimized, although not eliminated. It is important to observe that, in a few experiments with water, this phenomenon was not observed, presumably due to the much slower rate of flash evaporation of water.

The amount of HCFC-22 required to extinguish the flame was uniformly less than the cup-burner value of 11.6 percent by volume (Reference 4). The variability from experiment to experiment was significant and was attributed to the residual hydrodynamic disturbances caused by the flash evaporation. Attempts to reduce further the hydrodynamic disturbances included placement of a screen between the valve and the flame (this had no noticeable effect), and placement of a convergent-divergent nozzle between the valve and the cup (this made a noticeable improvement, depending on the location).

4. Assessment

Unfortunately, failure of the pulsed valve resulted in premature cessation of the experiments. However, the pulsed-valve experiments appeared to have considerable promise. As a start, experiments should be done to assess the statistical variance. It may be that the additional cooling due to the vaporization of the liquid can be shown to make a significant contribution to the extinguishment. In addition, other agents, especially those with lower vapor

pressures, should be examined. These can be forced through the nozzle by pressurizing the delivery cylinder (with N_2, for example). It appears that the pulsed-valve delivery system opens up the cup-burner technique to many more candidate agents of more than just casual interest.

SECTION III

ATMOSPHERIC PRESSURE FLAMES—SAPPHIRE 0

A. INTRODUCTION

Flame velocity is a measure of the progress toward extinguishment of inhibited flames. As the flame speed approaches zero, the flame loses its ability to propagate; extinguishment corresponds to zero flame speed.

In an early and enduring paper, Botha and Spalding determined the adiabatic flame speed by relating the observed flame speed to the amount of heat removed by the burner as the mixture ratio was changed; a nearly linear relationship was found (Reference 5). It follows that it should be possible to relate the observed heat removed by the burner to the progress toward extinguishment of inhibited flames. Based on this idea, it was decided to measure the heat extracted by the burner as a function of the amount of extinguishant added.

The first heat extraction experiments conducted in this project were performed in the Sapphire 1 instrument and are detailed in Section V of this report. However, it was quickly found that the Sapphire 1 experiments were complicated to an undue degree by the fact that the flame was generated in an atmosphere of combustion products. For the first of the atmospheric pressure experiments, the burners were removed from the Sapphire 1 chamber and operated at atmospheric pressure in a hood. As experience was gained, burners designed especially for atmospheric pressure operation were constructed. These have become known collectively as the Sapphire 0 burners. The work with these burners is collected in two sections. Section III describes the characteristics of these burners and of typical experiments, while Section IV collects the data from all of the Sapphire 0 experiments and compares the results obtained for several different agents.

As mentioned in Section II, two types of experiments were conducted with Sapphire 0 burners.

Heat extracted *vs.* Flow Rate Experiments. The flow rate of extinguishing agent was changed while all other flow rates were held constant; beginning with an uninhibited flame, extinguishing agent was added incrementally until flameout was achieved. These experiments are described in II.B.

Heat Extracted *vs.* Fuel/Oxygen Equivalence Ratio Experiments. The flow rate of methane was changed (thus changing the fuel/oxygen equivalence ratio, ϕ) while all other flow rates (including that of the extinguishing agent) were held constant. The fuel/oxygen equivalence ratio was scanned incrementally from the lean inflammability limit to the rich inflammability limit. These experiments are described in II.C.

B. HEAT EXTRACTED *vs.* FLOW RATE EXPERIMENTS

1. Experiments with Thermal Agents

The unique characteristic of experiments with thermal agents, such as argon and nitrogen, was the linear relationship between the heat extracted by the burner and the flow rate of extinguishing agent added to the flame. An early experiment with argon as the diluent and nitrogen as the inhibitor is illustrated by Figures 13 and 14. In this experiment, the total flow rate in the uninhibited flame was 3705 cc/min (@ 637 torr), and the mole fractions of Ar, O_2, and CH_4 were 0.757, 0.154, and 0.088, respectively; $\phi = 1.15$ for this flame. With the flow rates of diluent, oxidizer, and fuel held constant, the amount of nitrogen was increased incrementally, and the temperature increase of the EG in the cooling loop was measured after a suitable delay for thermal equilibration. Because of the thermal mass of the burner, about 6 minutes was required for the system to achieve thermal equilibrium. The EG at the entrance to the cooling loop was maintained at room temperature by a constant temperature bath; the objective of this provision was to minimize heat transfer from the (nearly ambient temperature) atmosphere near the burner. The flow rate of the EG coolant was selected so that, for an uninhibited flame, the temperature rise in the coolant was about 10 °C (18 °F).

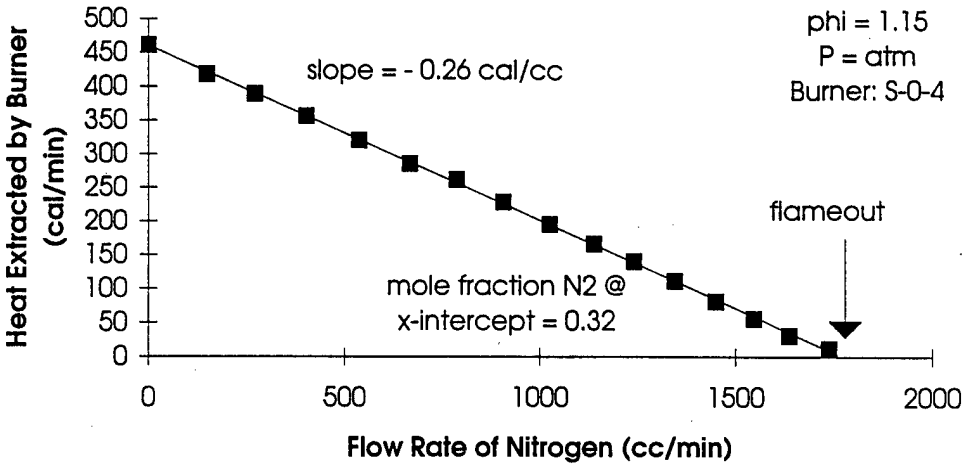

Figure 13. Inhibition of a Methane-Oxygen-Argon Flame by Nitrogen: Heat Extracted by the Burner.

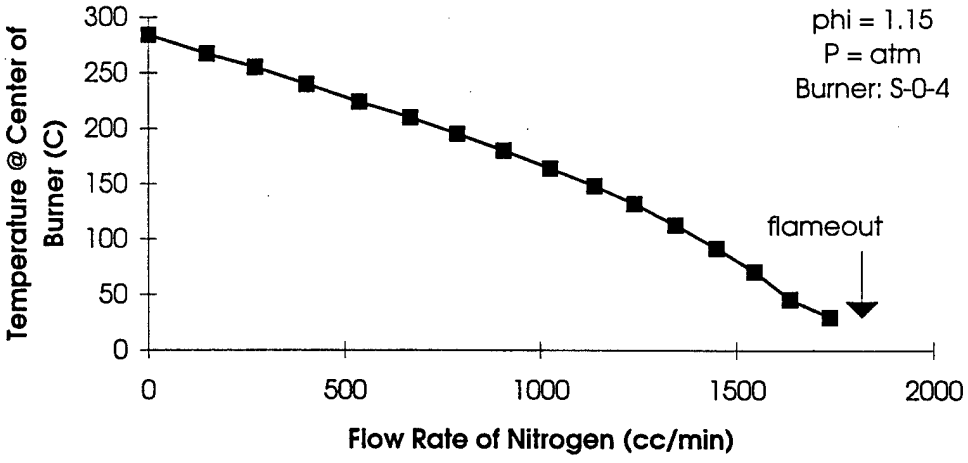

Figure 14. Inhibition of a Methane-Oxygen-Argon Flame by Nitrogen: Temperature at the Center of the Burner.

As expected, the heat extracted by the burner from an uninhibited flame was a strong function of the flow rate of methane; for this reason, many of the heat extraction data were normalized by dividing the observed heat extracted by the flow rate of methane. The reader is cautioned, however, that some of the data in this report were not treated in this manner; see especially the results reported in Section V.

In typical experiments, the total energy released was 1500 to 2500 cal/min (calculated from the standard heat of combustion of methane). Of this, between 5 and 15 percent were extracted from the uninhibited flame by the cooled burner at the beginning of the experiment. The fraction of the total heat actually extracted by the burner depended primarily on the fuel/oxygen equivalence ratio. The fraction of the heat transferred to the burner was the largest for the stoichiometric flames and was significantly less both for rich and for lean flames.

The heat extracted by the burner was found to be burner dependent; thus, data such as the slope of the curve obtained for a particular agent could be compared only against the data for another agent using the same burner. However, the point of extinguishment was independent of the burner used and thus permitted comparison with experiments by other workers.

The experiment illustrated by Figures 13 and 14 was conducted in an ambient air atmosphere, with provisions to prevent disturbance by air currents, but with no provisions to prevent entrainment of air into the flame. It was particularly interesting to note that, although this flame was fuel-rich and entrained oxygen from the surrounding atmosphere, all of the experimental data points nevertheless fell on a straight line. Flameout occurred at the point that was predicted by extension of the line to the point at which no heat was transferred to the burner from the flame. This result was characteristic of experiments with moderately fuel-rich flames, such as the experiment illustrated here.

The temperature measured at the center of the burner was also an excellent predictor of extinguishment; as expected, this temperature was very near room temperature at extinguishment (Figure 14). However, while the heat extracted by the burner was a linear function of the amount of extinguishant added (for thermal agents such as N_2), the temperature at the center of the burner was a decidedly non-linear function of this variable. Nevertheless, it was

possible to correlate the temperature at the center of the burner with the heat extracted by the burner, provided variables such as the flow rate of ethylene glycol were held constant. As an example, consider the data for a set of five experiments with methyl chloride (Figure 15); for these experiments, the Heat Extracted *vs.* Temperature at the Center of the Burner data were fitted to a single curve.

Liftoff was not measured for the atmospheric pressure experiments. With the exception of the data points immediately before extinguishment, the flame remained tightly attached to the flame holder, and liftoff was immeasurably small.

2. Slope of the Heat Extracted Line

The slope of the Heat Extracted line was of particular interest. It was a direct measure of the effectiveness of the agent—the more negative the slope, the less agent required to achieve extinguishment. Since the slope was expressed in terms of calories/cubic centimeter of agent, it was a measure of the capacity of the agent to absorb heat from the flame, and it was of interest to determine the relationship between this slope and more conventional measures of the capacity of the agent to absorb heat.

Data for five thermal agents are presented in Figure 16. Here, the experimental slopes were plotted as a function of the change of enthalpy (ΔH) of the agent upon being heated from 298 K to a presumed extinguishment temperature of 1600 K. In essence, the independent variable (x-axis) for this presentation of the data was the amount of heat that the agent would have absorbed on reducing an uninhibited adiabatic flame to an inhibited adiabatic flame at the point of extinguishment. The enthalpy data were taken directly from Reference 6.

For further discussion of the conditions at extinguishment, the reader is referred to Section IV.H. It is sufficient to note at this point that, because of the linear velocity of the cold gases in the Sapphire 0 burner, extinguishment (liftoff) was observed at an adiabatic flame temperature higher than that expected for extinguishment in a quiescent mixture of gases.

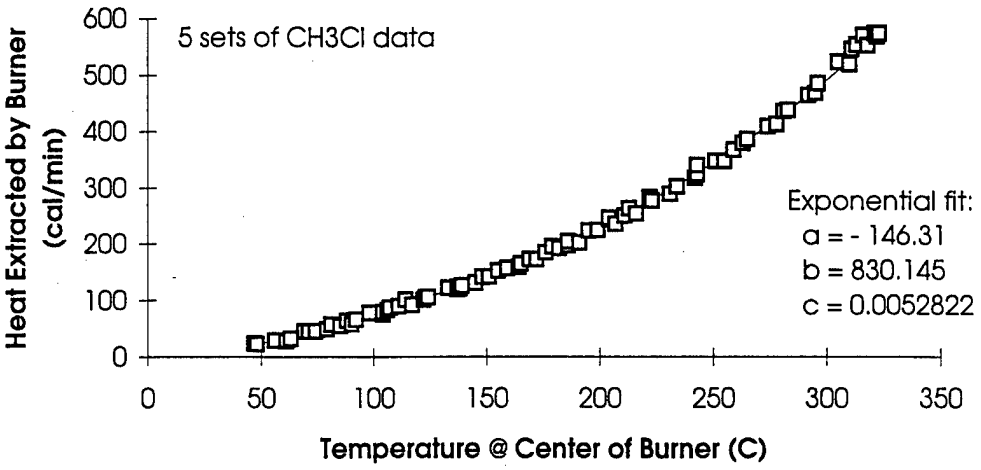

Figure 15. Relation between Heat Extracted by the Burner and the Temperature at the Center of the Burner.

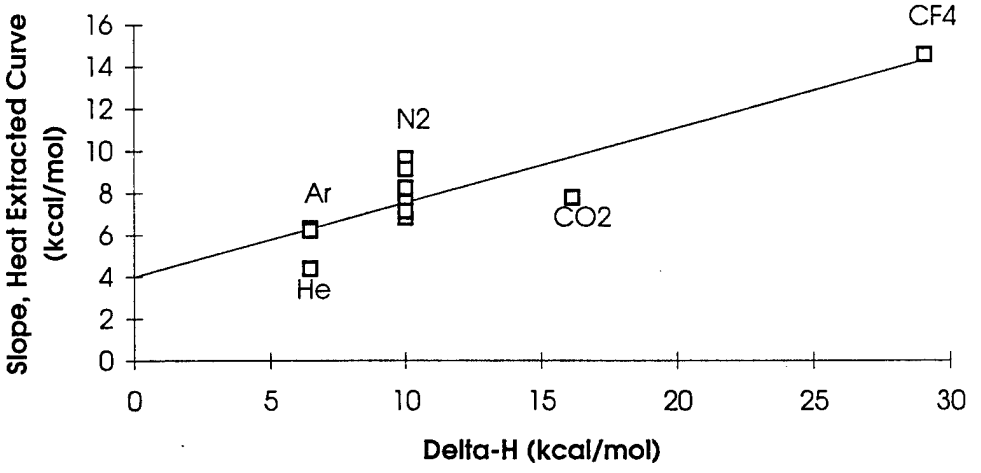

Figure 16. Relation between the Slope of the Heat Extracted Curve and ΔH [= H^0(1600 K) -H^0(298.15 K)] for Thermal Extinguishants.

Within experimental uncertainties, all the data presented in Figure 16 were obtained with flames having the same fuel/oxygen equivalence ratio ($\phi = 1.17$) at the prevailing atmospheric pressure (ca. 630 torr), and with argon as a diluent. It was immediately apparent that while there was a general relationship, there was also a great deal of scatter in the data. In defense of the data, it is noted that the data were collected over an extended period of time, early in the program. Moreover, since other objectives were foremost at that time, some of the experimental parameters that might have enabled a "tightening" of the data, were not carefully controlled. As an example, consider the flow rate of the EG coolant. Data for two experiments, conducted on the same day with all other parameters being the same, are presented in Figure 17. The 10 percent difference in the slopes was unexpected and reflected (primarily) the fact that the amount of heat apparently extracted by the burner was larger for the experiment with the lower EG flow rate. In retrospect, it seems more likely that this particular difference in slope should be attributed to the practical difficulties associated with sensing the temperatures of a flowing liquid in a copper tube with a thermal gradient that extended to either side of each of the two discrete points at which the temperatures were measured. Nevertheless, the point was made—small changes in experimental parameters did result in variances in the observed slope.

In spite of the obvious uncertainties in the data, and the fact that only one or two data points were obtained for some of the agents, the results provided a useful benchmark. Figure 18 shows the data for all the agents studied. Without exception, the slopes of the heat extracted lines for all other agents were above the line defined in Figure 16 (and repeated in Figure 18). This suggested that factors other than simple absorption of heat were important for these other agents, and that, with more careful control of the experimental variables, one had the potential for making quantitative estimates of the relative importance of thermal and other mechanisms of inhibition.

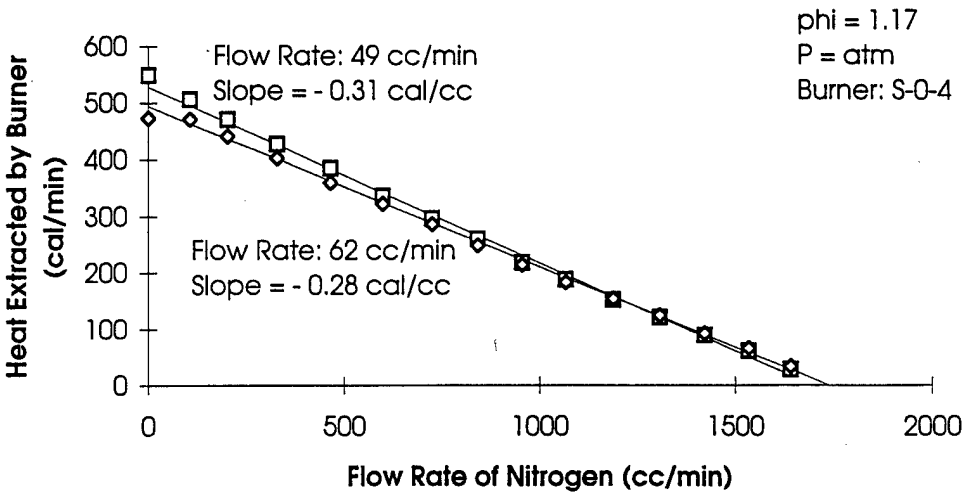

Figure 17. Effect of Ethylene Glycol Flow Rate on Slope of Heat Extracted Curves.

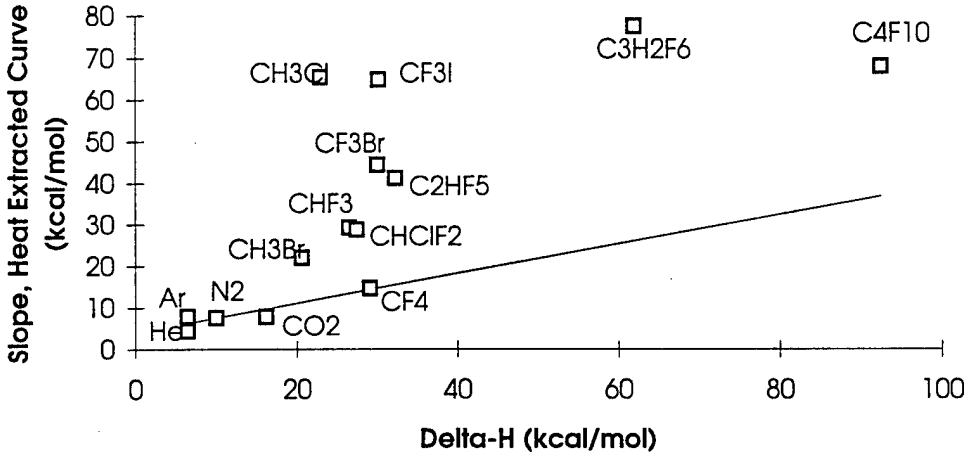

Figure 18. Relation between the Slope of the Heat Extracted Curve and ΔH [$\Delta H = H^0(1600K) - H^0(298.15\ K)$] for All Extinguishants Studied.

3. Experiments with Fuel-Rich Flames

A typical result for a fuel-rich flame is illustrated by Figures 19 and 20. Except for the fuel/oxygen equivalence ratio and different burner, this experiment was essentially identical to that illustrated by Figures 13 and 14. The significant difference was the departure from straight-line behavior for nitrogen at flow rates greater than 1200 cc/min. The additional heat extracted by the burner at these high flow rates was attributed to the combustion of the excess methane with entrained oxygen from the ambient air environment. This hypothesis was supported by the observation that the flame remained attached around the rim of the burner until flameout was finally observed at about 1700 cc/min, although the flame lifted off from the center of the burner (as evidenced by the temperature at the center of the burner) at about the 1200-cc/min point. In effect, the fuel/oxygen equivalence ratio (ϕ) did not remain constant throughout this experiment.

4. Experiments with Agents Having "Fuel-Character"

There has been a great deal of interest in candidate agents having one or more hydrogen atoms on the carbon backbone. Because of the presence of the H atom, these molecules are subject to reaction with tropospheric OH molecules and hence to degradation in the troposphere. As a consequence, these molecules have significantly smaller ozone depletion potentials (ODP) than their completely halogenated counterparts. Because of the presence of the H atom, these molecules also have what may be called "fuel-character"; some are even flammable.

A classic example of the behavior of one of these molecules, methyl chloride (CH_3Cl), in the Sapphire 0 burner is illustrated by Figure 21. For CH_3Cl flow rates greater than 125 cc/min, the flame lifted off at the center, but it remained attached around the periphery of the burner, suggesting that the fuel and CH_3Cl were continuing to burn in the presence of entrained oxygen. In this respect, the experiment mirrored the experiment, mentioned above, in which a fuel-rich flame was inhibited by nitrogen. The experimental result here also was a very obvious "tail" on the curve. However, there were additional consequences that did not become evident until the entrainment of air was eliminated.

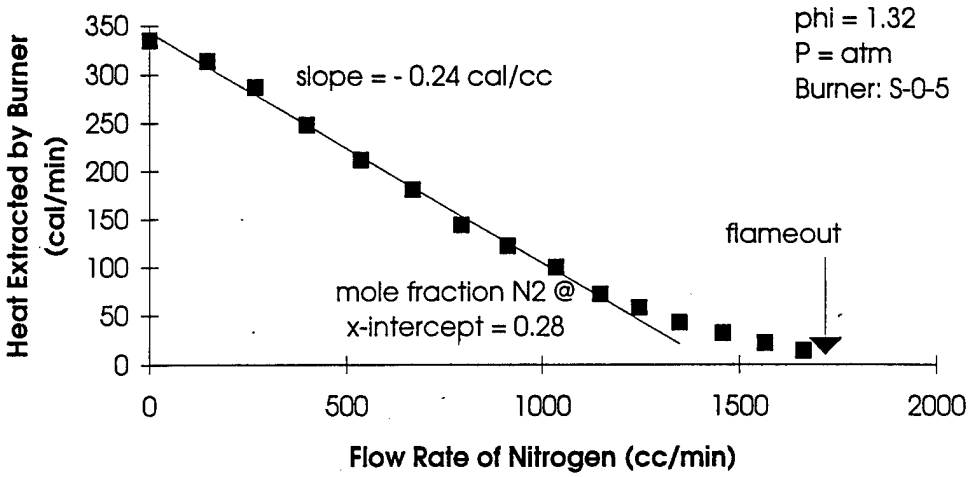

Figure 19. Inhibition of a Fuel-Rich Methane-Oxygen-Argon Flame by Nitrogen: Heat Extracted by Burner.

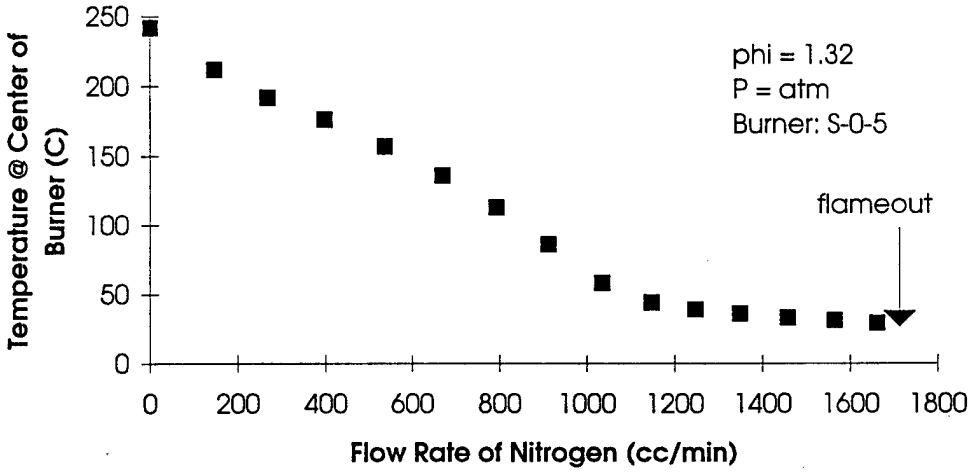

Figure 20. Inhibition of a Fuel-Rich Methane-Oxygen-Argon Flame by Nitrogen: Temperature at Center of Burner.

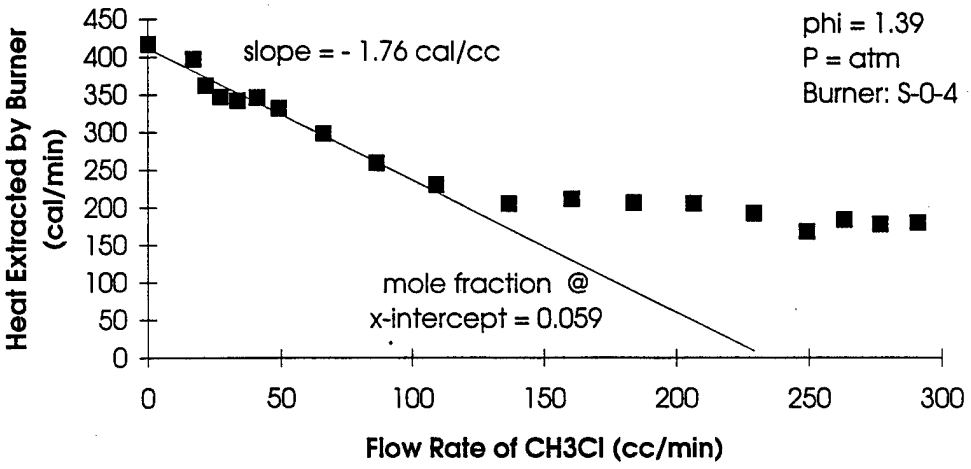

Figure 21. Inhibition of a Methane-Oxygen-Argon Flame by CH_3Cl.

To eliminate the effect of the entrained air, the burner was reconfigured so that the flame would burn in a slow-flowing nitrogen atmosphere. The burner was placed in a borosilicate glass cylinder, and a coaxial flow of dry nitrogen, stilled by iron wool packed around the burner, was introduced. The linear flow rate of the nitrogen flow was similar to that of the premixed gases as they flowed from the burner. The results of the first experiment with the nitrogen sheath are displayed in Figure 22. The "tail" of the curve, attributed to the reaction with entrained oxygen, was completely absent. However, two other differences were even more significant. For the nitrogen-sheathed flame, the slope of the heat extraction curve was more negative, and the predicted mole fraction at extinguishment was smaller.

The understanding of these findings was predicated on the realization that the extinguishing effectiveness of an agent with "fuel character" was, to a significant degree, the result of increasing the fuel/oxygen equivalence ratio (ϕ), thus yielding what may be called an "effective ϕ." As the "effective ϕ" of the premixed gases was increased, the upper inflammability limit was approached, and less extinguishing agent was required. In the CH_3Cl experiments illustrated here, the entrainment of oxygen, and the contribution of the diffusion flame around the periphery of the burner, effectively reduced the fuel/oxygen equivalence ratio from the value established for the premixed gases. As a direct consequence, the flame lifted off

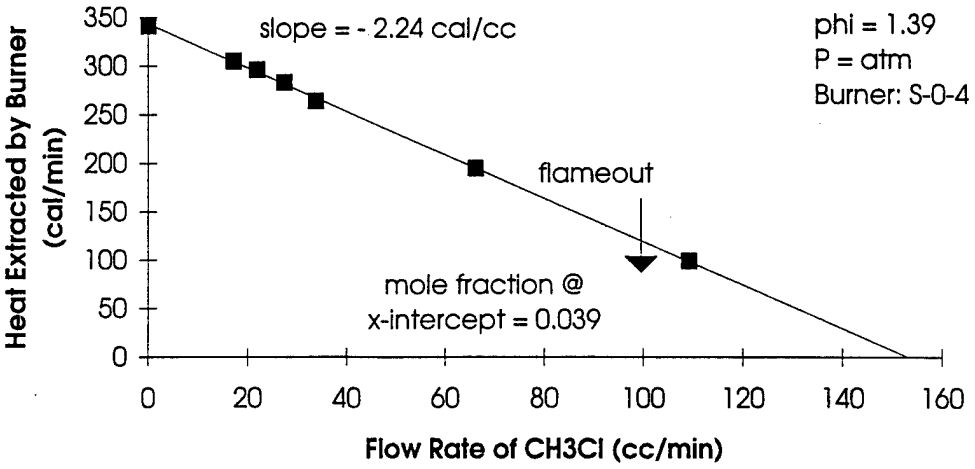

Figure 22. Effect of Providing an N_2 Sheath for Methane-Oxygen-Argon Flames Inhibited by CH_3Cl.

at the center of the burner, but remained attached around the periphery. The addition of the nitrogen sheath prevented the entrained oxygen from enabling the flame to remain attached around the periphery of the burner. Thus the nitrogen sheath accounted both for the increased steepness of the Heat Extracted curve and for the smaller amount of CH_3Cl required to achieve extinguishment. As a result of these experiments, all future Sapphire 0 experiments employed a nitrogen sheath.

Flames doped with agents with fuel content were frequently observed to be luminous (reminiscent of candle flames) near the extinguishment point. Some of these flames also displayed cellular structure, in which a small number of flamelets were observed; the scale of these flamelets was larger than that of the spacing of the elements in the flame holder (0.1 in by 0.1 in). Flames with 3, 4, and 7 cells were sometimes observed just before extinguishment.

5. Experiments with Catalytic Agents

By comparison with the thermal agents, catalytic inhibiting agents displayed a dramatically different behavior. An experiment with methyl bromide (CH_3Br) is illustrated by Figure 23. In this experiment, the total flow rate in the uninhibited flame was 3698 cc/min

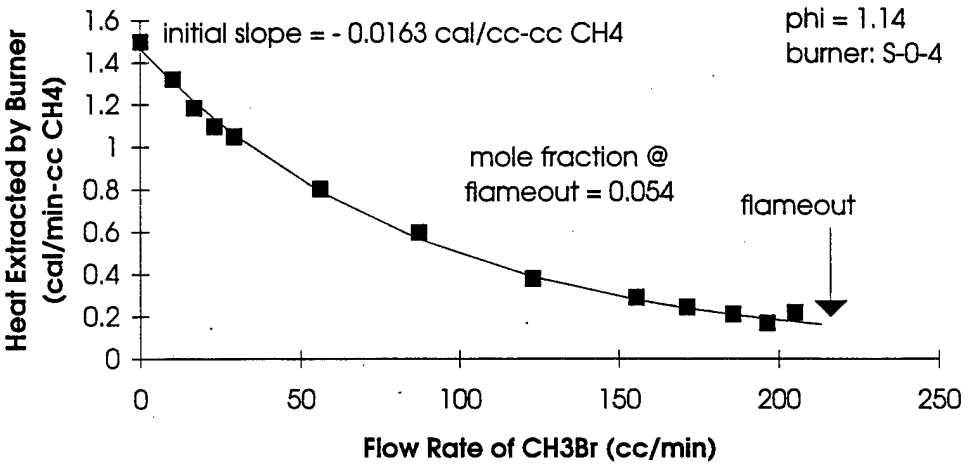

Figure 23. Inhibition of a Methane-Oxygen-Argon Flame by CH_3Br.

(@ ca. 630 torr), and the mole fractions of Ar, O_2, and CH_4 were 0.758, 0.154, and 0.088, respectively; $\phi = 1.14$ for this flame. While, the heat capacity of methyl bromide contributed significantly to the extinguishment of the flame, the characteristic linear relationship typical of a physical (thermal) extinguishing agent was absent, and the data points in this figure were best fitted using an exponential equation of the form $y = a + be^{-cx}$.

C. HEAT EXTRACTED *vs.* FUEL/OXYGEN EQUIVALENCE RATIO EXPERIMENTS

1. A Typical Experiment

Heat Extracted *vs.* Fuel/Oxygen Equivalence Ratio experiments were conducted for four compounds: CF_4, CHF_3, $CBrF_3$, and $Fe(CO)_5$. The CF_4 experiments are discussed here; the experiments with CHF_3 and $CBrF_3$ are discussed in Section IV; and the experiments with $Fe(CO)_5$ are discussed in Section VII. While all of the experiments were essentially identical, the results were quite different and provided important insights into the extinguishment mechanisms characteristic of the individual compounds.

A typical Heat Extracted *vs.* Fuel/Oxygen Equivalence Ratio experiment is Figures 24 and 25. The first step in this experiment was to measure the heat extracted as a

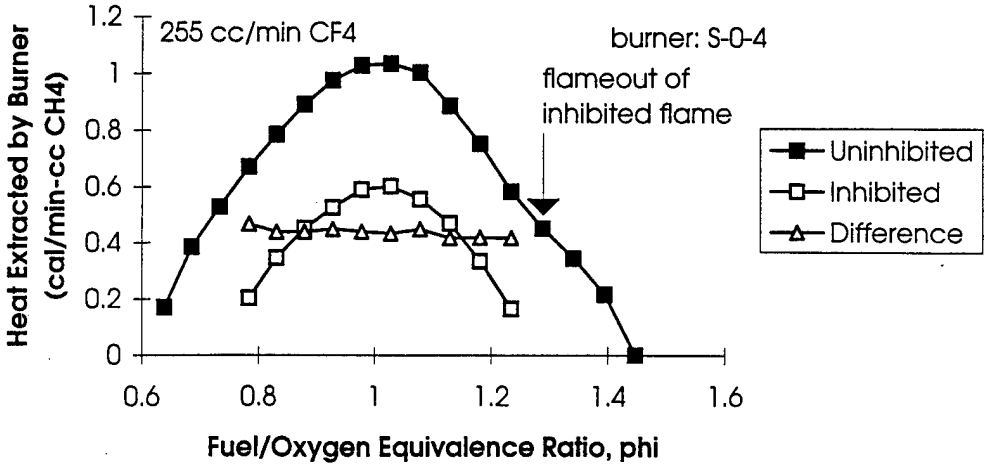

Figure 24. Inhibition by CF_4: Heat Extracted by Burner.

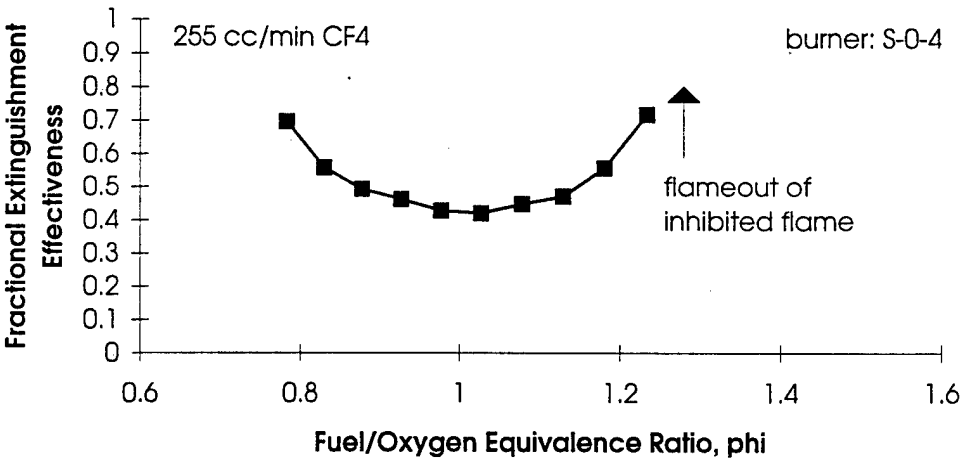

Figure 25. Inhibition by CF_4: Fractional Extinguishment Effectiveness.

function of the fuel/oxygen equivalence ratio of the uninhibited methane/air flame from the lean inflammability limit to the rich inflammability limit. A fixed flow rate of extinguishing agent was then introduced, and the experiment was repeated. In this experiment, the flow rates of O_2, N_2, and CF_4 (for the inhibited flame) were fixed at 732, 2793, and 255 cc/min, respectively (measured at the prevailing atmospheric pressure of about 630 torr), and the flow rate of CH_4 was varied to achieve the change in the fuel/oxygen equivalence ratio.

As expected, the uninhibited flame yielded a nearly symmetrical Heat Extracted curve, denoted by the filled squares, with a peak at the stoichiometric composition. Extrapolation of the curve to the x-axis yielded inflammability limits for this burner, under these experimental conditions. The true inflammability limits for methane-air mixtures have been reported to be $\phi = 0.46$ and $\phi = 1.64$ (Reference 7). The difference between these literature values and the experimental values found with the Sapphire burners is discussed in Section II.D. It suffices at this point to note that, because of the finite flow of the premixed gases at the top of the Sapphire burner, the range of values accessible with the Sapphire burner was narrower than the range cited in the literature.

The Heat Extracted curve for the inhibited flame is denoted by open squares (Figure 24). This curve, like the curve for the uninhibited flame, was nearly symmetrical and had a maximum value at $\phi = 1.00$. Although no experiments of this type were performed with the thermal agents such as argon or nitrogen, the observed result was precisely what one would have expected for a thermal agent. Indeed, CF_4 is thought to be a thermal agent. However, it would be unwise to imply that the experimental results displayed here demand that CF_4 be strictly a thermal agent. Rather, the results require only that the CF_4 not upset the chemistry in such a manner as to displace the peak of the Heat Extracted curve to a lower (or higher) value of ϕ. In sharp contrast, as will be discussed later, the other three agents did indeed perturb the chemistry and cause the peak of the Heat Extracted curve for the inhibited flame to be displaced from $\phi = 1.00$.

The third curve in Figure 24, denoted by the open triangles, is the pointwise difference between the curve for the uninhibited flame and the curve for the inhibited flame. In essence, this "difference" curve represents the amount of heat that was not extracted by the

burner as the result of addition of the CF_4. The fact that this curve was essentially flat was one more indication that the CF_4 inhibited the flame equally well at all values of ϕ.

The results presented in Figure 25 (for this same experiment) were derived from the data presented in Figure 24. The fractional extinguishment effectiveness (FEE)* is defined as follows:

$$FEE = \frac{Q(uninhibited) - Q(inhibited)}{Q(uninhibited)} \qquad [1]$$

Where: Q(uninhibited) = Heat extracted by the burner from the uninhibited flame

Q(inhibited) = Heat extracted by the burner from the inhibited flame

In essence, the FEE is defined at each data point as the value on the "difference" curve divided by the value on the curve for the uninhibited flame. Note that the extrapolated value of this curve is 1.0 at each of the inflammability limits of the inhibited flame. As expected, the bottom of this bowl-shaped curve was found at $\phi = 1.00$, implying that the stoichiometric flame was the most difficult for the CF_4 to extinguish.

D. INFLAMMABILITY LIMITS

Following the completion of several Heat Extracted *vs.* Flow Rate experiments with N_2 as the extinguishing agent, the extinguishment data were collected and plotted as a function of the fuel/oxygen equivalence ratio. The results are presented in Figure 26, along with the literature values for the lean and rich inflammability limits of methane-air flames at a pressure of 1.0 atm (Reference 7). It was evident that, when the experimental data for the Sapphire burner were extrapolated to the x-axis, the intercepts did not correspond to the published values for the inflammability limits for methane-air flames. The fuel-lean intercept was greater than the

*Throughout this report, equation numbers are inserted in brackets, [], and chemical reaction numbers are placed in parentheses, ().

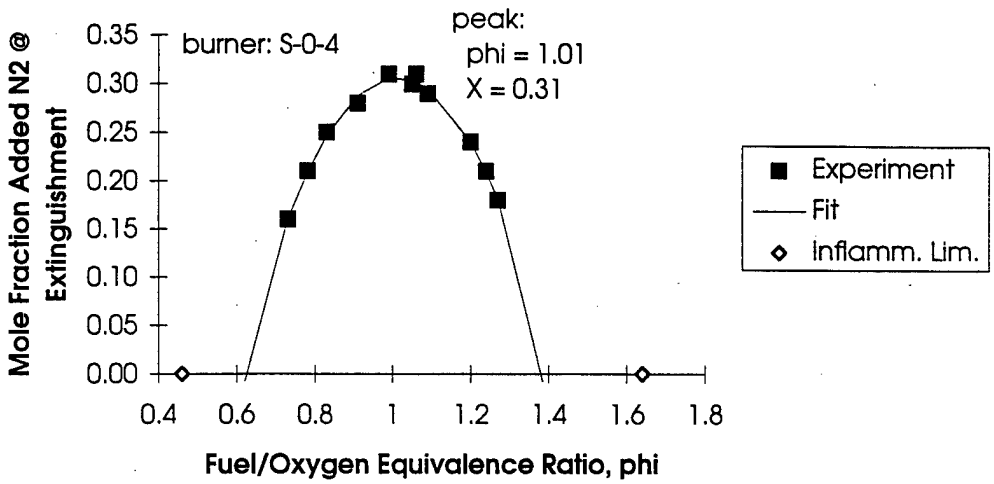

Figure 26. Inhibition by N_2: Mole Fraction at Flameout as a Function of Fuel/Oxygen Equivalence Ratio.

literature value for the lean inflammability limit, and the fuel-rich intercept was less than the literature value for the rich inflammability limit.

This finding was the result of the fact that the linear velocity of the cold gases in the burner was not zero, and extinguishment was observed when the flame speed had fallen to a value equal to the linear velocity of the cold gases. At this point, the flame detached from the burner, no heat was extracted by the burner, and the adiabatic flame speed of the gas-inhibitor mixture was equal to the measured linear velocity of the cold gases. It follows that, since the actual flame speed at the observed flameout was not zero, additional extinguishing agent would have been required to reduce the actual flame speed to zero (a common measure of the point of extinguishment).

With this problem in mind, a simple algorithm was sought, which could be used to relate the mole fraction at extinguishment in a flowing stream to the mole fraction at extinguishment in a still mixture. The algorithm is still being sought. Meanwhile, it is interesting to observe that the mole fraction of nitrogen required to extinguish a $\phi = 1.00$ flame is in excellent agreement with the published data from cup-burner experiments.

E. CORRELATION OF FLAME SPEED AND HEAT EXTRACTED BY THE BURNER

As noted earlier in this report, the basis of the Heat Extracted experiments was the Botha and Spalding finding that the flame speed was very nearly a linear function of the heat extracted by the burner (Reference 5). The Botha-Spalding burner differed from the Sapphire burners in several respects, perhaps the most important difference being the temperature at the center of the burner. The Botha-Spalding burner had a porous frit as a flame holder and was cooled to nearly room temperature at all points. By contrast, the flame holder in the Sapphire burner was an open grid, and had a temperature gradient from the center of the grid to the edge (where the cooling coils were located); in typical Sapphire experiments, the center of the grid was 200 to 300 °C (392 to 572 °F). Therefore, it was of importance to discover whether (1) the Sapphire burners were characterized by a linear relationship between flame speed and heat extracted by the burner, and (2) the value of the adiabatic flame speed extrapolated from data acquired with a Sapphire burner would agree with the literature values.

The data for this investigation were collected using uninhibited flames. In a typical experiment, the flow rate of air was fixed, and the flow rate of methane was varied from the lean inflammability limit to the rich inflammability limit. The flame speed at each point along the experimental curve was found by dividing the volumetric flow rate of the unburned gases, assuming that they were at room temperature, by the cross-sectional area of the burner. (Note: For this calculation, the area immediately *above* the grid was used, and not the area *in* the grid.) The flow rate of air was changed, and the experiment was repeated. After several experiments at different air flow rates, the flame speed data for each value of ϕ were collected and plotted as a function of the heat extracted by the burner. The y-intercept (no heat extracted by the burner) was taken to be the adiabatic flame speed. The results for $\phi = 1.00$ are presented in Figure 27. While a trend was apparent, no confidence could be placed in the results. The cause of the scatter of the data remains unknown.

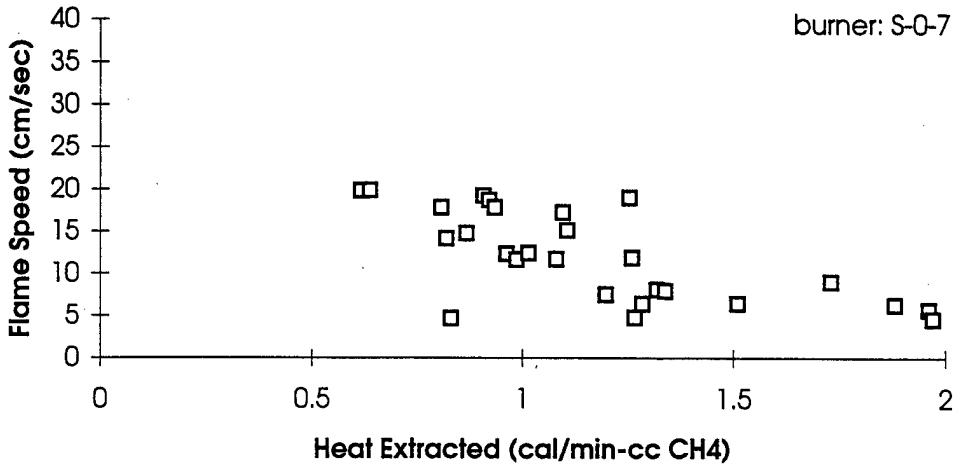

Figure 27. Flame Speed for Stoichiometric Methane-Air Flames. Each point represents an individual experiment.

Two questions arose during the course of this investigation.

1. Cross-sectional Area of the Burner. Since the burner had an open grid as the flame holder, should the open area of the grid (64 percent of the total cross-sectional area of the burner) be used, or should the total cross-sectional area be used (thus accounting for the fact that the flame expanded to fill the entire cross-sectional area immediately after escaping from the grid)? It was concluded that the latter procedure was proper.

2. Temperature Gradient across the Burner. Should the fact the flame holder into which the heat was extracted had a temperature gradient instead of a constant temperature across the entire diameter (as in the Botha-Spalding experiments) be considered? The answer is probably "yes" and "no." As a consequence of the gradient, the plot of flame speed as a function of heat extracted might not be linear. (The data were too badly scattered to tell.) Nevertheless, at the adiabatic flame speed (flame speed extrapolated to zero heat extracted by the burner), the gradient across the burner would be zero, just as in the Botha-Spalding experiments.

In view of the magnitude of the scatter of the data collected to this point, a more direct approach was taken: The experimental protocol was changed so that several measurements of the flame speed as a function of the heat extracted could be made in a single experiment. In these

experiments, the fuel/oxygen equivalence ratio was fixed at $\phi = 1.00$. For a typical data point, the flow rate of methane was set, the flow rate of air was adjusted to give the desired value of ϕ, and the heat extracted was measured; then a new value was selected for the flow rate of methane, and the process was repeated. A representative experiment is illustrated by Figure 28. It was encouraging to note at this point that the experimental data generally fell in the middle of the data collected in the previous experiments, and that the extrapolated adiabatic flame speed was reasonable. For comparison, Fristrom lists a maximum flame velocity of 39 cm/sec at $\phi = 1.06$ (Reference 7).

Despite the reasonable appearance of the results presented in Figure 28, the small upturn of the data at the highest values of flame speed was worrisome, and it seemed prudent to push the experiment to lower values of heat extracted by increasing the experimentally observed the flame speeds. Figure 29 displays the results of the best of this next set of experiments. Clearly, something was wrong. At the high flow rates, the experimentally observed flame speeds were very much too large. It was thought that the explanation might lie in the fact that the flow rate of the N_2 sheath gas was not matched to the velocity of the cold gases, so yet another experiment was conducted in which the flow rate of the sheath gas *was* matched to the flow rate of the cold gases; this made no difference. However, it was noted that, at a linear flow rate of cold gases of 20 cm/sec, the flame lifted off at the center of the burner while remaining attached around the periphery. It, therefore, seemed very likely that this observation could be attributed to the fact that the sheath gas flow was not parallel to the flow of cold gases at the top of the burner, as a result of the presence of the 1/4 in (0.64 cm)-OD cooling loop soldered to the periphery of the burner. It is proposed that the sheath gas "curled" around the cooling loop and forced the flame to remain attached at the edge of the burner. Note that low flame speed data points (from 0.8 to 1.2 cal/min-cc CH_4) fell on a reasonably straight line and were extrapolated to an adiabatic flame speed of 35 cm/s (14 in/s), essentially the same as the value found in experiment FS_D* (Figure 28). Note further that, except for these flame speed experiments (where the heat

*Experiment numbers generally designate the type of experiment (for example, FS means flame speed and is followed by an underscore and a number or letter in the series).

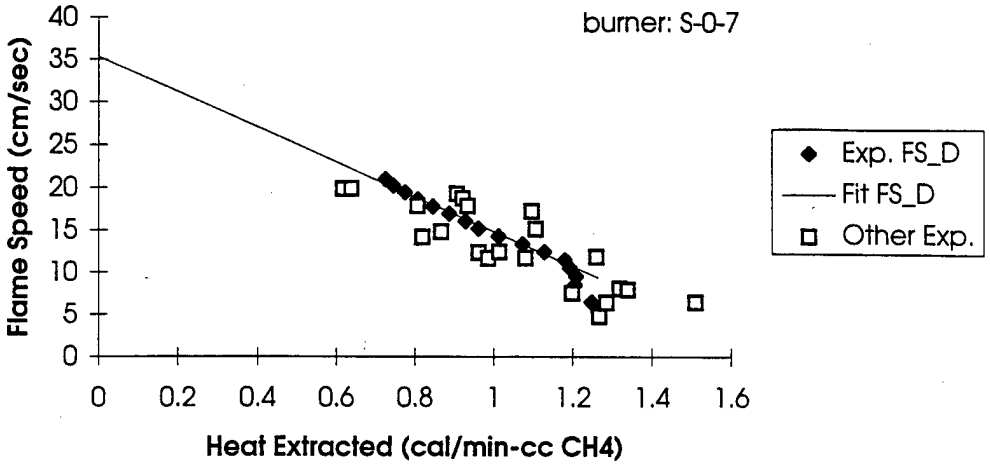

Figure 28. Experiment FS_D: Flame Speed as a Function of Heat Extracted. Data from individual experiments are superimposed.

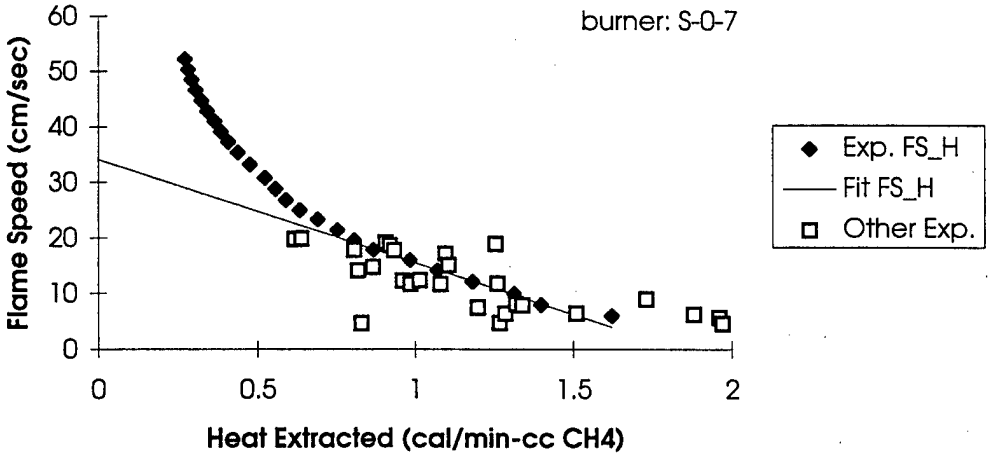

Figure 29. Experiment FS_H: Flame Speed as a Function of Heat Extracted.. Data from individual experiments are superimposed.

extracted was pushed to values below 0.8 cal/min), all experiments reported herein were conducted in the linear range, i.e., from 0.8 to 1.2 cal/min-cc CH_4.

F. INFRARED SPECTROSCOPY OF POST-REACTION GASES

1. Introduction

While some strictly "physical" extinguishing agents (e.g., Ar, N_2, CO_2) pass through a flame without interacting chemically with flame radicals ("burning"), this is not true for the vast majority of agents. The exceptional effectiveness of Halon 1301 ($CBrF_3$), for example, is directly attributable to the initial abstraction of the Br atom by an H atom, and by the subsequent reactions of various Br-containing species. It follows that at least one Br-containing species must be present in the post-combustion gases. In addition, the further reactions of the CF_3 radical must yield at least one F-containing species. In the case of Halon 1301, the principal halogen-containing products are F_2CO, HF, and Br atoms (Reference 8). While these compounds have significant toxicities, the risks have been weighed against the benefits, and have been found to be acceptable. Moreover, it is known that the absolute amount of HF generated during extinguishment by Halon 1301 depends on the rate of application of the agent, and that the amount is smaller in scenarios in which the flame is extinguished quickly by liberal application of agent.

As illustrated by this example, it is apparent that, when the mechanism of inhibition involves the chemical intervention of the agent in the flame reactions, uniquely characteristic molecules should appear in the post-combustion gases. To explore the relative ease and merits of experiments designed to characterize the post-combustion gases, a preliminary set of experiments was conducted with a set of phosphorous-nitrogen (PN) compounds available through another USAF contract. It was decided to introduce the compounds into the Sapphire burner and to examine the composition of the post-combustion gases by passing these gases through the optical path of an FTIR spectrophotometer. This arrangement had two significant advantages: (1) relatively small amounts of extinguishing compound could be studied with the Sapphire burner, and (2) the Sapphire burner system allowed careful control of experimental

variables and permitted measurement of the amount of each product compound as a function of the amount of agent introduced into the flame.

As detailed below, a third very important benefit from these experiments was significant new information concerning the interaction of these PN compounds with flames.

2. Experimental

The Sapphire 0-7 burner was used for these experiments. The technique for introducing the PN compounds was adopted directly from experiments with tris(hexafluoro-acetylacetonato)iron(III) ($Fe(hfac)_3$) (Figure 3). In this configuration, the premixed fuel and oxidizer swept past the orifice of a quartz effusion cell containing the PN compound, and the rate of injection of the PN compound into the premixed gas stream was determined by the temperature to which the effusion cell was heated.

The optical path of the FTIR spectrophotometer was positioned to monitor the combustion gases continuously. The optical axis of the spectrophotometer was 8 in (20 cm) above the burner; direct access to the gases was provided by two openings in the 3.0 in (7.6-cm) diameter borosilicate glass envelope, which surrounded the flame zone and protected it from disturbance by external air currents. A coaxial sheath of N_2 gas surrounded the flame to minimize recirculation in the flame zone and to carry the combustion gases uniformly up the borosilicate glass envelope. Since the openings were very near the top of the borosilicate glass envelope, no difficulties were encountered that might have been ascribed to "chimney effects" (and potentially could have led to variability of path length through the combustion gases). Moreover, it was observed that no hot gases escaped through the windowless openings.

This experimental arrangement proved to be quite satisfactory. A background spectrum was obtained with the flame lighted; subsequently, it was subtracted from the spectra obtained with varying amounts of agent added to the premixed gases. Starting with an uninhibited flame, spectra were recorded as increasingly larger amounts of agent were added to the flame, and, after the flame was extinguished, one more spectrum was recorded as a direct measure of the amount of agent required to extinguish the flame.

Three compounds, provided by the USAF Advanced Streaming Agent Program, were examined: hexafluorocyclotriphosphazene (HFCTP), hexakis(2,2,2-triflouro-ethoxy) cyclotriphosphazene (TFECTP), and hexakis(2,2,3,3,3-pentafluoropropoxy) cyclotriphosphazene (PFPCTP).

3. Hexafluorocyclotriphosphazene

Hexafluorocyclotriphosphazene (HFCTP), while not a candidate extinguishing agent, was by far the easiest to study because of its relatively high vapor pressure. HFCTP provided a valuable starting point for comparison with the other two compounds. Figure 30 was obtained near the extinguishing limit. Figure 31 was obtained after the flame was extinguished; in this spectrum, the agent was still flowing, but the methane was turned off. The product gases were readily identified in Figure 30: HF (two sets of sharp lines, the R and P branches, on either side of 3961 cm^{-1}) and PF_5 (two broad absorptions, the R and P branches, on either side of 995 cm^{-1}). No nitrogen-containing compounds were found, and it was presumed that any nitrogen compounds (other than N_2) were present in such small concentrations that they could not be seen readily.

The four principal bands attributable to HFCTP are shown at 1303, 976, 864, and 466 cm^{-1} (Figure 31). It is important to note that no unreacted HFCTP was seen in Figure 30, suggesting that this compound was completely destroyed by the flame.

All of the other features seen in Figures 30 and 31 were attributable to H_2O and CO_2. These features were observed to be *below* the baseline in Figure 31, due to the fact that the flame had been extinguished when this spectrum was recorded.

4. Hexakis(2,2,2-triflouroethoxy)cyclotriphosphazene

Figures 32, 33, 34, through 35 are representative spectra for an experiment with hexakis(2,2,2-triflouroethoxy)cyclo-triphosphazene (TFECTP). As in the case of HFCTP, the two readily identifiable products were HF and PF_5 (Figure 32).

When more TFECTP was added, the flame began to liftoff and dance around the burner surface, and Figure 33 was obtained. Two features are worthy of note. First, neither the

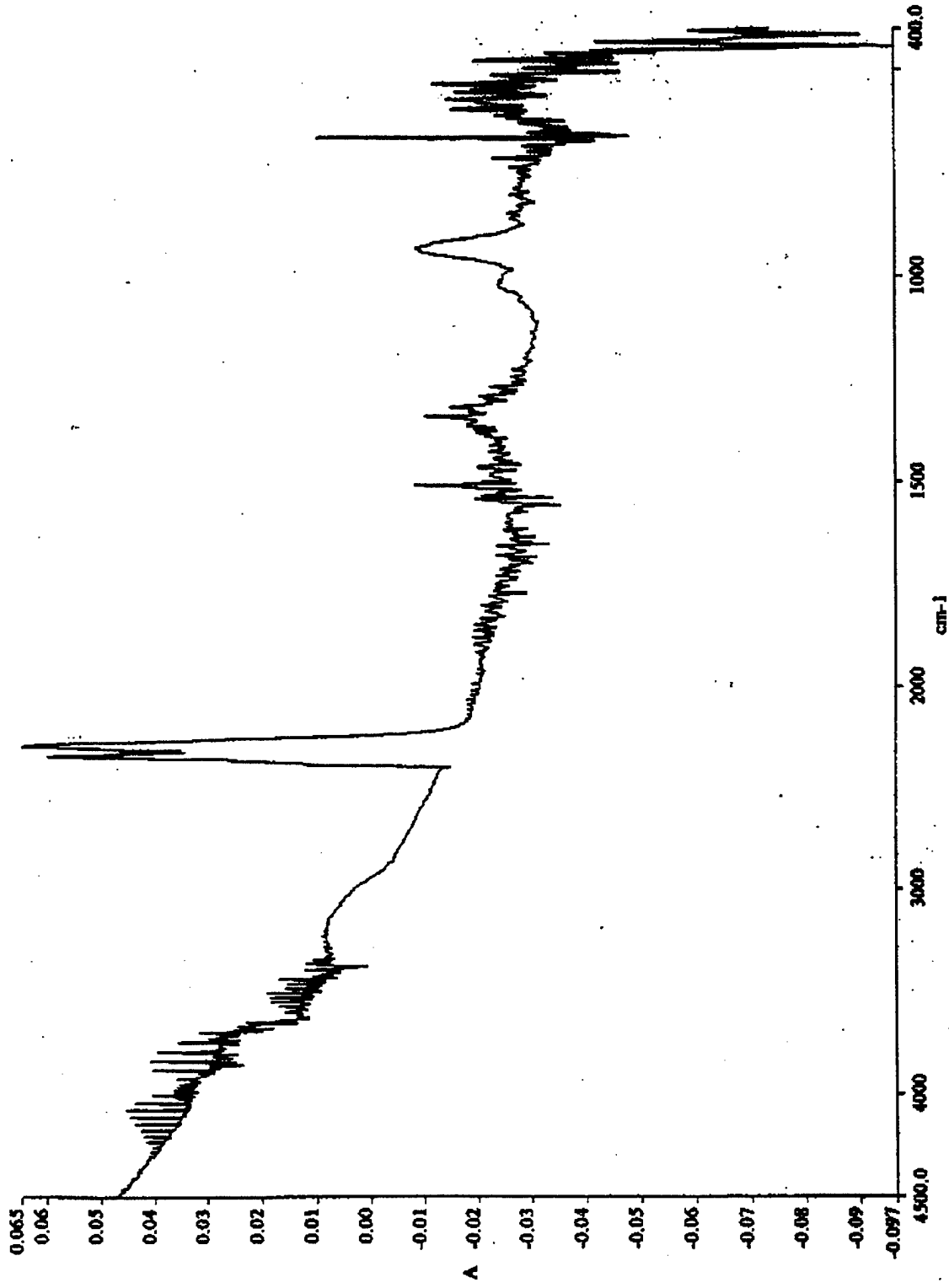

Figure 30. IR Spectrum of HFCTP: With Flame Lifted Off the Burner.

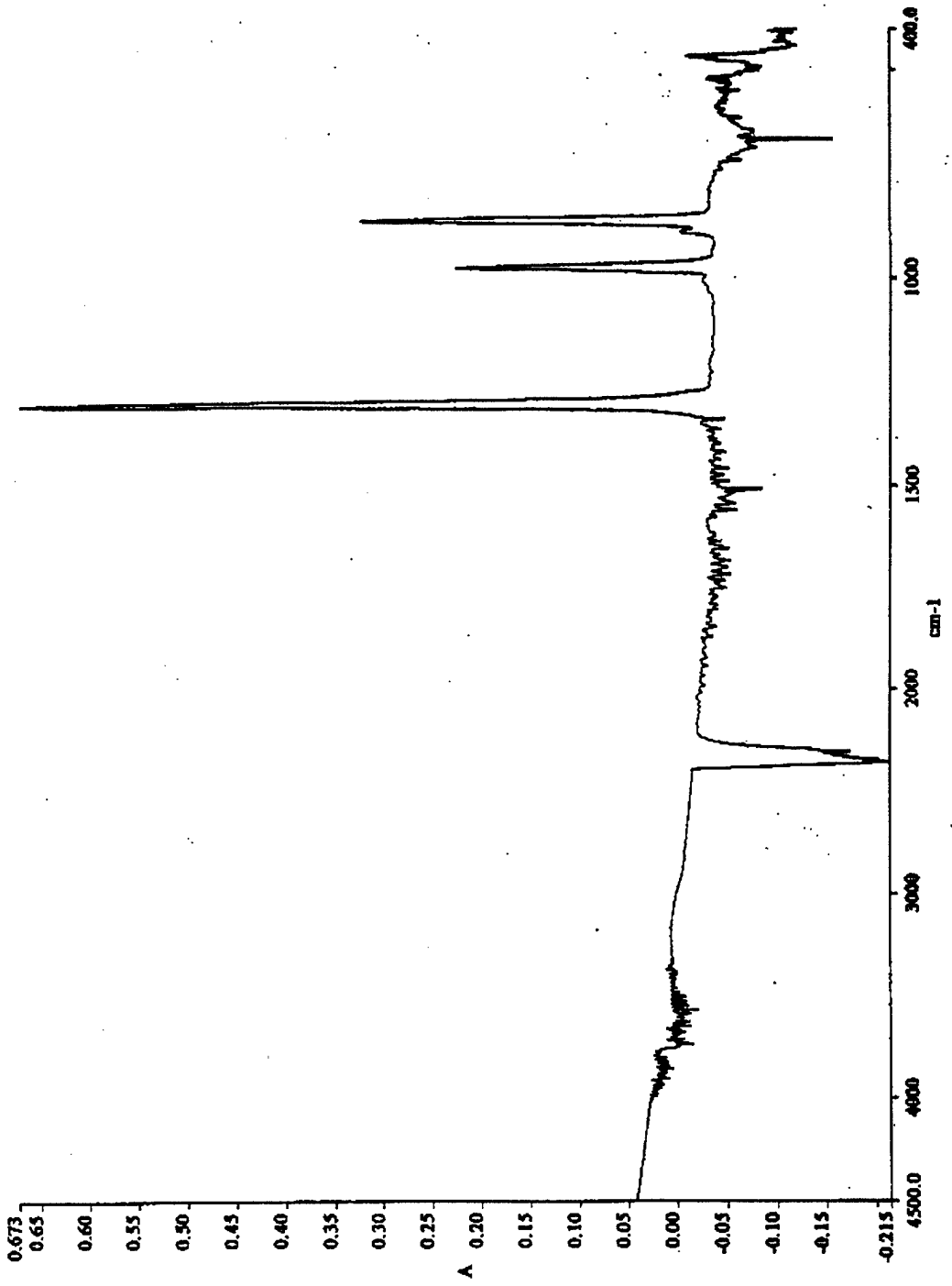

Figure 31. IR Spectrum of HFCTP: With Flame Extinguished and Methane Off.

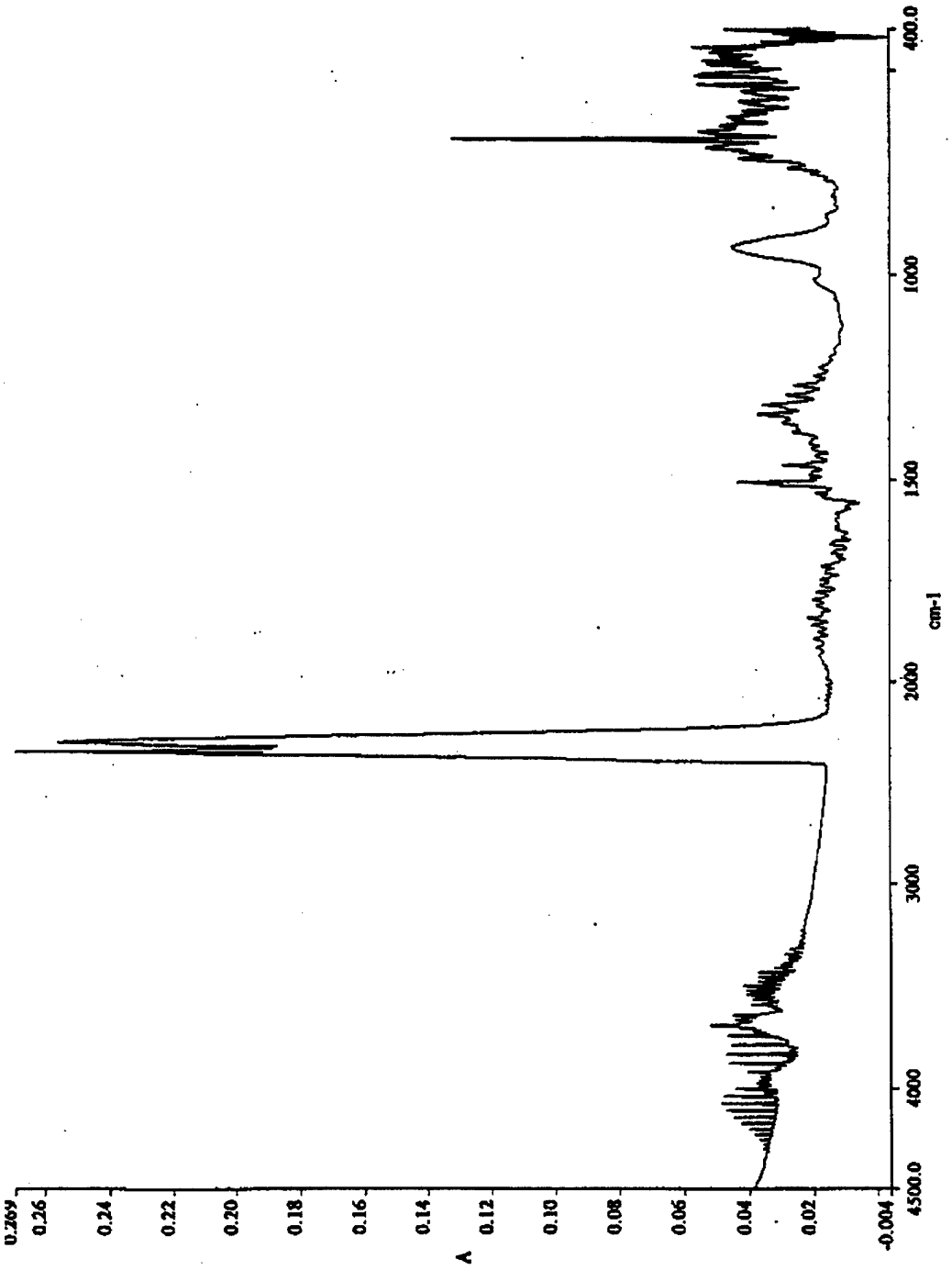

Figure 32. IR Spectrum of TFCTP: With Intense Orange Flame.

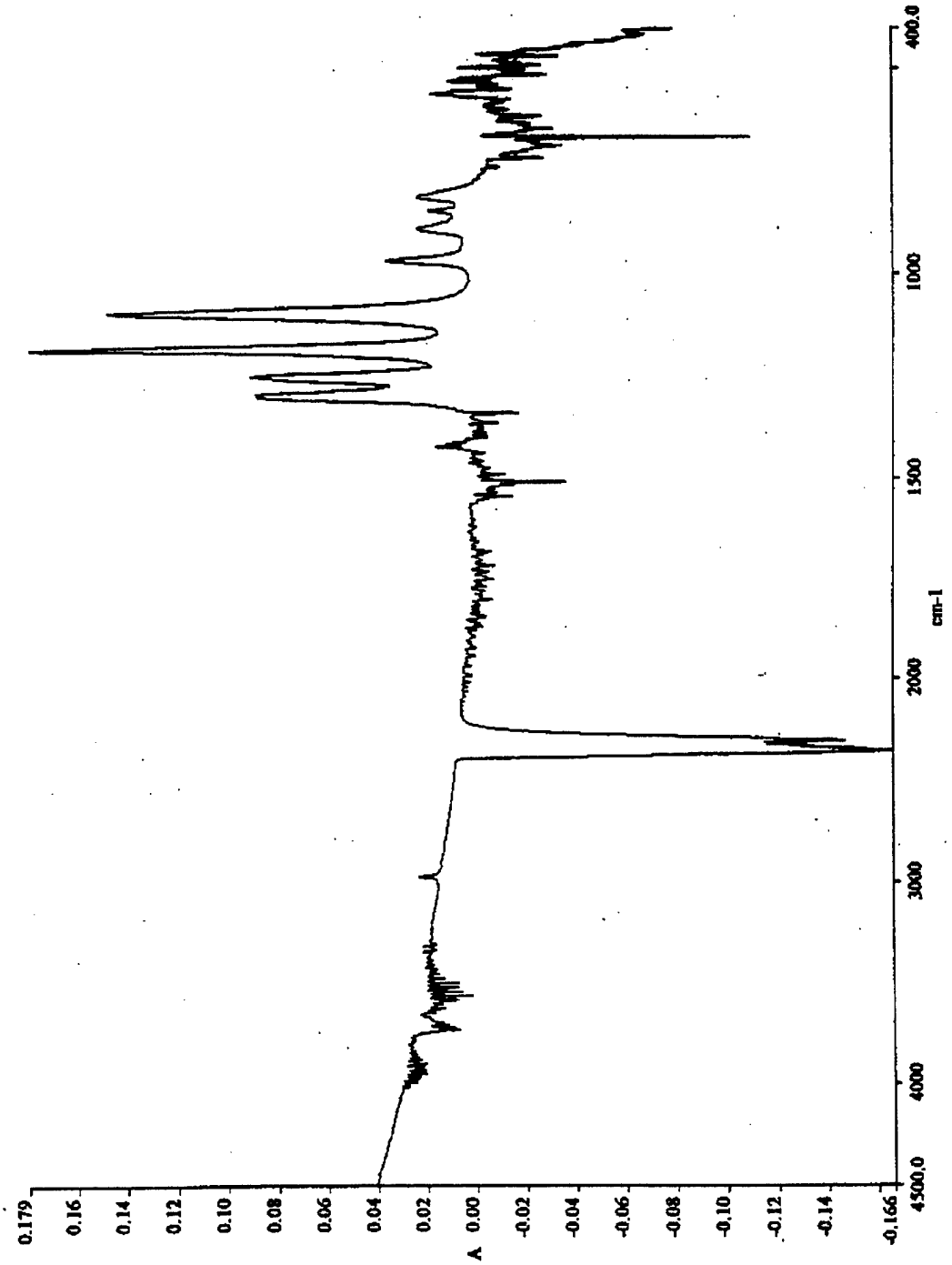

Figure 33. IR Spectrum of TFCTP: With Flame Dancing and Curling Up on Edges.

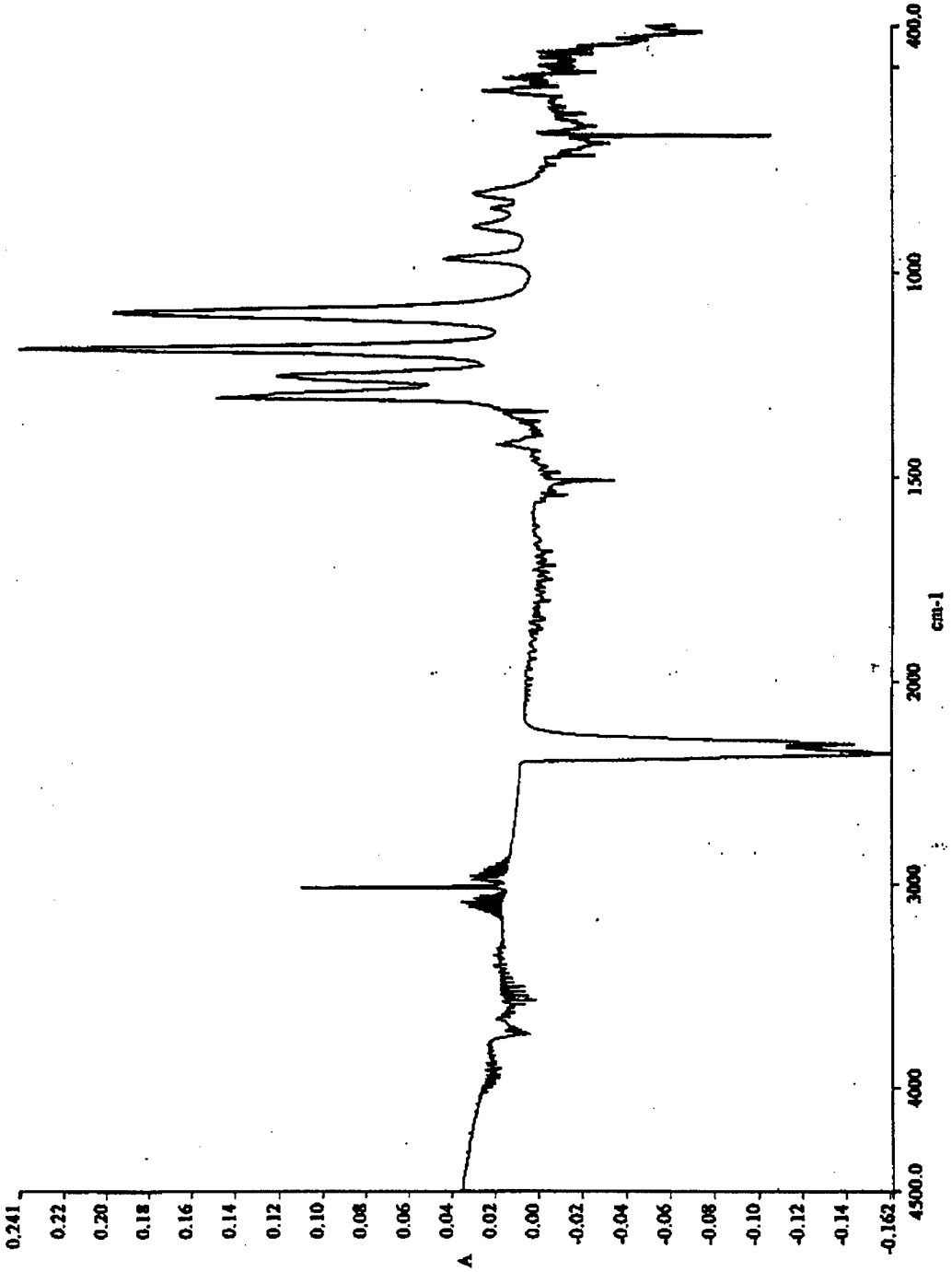

Figure 34. IR Spectrum of TFCTP: With Flame Above Burner.

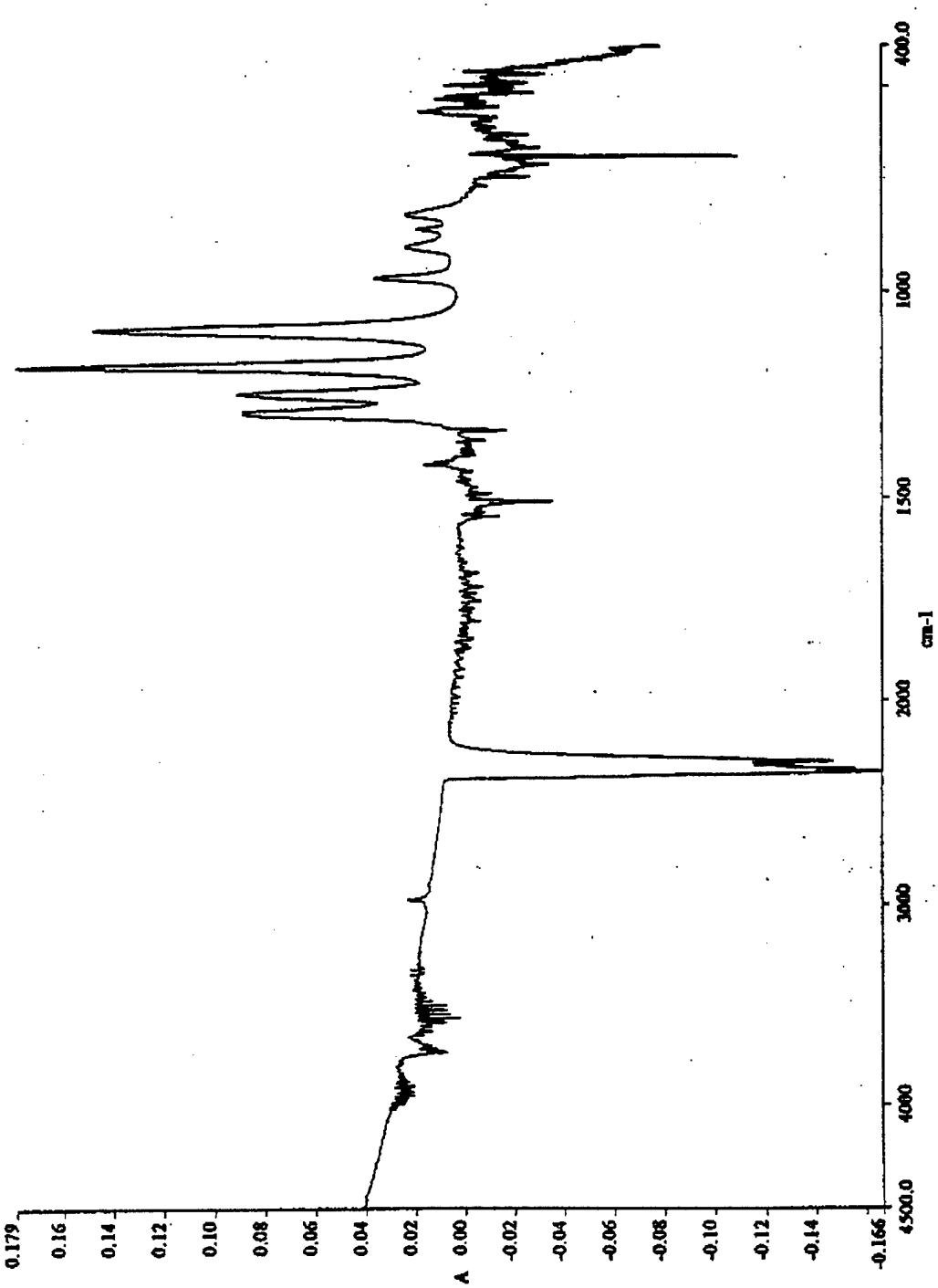

Figure 35. IR Spectrum of TFCTP: With Flame Extinguished and Methane Off.

HF nor the PF_5 was observable. Second, unreacted TFECTP was evident; note the exact correspondence of the observed bands between 750 cm^{-1} and 1500 cm^{-1} with those in Figure 35. The preliminary assessment of this behavior suggests that, under these conditions, the TFECTP was acting strictly as a physical agent and had cooled the flame sufficiently to cause liftoff and prevent burning of the TFECTP.

When even more TFECTP was added, the flame lifted off, but continued to burn several millimeters above the burner (Figure 34). The new feature in Figure 34 was the set of bands with a Q branch at 3017 cm^{-1}; this feature was assigned to unburned methane and indicated (most likely) that some of the methane had escaped combustion due to the "nearly-extinguished" state of the flame.

Following extinguishment, Figure 35 was obtained, which illustrates the spectrum of pure TFECTP in the gas phase. Since the methane was routinely turned off at extinguishment, the spectrum of this molecule is absent in Figure 35.

5. Hexakis(2,2,3,3,3-pentafluoropropoxy)cyclophosphazene

The behavior of hexakis(2,2,3,3,3-pentafluoropropoxy)cyclophosphazene (PFPCTP) is illustrated by Figures 36, 37, and 38. As with the two compounds discussed above, the initial products were HF and PF_5 (Figure 36).

However, as more PFPCTP was added, the spectrum became considerably more complex, indicative of additional chemistry, as seen in Figure 37, which was obtained when the flame was very close to extinguishment. In addition to HF and PF_5, carbonyl fluoride (F_2CO, with bands near 1959, 1929, and 1239 cm^{-1}, and a contribution to the 949 cm^{-1} band) and PN (in the vicinity of 1355 cm^{-1}) were also observed. Note, however, that pure PFPCTP was not observed at this point.

Figure 38, obtained following extinguishment, illustrated the spectrum of gas phase PFPCTP. Again, the methane had been shut off at extinguishment.

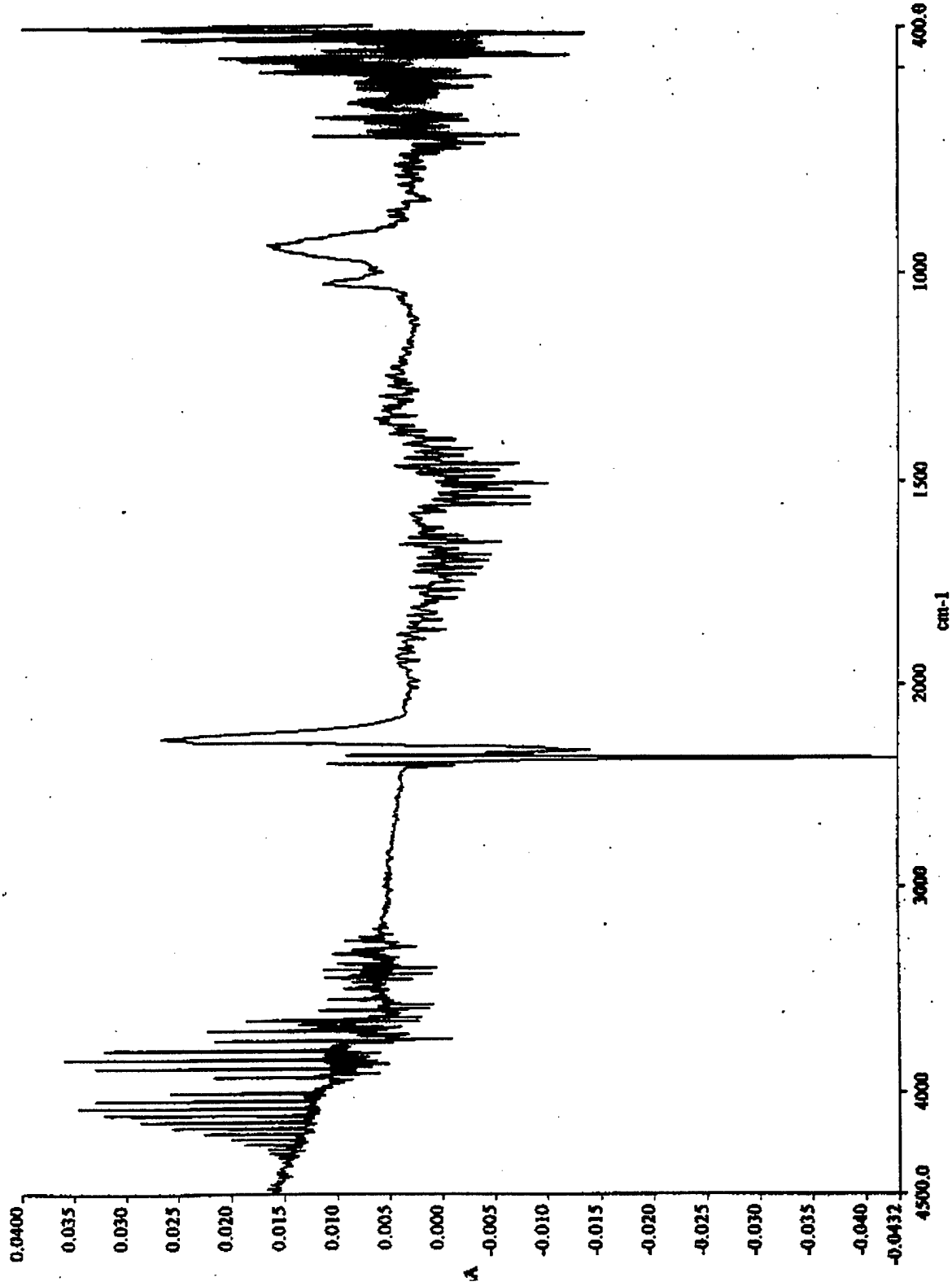

Figure 36. IR Spectrum of PFPCTP: With Flame Just Beginning to Liftoff.

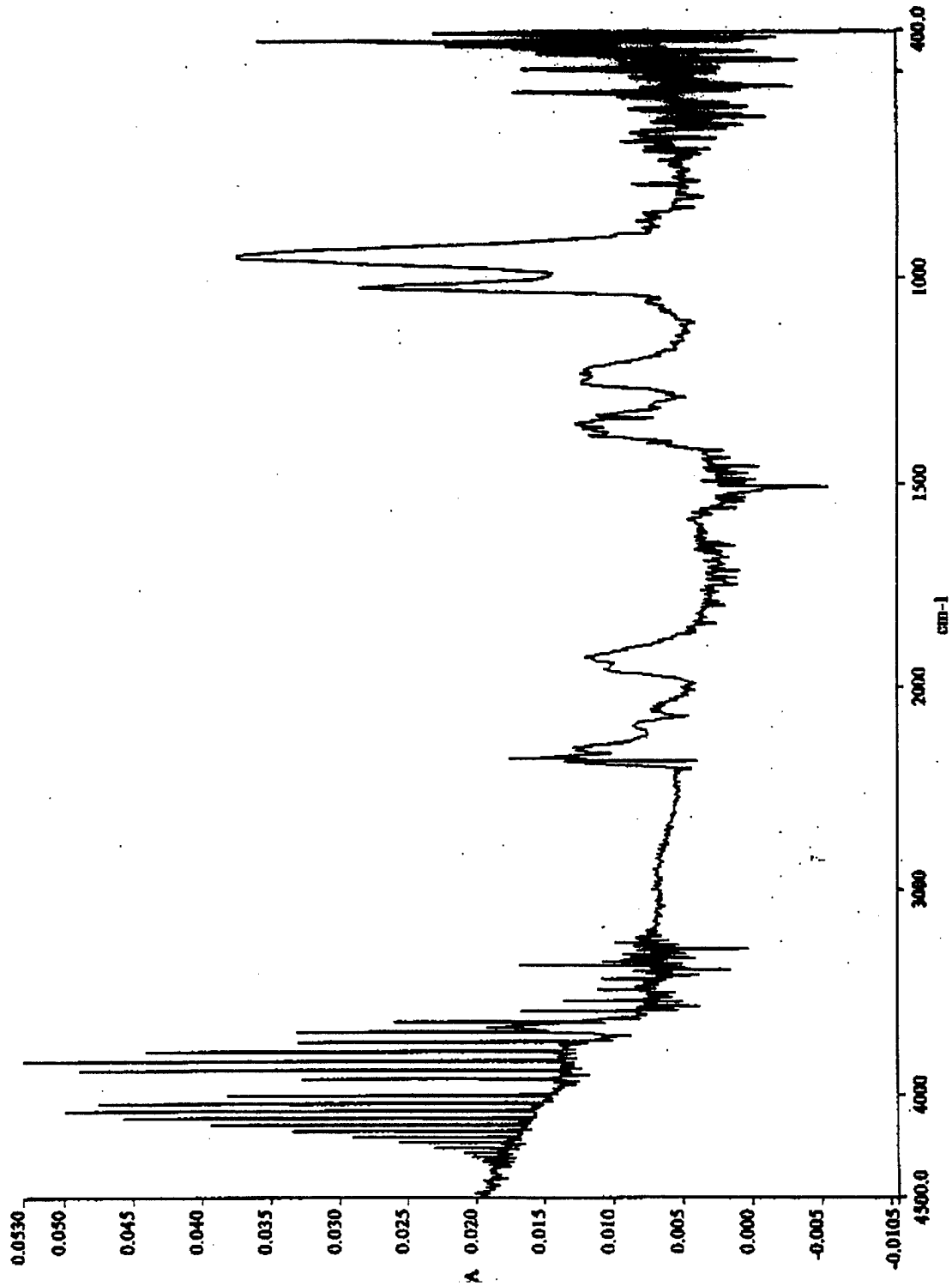

Figure 37. IR Spectrum of PFPCTP: With Flame Very Close to Extinguishment.

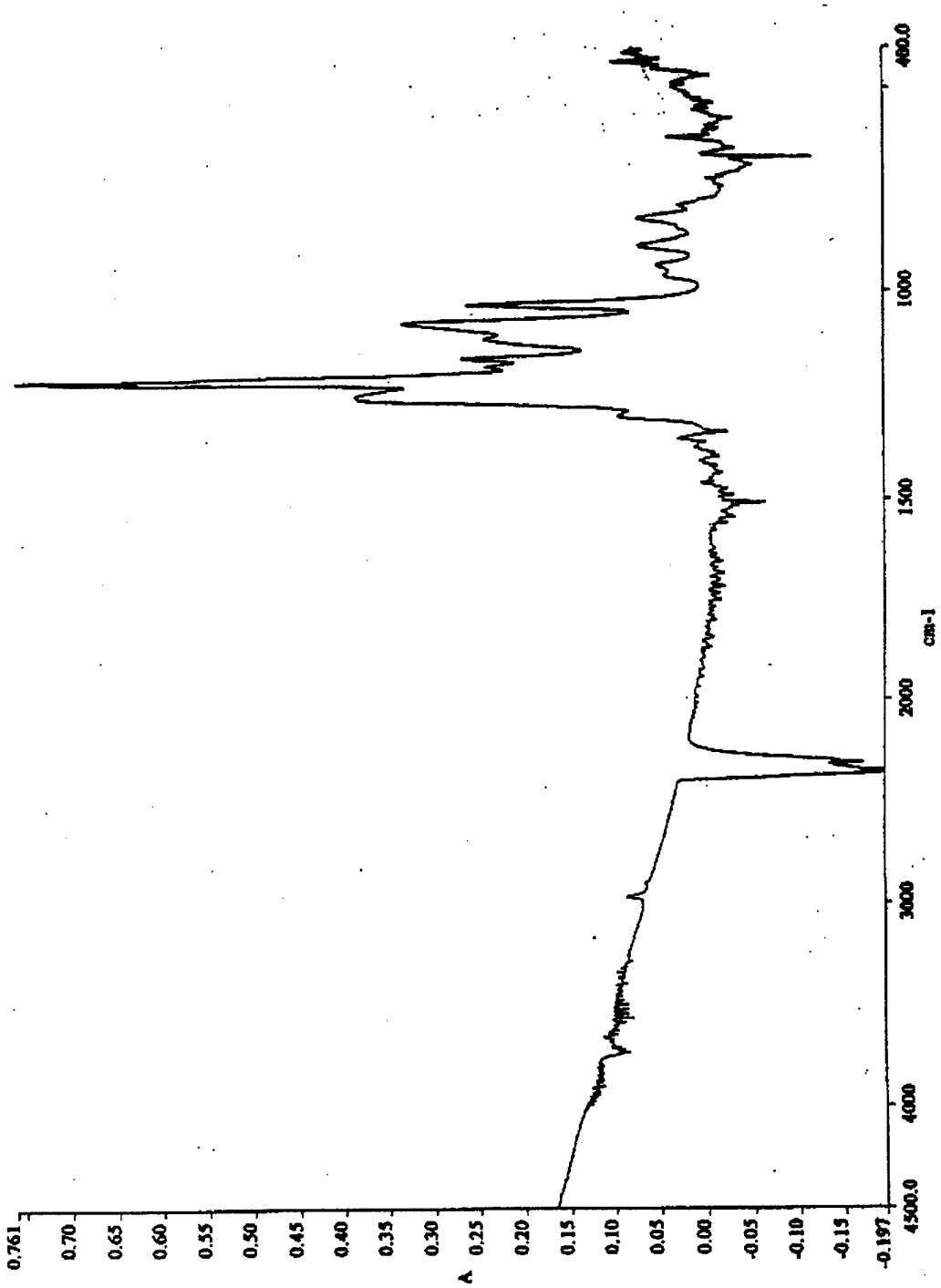

Figure 38. IR Spectrum of PFPFCTP: With Flame Extinguished and Methane Off.

6. Assessment

While the data presented here do not represent an exhaustive exploration of the three compounds tested, several useful results are already apparent.

(a) The appearance of TFECTP in the product gases while the flame was still burning was a surprise, and most probably indicated a change in the dominant extinguishment mechanism during the course of adding additional agent. Further experiments are warranted to quantify the relationship between the degree of extinguishment and the composition of the post-combustion gases.

(b) The appearance of unreacted TFECTP in the product gases of strongly inhibited flames is entirely consistent with the observation that the yield of HF in flames inhibited by Halon 1301 decreases as the amount of Halon 1301 is increased. The implication is clear: A chemical mechanism (involving chemical intervention of the inhibitor with the flame radicals, and perhaps catalytic) dominates when only small amounts of agent are used; however, the thermal mechanism becomes increasingly preeminent as the concentration of agent in the flame is increased.

(c) Although pure agent was not observed while the flame was still burning in the HFCTP or PFPCTP experiments, a more careful examination of these systems is needed. In particular, it is important to discover whether TFECTP is unique with respect to the apparent change in extinguishment mechanism.

(d) While HF was observed in experiments with all three compounds, it is important to quantitatively estimate the yield of HF as a function of the degree of extinguishment. The current experimental configuration appears to be nearly ideal for this purpose. Similar experiments with Halon 1301, $CBrF_3$, would provide a direct comparison and enable an initial evaluation of the relative adverse impact of HF in combustion gases in a typical fire scenario.

(e) At the same time that HF is being studied, the relative yields of the other potentially hazardous products (F_2CO, PN, and PF_5) should also be measured.

(f) The importance of post-combustion gas analysis cannot be over-emphasized. It is well known that, for some compounds such as $Fe(CO)_5$ and $Fe(hfac)_3$, the degree of extinguishment is not a linear function of the amount of compound added. Post-combustion gas analysis has the potential to shed light on this non-linear behavior. Moreover, post-combustion gas analysis may provide the information needed to explain why the amount of $Fe(CO)_5$ and similar chemical agents required for extinguishment is remarkably similar to the amount estimated on the basis of simple physical heat absorption mechanisms.

(g) Finally, it should be noted that post-combustion analysis has the potential to yield important information on delivery techniques including how much of the unreacted compound passes through the flame.

G. FUELS OTHER THAN METHANE

1. Experimental Details

Two other fuels, propane and isobutane, were briefly studied in the Sapphire 0-7 burner. Because of the very different heats of combustion of these fuels, very different operating points were expected. To minimize the uncertainties, a fixed oxygen flow rate was selected for all experiments, and the fuel flow was adjusted to obtain data on either side of $\phi = 1.00$. There was one interesting uncertainty: When the fuel flow is reduced while holding the N_2 and O_2 flows constant, the flame speed is also reduced, and hence the fraction of the energy extracted by the burner is increased. To compensate for this, it was decided to compensate (on a volume for volume basis) with nitrogen, thus keeping the total flow rate of cold gases constant.

2. Results

To a first approximation, the amount of heat extracted by the burner was found to be proportional to the available energy as determined from the literature value of the heat of combustion. The uncertainty was on the order of ±5 percent, and probably reflected the microscopic behavior of the flame. (Note that the H_2O/CO_2 ratio changes from fuel to fuel. Differences in the concentration of H atoms, carrying energy upstream, should also be expected.) One very important lesson was learned: It is critical to establish a baseline, using methane, for

each experiment. By so doing, one can "calibrate" the heat extracted by the burner against a fuel of known heat content and thus better predict the heat content of another fuel. This lesson arose from prior experience and was validated by the observation that two methane runs, apparently identical, on different days had markedly different values for heat extracted. It is, therefore, considered important to precede each test run with a calibration run without changing any other parameters.

3. Measurement of the Fuel Content of an Unknown

A gaseous "fuel" of unknown composition was added to the Sapphire 0-7 flame in the same manner as an ordinary extinguishing agent. From a trace of heat extracted by the burner as a function of the amount of "fuel" added, it was determined that the "fuel" neither promoted combustion nor inhibited combustion. Subsequent analysis of the "fuel" showed that, it was mostly CO_2, with a small amount of combustible hydrocarbons.

SECTION IV
ATMOSPHERIC PRESSURE FLAMES— INDIVIDUAL COMPOUNDS AND COMPARATIVE RESULTS

A. INTRODUCTION

Most of the atmospheric pressure experiments were conducted with air/methane flames (and hence with nitrogen, in the natural abundance found in air, as the diluent). The data for these experiments are presented in individual paragraphs below, with a separate paragraph dedicated to each compound. At this end of this section, some comparisons are made among the results of these experiments.

However, before considering these fuel-air experiments, results of an early set of experiments in which the diluent was argon are discussed. Argon was used as a diluent in these experiments, partly because considerable experience had already been gained with the methane-oxygen-argon system, and partly to establish a database for comparison with the low-pressure experiments, in which argon was used exclusively as the diluent.

The results of the atmospheric-pressure heat-extracted experiments for iron-containing compounds are presented separately in Section VII.

B. COMPARATIVE DATA FOR CH_4-O_2-Ar FLAMES

1. General Observations

Table 2 collects the data from a series of early experiments with argon as the diluent. Except as noted, these were fuel-rich flames with $\phi = 1.17$. The total flow rate was about 3720 cc/min, and the mole percents of the gases in the uninhibited flames at the start of the experiments were as follows: Ar — 75.9 percent, CH_4 — 8.9 percent, and O_2 — 15.2 percent. A nitrogen sheath was provided only for the experiments noted in the table.

TABLE 2. COMPARATIVE DATA FOR CH_4-O_2-Ar FLAMES.

Agent	Experiment	Mole fraction @ x-intercept	Slope, heat extracted curve, cal/cc	Notes. (S-0-x is the Sapphire burner number) ϕ = 1.17, except as noted
He	A091	0.44	- 0.15	S-0-4
Ar	A071[a]	0.37[b]	- 0.22	S-0-1
	A072	0.40[b]	- 0.21	S-0-1
N_2	A085	0.33	- 0.28	S-0-3
	A086	0.35	- 0.33	S-0-4
	A089	0.32	- 0.26	S-0-4
	A090	0.33	- 0.24	S-0-4
	A091A	0.32	- 0.25	S-0-4
	A093	0.31	- 0.32	S-0-4
	A094	0.32	- 0.28	S-0-4
	A121A	0.30	- 0.19	S-0-5, ϕ = 0.94
	A121B	0.28[c]	- 0.24	S-0-5, ϕ = 1.32
	A127	0.32	- 0.26	S-0-4
	A146	0.30	- 0.25	S-0-4; N_2 sheath; ϕ = 1.12
	A155	0.36	- 0.27	S-0-4; N_2 sheath; ϕ = 0.97
CO_2	A115	0.20	- 0.27	S-0-5
CF_4	A118	0.14	- 0.50	S-0-5; ϕ = 1.12
C_4F_{10}	A129	0.054	- 2.33	S-0-5
$C_3H_2F_6$	A130[a]	0.037[c]	- 3.83	S-0-4; ϕ = 1.15
	A132	0.042[c]	- 2.65	S-0-4; ϕ = 1.15
CH_3Cl	A136	0.096[c]	- 1.12	S-0-4; ϕ = 1.01
	A138	0.059[c]	- 1.76	S-0-4; ϕ = 1.39
	A139	0.039	- 2.24	S-0-4; N_2 sheath; ϕ = 1.39
	CH3CL_D	0.047	- 1.82	S-0-4; N_2 sheath; ϕ = 1.13
	CH3CL_E	0.073	- 1.62	S-0-4; N_2 sheath; ϕ = 1.02
	CH3CL_F	0.039	- 1.98	S-0-4; N_2 sheath; ϕ = 1.18
	CH3CL_G	0.055	- 1.76	S-0-4; N_2 sheath; ϕ = 1.10
	CH3CL_H	0.081	- 1.63	S-0-4; N_2 sheath; ϕ = 0.97
	CH3CL_J	0.029	- 2.00	S-0-4; N_2 sheath; ϕ = 1.25
	CH3CL_K	0.030	- 0.75	S-0-4; N_2 sheath; ϕ = 1.34
$CHClF_2$	CHCLF2_A	0.070	- 1.26	S-0-4; N_2 sheath; liquid
	CHCLF2_B	0.068	- 1.27	S-0-4; N_2 sheath; liquid
	CHCLF2_C	0.077	- 0.98	S-0-4; N_2 sheath; gas
CH_3Br	A133		- 5.3[d]	S-0-4
$CBrF_3$	A080[a]		- 8.7[d]	S-0-3
	A081[a]		- 8.7[d]	S-0-3
	A082		- 9.9[d]	S-0-3
CF_3I	A123		- 7.5[d]	S-0-5

[a]Flameout not observed.
[b]Argon *added* to the amount already present in the basic flame.
[c]Linear Heat Extracted curve with "tail" having a less negative slope.
[d] Initial slope (cal/cc)

There were no surprises. The salient features are briefly summarized below.

The last three compounds listed in Table 2 (CH_3Br, $CBrF_3$ and CF_3I) displayed similar behaviors, typical of catalytic inhibiting agents; the Heat Extracted curves were exponential with a steep initial slope. The feature in common was, of course, the heavy halogen atom. The overwhelming weight of evidence supports the conclusion that both the Br atom and the I atom engage in catalytic recombination of H atoms in flames. With the exception of the CH_3Br experiment, flameout was not observed. The objective of these experiments was to take a careful look at the initial part of the Heat Extracted curves; the experiments were stopped before flameout was achieved.

The first six compounds listed in Table 2 (He, Ar, N_2, CO_2, CF_4, and C_4F_{10}) were characterized (with one exception) by linear Heat Extracted curves, typical of thermal agents. The one exception was the N_2 experiment with a richer flame ($\phi = 1.32$); this curve had a "tail" with a less negative slope. As expected for thermal agents, the effectiveness was directly proportional to the heat capacity.

The three remaining agents ($C_3H_2F_6$, CH_3Cl, and $CHClF_2$) displayed "fuel-character"; after an initial straight-line segment, the Heat Extracted curve had a "tail." This feature, characteristic of all agents with "fuel character," was not present in experiments in which the flame was provided with a nitrogen sheath; this is discussed in Section III.B.

2. Comparative Data for CH_3Cl

Comparative data for CH_3Cl as a function of the fuel/oxygen equivalence ratio, ϕ, are included in Table 2, and are displayed graphically in Figure 39. In this series of experiments, both the argon and methane flow rates were held constant, and ϕ was changed by varying the flow rate of O_2. A nitrogen sheath was used in all cases. The "fuel character" of CH_3Cl was especially evident for the two experiments near $\phi = 1.0$. In the nearly stoichiometric flames, the CH_3Cl contributed to the heat released in the flame and to the heat extracted by the burner, which accounted for the fact that extinguishment did not appear to begin until after substantial amounts of CH_3Cl had already been introduced.

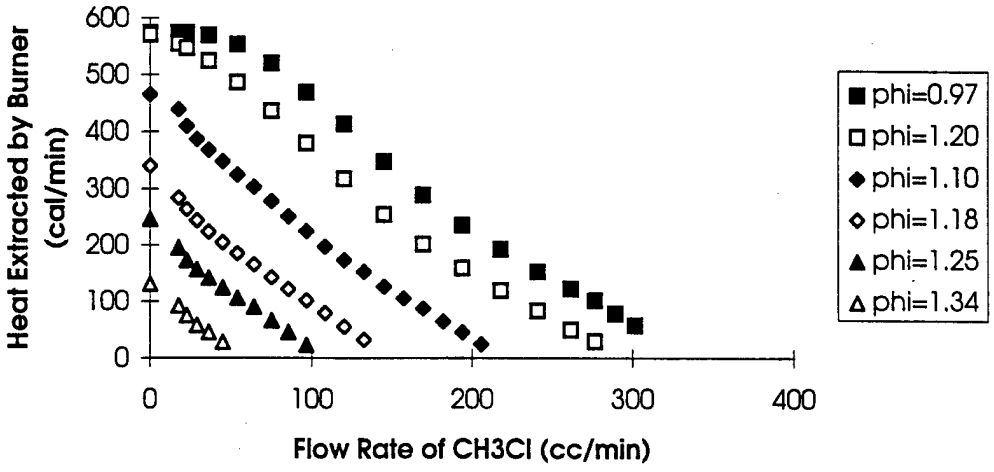

Figure 39. Inhibition of Six Different CH_4-O_2-Ar Flames by CH_3Cl.

The slopes of the six curves displayed in Figure 39, while similar, became slightly more negative as ϕ increased. One phenomenon remains unexplained: Each Heat Extracted curve seemed to have two straight-line segments with different slopes. This was particularly evident for the curves for experiments with ϕ = 0.97, 1.02, 1.10, and 1.18. If the second part of each of these curves was some sort of "tail," it would have been interesting to redo these experiments with a higher flow rate of the N_2 sheath gas.

C. DIRECT INJECTION OF HCFC-22 AS AN AEROSOL

1. Experimental Procedures

Buried in Table 2 are the data for three experiments with HCFC-22 ($HCClF_2$) in which a comparison was made between the introduction of the agent as a room-temperature gas and as an aerosol. In the two aerosol experiments, liquid $HCClF_2$ was drawn from a pressurized cylinder and expanded through a throttling valve located at a "T" in the premixed gas stream, immediately below the burner. It was known from separate experiments that an aerosol was generated by this configuration. Whether any of the aerosol survived the transit into the flame was unknown. Even if the aerosol completely vaporized before it reached the flame, the vaporization had some cooling effect on the premixed gases.

2. Results

The results of the three experiments are displayed in Figure 40. The two aerosol experiments were, at best, difficult. Especially at higher flow rates of $HCClF_2$, the throttling valve tended to freeze up and give an unsteady rate of introduction of the agent. For this reason, more weight was given to the low flow rate data points. With this caveat, it was found that the slopes of the Heat Extracted curves for the aerosol experiments were more negative than the slope for the room-temperature gas-phase experiment.

3. Assessment

The slope of the Heat Extracted curve for the gas phase experiment was 1.00 cal/cc $HCClF_2$, while the slopes of the Heat Extracted curves for the early data points of the aerosol experiments were about 1.26 cal/cc. It was easy to rationalize this difference in terms of the additional cooling due to vaporization of the aerosol. However, these results must be considered, at best, preliminary and indicative, and by no means conclusive.

Partly in response to these findings, some effort was devoted to development of an alternate method for introducing agents such as $HCClF_2$, which could be delivered as an aerosol. The pulsed valve work, described in Section II, was an outgrowth of this effort.

D. NITROGEN

1. Summary

A typical Heat Extracted experiment with nitrogen as the extinguishing agent is illustrated by Figure 41 and the set of experiments reported here is summarized in Table 3. For these experiments, the "air" for the flames was made by premixing O_2 and N_2 in a 0.208:0.792 ratio, and additional nitrogen was added to inhibit the flame.

Flameout was observed in each case; flameout typically occurred slightly before the point predicted by the extrapolation of the straight line to the x-axis. All of the Heat Extracted curves were similar to that displayed in Figure 41; the lines were straight, as expected for a thermal agent.

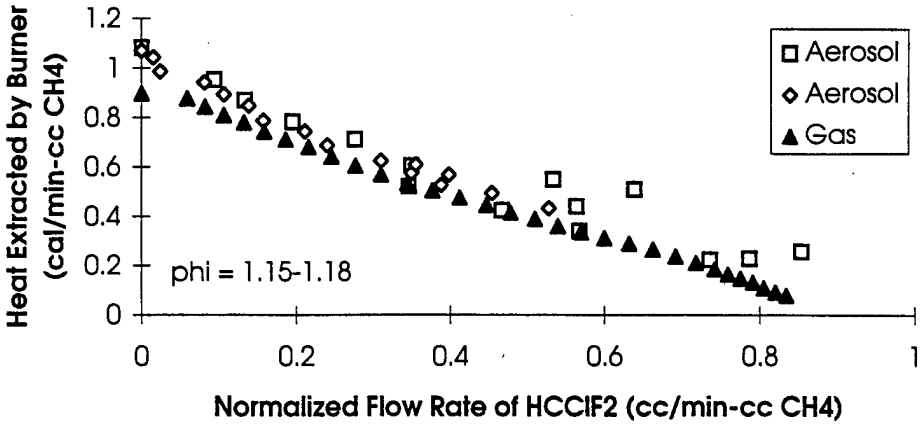

Figure 40. Inhibition of CH_4-O_2-Ar Flames by $HCClF_2$ as an Aerosol and in the Gas Phase.

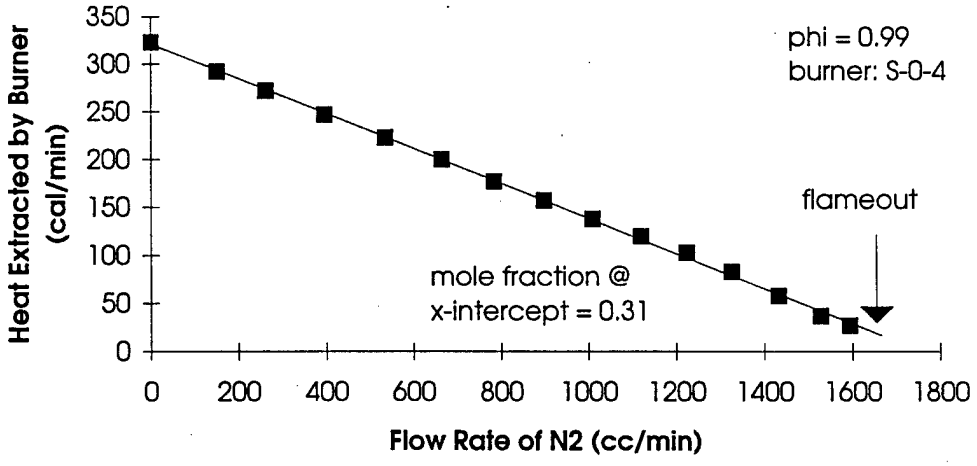

Figure 41. Inhibition of a Stoichiometric CH_4-O_2-N_2 Flame by N_2.

TABLE 3. HEAT EXTRACTED EXPERIMENTS WITH NITROGEN.

Experiment	ϕ	Mole fraction @ extinguishment	
		x-Axis intercept	@ Flameout
N21183	0.73	0.16	0.13
N2_A	0.78	0.21	0.20
N21182	0.83	0.25	0.22
N2_B	0.91	0.28	0.27
N2_I	0.99	0.31	0.30
N2_H	1.05	0.30	0.29
N2_C	1.06	0.31	0.30
N2_G	1.09	0.29	0.29
N2_F	1.20	0.24	0.23
N2_E	1.24	0.21	0.20
N2_D	1.27	0.18	0.16

Figure 42 summarizes the extinguishment data as a function of the fuel/oxygen equivalence ratio (ϕ). Figure 42, repeated from Section III, was discussed in detail in that section. Note that the stoichiometric ($\phi = 1.0$) flame was the most difficult to extinguish, and that the curve was essentially symmetric about $\phi = 1.0$.

2. Assessment

Nitrogen behaved, as expected, as a thermal agent. Two features of the experimental data were consistent with this conclusion: (1) the linearity of the Heat Extracted curves, and (2) the symmetry about $\phi = 1.0$ of the data presented in Figure 42.

E. TETRAFLUOROMETHANE

1. Summary

Two types of experiments were performed with tetrafluoromethane (CF_4). The heat extracted by the burner was measured both as a function of the flow rate of CF_4 added and as a function of the fuel/oxygen equivalence ratio. In both types of experiments, the "air" was made by premixing O_2 and N_2 in a 0.208:0.792 ratio.

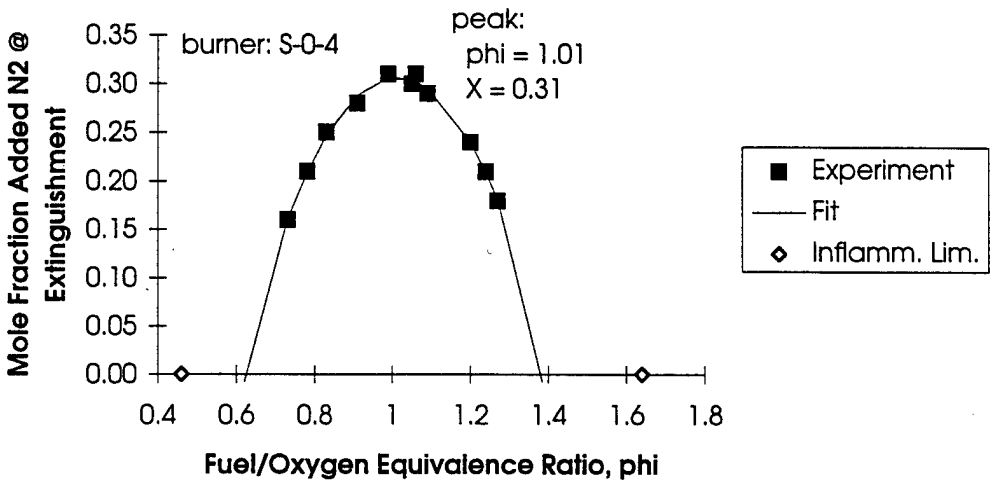

Figure 42. Influence of Fuel/Oxygen Equivalence Ratio on Mole Fraction of N_2 Required to Extinguish CH_4-Air Flames.

2. Heat Extraction *vs.* Flow Rate of CF_4 Experiments

A typical experiment is illustrated by Figure 43; the experiments are summarized in Table 4. Straight lines were observed in all experiments, as in the case of the nitrogen experiments. Flameout typically occurred slightly before the point predicted by the extrapolation of the straight line to the x-axis; as the flow rate of CF_4 approached the value required for extinguishment, small instabilities in the flame frequently resulted in flameout somewhat in advance of the value at the intersection of the straight line with the x-axis.

Figure 44 summarizes the extinguishment data as a function of the fuel/oxygen equivalence ratio (ϕ). Each experiment is represented by two points on the graph—a solid square and an empty square. The solid square represents the mole fraction of CF_4 at the observed flameout; the empty square represents the x-axis intercept of the straight line through the data points. The line in this figure was obtained by fitting the data for the intercepts to an equation of the form $y = a + bx + cx^2$. Note that, as in the case of N_2 as an extinguishing agent, the stoichiometric ($\phi = 1.0$) flame was the most difficult to extinguish, and that the curve was essentially symmetric about $\phi = 1.0$.

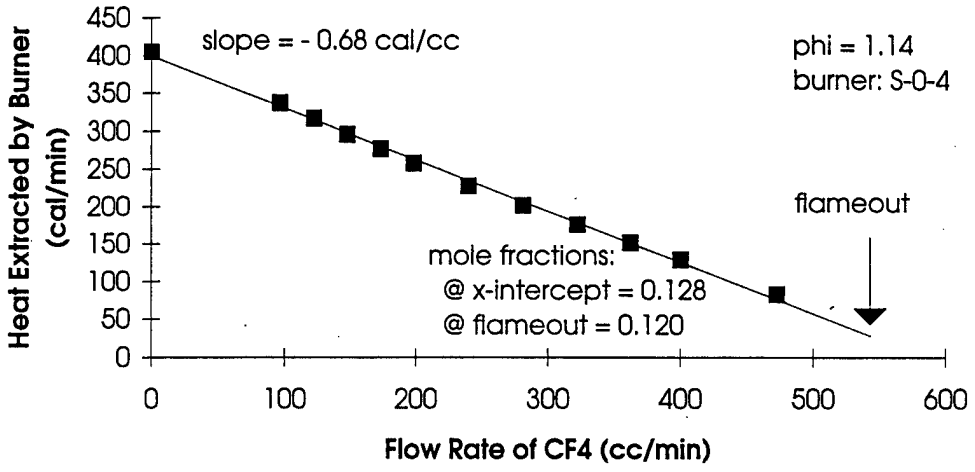

Figure 43. Inhibition of a Fuel-Rich CH_4-Air Flame by CF_4.

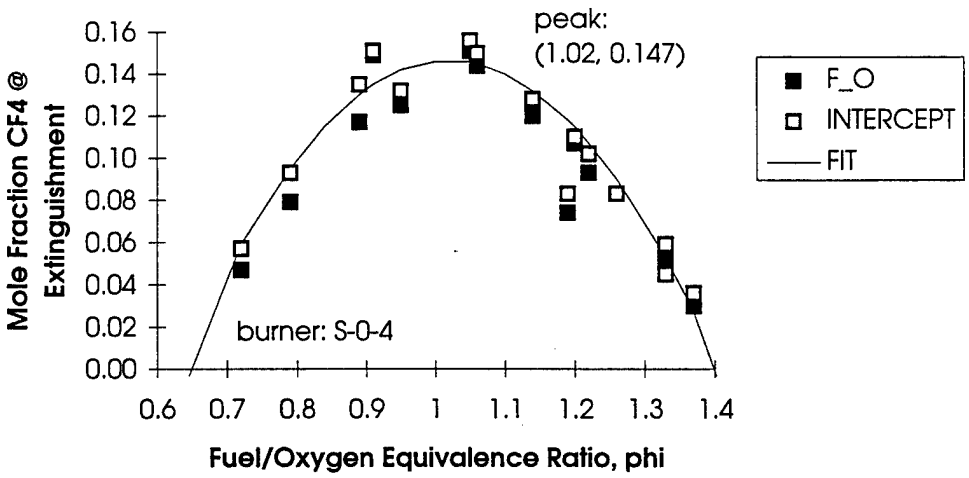

Figure 44. Inhibition of a CH_4-Air Flame by CF_4 as a Function of Fuel/Oxygen Equivalence Ratio.

TABLE 4. HEAT EXTRACTED *vs.* FLOW RATE OF CF_4.

Experiment	ϕ	Mole Fraction @ extinguishment	
		x-Axis intercept	@ Flameout
CF4_R	0.72	0.057	0.047
CF4_U	0.79	0.093	0.079
CF4_P	0.89	0.135	0.117
CF4_C	0.91	0.151	0.149
CF4_T	0.95	0.132	0.125
CF4_A	1.05	0.156	0.151
CF4_O	1.06	0.150	0.144
CF4_V	1.14	0.128	0.120
CF4_G	1.19	0.083	0.074
CF4_B	1.20	0.110	0.107
CF4_S	1.22	0.102	0.093
CF4_E	1.26	0.083	no f/o
CF4_W	1.33	0.059	0.052
CF4_D	1.33	0.045	no f/o
CF4_F	1.37	0.036	0.030

3. Heat Extracted *vs.* Fuel/Oxygen Equivalence Ratio Experiments

Figures 45 and 46 illustrate the results of a typical experiment, and Table 5 summarizes the extinguishment data as a function of the fuel/oxygen equivalence ratio (ϕ) for the complete set of experiments. Figures 45 and 46, repeated from Section III, were discussed in detail in that section. Figures 47 and 48 show data for six of the seven experiments listed in Table 5. While the Difference curves displayed in Figure 47 were very nearly horizontal, the differences were distinctly smaller for fuel-rich flames than for fuel-lean flames. By contrast, the corresponding Difference curves for $CBrF_3$ were characterized by a positive slope as a function of fuel/oxygen equivalence ratio; these data are presented in Section IV.K. The FEE curves (Figure 48) had the expected concave up shapes, with minima at $\phi = 1.0$.

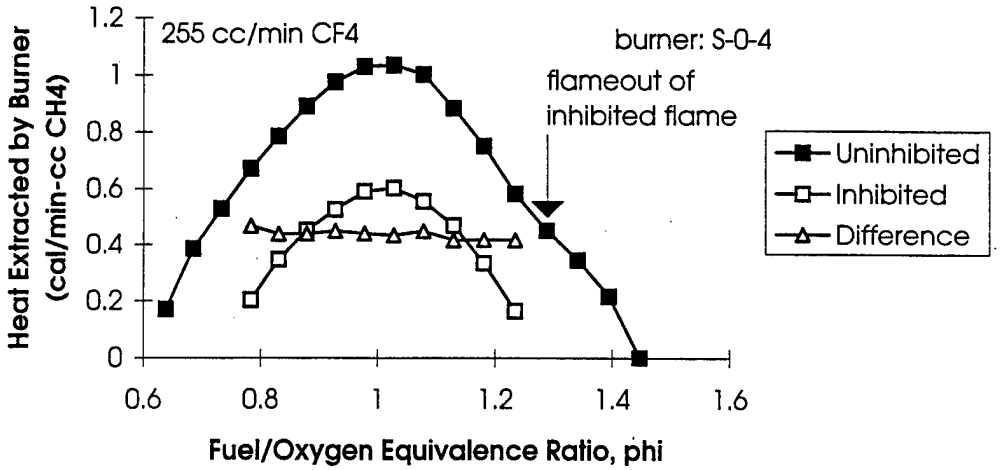

Figure 45. Inhibition of a CH_4-Air Flame by CF_4: Heat Extracted by Burner.

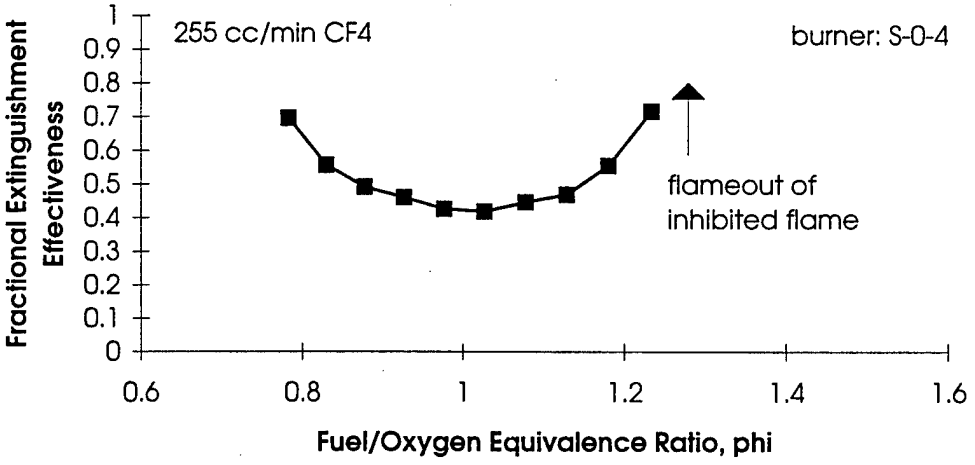

Figure 46. Inhibition of a CH_4-Air Flame by CF_4: Fractional Extinguishment Effectiveness.

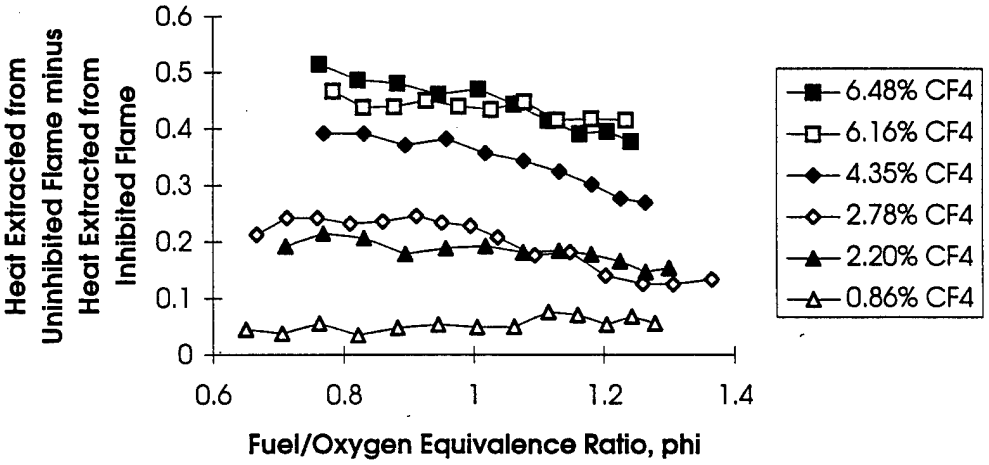

Figure 47. Effect of Various Amounts of CF_4 on the Heat Extracted.

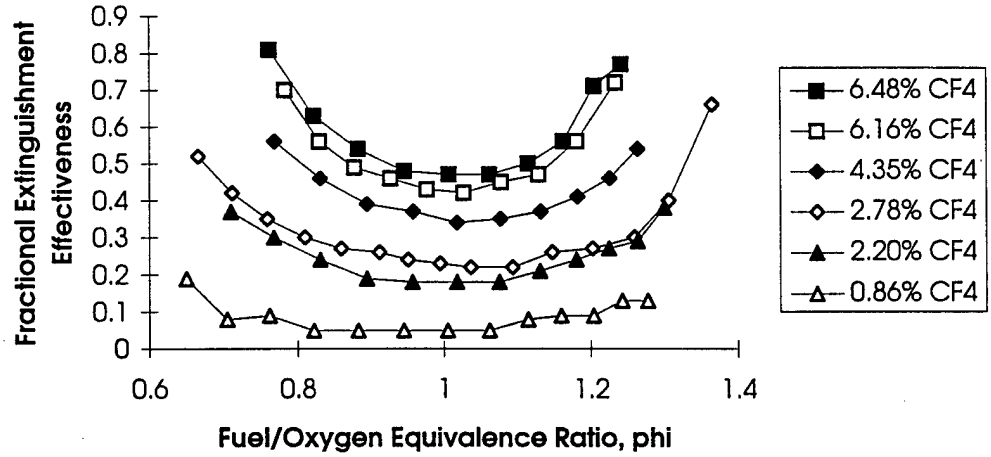

Figure 48. Effect of Various Amounts of CF_4 on the Fractional Extinguishment Effectiveness.

TABLE 5. CF_4 HEAT EXTRACTED *vs.* FUEL/OXIDIZER EQUIVALENCE RATIO EXPERIMENTS.

Experiment	CF_4 Flow Rate (cc/min)	X_{CF4} @ $\phi = 1.00$	FEE @ $\phi = 1.00$
CF4_H	35	0.0086	FEE = 0.040
CF4_I	88	0.022	0.174
CF4_J	178	0.0435	0.341
CF4_K	273	0.0648	0.449
CF4_L	112	0.0228	0.203
CF4_M	255	0.0616	0.411
CF4_N	280	0.0661	0.508

In Figure 49, the FEE data at $\phi = 1.0$ for the seven experiments are presented as a function of the mole fraction of CF_4. It is important to note that (1) the curve was linear, (2) the line passed through the origin (within experimental uncertainty), and (3) the extrapolated value of the mole fraction at extinction, $X = 0.14 \pm 0.01$, was in good agreement with the data obtained with the Heat Extracted *vs.* Flow Rate of CF_4 experiments, the data for which are summarized in Figure 44.

4. Assessment

The data for CF_4 were similar in every respect to those for N_2. Given that N_2 is known to be a thermal (only) agent, there is then strong support for the same conclusion regarding CF_4. A certain amount of caution is warranted, however. While a thermal agent has been shown to yield a linear Heat Extracted *vs.* Flow Rate curve, the reverse may not necessarily be true. The most that can be said, when it is observed that the Heat Extracted *vs.* Flow Rate curve is linear, is that the processes (including thermal heat absorption) were linear functions of the amount of agent added.

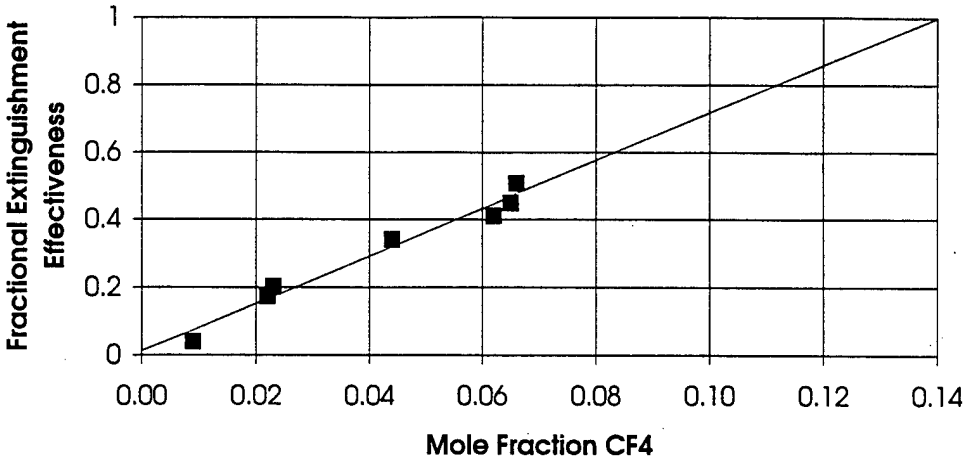

Figure 49. Fractional Extinguishment Effectiveness as a Function of Mole Fraction of CF_4.

F. HFC-23, TRIFLUOROMETHANE

1. Summary

To facilitate a comparison between tetrafluoromethane (CF_4) and trifluoromethane (CHF_3) the same types of experiments were performed with both compounds. As in the CHF_4 experiments, the "air" for the CHF_3 experiments was made by premixing separately metered streams of O_2 and N_2 in a 0.208:0.792 ratio. As closely as possible, all experiments were performed with constant flow rates of O_2 and N_2; changes in ϕ were achieved by changing the flow rate of the methane stream. The results for CHF_3 were quite different from the results for CF_4; the differences are pointed out in this paragraph and are discussed further in the following paragraph.

2. Heat Extracted *vs.* Flow Rate of CHF_3 Experiments

Six representative sets of data are presented in Figure 50; the complete set of experiments is summarized in Table 6. While it was observed that, for flames with $\phi > 1.0$, the Heat Extracted curves were quite straight, fuel-lean flames were characterized by Heat Extracted curves with "knees." The curves were best described as consisting of two segments with

distinctly different slopes. For the fuel-lean experiments, the initial slopes (at small flow rates of CHF_3) of the Heat Extracted curves were quite dependent on the stoichiometry of the flame and were much less negative than the final slopes. For the first five experiments listed in Table 6, only the first segment was observed; in each case, it intercepted the x-axis at a quite large value of the mole fraction.

To gain additional insight into the chemistry underlying the Heat Extracted experiments, the data in Figure 50 were recast by normalizing both the Heat Extracted and the Flow Rate of CHF_3 by the flow rate of CH_4 (Figure 51). Two features were noted. First, it was observed that the "knees" in the curves for the fuel-lean flames were all found at the same flow rate of CHF_3, which was suggestive of a change in the dominant process as the composition passed through a 1:1 ratio of CHF_3 to CH_4. Second, the $\phi = 0.76$ flame required the largest flow of CHF_3 for extinguishment and was the most challenging flame for this agent.

A similar conclusion was reached when the mole fraction at extinguishment was plotted as a function of the fuel/oxygen equivalence ratio (Figure 52). In Figure 52, both the actual mole fraction at flameout and the predicted value of the mole fraction at extinguishment (based on the extrapolation of the Heat Extracted curve to the x-axis) were plotted. The curved line in the Figure 52 was obtained by a non-linear fit to the observed values of mole fraction at flameout; the mole fraction of CHF_3 required to extinguish the flame at the peak ($\phi = 0.89$) was $X = 0.10$. While this statistical treatment of the data yields a reasonable value for the mole fraction required to extinguish a flame, visual inspection of the data in Figure 52 suggests that an equally reasonable estimate of the mole fraction at extinguishment would be $X = 0.12$ (at a value of ϕ of about 0.7).

3. Heat Extracted *vs.* Fuel/Oxygen Equivalence Ratio Experiments

A typical experiment is illustrated by Figures 53 and 54. Table 7 collects the data for the entire set of experiments, and Figure 55 presents the FEE results for this set. The results of these experiments, with the minima in the FEE curves near $\phi = 0.75$, were entirely consistent with the results of the Heat Extracted *vs.* Flow Rate of CHF_3 experiments, described above.

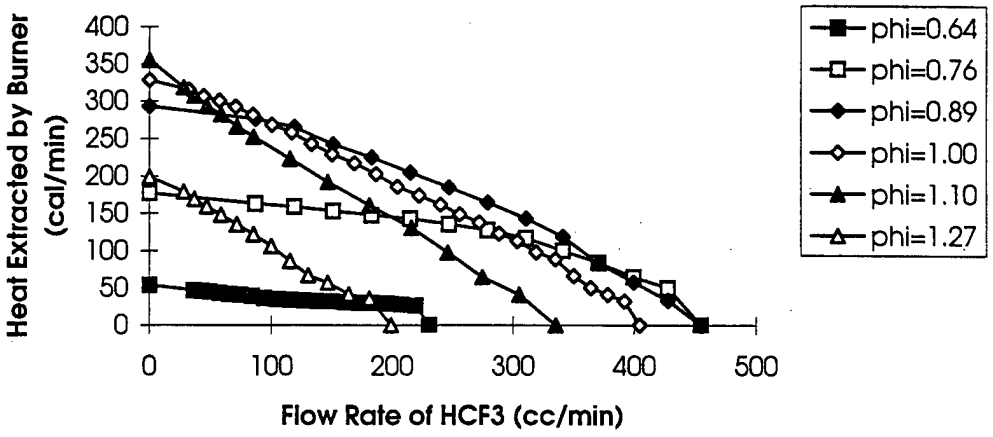

Figure 50. Inhibition of Six Different CH_4-Air Flames by CHF_3.

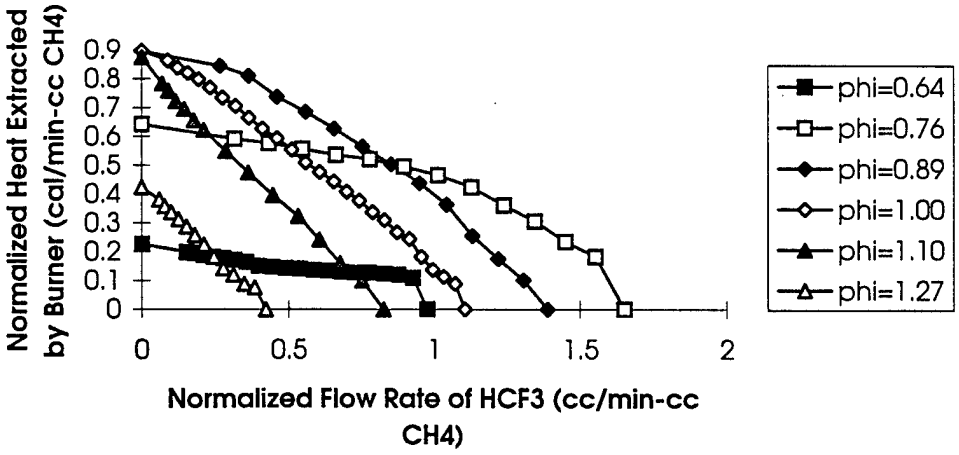

Figure 51. Inhibition of Six Different CH_4-Air Flames by CHF_3: Normalized Data.

TABLE 6. HEAT EXTRACTED *vs.* FLOW RATE OF CHF_3 EXPERIMENTS.

Experiment	ϕ	Mole fraction @ extinguishment	
		x-Axis intercept	@ Flameout
CHF3_AD	0.64	[a]	0.059
CHF3_O	0.65	[a]	no f/o
CHF3_P	0.66	[a]	0.052
CHF3_AE	0.66	[a]	0.092
CHF3_S	0.68	[a]	0.087
CHF3_V	0.70	0.127	0.106
CHF3_I	0.74	0.120	no f/o
CHF3_N	0.74	0.098	0.084
CHF3_T	0.76	0.118	0.105
CHF3_R	0.77	0.120	no f/o
CHF3_AG	0.77	0.120	0.112
CHF3_X	0.87	0.107	0.096
CHF3_H	0.89	0.107	0.099
CHF3_U	0.89	0.106	0.105
CHF3_AF	0.94	0.102	0.098
CHF3_E	0.98	0.105	0.096
CHF3_G	1.00	0.103	0.094
CHF3_F	1.01	0.107	0.098
CHF3_W	1.01	0.095	0.093
CHF3_J	1.10	0.081	0.078
CHF3_Y	1.10	0.080	0.079
CHF3_K	1.17	0.063	0.064
CHF3_AA	1.20	0.057	0.054
CHF3_L	1.25	0.046	0.044
CHF3_AB	1.27	0.048	0.047
CHF3_M	1.32	0.033	0.028
CHF3_AC	1.34	0.025	0.026

[a]Only the first segment, intercepting the x axis at a large value, was observed.

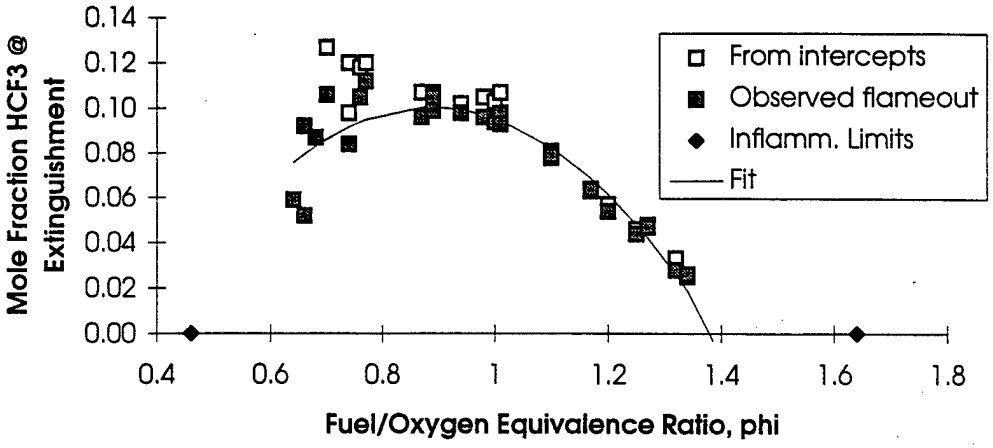

Figure 52. Influence of Fuel/Oxygen Equivalence Ratio on Mole Fraction of CHF_3 Required to Extinguish CH_4-Air Flames.

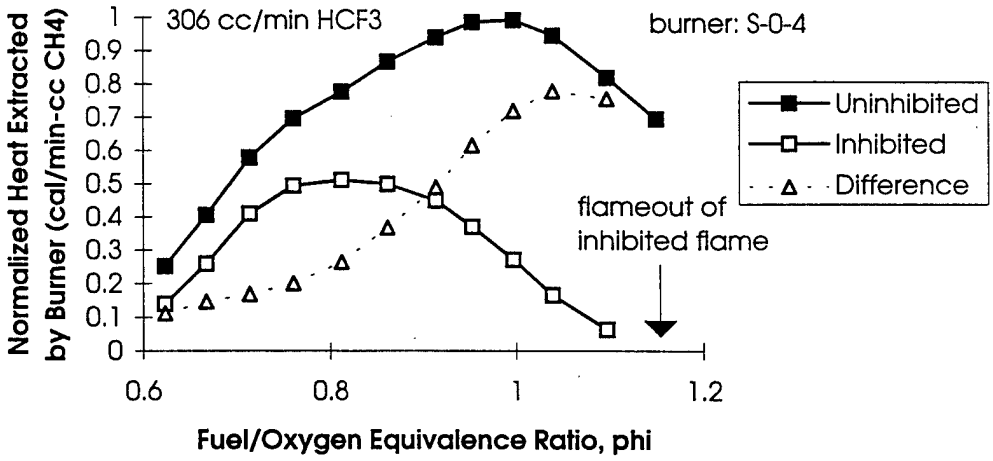

Figure 53. Inhibition of a CH_4-Air Flame by CHF_3: Heat Extracted.

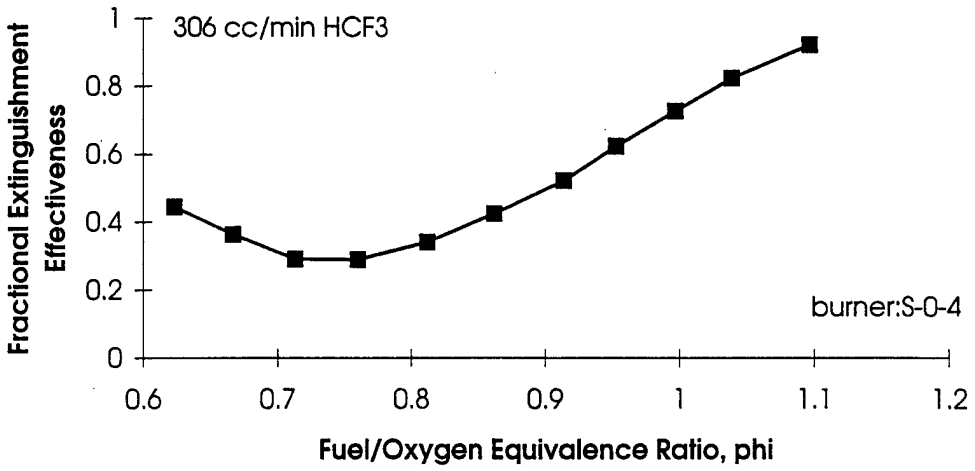

Figure 54. Inhibition of a CH_4-Air Flame by CHF_3: Fractional Extinguishment Effectiveness.

TABLE 7. CHF_3 HEAT EXTRACTED *vs.* FUEL/OXIDIZER EQUIVALENCE RATIO EXPERIMENTS.

Experiment	CHF_3 flow rate (cc/min)	X_{chf3} @ $\phi = 1.00$	FEE @ $\phi = 1.00$
CHF_3_AK	24	0.0061	0.05
CHF_3_AH	57	0.0143	0.05
CHF_3_AI	126	0.0310	0.19
CHF_3_AJ	202	0.0493	0.14
CHF_3_AL	265	0.0638	0.21
CHF_3_AM	306	0.0726	0.29

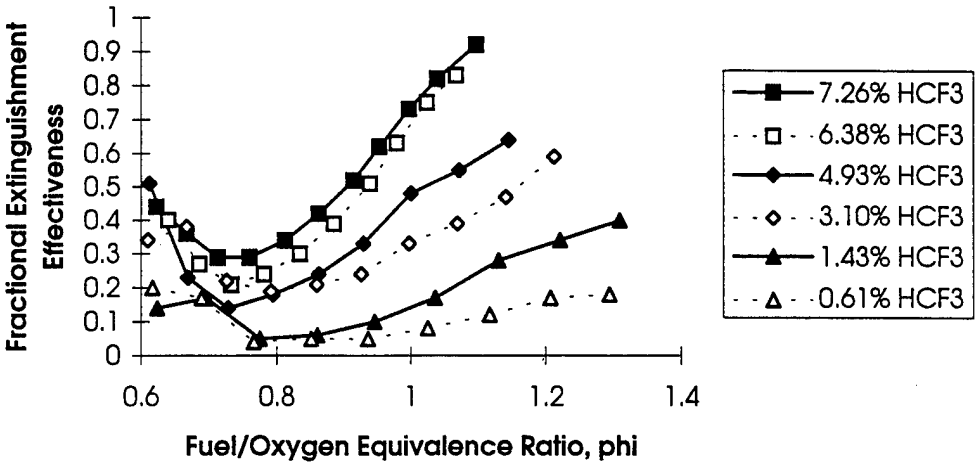

Figure 55. Fractional Extinguishment Effectiveness of CHF_3 as a Function Fuel/Oxygen Equivalence Ratio.

4. Assessment

This behavior of CHF_3 is readily attributed to the "fuel character" of this agent. It is noted, however, that, despite of the contribution of the combustion of CHF_3 to the total heat extracted by the burner, the Heat Extracted curves had negative slopes for all values of ϕ. Thus, the net effect of the CHF_3 was to serve as an extinguishing agent at all stoichiometries. There is one additional interesting observation. When the FEE data, obtained for the minima in the curves (near $\phi = 0.75$) were plotted as a function of mole fraction of CHF_3, Figure 56 was obtained. Extrapolation to a Fractional Extinguishment Effectiveness of 1.0 yielded a required mole fraction of 0.24 to 0.30. This value was 2 to 4 times the experimental value found for the mole fraction required to extinguish a $\phi = 0.75$ flame, which indicates that caution in interpreting FEE data, especially for fuel-lean flames, must be observed.

One additional question remains: Does the $\bullet CF_3$ radical play an important role in extinguishment? Thoughts on this topic are included in the next two paragraphs.

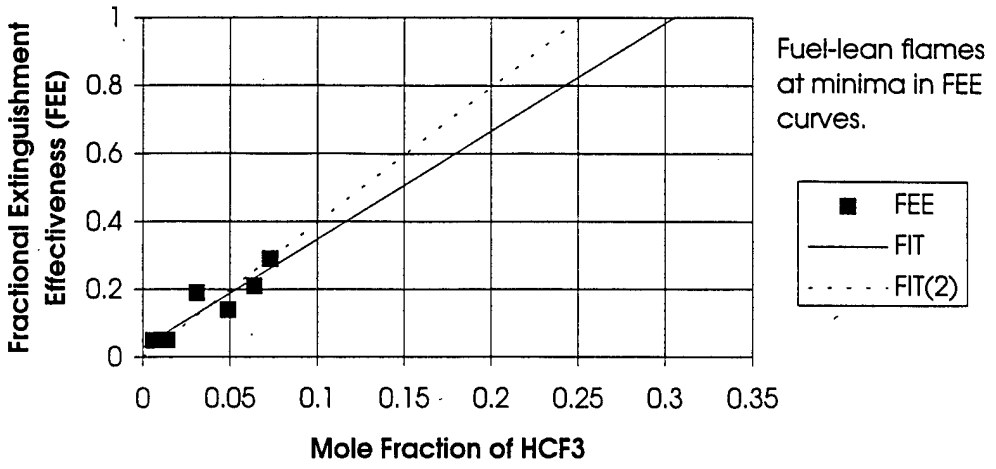

Figure 56. Fractional Extinguishment Effectiveness as a Function of Mole Fraction of CHF_3.

G. THE ROLE OF THE $\bullet CF_3$ RADICAL

1. Introduction

Among the reactions that can be written for the $\bullet CF_3$ radical are the following:

$$CHF_3 + \bullet H \rightarrow H_2 + \bullet CF_3 \quad (1)$$

$$\bullet CF_3 + \bullet H \rightarrow CHF_3 \quad (2)$$

$$CHF_3 + \bullet OH \rightarrow H_2O + \bullet CF_3 \quad (3)$$

Taken as a group, these three reactions suggest that the $\bullet CF_3$ radical might be involved in one or more catalytic cycles that remove flame propagating radicals from the flame. Reaction (1) is, of course, the primary elementary reaction by which CHF_3 is introduced into the chemistry of the flame and occurs readily in typical flames. By contrast with CHF_3, CF_4 is relatively unreactive in flames; the abstraction of an F atom does not occur easily. This then suggests that a comparison of the extinguishment effectiveness of CHF_3 with the extinguishment effectiveness of CF_4 should yield useful information as to the potential role of the $\bullet CF_3$ radical.

2. Experimental Results

The Heat Extracted *vs.* Fuel/Oxygen Equivalence Ratio experiments provided a useful vehicle for comparing these two extinguishing agents. Figure 57 compares the heat extracted by the burner from the uninhibited flame with the heat extracted by the burner from flames inhibited by equal amounts of CF_4 and CHF_3. Note that, while CHF_3 removed very little heat from lean flames, CF_4 extinguished these flames; conversely, fuel-rich flames were extinguished by CHF_3, but not by CF_4.

Figure 58 plots these data in a different fashion, and illustrate the regions in which each agent is more effective. In this figure, the energy absorbed by the burner from an uninhibited flame is once again displayed. Superimposed for each agent is a data set that shows the magnitude by which the agent reduced the amount of heat absorbed by the burner. It is evident from Figure 58 that CF_4 was nearly equally effective at all values of ϕ, while CHF_3 had very little effect on lean flames, but had a larger effect than CF_4 on rich flames.

3. Assessment

It is proposed that these differences can be explained simply in terms of the "fuel content" of CHF_3 as illustrated by the following overall stoichiometry.

$$2\ CHF_3 + 2\ H_2O + O_2 \rightarrow 6\ HF + 2\ CO_2 \qquad (4)$$

This reaction suggests that some of the oxygen was used in combustion of the CHF_3 and that the fuel/oxygen equivalence ratio (ϕ) for combustion of CH_4 should be altered to reflect the availability of less oxygen. When this was done, Figure 59 was obtained, and the heat extracted by the burner as a function of ϕ was seen to be nearly identical for both agents. This finding is consistent with a model in which the dominant mechanisms of the two agents are both thermal.

CHF_3 altered the chemistry of the flame by serving as a fuel and shifting the stoichiometry of the flame closer to the rich inflammability limit. The observation that rich flames were more easily extinguished by CHF_3 than by CF_4 directly followed from this fact.

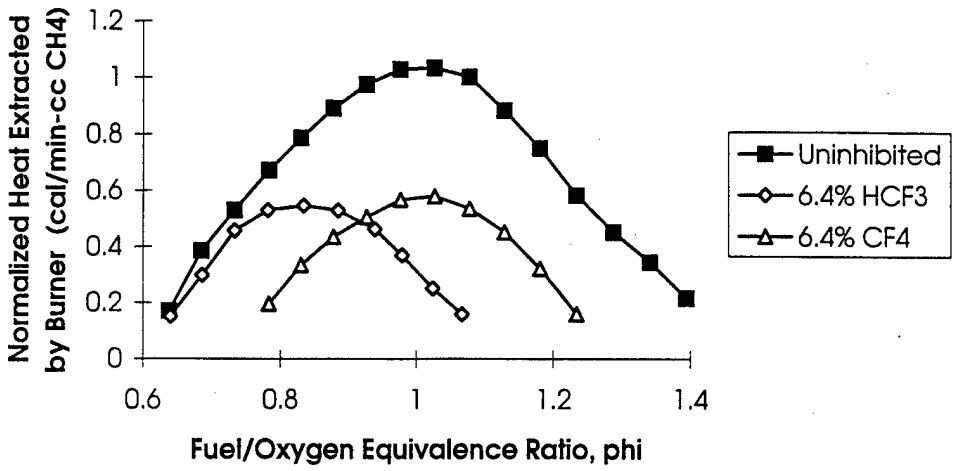

Figure 57. Comparison of CHF_3 and CF_4: Heat Extracted by Burner.

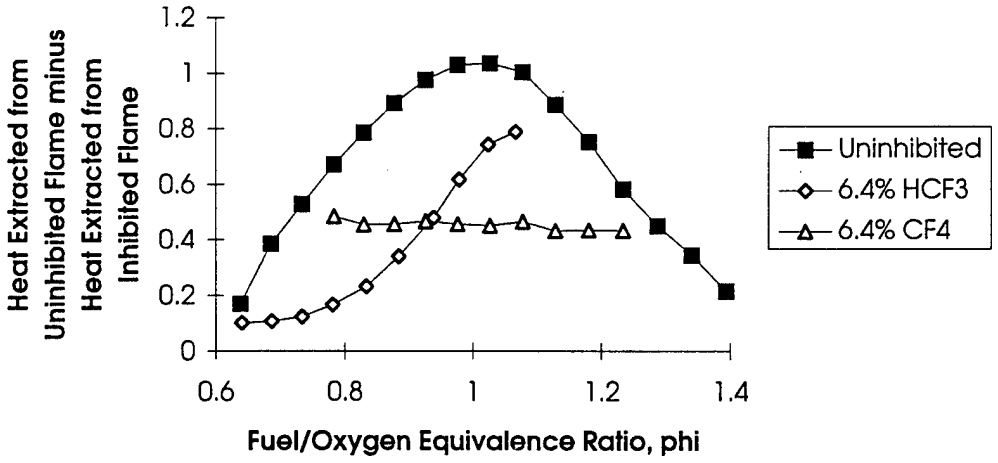

Figure 58. Comparison of CHF_3 and CF_4: Reduction in Heat Extracted by Burner.

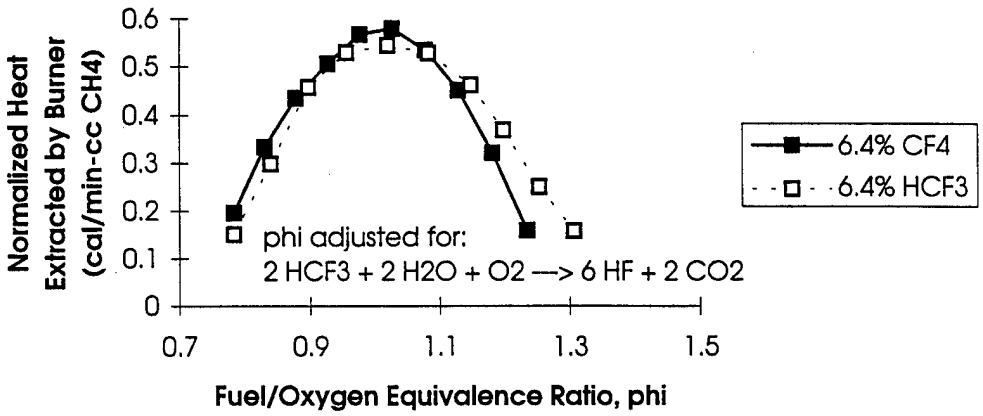

Figure 59. Comparison of CHF_3 and CF_4: After Adjustment for Shift in Fuel/Oxygen Equivalence Ratio.

Although CHF_3 and CF_4 are very similar, they do have slightly different heat capacities; at typical flame temperatures, the heat capacity of CF_4 is about 10 percent greater. And yet, it is noted in Figure 59 that CHF_3 was somewhat more effective than CF_4 in inhibiting the flame, in spite of the fact that the heat capacity of CHF_3 is smaller. This fact is considered in more detail in the next section. Thus a small, but apparently real, difference was found that may be evidence for a flame-inhibiting role for the $\bullet CF_3$ radical. This "back-of-the-envelope" argument should be substantiated by careful modeling. Moreover, it would be of value to test this conclusion on another pair of compounds such as C_2F_6 and C_2HF_5 or C_3F_8 and $CF_3CH_2CF_3$.

H. A FURTHER LOOK AT THERMAL AGENTS

1. Introduction

To this point, a great deal of information has been presented on N_2, the prototypical thermal agent. Data have also been presented on CF_4, which is also thought to be principally a thermal agent even though it is known that some combustion of CF_4 does occur. Conversely, while it is apparent that CHF_3 reacts with O_2 in the flame, it is unknown whether the dominant extinguishment mechanism in this last compound might nevertheless be thermal. Some "back of the envelope" calculations shed considerable light on this question.

The calculation was performed as follows. First, based on the stoichiometry of the flame, the total energy released by combustion of the methane was calculated. Second, given the amount of energy released and the heat capacities of the post combustion species, the adiabatic flame temperature was estimated. Third, the extinguishing agent was added to the post-combustion species and the adiabatic flame temperature was recomputed.

The actual temperature reached by the burner-cooled flame was, of course, lower than the adiabatic flame temperature; thus the adiabatic flame temperature of the uninhibited flame was a somewhat artificial (but useful) reference point. By contrast, at extinguishment, the burner no longer extracted heat from the flame, and the actual temperature was essentially the adiabatic flame temperature of the inhibited flame. The difference between these two temperatures was then a measure of thermal (only) cooling of the flame by the inhibiting agent. Incidentally, for these calculations it was assumed that the molecules of inhibiting agent remained intact, and that the thermal effect of the inhibiting agent was due solely to its heat capacity.

For stoichiometric and lean flames, it was assumed that methane was completely converted to $H_2O(g)$ and $CO_2(g)$. The standard heat of reaction at 1 bar (14.7 psia) and 25 °C (77 °F) was calculated from the standard heats of formation; tabulated data for the enthalpy as a function of temperature [$\Delta H = H°-H°(T_r)$] were then used to calculate the temperature to which the heat of combustion would raise the combustion products. With regard to interpolating the enthalpy data as a function of temperature between 1500 K and 2500 K, it was convenient to fit the tabulated data to an equation of the form $\Delta H = A + BT$. Data were obtained from the *JANAF Thermochemical Tables* (Reference 6). The values used in the fitting equations are included in Table 8.

For fuel-rich flames, it was assumed that both CO_2 and CO were formed, and that the ratio of these two products was dictated by the availability of O_2. For flames with $\phi>1.333$ (at which point, only CO was assumed to be formed), it was assumed that the excess methane remained unreacted. While these assumptions overly simplify the chemistry, they provide a useful point of departure for these back-of-the envelope estimates.

TABLE 8. VALUES FOR CALCULATION OF $\Delta H = H°-H°(TR) = A + BT$.

Compound	A (kJ/mol)	B (kJ/mol-K)
$CH_4(g)$	-63.815	0.093996
$O_2(g)$	-16.1748	0.0377326
$N_2(g)$	-15.607	0.0359143
$CO(g)$	-15.5277	0.0361714
$CO_2(g)$	-28.9201	0.0602533
$H_2O(g)$	-28.923	0.0510237
$CF_4(g)$	-47.0729	0.105430
$CHF_3(g)$	-52.7248	0.102229

2. Nitrogen

The results for N_2 are shown in Figure 60. It was not surprising that this curve looked very much like the curve in Figure 26 since both curves were derived from the same data. The significant difference between the two curves was the explicit accounting for the heat absorbed by the added N_2 (Figure 60). The general shape of the curve was very much in accord with expectations. The curve was found to be very nearly symmetric about $\phi = 1.02$; although the calculated location of the peak was slightly on the fuel-rich side of a stoichiometric flame, little weight should be assigned to the precise location of the maximum because of the scatter in the experimental data points. As a point of reference, the maximum flame velocity for methane-air flames is reported to be at $\phi = 1.06$; at this fuel/oxygen equivalence ratio, the adiabatic flame temperature is calculated to be 2236 K, and the flame speed is 39 cm/sec (Reference 7).

For the data displayed in Figure 60, at $\phi = 1.06$, the adiabatic flame temperatures were calculated to be 2270 K and 1752 K, for the uninhibited flame and the flame at flameout, respectively. Note that the adiabatic temperature at flameout was about 150 K higher than the generally accepted value for methane-air flames at extinction. In addition, the inflammability limits *for this burner under these flow conditions,* spanned a narrower range of values of ϕ than expected for methane-air flames. Both of these facts were the result of the finite rate of gas flow

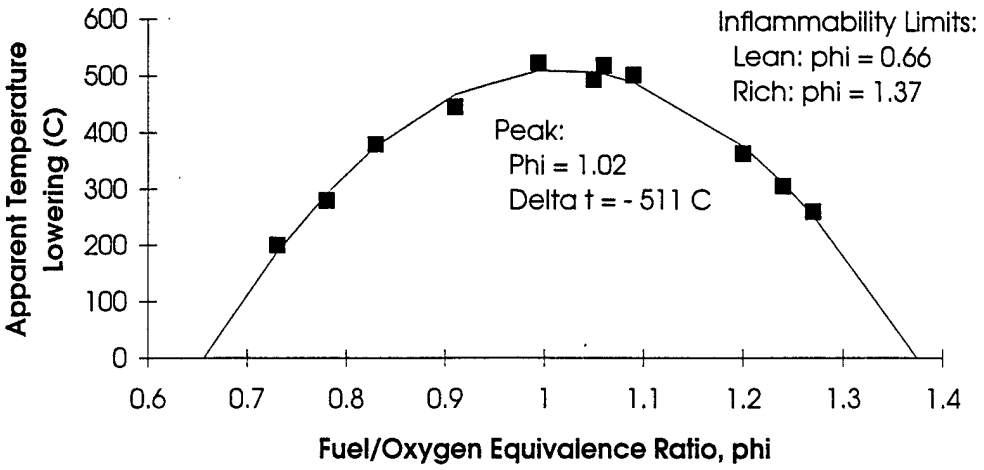

Figure 60. Apparent Flame Temperature Lowering Due to Inhibition by N_2 as a Function of Fuel/Oxygen Equivalence Ratio.

from the burner at flameout. Note in this regard that the linear velocity at flameout (10 cm/sec) was about 25 percent of the adiabatic flame speed of an uninhibited flame, and that the additional increment of temperature (150 K) was about 25 percent of the difference between the adiabatic flame temperature of the uninhibited flame and the adiabatic flame temperature expected for a flame at flameout.

3. Tetrafluoromethane

The results calculated for tetrafluoromethane (CF_4) were nearly identical to those for N_2 and are displayed in Figure 61. Indeed, when both sets of data were plotted on a single chart, it was not possible to distinguish one data set from the other. This finding lent credence to the suggestion that a temperature difference of about 510 K was a useful benchmark for thermal quenching of flames with this burner under these flow conditions.

4. Trifluorimethane

Similar treatment of the experimental data for trifluorimethane (CHF_3) yielded Figure 62. The obvious differences were the location of the maximum ($\phi = 0.88$) and the smaller value of the apparent temperature decrease (-384 K). The effect of the "fuel-content" of the

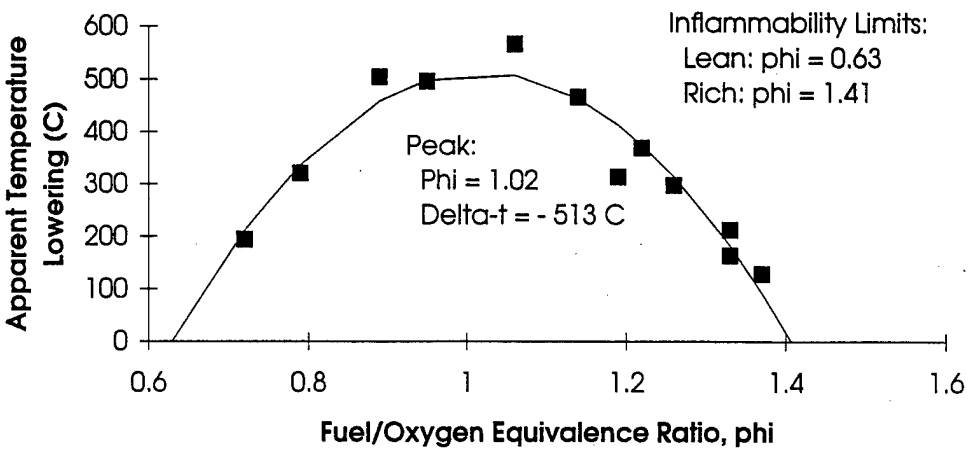

Figure 61. Apparent Flame Temperature Lowering Due to Inhibition by CF_4 as a Function of Fuel/Oxygen Equivalence Ratio.

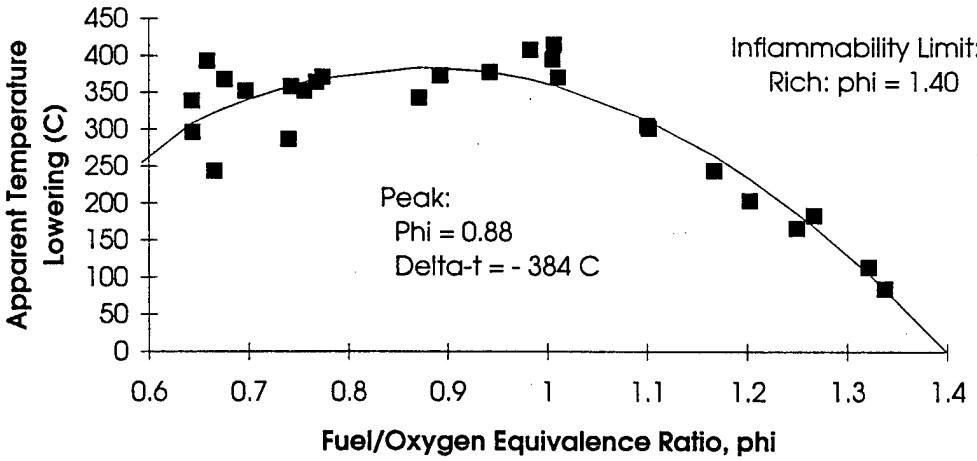

Figure 62. Apparent Flame Temperature Lowering Due to Inhibition by CHF_3 as a Function of Fuel/Oxygen Equivalence Ratio.

CHF_3 has already been discussed. The fact that the apparent lowering of the temperature was about 75 percent of the value for CF_4 suggests that the thermal contribution to the overall effectiveness of CHF_3 was about 75 percent of the total. The other 25 percent must then be accounted for by other mechanisms. The fact that CHF_3 clearly was involved in combustion and that HF was an end product suggests that F-atom scavenging of H-atoms was the most likely candidate.

I. HFC-125, PENTAFLUOROETHANE

1. Summary

Tabulated data for the HFC-125 (C_2HF_5) are presented in Table 9. Only Table 9 experiments were performed; the "air" was made by mixing separately metered streams of O_2 and N_2. The two experiments in which flameout was not observed were the result of an experimental limitation and not an inherent characteristic of the inhibited flame.

TABLE 9. HEAT EXTRACTED *vs.* FLOW RATE OF C_2HF_5 EXPERIMENTS.

Experiment	ϕ	Mole fraction @ extinguishment	
		x-Axis intercept	@ Flameout
C2HF5_H	0.77	0.077	0.075
C2HF5_F	0.88	0.079	no f/o
C2HF5_G	0.90	0.070	0.068
C2HF5_A	0.98	0.072	no f/o
C2HF5_I	1.00	0.065	0.059
C2HF5_B	1.08	0.056	0.053
C2HF5_C	1.16	0.045	0.043
C2HF5_D	1.25	0.035	0.032
C2HF5_E	1.32	0.023	0.022

2. Results

Eight of the experiments are illustrated in Figure 63. By far, the most difficult flame to extinguish was the leanest of the flames examined ($\phi = 0.77$). Note especially that, for this flame, the initial slope of the Heat Extracted curve was positive, and that, for the $\phi = 0.90$ flame, the initial slope was zero.

Extinguishment data for the entire set of experiments are illustrated in Figure 64. Since no experiments were conducted with $\phi < 0.77$, it was not possible to determine with certainty where the peak of the extinguishment curve might lie. Nevertheless, considerable confidence was placed in the maximum mole fraction, estimated to be $X = 0.080$, required to extinguish the most difficult flame.

3. Assessment

The results of the experiments with C_2HF_5 were quite similar to those with CHF_3. Like CHF_3, C_2HF_5 was found to have "fuel character." It was a surprise to note that C_2HF_5 apparently promoted the very lean flames (while this was not true of CHF_3).

On the other side of the ledger, it was found that HC_2F_5 was considerably more effective on a molar (volume of gaseous agent) basis. A good measure of the effectiveness is the slope of the Heat Extracted curve at flameout. A quick glance at Figure 63 reveals that, for all of the experiments, the final slopes were quite similar. For flames with $\phi \geq 0.98$, the average value was -1.40 cal/cc C_2HF_5. A comparable value for the CHF_3 experiments was -0.93 cal/cc CHF_3. The ratio of these two slopes was similar to the ratio of the room temperature heat capacities of these two compounds. Based on this comparison, it has been concluded that the dominant mechanism of inhibition is thermal for HC_2F_5, as in the case of CHF_3. (The ratio of slopes was actually larger that the ratio of room temperature heat capacities; however, the statistical uncertainty associated with the ratio of the slopes makes one wary about assigning any significance to this apparent difference.)

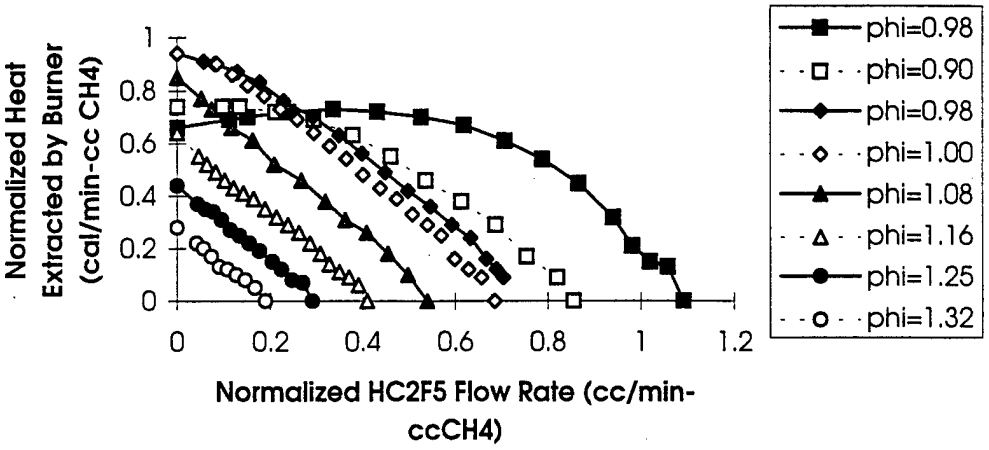

Figure 63. Inhibition of Eight CH_4-Air Flames by C_2HF_5: Normalized Data.

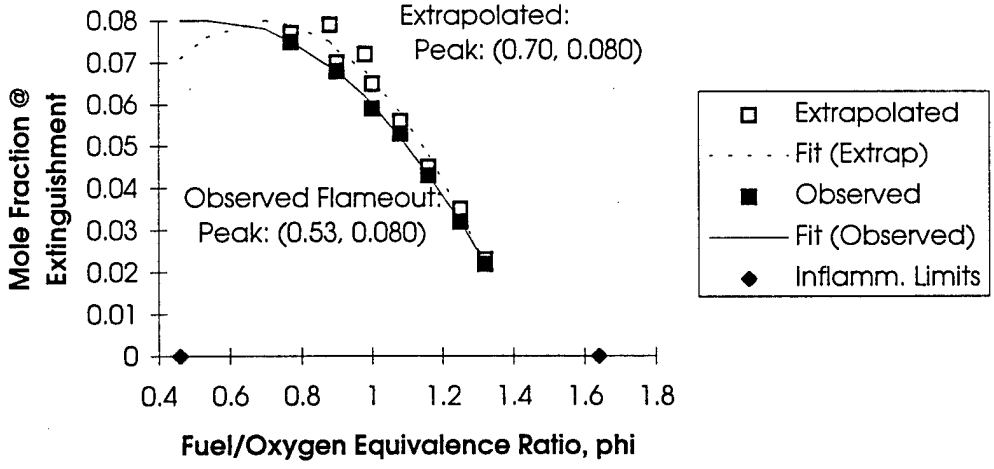

Figure 64. Influence of Fuel/Oxygen Equivalence Ratio on Mole Fraction of C_2HF_5 Required to Extinguish CH_4-Air Flames.

J. HCFC-22, CHLORODIFLUOROMETHANE

Two Heat Extraction *vs.* Flow Rate of $HCClF_2$ (HCFC-22) experiments were performed with nitrogen as the diluent (using air as the oxidant), and the results are displayed in Figure 65. Since both experiments were conducted with fuel-rich flames (one at $\phi = 1.16$, and the other at $\phi = 1.18$), the straight Heat Extracted curves were not a surprise. In spite of the "fuel-content" of this agent, noticeable curvature of the Heat Extracted curve would have been expected only for values of ϕ less than about 1.1. No data were collected for fuel-lean flames; nevertheless, these flames would have been expected to have been more difficult to extinguish.

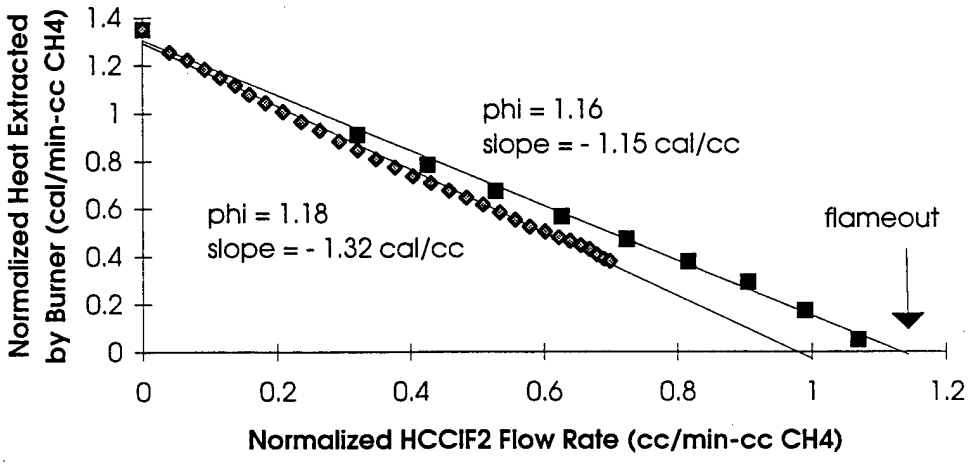

Figure 65. Inhibition of Two CH_4-Air Flames by $HCClF_2$: Normalized Data.

K. HALON 1301

1. Heat Extracted *vs.* Flow Rate of $CBrF_3$ Experiments

The data for six representative experiments, at different values of ϕ, are presented in Figure 66, and Table 10 summarizes the data for these and other experiments with Halon 1301 ($CBrF_3$). The Heat Extracted curves were remarkably similar, and did not display significant changes in shape as a function of ϕ. Each curve was characterized by an initial steep slope and, as extinguishment was approached, a straight-line segment with a lesser slope. The data were

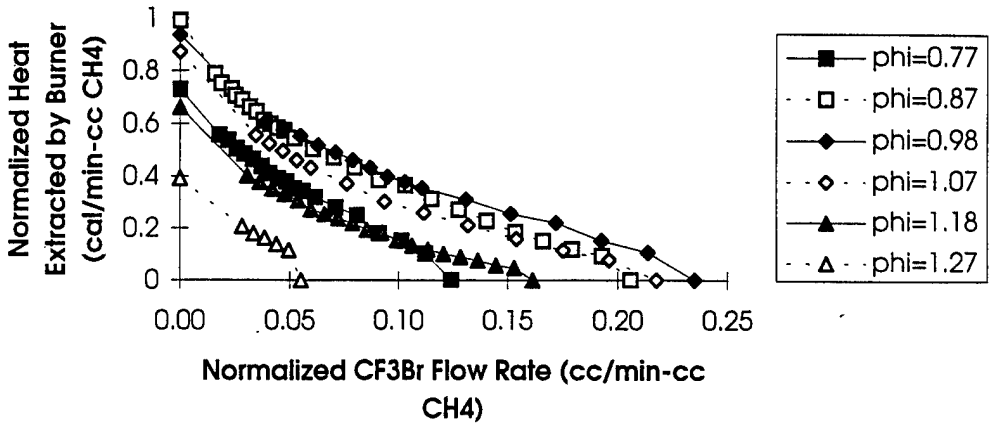

Figure 66. Inhibition of Six Different CH_4-Air Flames by $CBrF_3$: Normalized Data.

TABLE 10. HEAT EXTRACTED *vs.* FLOW RATE OF $CBrF_3$.

Experiment	ϕ	Slope (cal/cc $CBrF_3$)		Mole fraction @ extinguishment	
		Initial	Final	x-Axis intercept	@ Flameout
CBRF3_D	0.76	[b]	- 5.02	0.010	0.009
CBRF3_H[a]	0.77	- 12.7	- 4.27	0.010	0.009
CBRF3_L	0.77	- 10.3	- 3.56	0.010	0.010
CBRF3_A	0.79	[b]	- 4.21	0.012	0.010
CBRF3_I[a]	0.87	- 17.0	- 3.37	0.018	0.017
CBRF3_N	0.87	- 12.6	- 2.59	0.019	0.020
CBRF3_B	0.89	- 14.1	- 2.60	0.018	0.017
CBRF3_C	0.98	- 18.5	- 2.78	0.022	0.020
CBRF3_O[a]	0.98	- 12.6	- 2.45	0.023	0.021
CBRF3_J[a]	1.07	- 13.7	- 2.31	0.022	0.022
CBRF3_E	1.10	- 19.1	- 2.77	0.020	0.019
CBRF3_F	1.16	- 16.2	- 3.12	0.017	0.016
CBRF3_K[a]	1.18	- 7.7	- 2.86	0.018	0.017
CBRF3_G	1.25	[b]	- 3.42	0.010	0.006
CBRF3_M[a]	1.27	- 11.3	- 4.06	0.009	0.006

[a]Illustrated in Figure 66.
[b]Not observed.

best treated by first fitting a straight line to the data points at larger flow rates of $CBrF_3$. Subtraction of the values on the straight line from the experimental data points yielded a set of residuals, and these residuals were fitted to an exponential curve of the form $y = a + b\,e^{-cx}$. This procedure yielded an excellent fit to the experimental data and permitted estimates of the initial (@ Flow Rate = 0) and final (@ flameout) values for the slope of the Heat Extracted curve. These results are reported in Table 10. Perhaps because there was considerable scatter among the values of the initial slope, it was found that there was no obvious trend as a function of ϕ; a good estimate of this initial slope was about 13 cal/cc $CBrF_3$. The uncertainty in the initial slope was in part the result of the fact that many experiments (especially CBRF3_A through CBRF3_I) lacked data points at small values of the flow rate of $CBrF_3$. The final slope did show some dependence on ϕ; near $\phi = 1.0$, the final slope was about 2.5 cal/cc $CBrF_3$, and it was about twice this value for very rich flames and for very lean flames.

The mole fractions of $CBrF_3$ at flameout are displayed in Figure 67. As expected, the observed values were somewhat smaller than the values obtained from the linear extrapolation of the straight-line segments of the Heat Extracted curves. The line in Figure 67 represents a fit to the values obtained by linear extrapolation. Within experimental uncertainty, the data for the mole fraction at extinguishment were found to be symmetrical with respect to $\phi = 1.00$, and to have a maximum value of $X = 0.023$.

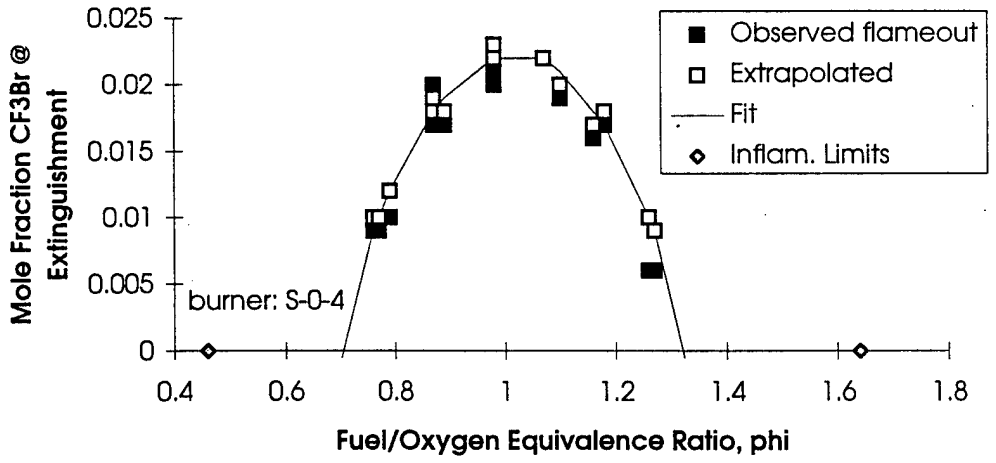

Figure 67. Influence of Fuel/Oxygen Equivalence Ratio on Mole Fraction of $CBrF_3$ Required to Extinguish CH_4-Air Flames.

2. Heat Extracted *vs.* Fuel/Oxygen Equivalence Ratio

These experiments yielded the same conclusions. A typical experiment is illustrated by Figure 68 and Figure 69. The data for several experiments are presented in Table 11.

The FEE curves for seven experiments with different amounts of $CBrF_3$ added are shown in Figure 70. Within experimental uncertainty, the FEE curves were symmetrical about $\phi = 1.00$. The "difference" curves for these same experiments are collected in Figure 71. These are distinctly different from the corresponding curves for CF_4; while the curves in the CF_4 experiments were characterized by small negative slopes as a function of fuel/oxidizer equivalence ratio, the curves for $CBrF_3$ were characterized by maxima on the fuel-rich side of $\phi = 1.0$.

3. Assessment

It was concluded long ago that Halon-1301 extinguishes flames, in part, through catalytic recombination of flame radicals. The fact that the Heat Extracted curves were non-linear was entirely consistent with this conclusion. When the FEE data for $\phi = 1.00$ (the most difficult flame for $CBrF_3$ to extinguish) were plotted as a function of the amount of $CBrF_3$ added to the flame, Figure 72 was obtained. With the exception of the first three data points (at the lowest concentrations of $CBrF_3$), the data fell on a reasonably straight line, and the extrapolated value at extinguishment (FEE = 1.00), was, within experimental uncertainty, in agreement with the Heat Extracted *vs.* Flow Rate of $CBrF_3$ experiments at values of ϕ near 1.0. The fact that the straight line in Figure 72 did not pass through the origin, and that the first three data points were below the line, reinforced the conclusion that the non-linear behavior was important only up to a volume of about 0.5 percent. Beyond this point, the extinguishing effectiveness of $CBrF_3$ was found to be a linear function of the amount of agent added to the premixed gases. (For comparison with the data presented in Figure 66, 0.5 percent $CBrF_3$ by volume corresponded to a normalized flow rate of about 0.05 cc $CBrF_3$/min-cc CH_4.)

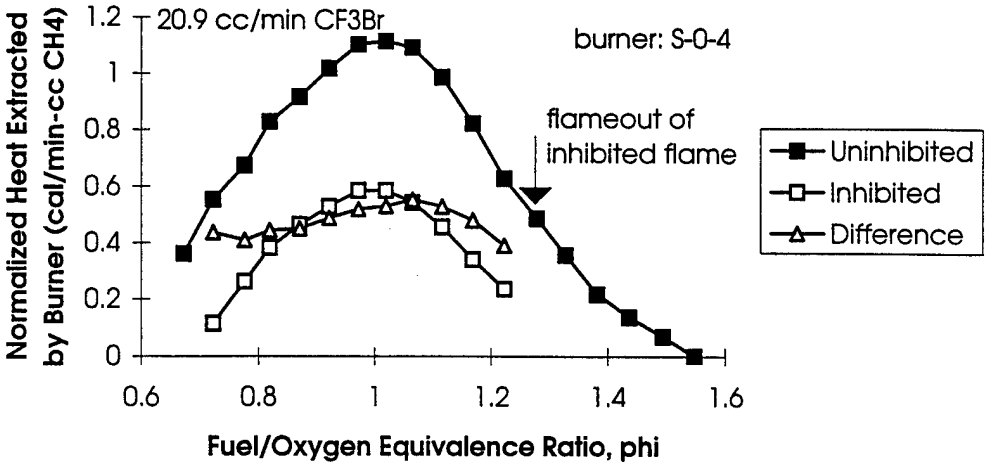

Figure 68. Inhibition of a CH_4-Air Flame by $CBrF_3$: Heat Extracted.

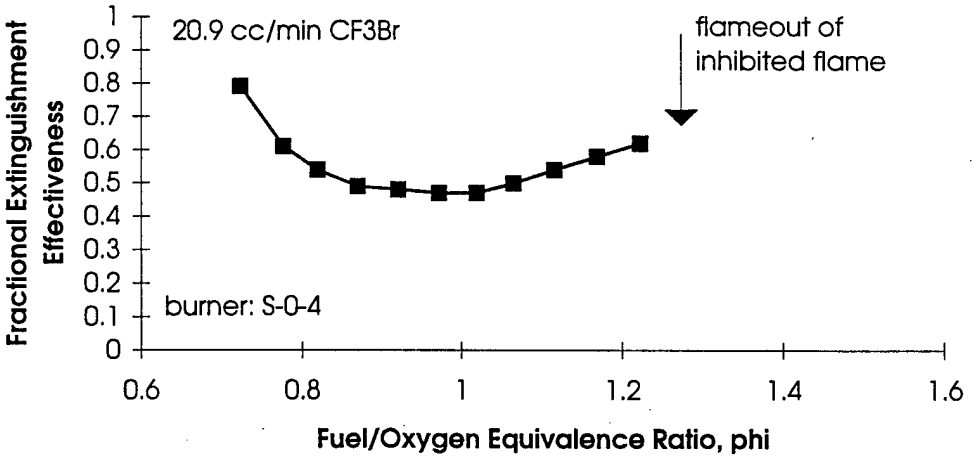

Figure 69. Inhibition of a CH_4-Air Flame by $CBrF_3$: Fractional Extinguishment Effectiveness.

TABLE 11. $CBrF_3$ HEAT EXTRACTION *vs.*FUEL/OXYGEN EQUIVALENCE RATIO EXPERIMENTS.

Experiment	$CBrF_3$ flow rate (cc/min)	Mole fraction $CBrF_3$, X=	FEE @ ϕ = 1.00
CBRF3_V	44.3	0.0110	0.672
CBRF3_T	35.0	0.0088	0.589
CBRF3_U	25.3	0.0064	0.521
CBRF3_X	20.9	0.0052	0.460
CBRF3_R	15.1	0.0039	0.293
CBRF3_W	11.3	0.0029	0.259
CBRF3_S	7.5	0.0020	0.079

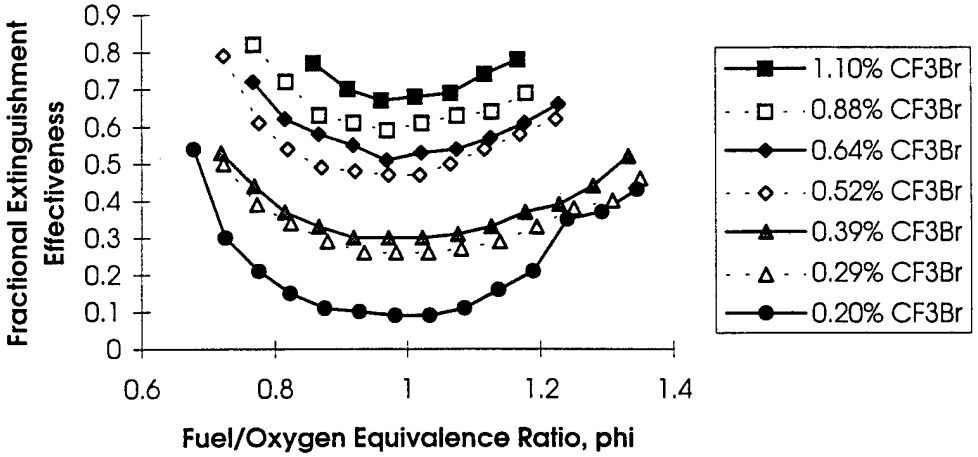

Figure 70. Fractional Extinguishment Effectiveness as a Function of Volume Percent $CBrF_3$.

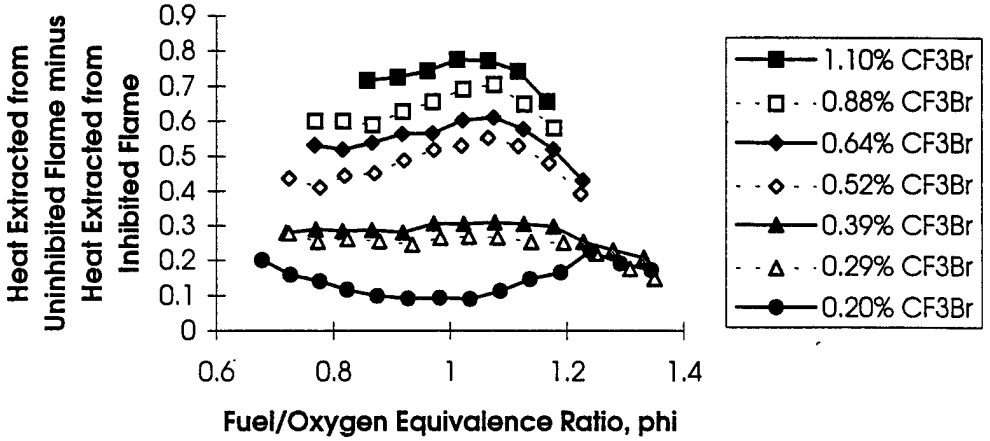

Figure 71. Effect of Various Amounts of $CBrF_3$ on the Heat Extracted by the Burner.

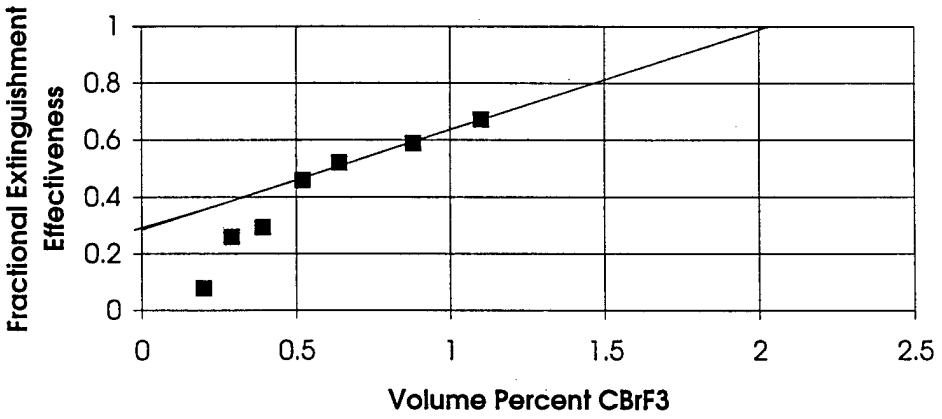

Figure 72. Effect of Various Amounts of $CBrF_3$ on the Fractional Extinguishment Effectiveness.

L. COMPARISON OF SAPPHIRE RESULTS WITH CUP-BURNER EXPERIMENTS

Table 12 compares the results of atmospheric-pressure, methane-oxygen Sapphire 0 experiments with the results of cup-burner experiments. There are, of course, major differences between these two types of experiments. While the Sapphire 0 experiments were conducted with premixed methane-air flames, cup-burner measurements typically use *n*-heptane-fueled diffusion flames. Since it was of some interest to compare methane flames with *n*-heptane flames, some comparative data are included in Table 12.

The data obtained in the Sapphire 0 experiments were in surprisingly good agreement with the cup-burner results. Note that, for each of the compounds studied with the Sapphire 0 burner, the volume percent at extinguishment is reported for that value of the fuel/oxygen equivalence ratio at which the flame was most difficult to extinguish. In this respect, the Sapphire datum for each compound is very much like the datum for the corresponding cup-burner experiment; in the cup-burner experiment (indeed, in any diffusion flame), the reaction zone is established at the location (and corresponding value of ϕ) where the flame is most stable.

While there is a general feeling in the literature that methane flames are easier to extinguish than *n*-heptane flames, the limited data set presented in Table 12 is not persuasive in this regard.

One other comment seems to be in order. It was noted that, of the five compounds compared in Table 12, there was a significant discrepancy between the Sapphire 0 and cup-burner data only in the case of Halon 1301. This difference is real, and not a matter of experimental uncertainty, and could result from the fact that Halon 1301, unlike the other four compounds, is a catalytic recombination agent.

TABLE 12. COMPARISON OF SAPPHIRE 0 EXPERIMENTS WITH CUP-BURNER EXPERIMENTS.

Agent	Literature data		Sapphire 0 experiments	
	n-Heptane percent (v/v) @ extinguishment	Methane percent (v/v) @ extinguishment	CH_4/O_2 equivalence ratio	Methane percent (v/v) @ extinguishment
$CF_3CH_2CF_3$ [FM-200]	5.8 (6)[a] 7.5 (6)[a] 6.3 (2)[a]	6.2 (6)[a]		
NAF-S-III	9.9 (4, 6)[a]	13.7 (6)[a]		
CF_3I	3.0 (2, 6)[a]	2.0 (6)[a]		
$CBrF_3$ [Halon 1301]	2.9 (2, 6)[a] 2.9 (5)[a] 3.1 (5)[a] 3.5 (5)[a] 2.7 (5)[a] 3.0 (5)[a] 3.9 (5)[a]	3.1 (6)[a]	$\phi = 1.01$	2.3
N_2-Ar-CO_2 (50:40:10) [Inergen]	29 (7)[a]	15 (7)[a]		
N_2-Ar (50:50) [Argonite]	28 (7)[a] 29 (4)[a]	27 (7)[a]		
Ar	38 (4, 7)[a]	29(7)[a]		
N_2	30 (4)[a] 30 (5)[a] 30 (5)[a] 31 (5)[a] 30 (5)[a]		$\phi = 1.01$	31
CF_4	13.8 (2)[a]		$\phi = 1.02$	14.7
CHF_3 [FE-13]	12.6 (2)[a]		$\phi = 0.8$	12
C_2HF_5 [FE-25]	9.4 (2)[a] 9.4 (5)[a] 8.8 (5)[a] 9.3 (5)[a] 8.1 (5)[a]		$\phi = 0.7$	8.0

[a]Number in parentheses refers to a table (Reference 4).

SECTION V

LOW PRESSURE FLAME CHAMBER—SAPPHIRE 1

A. GENERAL CHARACTERISTICS OF THE SAPPHIRE 1 INSTRUMENT

1. Introduction

The Sapphire 1 instrument was assembled largely from available pieces of hardware. The original objectives were (1) to obtain experience with low pressure flames, (2) to work out a technique for introducing aerosols into low pressure flames, and (3) to explore the quantitative relationship between the heat extracted from the flame and the degree of inhibition of the flame. All three objectives were achieved. Experience with low pressure flames and with introduction of aerosols into low pressure flames was directly transferred to the Sapphire 2 experiments, and the work on heat extraction as a technique for elucidating the mechanisms of extinguishment was shifted to the inherently less complicated Sapphire 0 atmospheric pressure experiments. The last experiment conducted with the Sapphire 1 instrument was during April 1995.

Although the original objectives for the Sapphire 1 instrument were very limited, it became clear from the very early heat extraction experiments with this instrument that these experiments could provide important insights into the mechanisms of extinguishment. The results of these experiments are detailed in Section V.B.

Most of the heat extraction experiments were conducted with the sintered bronze burner, Sapphire 1-1, while the aerosol experiments were conducted exclusively with the modified Meker burner, Sapphire 1-2.

2. Temperature Measurements

A few flame temperature measurements were made with a platinum-platinum(13% rhodium) thermocouple. A representative value was 1520 °C (2770 °F) for a ϕ = 1.11 flame @ 25 torr; the thermocouple was located 7.8 in (2 cm) above the surface of the burner, well into the recombination zone. The thermocouple was not coated, and no corrections

were made for radiative or conductive losses. Temperature measurements were not pursued, largely because of their limited utility with respect to the objectives of the project. It was also recognized that many of the compounds of primary interest in the project would build up deposits on the thermocouples and that these deposits would make interpretation of the observed voltages very difficult.

3. Flow Field

The flow field in the vicinity of the flame can best be characterized as "complex." A typical flow rate for the premixed gases was 27 cc/sec, measured at room temperature and local prevailing atmospheric pressure (633 torr). At this flow rate, the linear velocity of the premixed gases at the surface of the 1.50-in (3.81 cm)-diameter Sapphire 1-1 burner, operating at 30 torr, and assuming that the gases were still at room temperature, was 20 in/sec (50 cm/sec).

The linear velocity immediately above the Sapphire 1-2 burner was similar, 24 in/sec (62 cm/sec). For this burner, the linear velocity in the "channels" formed by the flame holder was also estimated: 3.8 in/sec (97 cm/sec). The situation was complicated by the fact that the 0.020-in (0.5 cm) metal foils from which the flame holder was constructed were known to be at a temperature above room temperature. A typical temperature at the center of the flame-holding grid was 300 °C (572 °F).

Because a sheath of inert gas was not provided for the flame, the flame was burning in a nearly stagnant "atmosphere" of burned gases. The "atmosphere" was, of course, set in motion by the flow field induced by the flame. To a significant degree, this "atmosphere" impeded the flow of the flame and stabilized it near the burner. It was also true that burned gases were entrained in the flame around the periphery of the burner. The shape of the flame in the vicinity of the burner was ample evidence of this entrainment. Although the luminous zone was reasonably flat, the edge was raised, a bit like the edge of a plate or of a rather shallow soup bowl. Additional evidence of the perturbation (and stabilizing effect) of the relatively stagnant "atmosphere" of burned gases was the fact that the magnitude of the perturbation depended on the location of the burner relative to the top of the chamber. As noted elsewhere in this report, the temperature at the center of the Sapphire 2-2 burner depended on the distance between the

surface of the burner and the top of the chamber, and decreased as the distance between the surface of the burner and the top of the chamber was decreased.

The "atmosphere" in which the flame was burning was, of course, well above ambient temperature. A measurement of this temperature is described below, along with a discussion of its implications.

Concern with the complexity of the flow field was somewhat alleviated by the realization that the flow at the center of the flame was less perturbed than the flow at the edges. Nevertheless, this potential impact on observed phenomena was considered. No attempts were made to quantitatively take account of the impact on the observed results.

4. Heat Extracted by the Burner

As a baseline for evaluating the effectiveness of candidate extinguishing agents, the heat extracted by the burner was profiled as a function of the fuel-oxidizer equivalence ratio (ϕ) for an uninhibited flame. In this experiment (Figure 73), only the flow rate of methane was varied; the chamber pressure and flow rates of argon and oxygen were held constant. To account for the fact that the methane flow rate was varied, the measured heat extracted by the burner was normalized by the flow rate of the methane. For these normalized data, it was found that the flame with a nearly stoichiometric ($\phi = 0.94$) composition yielded the largest amount of heat extracted by the burner per cc of methane. The fact that the observed maximum was slightly on the fuel-lean side of the stoichiometric flame was of some interest. Since the heat extracted by the burner depended not only on the total heat in the flame but also on the separation of the flame from the surface of the burner ("liftoff"), it was not surprising that the lean flame (which was characterized by a lower methane flow rate and lower flow rate of total gases) was characterized by smaller liftoff and larger heat extracted by the burner.

The finding that the peak in the heat extracted curve was found at a value of ϕ very nearly equal to 1.00 was especially encouraging and strongly implied that, in spite of the complexities of the flow field, the results were not irretrievably compromised by these complexities.

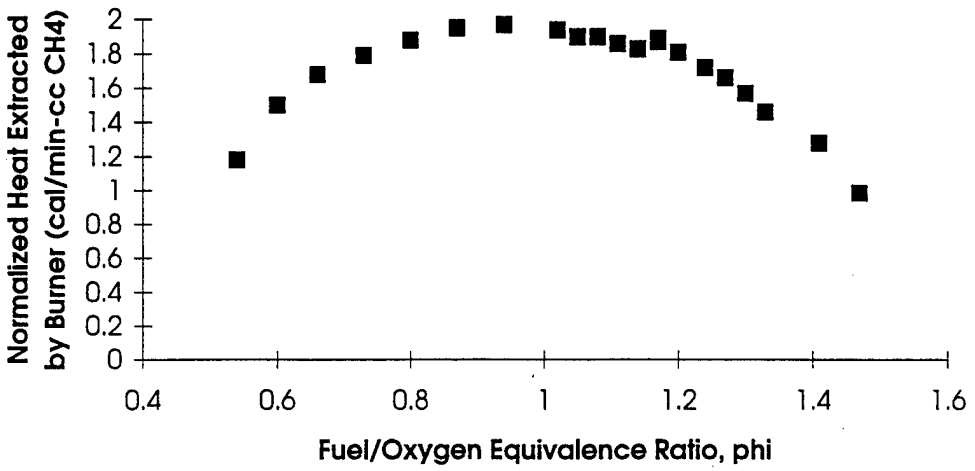

Figure 73. Heat Extracted by the Burner in the Sapphire 1 Instrument as a Function of Fuel/Oxygen Equivalence Ratio.

In the experiment illustrated by Figure 73, the actual (unnormalized) heat extracted by the burner was highest at $\phi = 1.17$, and many of the experiments reported here were conducted at this value of ϕ.

5. Liftoff

The "liftoff" was defined as the vertical distance between the top of the burner and the bottom of the luminous zone. It was measured with a transit mounted on a fixture that could raise or lower the transit. The baseline was established by aligning the crosshair with the top of the burner, and all subsequent measurements were referenced to this baseline. Although the lower edge of the luminous zone was somewhat diffuse, it was relatively easy to make reproducible measurements within ±0.008 in (±0.2 mm).

The liftoff was found to be a monotonic, but very non-linear, function of the amount of inhibiting agent added to the flame. For the first few incremental additions of agent to the premixed gases, very small changes in liftoff were observed. As extinguishment was approached, it was not uncommon to observe a liftoff of 0.8 in (2 cm), or more. The fact that a flame could be stabilized at such a long distance from the cooled burner reflected the fact that the flame was stabilized by the cooled burner, by the top of the flame chamber (also cooled), and by

the quasi-stagnant "atmosphere" of burned gases (cooled to a significant degree by the cooled walls of the chamber).

B. RESULTS OF HEAT EXTRACTED EXPERIMENTS

1. Protocol

With two exceptions, noted in the tabulated data, all experiments were conducted at a chamber pressure of 30 torr and with a flame of the following composition: O_2, 521 cc/min; Ar, 769 cc/min; CH_4, 330 cc/min (all measured at ambient laboratory temperature and pressure). For this flame, $\phi = 1.17$. The temperature increase of the coolant passed through the cooling coils on the periphery of the burner was measured as a function of the amount of extinguishing agent added to the premixed gases. The liftoff was measured at each data point.

2. Inhibition by Nitrogen

Typical results for inhibition by nitrogen were obtained in experiment A056, and are illustrated by Figures 74, 75, and 76. The most significant finding was the fact that, up to a N_2 flow rate of 1000 cc/min, the heat extracted by the burner was a linear function of the amount of nitrogen added. The units of the slope of this straight-line portion of the curve (cal/cc N_2) are especially noteworthy, and imply that the slope of this line is a clear figure of merit for the inhibiting agent. In essence, the slope is a measure of the ability of the agent (N_2) to absorb heat, which otherwise would have been extracted by the burner. However, the interpretation is considerably more complex. By reducing the temperature of the flame, the N_2 reduced the number density (number of molecules per cc) of the flame radicals that were capable of migrating upstream and participating in the flame initiation and flame propagation reactions that characterize the induction zone. Here, the "induction zone" is identified as the dark zone below the luminous zone. The net result was to stretch the induction zone, as evidenced by the increased liftoff (a direct measure of the length of the induction zone). Figure 75 displays data for liftoff as a function of the amount of N_2 added to the premixed gases.

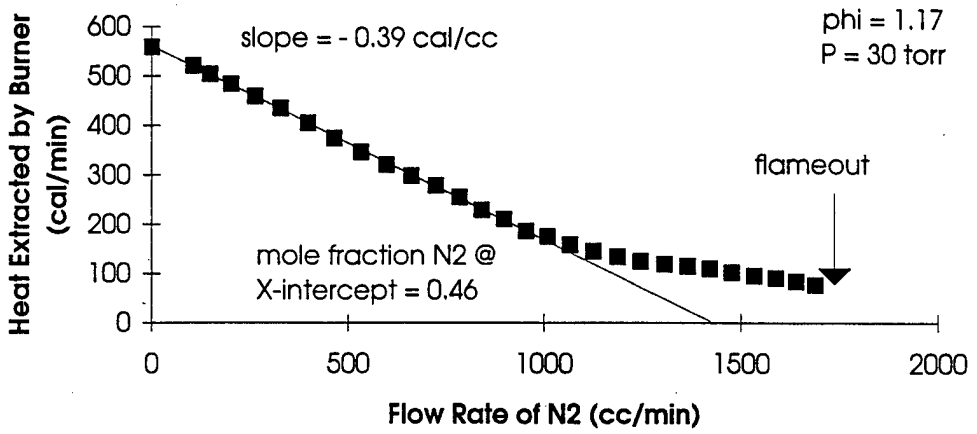

Figure 74. Inhibition of a 30-torr Flame by N_2: Heat Extracted by the Burner.

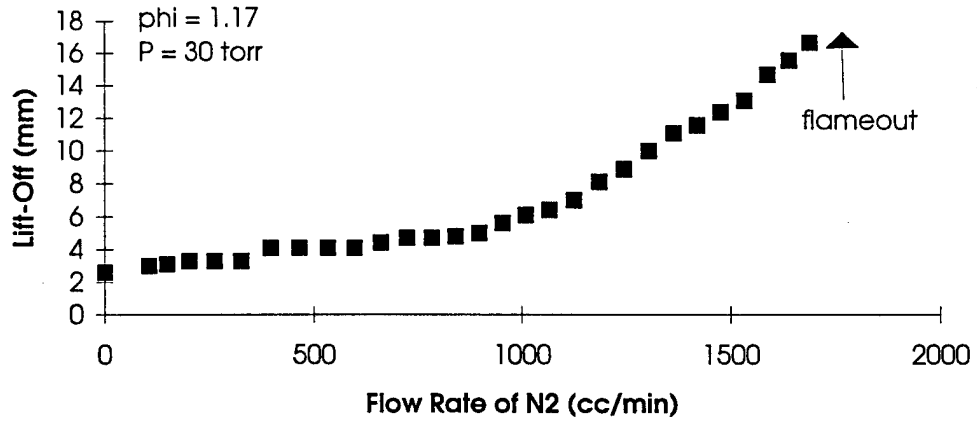

Figure 75. Inhibition of a 30-torr Flame by N_2: Liftoff.

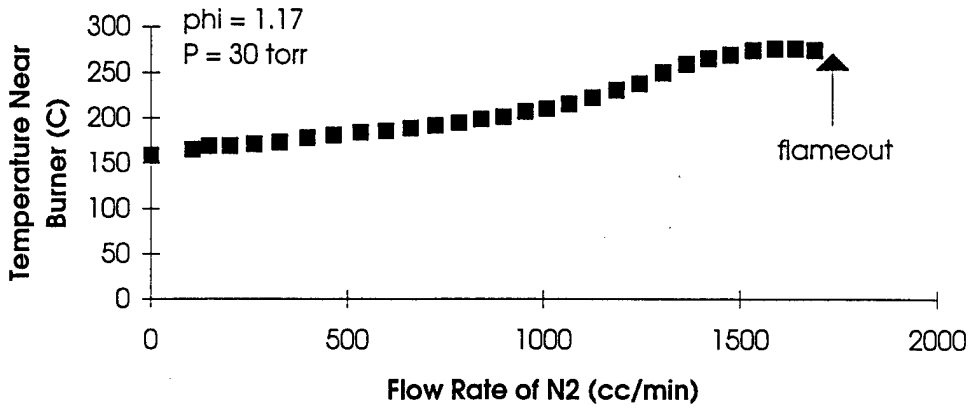

Figure 76. Inhibition of a 30-torr Flame by N_2: Temperature of the Burned Gases Near and Below the Edge of the Burner.

The intersection of the straight-line with the x-axis (Figure 74) was the point at which the inhibiting agent should have extinguished the flame. When the flame speed was reduced to the point that no heat was deposited in the burner (and into the fresh, premixed gases), extinguishment should be expected. It was, therefore, of more than casual interest to compare the observed intersection (at a mole fraction, X = 0.46 in this case) with the mole fraction at extinguishment observed in other experiments, e.g., cup-burner. For nitrogen, the cup-burner value is X = 0.31. There were, of course, many differences between the A056 experiment and the Cup-Burner experiment including fuel, pressure, and ϕ. A systematic comparison for several agents may be found in the Section IV.B.4.

Departure of the Heat Extracted data from the straight line (Figure 74) occurred at a N_2 flow rate of 1000 cc/min; it was coincidental with the change in slope of the graph of liftoff as a function of N_2 flow rate (Figure 75). An explanation for the "tail" of the curve was needed. It will be recalled that the heat was extracted from the burner by cooling coils soldered to the periphery of the burner. (Refer to Figure 4 in Section II for a diagram of the Sapphire 1 instrument.) It follows that some heat should have been picked up by these coils from the hot "atmosphere" of burned gases. Moreover, it might have been suspected that, as decreasing amounts of heat were extracted by the burner, the temperature of the hot "atmosphere" would increase, and the amount of heat extracted by the cooling coils from the "atmosphere" would also

increase. To explore this hypothesis, a thermocouple was located in the "atmosphere," near the burner, but below the surface so that radiative heating by the flame would be minimized. The results are displayed in Figure 76. It was noted that the temperature differential between the "atmosphere" and the cooling coils increased from about 120 °C (216 °F) at the beginning of the experiment to about twice this value at extinguishment. This observation lent strong support to the hypothesis. It was also noted that the temperature rise in the "atmosphere" departed from linearity at about the same point at which both the Heat Extracted curve and the liftoff curve departed from linearity, adding further credence to the hypothesis.

3. Inhibition by Halon 1301

Data for inhibition by Halon 1301 ($CBrF_3$) are displayed in Figures 77 and 78. In all respects, this experiment was similar to that for nitrogen, but the result had one very significant difference: Unlike the nitrogen experiment, the Heat Extracted curve could not be described as a straight line with a "tail." The entire set of data was best fit by a single exponential equation of the form $y = a + be^{-cx}$. This observation suggested that there was a fundamental difference in the Heat Extracted behavior of typical thermal agents (such as N_2) on one hand, and typical catalytic agents (of which $CBrF_3$ is representative) on the other hand. To eliminate the complicating factor associated with the hot "atmosphere" of burned gases in the Sapphire 1 experiment, the Heat Extracted experiments were moved to the atmospheric, Sapphire 0, burners, and the Sapphire 1 instrument was turned to other objectives.

4. Comparative Results

Comparative results for several different extinguishing agents are compiled in Table 13. With the two exceptions noted in the table, all data were obtained with $\phi = 1.17$ flames at a chamber pressure of 30 torr.

Two measures of effectiveness were recorded: the slope of the straight-line portion of the heat extracted curve, and the mole fraction at extinguishment (obtained by extrapolating the straight-line portion of the curve to the x-axis). The observed results were very much in accord with expectations. For reference, the heat capacities (C_P) at 25 °C (77 °F) are also listed in Table 13. Of the seven agents, the first six are typical thermal agents, and the

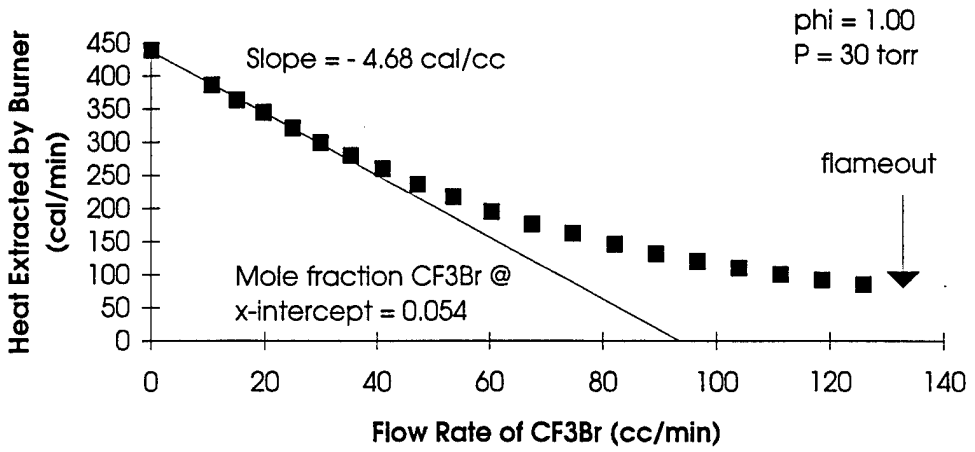

Figure 77. Inhibition of a 30-torr $CH_4/O_2/Ar$ Flame by $CBrF_3$: Heat Extracted.

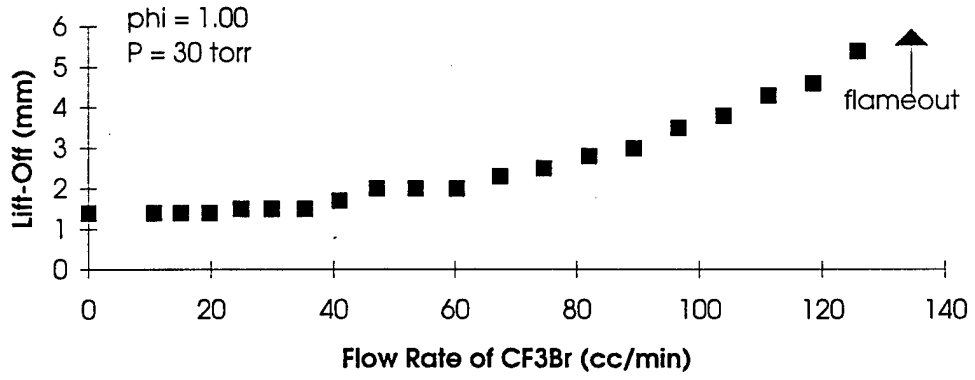

Figure 78. Inhibition of a 30-torr $CH_4/O_2/Ar$ Flame by $CBrF_3$ Liftoff.

TABLE 13. SAPPHIRE 1 EXPERIMENTS: COMPARATIVE DATA.

Agent	Experiment	Slope (cal/cc)	Mole fraction @ x-intercept	C_P @ 25 °C (cal/mol-K)	Notes
He	A060B	-0.34	0.49	4.97	
	A061	-0.38	0.44		
	A067	-0.37	0.47		
Ar	A035	-0.30	0.54[a]	4.97	
	A038	-0.29	0.51[a]		
	A066A	-0.30	0.51[a]		
	A066B	-0.32	0.46[a]		20 torr
	A078	-0.27	0.43[a]		Meker burner
N_2	A047	-0.37	0.42	6.96	
	A056	-0.39	0.46		
	A060A	-0.38	0.45		
	A079	-0.35	0.46		Meker burner
CO_2	A044	-0.79	0.28	8.87	
	A050	-0.84	0.24		
	A065	-0.75	0.30		
CF_4	A054	-1.06	0.23	14.59	
SF_6	A069	-2.12	0.12	23.17	
$CBrF_3$	A040	-4.68[b]	0.054	16.57	$\phi = 1.00$
	A042	-5.10[b]	0.056		

[a]Argon added to the amount already present in the basic flame.
[b]Initial slope of exponential curve (@ flow rate = 0 cc $CBrF_3$/min).

effectiveness was expected to be proportional to the heat capacity. It was observed that the initial slopes of the Heat Extracted curves increased as the heat capacities of the agents increased. Similarly, the intercept of the linear segment of the Heat Extracted curve with the x-axis (and hence the mole fraction of agent predicted to achieve extinguishment) was found to decrease with increasing C_P.

Of the seven agents, $CBrF_3$ (well known for its catalytic contributions to extinguishment), was the notable exception. Since the Heat Extracted curve was not linear, the initial slope of the curve was included in Table 13. The very large value of the initial slope (by comparison with the slopes for the six other agents) was indicative of the catalytic contributions.

It was of considerable interest to compare the Sapphire 1 data with Sapphire 0 (atmospheric flame) data. Table 14 summarizes the 30-torr data from Table 13, and presents atmospheric flame data for flames with the same stoichiometry, $\phi = 1.17$. There were some unforeseen results.

a. Result 1. The slopes of the Heat Extracted curves were more negative for the 30-torr experiments than for the corresponding atmospheric pressure experiments. Conversely, the predicted mole fractions at extinguishment were smaller for the atmospheric pressure experiments. While this contrast seemed contradictory on the surface, it was a reminder of the fact that the slope of the heat extraction curve depended not only on the mole fraction at

TABLE 14. COMPARISON OF 30-TORR EXPERIMENTS WITH ATMOSPHERIC EXPERIMENTS.

Agent	Slope (cal/cc)		Mole fraction @ intercept		C_P @ 25 °C
	30 torr	633 torr	30 torr	633 torr	(cal/mol-K)
He	-0.37	-0.15	0.47	0.44	4.97
Ar	-0.28	-0.27	0.50	0.72	4.97
N_2	-0.37	-0.29	0.45	0.33	6.96
CO_2	-0.79	-0.27	0.27	0.20	8.87
CF_4	-1.06	-0.50	0.23	0.14	14.59
SF_6	-2.12	[b]	0.12	[b]	23.17
$CBrF_3$	-5.10[a]	-10[a]	0.056[a]	0.013[a]	16.57

[a]Initial slope
[b]This experiment was not done.

extinction but also on a complex set of other factors including the total amount of heat in the uninhibited flame, liftoff, the heat extraction efficiency of the burner, etc. It is immediately apparent that caution must be taken in comparing the slopes of Heat Extracted curves for experiments with different experimental configurations.

b. Result 2. Although the slopes of the Heat Extracted curves were uniformly more negative in the 30-torr experiments than in the atmospheric experiments with the six

thermal agents, this was not true for $CBrF_3$. Note also that the mole fraction at extinguishment was larger in the 30-torr experiment than in the atmospheric experiment. This result suggests that the $CBrF_3$ was less effective at low pressure than at atmospheric pressure. This finding is in consonance with the results reported for $CBrF_3$ by Biordi and coworkers (Reference 2), and is reminiscent of the similar finding for $Fe(CO)_5$ (References 9 and 10).

C. INTRODUCTION OF AEROSOLS INTO LOW-PRESSURE FLAMES

1. Experimental

The ultrasonic aerosol generator and drying assembly are described in Section II. The premixed gases were introduced directly into the aerosol generator; the aerosol-laden gases were then passed through the heated borosilicate glass tube (typically at 140 °C [284 °F]) and the chemical condenser. An orifice located at the entrance to the burner provided a pressure drop between the aerosol generator and the burner. The principal difficulty with the experimental setup was the inability to maintain a steady rate of introduction of aerosol into the flame. Several factors contributed to this difficulty.

The principal diagnostic of the amount of aerosol introduced into the flame was the observed intensity of the emission of the alkali metal. The emission intensity was measured photometrically; however, in many cases, simple visual observation was adequate to distinguish among different experimental conditions. Needless to say, the emission intensity depended on several factors (such as flame temperature) in addition to the number density of atoms in the flame. A truer measure of the number density would have been obtained from the measured absorbance, provided the aerosol particles were completely atomized, and there was no subsequent formation of aggregates of metal-atom-containing species.

2. Geometry of the Hardware

Because it was necessary to provide a cold finger as a reservoir for the water condensed by the chemical condenser, the condenser was oriented at an angle of about 30 degrees relative to the vertical (Figure 10). As a consequence, the aerosol-laden premixed gases were forced to change directions several times between the aerosol generator and the flame.

Each change in direction provided an opportunity for some of the aerosol particles to be lost from the stream, a similar condition to the sandy beaches that "grow" on the inside of each bend in the Colorado River as it courses through the Grand Canyon. While the rate of deposition of aerosol particles was not catastrophic, the aerosol density was reduced, and it was necessary to clean the hardware after a few hours of operation.

3. Pressure Control Orifice

Orifices of two different diameters were employed: 0.040 in (1 mm) and 0.078 in (2 mm). The smaller orifice was used in earlier experiments. While the pressure in the aerosol generator was not measured in these experiments, it was probably more than half of the prevailing atmospheric pressure. Under these conditions, the aerosol was easily seen in the generator.

The larger orifice was installed to increase throughput of aerosol into the burner and to reduce problems associated with deposition of aerosol particles at the orifice (leading to eventual blockage). With the larger orifice, the observed pressure in the aerosol generator was on the order of 100 torr. With this arrangement, there was very little visual evidence of aerosol generation; presumably, the number density of aerosol particles was lower in the lower pressure gases.

4. Concentration of Aqueous Solutions

It was no surprise to discover that a 1.0 M solution of $NaHCO_3$ gave a much more highly colored flame than a 0.1 M solution. However, as the water evaporated (under the reduced pressure in the aerosol generator), the solution rapidly became saturated with the salt. This resulted in formation of a crust on the surface of the pool of solution, and in significantly reduced aerosol generation efficiency. Whether the reduction in generation efficiency was primarily mechanical or was strongly dependent on the reduction of the vapor pressure of the water is not known. However, it was found that, when distilled water was added to a saturated solution, the color of the flame increased considerably, suggesting an increase in efficiency of aerosol generation.

5. Aerosol Generator Temperature

Especially with the larger orifice, the temperature of the solution (and of the hardware) dropped significantly, due to the evaporation of the water. The net result was a marked reduction in the efficiency of aerosol generation. To compensate for this cooling, a 1/4-in (0.64-cm) OD copper tube was silver-soldered to the periphery of the base of the aerosol generator and used to circulate ethylene glycol from a constant temperature bath. Holding the temperature at room temperature significantly improved the rate of aerosol generation; raising the temperature to 30 °C (86 °F) resulted in a further increase in aerosol concentration in the gas stream.

6. Comparison of Solutions with Pure Water

Although the aerosol generator and drying system were presumed to yield essentially dry aerosols, it was unknown whether the effect of residual water could be separated from the effect of the dry aerosol particles. In an attempt to shed some light on this question, numerous measurements, both of the heat extracted by the burner and of the temperature at the center of the burner, were made. In general, there was some evidence that the aerosol particles produced a measurable degree of inhibition. However, the difficulties associated with generating aerosols at a constant rate were so severe that little or no confidence was placed in the quantitative data generated.

7. Summary and Conclusions

The technique for introducing aerosols in the low-pressure flames was easily worked out. However, the aerosol generator proved to be less than satisfactory for the task. The primary deficiency stemmed from the fact that the generator was a batch, rather than a continuous, device. As a result, experimental parameters varied rapidly over relatively short spans of time, and comparative data were very difficult to obtain. An apparently more effective generator was described by Fassel and Bear (Reference 11).

D. SPECTROSCOPY OF SAPPHIRE 1 FLAMES

1. General Characteristics

The visible spectroscopy of hydrocarbon-oxygen flames is, of course, dominated by CH, with bands near 3900Å and 4315Å, and by C_2, with band heads at 4737Å and 5165Å. Gaydon and Wolfhard (Reference 12) describe atmospheric hydrocarbon-oxygen flames as being green at the base and around the edges (due to C_2), and blue or blue-violet towards the top of the reaction zone (due to CH).

As expected, the relative intensities of the CH and C_2 bands (and the observed color of the flame) were a direct reflection of the stoichiometry. Fuel-lean flames were reddish-blue (characteristic of dominance by the CH radical), while fuel-rich flames were blue-green (as expected for flames with greater contributions by C_2).

2. $CBrF_3$-Doped Flames

The most dominant feature of flames doped with $CBrF_3$ was the rather bright orange color, especially in the recombination region; a paler, but nevertheless distinct, green "halo" surrounded the region dominated by the orange emission. A typical spectrum is shown in Figure 79. The principal bands in this figure were due to CH and C_2. It was observed that, upon addition of $CBrF_3$, the effect was similar to that of changing from a fuel-lean flame to a fuel-rich flame; the relative intensities shifted in favor of the C_2 bands over the CH bands. The broad continuum with a maximum near 5950Å was due to the orange emission; the emitter was probably Br_2O. The green halo was attributed to C_2. The small bands between 4800Å and 5000Å (blue-green) are particularly worthy of mention. These band heads, with literature values of 4811Å, 4881Å, 4957Å, and 5036Å, were due to the $A \rightarrow X$ system of CuBr and were the result of the reaction of the hot (and reactive) products of combustion with the numerous copper-containing parts of the burner (cooling tube, silver solder, brass shell, etc.). (The CuBr bands are not particularly prominent in Figure 79; they were much more evident in other spectra.) Interaction of the hot gases with the copper-containing parts was minimized by painting these parts with a high temperature varnish; this considerably reduced the intensity of the CuBr bands.

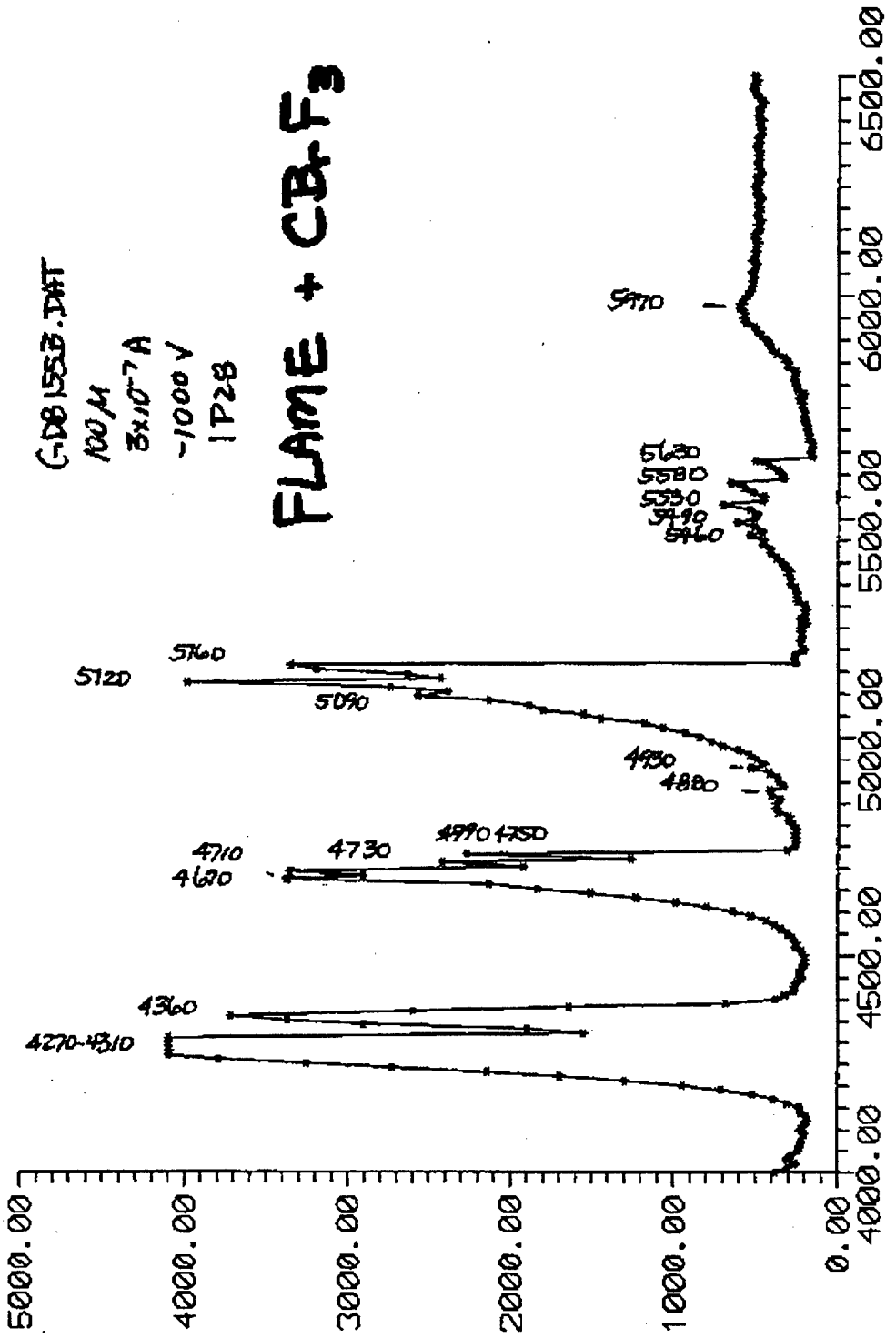

Figure 79. Visible Spectrum of a 30-torr CH4/O2/Ar Flame Inhibited by CBrF3.

Most of the spectra were recorded through a polymethylmethacrylate window, as the HF in the combustion products rapidly etched the glass window that was used for one experiment.

3. $NaHCO_3$- and $K_2C_2O_4$-Doped Flames

The $NaHCO_3$- and $K_2C_2O_4$-doped flames yielded the expected Na-D lines and the corresponding potassium lines, respectively. Since these very strong lines terminate in the ground states of the atoms, self absorption was anticipated at reasonable concentrations of the atoms in the flames. Accordingly, other emission lines were sought. For sodium, the $^2D \rightarrow {}^2P$ line at 5688Å was found to be an excellent candidate; the observed relative intensity of the 5688Å line was 0.004 of the intensity of the 5890Å line.

SECTION VI

FLAME-MOLECULAR BEAM-MASS SPECTROMETER—SAPPHIRE 2

A. GENERAL CHARACTERISTICS OF THE SAPPHIRE 2 INSTRUMENT

1. Introduction

Although a design was set for the Sapphire 2 instrument very early in the program, the design evolved as initial experiments were done and data were acquired. Indeed, as will be detailed toward the end of this section, it is likely that further significant performance enhancements could be achieved with relatively simple changes to the current design.

Two very different types of flame experiments are possible: (1) experiments in which only stable species are profiled, and (2) experiments in which radicals, transient species, and stable molecules are tracked. For the former of these two types of experiments, a quartz microprobe is used, and the sample is passed through a gas chromatograph-mass spectrometer (GC-MS). The Sapphire 2 instrument was designed for the latter of these two types of experiments. In these experiments it is desired to measure the concentrations of key flame radicals (especially the H atom and the OH radical) rather than infer their concentrations from measurements of the concentrations of stable species. Since flame radicals and other transient species are quite reactive, collisions with the walls or with other species are deleterious to the experiments proposed here.

It follows that the key to the performance of an instrument such as Sapphire 2 is the differential pressure chamber. If the pumping speed in this chamber were infinite, the path of the molecular beam would be collision free. This condition is, of course, unrealistic. For this reason, a great deal of attention was given to the pumping speed in the differential pressure chamber and to the ability of the molecular beam to transit this region unimpeded.

2. Initial Design

In the initial design, the diffusion pump was connected to the differential pressure chamber through two parallel bellows (2-in [5-cm] OD, 1.5-in [3.8-cm] ID), each with a 1.5-in

(3.8-cm) right-angle high vacuum valve. Initial characterization of the performance was a measurement of the pressure in the differential pressure chamber under a realistic flame chamber pressure of 30 torr. It was immediately apparent that the pressure in the differential pressure chamber was too high. At the observed pressure, the mean-free path of the species in the chamber was so short that virtually no molecules would be able to move from the quartz nozzle to the skimmer without encountering one or more collisions that would degrade the molecular beam.

3. Second Design

At this point, the initial design was abandoned; a 6-in (15.2-cm) gate valve (compatible with the 6-in [15.2-cm] diffusion pump) was acquired, the two right-angle valves were eliminated, and the two bellows were connected directly to a newly fabricated manifold on top of the gate valve. To aid in the characterization of the performance, an electromechanical (solenoid-operated) beam stop was installed. The flagged signal (the signal generated by the mass spectrometer with the beam stop in the path of the molecular beam) was compared with the unflagged signal (with the beam stop pulled out of the path of the molecular beam). These tests demonstrated that the pumping speed was still inadequate. With argon as a test gas at 30 torr in the flame chamber, a 5 percent difference was observed between the intensity of the flagged and unflagged beams. As expected, the performance improved a bit as the total pressure of argon gas in the flame chamber was reduced. Slightly better results were observed with helium as the test gas. At a helium pressure of 3 torr in the flame chamber, the flagged beam signal was about 10 percent less than the unflagged signal, indicating that at least some of the signal was due to He atoms "on the beam."

4. Third Design

The third design was a far more extensive departure from the original design. The differential pressure chamber was completely redesigned to replace the two bellows with a straight, 4-in (10.2-cm) OD stainless steel section. At the same time, the electromechanical beam stop was replaced with a 400-Hz tuning-fork chopper, the JB-5 Lock-In Amplifier was installed, and the Extrel C-50 was connected to the Vacuum Technologies, Inc., VTI, AEROSCAN 1600

Mass Spectrometer/RGA Interface. The following paragraphs describe the experiments performed with this configuration.

5. Modulation of the Mass Spectrometer Signal

The 400-Hz modulation of the signal generated by the mass spectrometer was observed at two slightly different places in the data processing electronic circuitry. First, the Extrel C-50 was modified by interrupting the circuit between the preamplifier and the buffer amplifier on the Electrometer/Ratemeter circuit board; two BNC connectors were mounted on the back panel of the Extrel C-50. In principle, a lock-in amplifier might be inserted in the circuit at this point. In practice, this modification also permitted the signal from the preamplifier to be observed directly with an oscilloscope.

Alternatively, the oscilloscope was connected to the AC OUT BNC connector on the back panel of the Extrel C-50. The signal at the AC OUT connector is also derived from the preamplifier, through a 1-μf capacitor. Thus, either the DC signal (with its AC component) or just the AC component could be observed. In practice, it made little difference with respect to the search for observable modulation of the signal. In both cases, it was very helpful to filter out the high frequency components with a 10-kHz bandwidth limiter (of the design suggested in the Extrel manual). The observed signal-to-noise ratio for argon as a test gas at typical flame pressures was about unity.

6. Performance Characterization

The performance of the Sapphire 2 instrument as a function of pressure of test gas in the flame chamber is described in detail in Section II. It suffices at this point to note that (1) the performance was limited by the size of the orifice in the quartz sampling nozzle and (2) significantly better data would have been obtained with a quartz sampling nozzle with a significantly smaller orifice. It was estimated that an improvement in the signal-to-noise ratio of a factor of 10 could have been achieved.

7. Temperature at the Center of the Burner

As noted elsewhere in this report, the temperature at the center of the burner was directly related to the heat extracted by the burner. Thus, the temperature at the center of the burner, like the heat extracted by the burner, was a measure of the degree of inhibition. However, it should not be forgotten that both of these measurements were also measures of the degree of stabilization of the flame by the burner, as well as measures of the degree of departure of the flame from adiabatic flame conditions (due to the perturbation by the cooled burner and to the proximity of the cooled copper disk above the flame in which the nozzle was mounted). It is, therefore, important to note that the temperature at the center of the burner was a function not only of the amount of inhibiting agent added to the flame, but also of the pressure in the flame chamber and of the position of the burner in the chamber.

The effect of changing the distance from the surface of the burner to the tip of the sampling nozzle, z, is illustrated by Figure 80. During the early part of the experiments ($z >$ 10 mm), it was observed that decreasing the distance between the burner surface and the nozzle tip resulted in a small but perceptible decrease in the temperature at the center of the burner. For distances less than about 10 mm, the effect was much more pronounced. The shape of the curves displayed in Figure 80 suggests that there were two zones of behavior, roughly separated at $z =$ 10 mm. Since this was approximately the interface between the luminous zone and the recombination zone, one is tempted to attribute the change in slope of the observed curves to a specific interaction with the flame. However, experimental data were too sparse to make a definite association of this sort. It will be of interest in future experiments with a longer nozzle to discover whether the steeper slope (at small distances between the burner surface and the nozzle tip) can be attributed to changes in flame structure, or whether the steeper slope is simply a reflection of the proximity of the cold copper plate.

The temperature at the center of the burner also was found to be a strong function of the pressure in the flame chamber (Figure 81). The explanation is straightforward: As the pressure in the flame chamber was decreased, the flame stretched and liftoff increased. This had the advantage of increasing the spatial resolution of the flame. The concomitant disadvantage was the more limited range over which experimental parameters could be varied. In particular, it

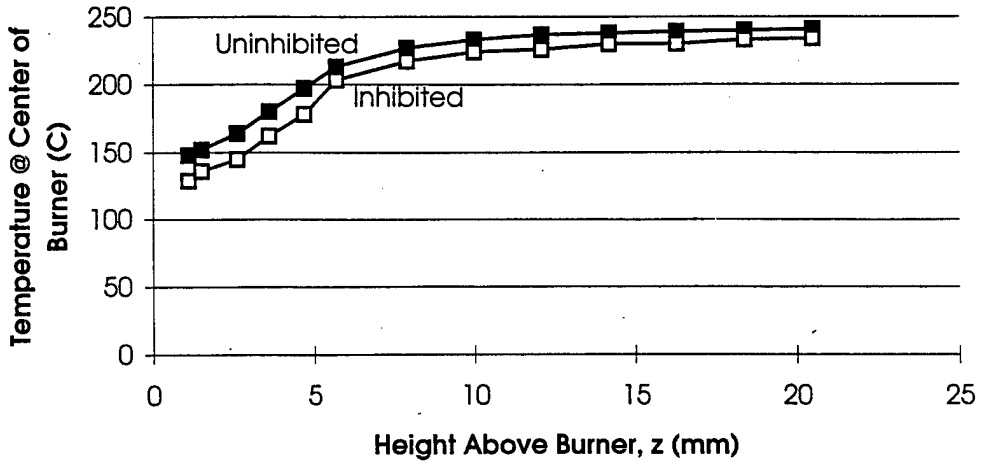

Figure 80. Effect of the Distance from the Tip of the Quartz Probe to the Surface of the Burner on the Temperature at the Center of the Burner.

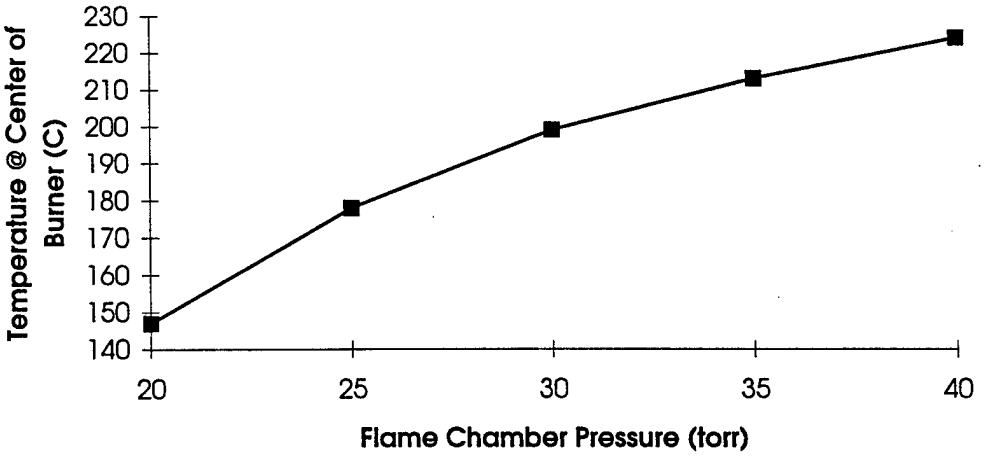

Figure 81. Effect of Flame Chamber Pressure on the Temperature at the Center of the Burner.

was found that, at low flame chamber pressures and small distances of the nozzle tip from the burner surface, addition of small amounts of $Fe(CO)_5$ resulted in extinguishment. Thus it was possible to probe the luminous zone with relative ease in flames sustained in the flame chamber at 40 torr, but with much more difficulty at a flame chamber pressure of 30 torr.

The one conclusion that should be drawn is that experiments with longer nozzles should be performed. Such experiments would determine whether the change in slope observed in Figure 80 was simply a function of distance between the burner surface and the cooled copper disk in which the nozzle was located, or a function of flame structure. It seems likely that, with longer nozzles, the net perturbation of the flame by the cooled copper disk would be reduced to the point that the flame could be probed to the surface of the burner. This was not possible with the configuration employed here.

B. FLAME EXPERIMENTS

1. Overview

The experiments of principal interest were those in which the flame was systematically profiled along the vertical (z) axis. Table 15 summarizes these experiments. Each experiment was begun with a separation of about 0.8 in (20 mm) between the surface of the burner and the tip of the quartz sampling nozzle. Several spectra were acquired for an uninhibited flame. $Fe(CO)_5$ was then added to the flame, and several additional spectra were acquired. At this point, the distance between the surface of the burner and the tip of the nozzle was reduced and the process was repeated. As the luminous zone was approached (about 0.2 in (5 mm) above the surface of the burner), smaller incremental changes in distance were made so that spatial resolution would be better in this region of the flame.

As detailed in Section II, the amount of $Fe(CO)_5$ added to the flame was controlled by a needle valve and found to be very reproducible. A suitable setting for the needle valve was determined by experience. It was quickly found that if too much $Fe(CO)_5$ was added to the flame, the nozzle was easily plugged. A satisfactory flow rate of $Fe(CO)_5$ yielded highly colored flames. These flames were not as bright as those typically observed in the Sapphire 0

TABLE 15. SAPPHIRE 2 EXPERIMENTS WITH $Fe(CO)_5$-INHIBITED FLAMES.

Experiment	Flame chamber pressure, torr	ϕ	Notes
C133_Z	40 torr	0.94	
C136_Z	30	1.00	
C143_Z	40	1.00	Unexplained decrease in intensities
C146_Z	35	1.00	Terminated early
C148_Z	35	1.00	
C151_Z	30	1.00	Terminated early

experiments; however, and there was no visual evidence of particulate formation. As noted in Section II, the mole fraction of Fe $(CO)_5$ in the premixed gases was estimated photometrically to be 0.0005 (0.05% by volume). With this concentration of $Fe(CO)_5$, it was found that the inhibited flame could be sustained for extended periods of time (hours) without appreciable changes in the intensities of the peaks in the mass spectra due to plugging of the nozzle.

During most of the experiments, a long-term variation in the apparent sensitivity of detection was observed. The origin of this variation was not known with certainty, and the variation was not monotonic. (Gradual plugging of the nozzle probably would have led to a monotonic increase in signal size; see the discussion of Sapphire 2 performance characterization, above.) To compensate for these slow changes in apparent sensitivity, the intensity of the argon (m/e = 40) signal was taken as the baseline, and all data were normalized to the argon signal.

2. Experiment C133_Z: Pressure = 40 torr, $\phi = 0.94$

The results of experiment C133_Z were typical. Figures 82 and 83 show the overall profiles of the principal species (CH_4, O_2, CO, CO_2, H_2O, and O atoms). The peak at m/e = 16 amu included both the CH_4 molecule and •O• atoms; experiments that would have distinguished between these two species were not performed. However, all the data are consistent with assignment of CH_4 as the dominant species in the initiation and reaction zones and of •O• atoms as the dominant species at m/e = 16 amu in the recombination zone. Data for

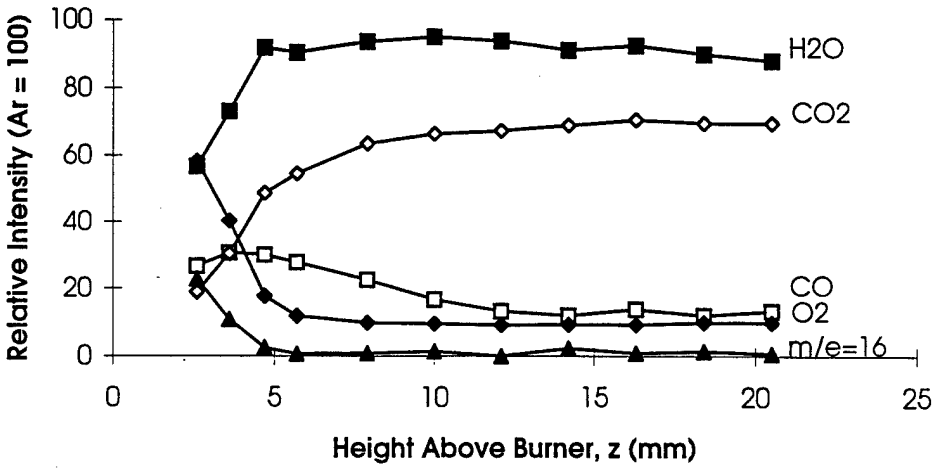

Figure 82. Experiment C133_Z: 40 torr, $\phi = 0.94$—Principal Species in the Uninhibited Flame as a Function of Distance of Quartz Probe from Burner.

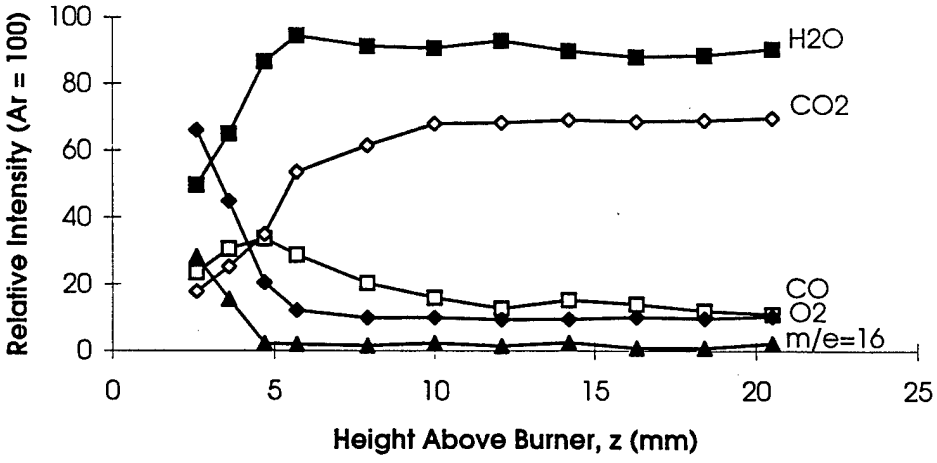

Figure 83. Experiment C133_Z: 40 torr, $\phi = 0.94$—Principal Species in the Inhibited Flame as a Function of Distance of Quartz Probe from Burner.

several minor species (•OH, •CH_3, CH_2, and •CH) were also acquired. Data for H_2 were not acquired; it is uncertain whether reliable data could have been obtained for H.

In this experiment, it was possible to penetrate into but not reach below the luminous zone; with the nozzle at the interface between the luminous zone and the initiation zone, the addition of $Fe(CO)_5$ to the flame caused extinguishment. As noted above, this no doubt reflects the fact that, at the relatively short distance between the burner surface and the copper plate (when the nozzle was at this location), the flame was quite close to extinguishment even before the $Fe(CO)_5$ was added. It is evident from the data that the interface between the recombination zone and the luminous zone was located about 0.2 in (5 mm) above the surface of the burner; the luminous zone was estimated to be slightly more than 0.08 in (2 mm) thick.

To obtain a value for the relative concentration of CH_4 in the flame, contributions at m/e = 16 amu due to fragmentation of O_2, CO_2, H_2O, and CO were subtracted using literature values for the fragmentation ratios (Reference 13). In the future, fragmentation ratios will be determined for the Sapphire 2 instrument and used in these calculations. However, the fact that the intensity of the m/e = 16 peak decreased dramatically in the reaction zone, and then remained essentially constant throughout the recombination zone, attests to the suitability of the use of literature values for the purposes of this preliminary investigation. The results for oxygen (m/e = 32) also were in accord with expectations. For this fuel-lean flame, the excess oxygen was essentially constant beyond the luminous zone.

In a similar manner, the contribution due to fragmentation of CO_2 was subtracted from the m/e = 28 amu peak, to obtain a value for the CO molecule. As expected, the CO intensities peaked in the luminous zone, and then decayed slowly in the recombination zone. The expected concomitant growth of the CO_2 intensities can also be seen in the figures. The slow oxidation of CO is well known. It is important to note that addition of $Fe(CO)_5$ did not make a dramatic impact on the behavior of the CO peak. Two comments are in order. First, the actual amount of CO contributed by decomposition of the $Fe(CO)_5$ was negligible with respect to the amount generated by the uninhibited flame. Second, although it is known that Fe atoms catalyze the oxidation of CO (Reference 14), there was no obvious evidence of this in the data presented here.

Figure 84 illustrates, at each distance between the burner surface and the nozzle tip, the changes in intensities resulting from addition of $Fe(CO)_5$. Note that, as the luminous zone was approached (at about 0.2 in (5 mm)), the concentrations of O_2 and CH_4 were larger in the inhibited flame than in the uninhibited flame, and the concentrations of CO_2 and H_2O were smaller. Given the uncertainty in the data, it was difficult to establish a trend for the CO. The rather random appearance of differences in the recombination zone (> 0.4 in (10 mm)) reflected the scatter in the data because the data were not "massaged" to remove the data points that did not conform to obvious preconceived notions.

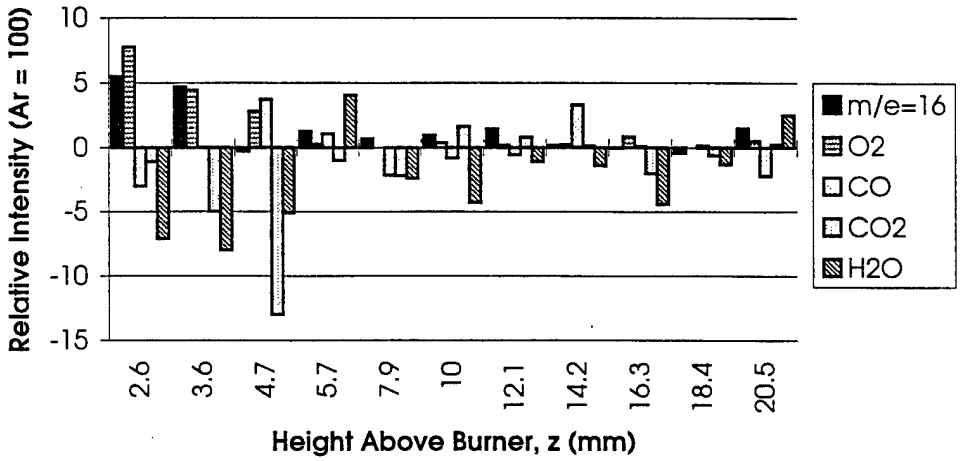

Figure 84. Experiment C133_Z: 40 torr, $\phi = 0.94$—Difference Between Intensities of Peaks as a Function of Distance of Quartz Probe from Burner.

Figures 85 and 86 illustrate the effect of adding $Fe(CO)_5$. From these figures, it is obvious that the net effect of addition of $Fe(CO)_5$ was to shift the combustion downstream. It can be estimated from these figures that the shift was on the order of 0.016 in (0.4 mm).

Selected data related to fragmentation ratios are displayed in Figures 87, 88, and 89. Figure 87 presents the data for the ratio of the m/e = 15 amu peak to the m/e = 16 peak; in a mass spectrum of pure methane, this ratio would be the ratio of the $\bullet CH_3$ fragment to the CH_4 parent molecule. It is evident from this figure that the $\bullet CH_3/CH_4$ ratio (15 amu/16 amu) was meaningful only for the smaller values of z (i.e., in the reaction zone), where the concentration of

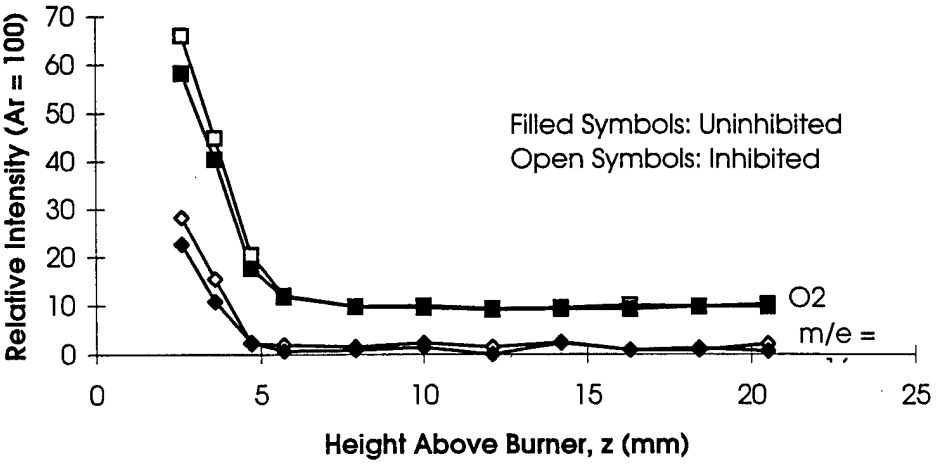

Figure 85. Experiment C133_Z: 40 torr, $\phi = 0.94$. Shift of m/e = 16 and O_2 Peaks as the Result of Inhibition by $Fe(CO)_5$.

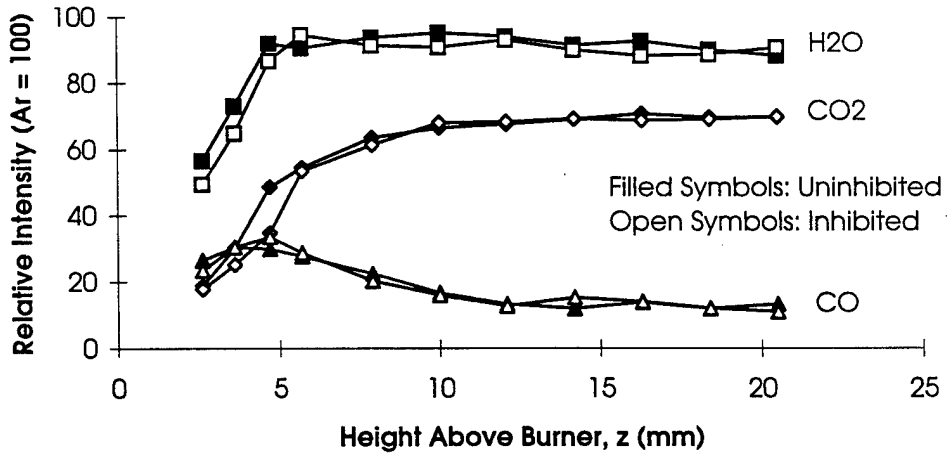

Figure 86. Experiment C133_Z: 40 torr, $\phi = 0.94$—Shift of CO_2, CO, and H_2O Peaks as the Result of Inhibition by $Fe(CO)_5$.

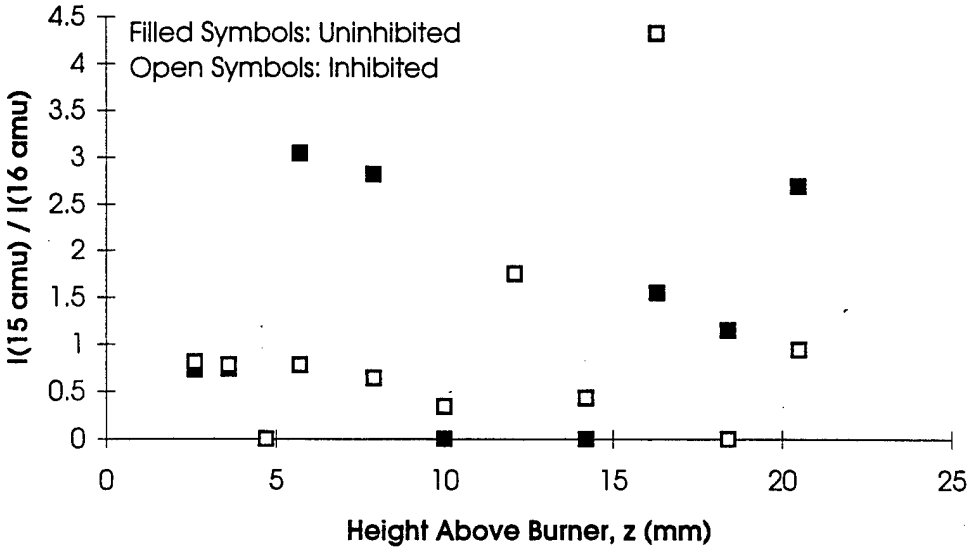

Figure 87. Experiment C133_Z: 40 torr, $\phi = 0.94$—Apparent Fragmentation Ratios (15 amu/16 amu).

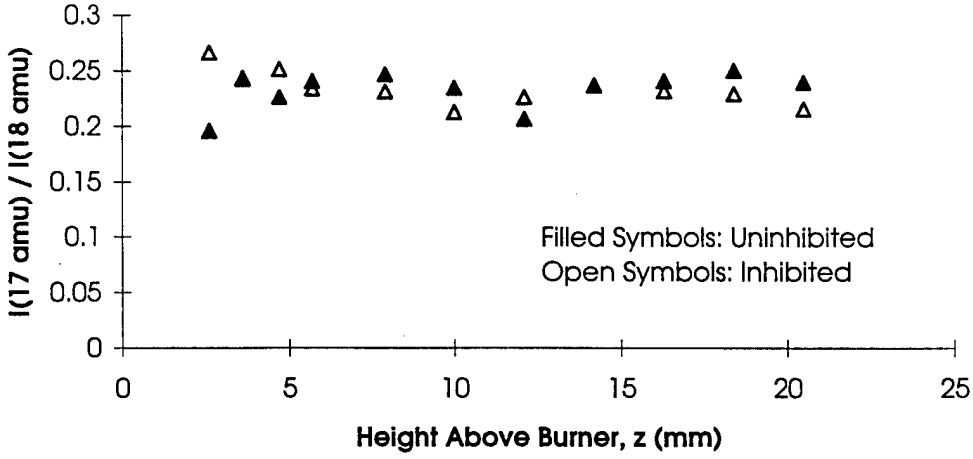

Figure 88. Experiment C133_Z: 40 torr, $\phi = 0.94$—Apparent Fragmentation Ratios (17 amu/18 amu).

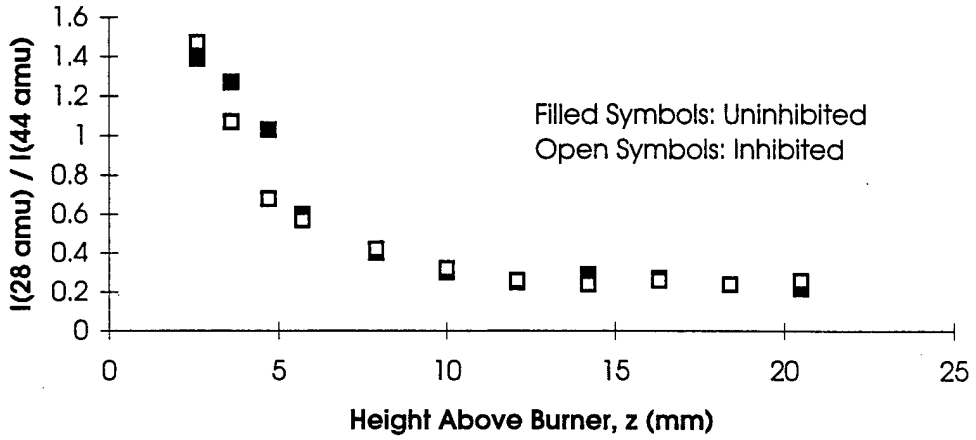

Figure 89. Experiment C133_Z: 40 torr, $\phi = 0.94$—Apparent Fragmentation Ratios (28 amu/44 amu).

CH_4 was significant. The values of the ratio for the two smallest values of z were 0.73 and 0.81, compared with a literature value of 0.856 (Reference 13). Values of the $\bullet CH_3/CH_4$ ratio at other values of z were essentially meaningless because of (1) the nearly zero value of the CH_4 peak and (2) the dominance of the •O• atom at these other values of z. It can be concluded that, in the recombination zone, the intensity of the CH_3 peak is not related to the concentration of the parent molecule, and is, therefore, a reasonable measure of the concentration of $\bullet CH_3$ radicals in the flame.

Figure 88 presents the data for the ratio of the m/e = 17 amu peak to the m/e = 18 peak; in a mass spectrum of pure water, this ratio would be the ratio of the •OH fragment to the H_2O parent molecule. The $\bullet OH/H_2O$ ratio was effectively constant, and very nearly equal to the literature value of 0.211 (Reference 13). In fact, most of the experimental values were larger than the literature value, suggesting that some flame-generated OH was indeed observed. However, the large uncertainties in the data, in conjunction with the relatively large magnitude of the m/e = 17 peak due to fragmentation of H_2O, precluded an estimate of the amount of •OH generated by the flame. Since a measure of the •OH concentration is crucial to the understanding of the interaction of $Fe(CO)_5$ with the flame, two other experiments should be considered. In one

experiment, the ionizing voltage should be reduced to the point that fragmentation of H_2O makes only a minor contribution to the overall m/e = 17 peak; this is a difficult experiment, because of the significantly reduced intensities of all peaks at the smaller ionizing voltage. In the second experiment, [•OH] should be measured spectroscopically in absorption, much as in the work of Biordi et al. (Reference 15).

Figure 89 presents the data for the ratio of the m/e = 28 amu peak to the m/e = 44 peak; in a mass spectrum of pure carbon dioxide, this ratio would be the ratio of the CO fragment to the CO_2 parent molecule. The ratio of CO to CO_2 varied with location in the flame and clearly reflected the presence of both species in the flame. If the observed m/e = 28 peak had been simply due to fragmentation of CO_2, the expected ratio would have been about 0.066 (Reference 13). Note particularly that the CO/CO_2 ratio was quite large in the reaction zone (z = 3 mm to z = 5 mm) and decayed only slowly with increasing z. This is evidence of the slow oxidation of CO to CO_2.

3. Experiment C136_Z: Pressure = 30 torr, ϕ = 1.00

Data from Experiment C136_Z are presented in Figures 90 through 96. While these data agree very well with those acquired in Experiment C133_Z, some details are worth examining. First, it should be noted that flameout was experienced at a greater distance of the sampling nozzle from the burner surface. This is directly attributable to the fact that the flame chamber pressure in Experiment C136_Z was 10 torr lower than that in Experiment C133_Z. This fact also accounts for the more gradual changes in intensities as a function of z. In addition, the downstream shift of the combustion was estimated to be 0.03 in (0.8 mm), about twice that for Experiment C133_Z. Second, since Experiment C136_Z was a stoichiometric flame (ϕ = 1.00) while Experiment C133_Z was oxygen-rich, the m/e = 32 peak was less intense in Experiment C136_Z. Third, with the somewhat better spatial resolution in this experiment, it can be said with some confidence that the CO concentration seemed to be tracking the CO_2 concentration, suggesting that the overall oxidation of carbon followed a single trend, whether or not $Fe(CO)_5$ was added.

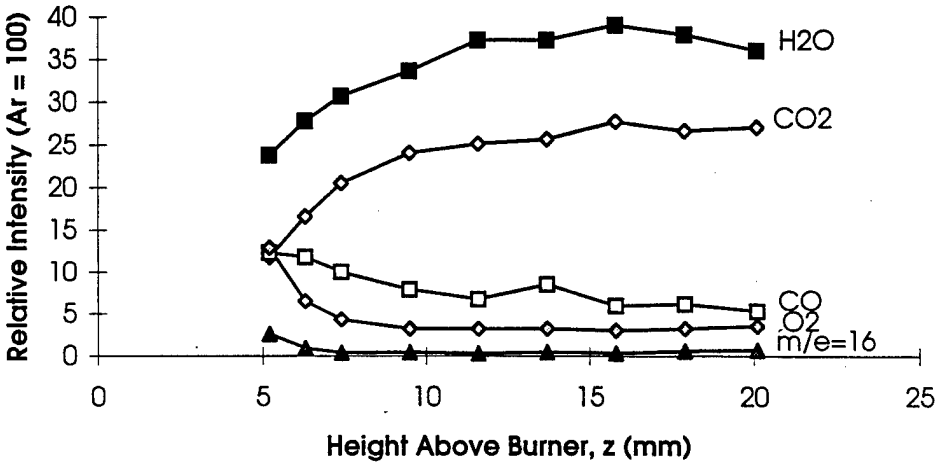

Figure 90. Experiment C136_Z: 30 torr, ϕ = 1.00—Principal Species in Uninhibited Flame as a Function of Distance of Quartz Probe from Burner.

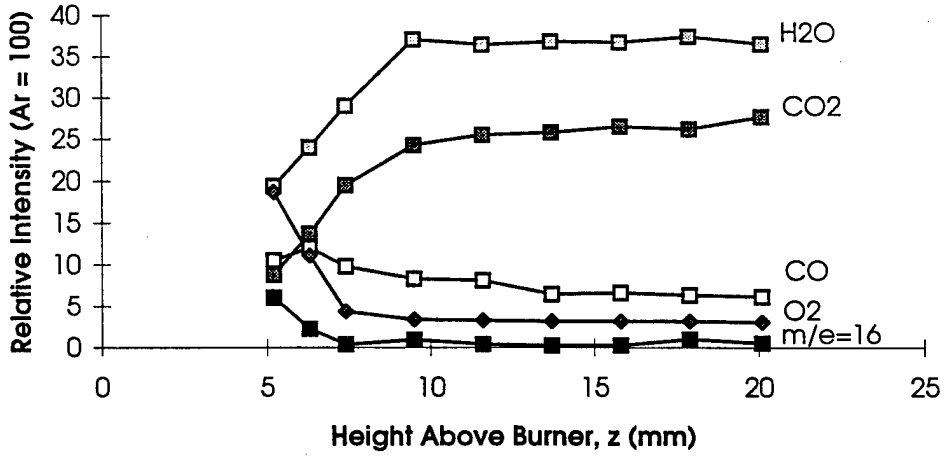

Figure 91. Experiment C136_Z: 30 torr, ϕ = 1.00—Principal Species in Inhibited Flame as a Function of Distance of Quartz Probe from Burner.

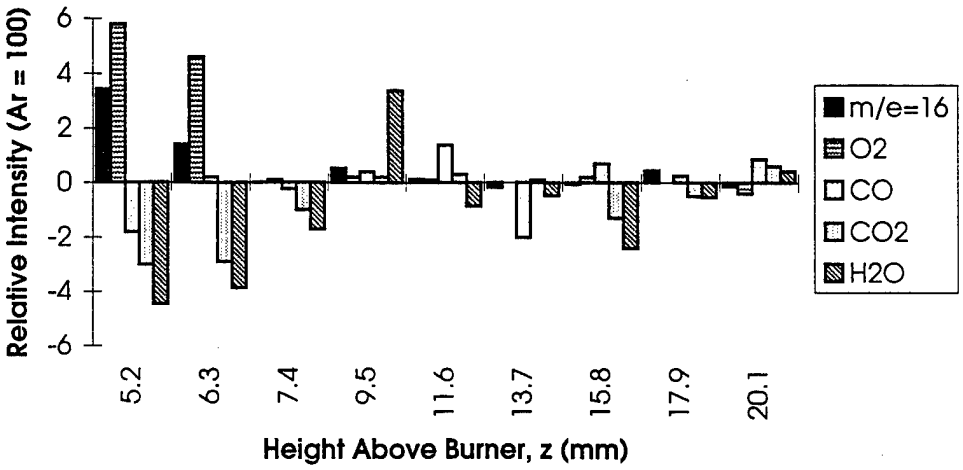

Figure 92. Experiment C136_Z: 30 torr, ϕ = 1.00—Difference between Intensities of Peaks as a Function of Distance of Quartz Probe from Burner.

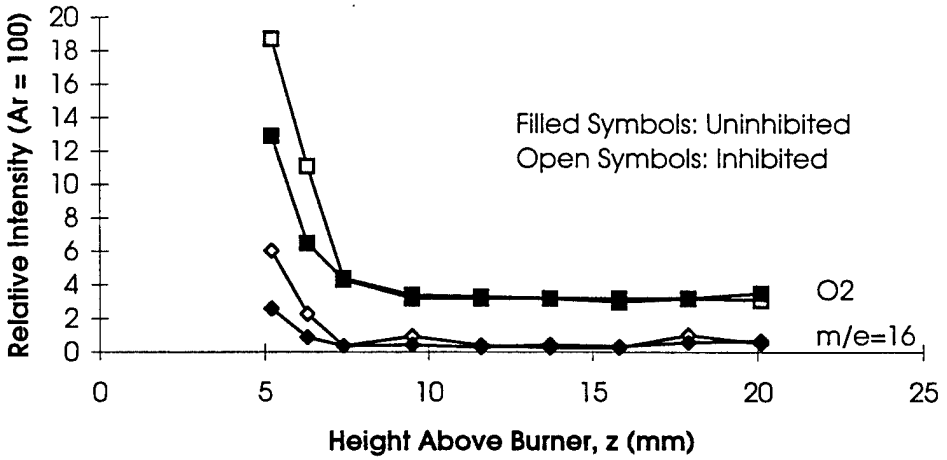

Figure 93. Experiment C136_Z: 30 torr, ϕ = 1.00—Shift of m/e = 16 amu and O_2 Peaks as the Result of Inhibition by $Fe(CO)_5$.

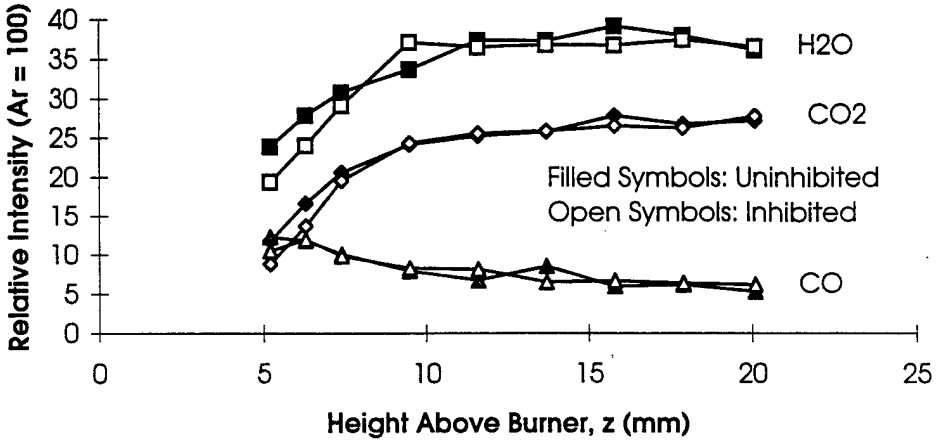

Figure 94. Experiment C136_Z: 30 torr, $\phi = 1.00$—Shift of CO_2, CO, and H_2O Peaks as the Result of Inhibition by $Fe(CO)_5$.

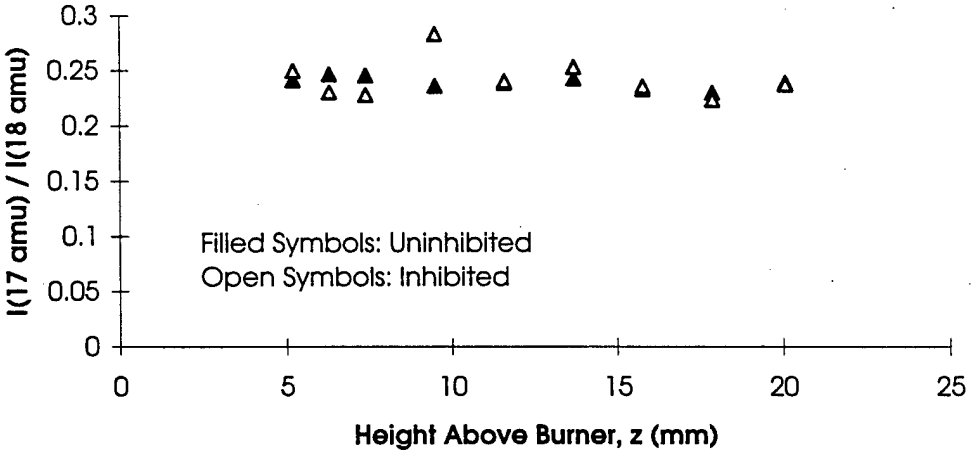

Figure 95. Experiment C136_Z: 30 torr, $\phi = 1.00$—Apparent Fragmentation Ratios (17 amu/18 amu).

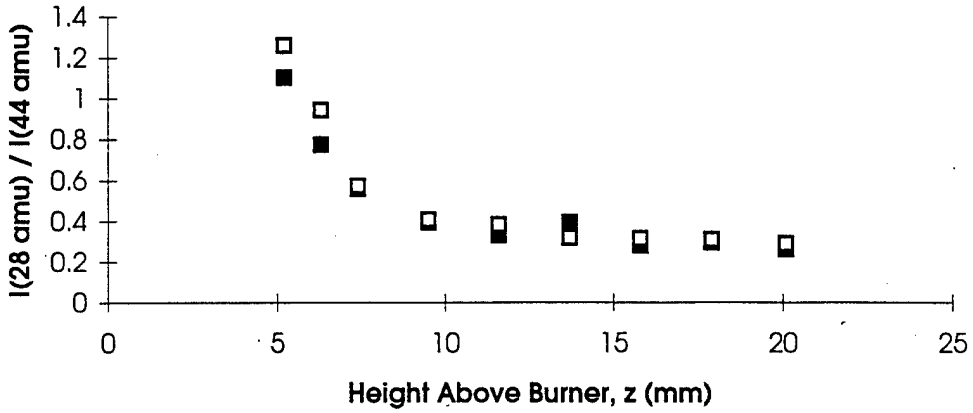

Figure 96. Experiment C136_Z: 30 torr, $\phi = 1.00$—Apparent Fragmentation Ratios (28 amu/44 amu).

4. Experiment C143_Z: Pressure = 40 torr, $\phi = 1.00$

Data from Experiment C143_Z are presented in Figures 97 through 104. Here again, the results were very similar to those reported in the two previous experiments. It is noted with interest that the luminous zone was completely penetrated in this experiment, and data were obtained near the bottom of the luminous zone. This is particularly evident from examination of Figures 99 through 101. While the maximum observable effect of the addition of $Fe(CO)_5$ occurred at about z = 4 mm, data were accumulated to a separation of just over 0.04 in (1 mm). There is one unexplained feature of Experiment C143_Z. As the experiment progressed from larger to smaller values of z, it was observed that the intensities of the m/e = 18 (H_2O) and m/e = 44 (CO_2) peaks increased. This was not expected and was not observed in other experiments. The data point at 0.31 in (8 mm) is considered to be "bad"; these data were taken during a period of time in which the instrument was experiencing an unexplained change in sensitivity.

5. Experiment C148_Z: Pressure = 35 torr, $\phi = 1.00$

Data from Experiment C148_Z are presented in Figures 105 through 111. It is immediately apparent that these data are much like the data of the preceding experiments. The estimated downstream shift of the reaction zone was about 0.16 in (4 mm).

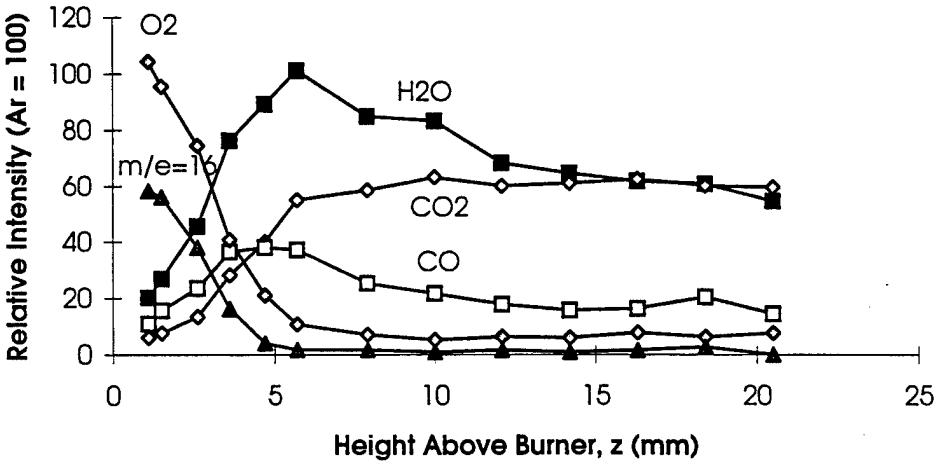

Figure 97. Experiment C143_Z: 40 torr, ϕ = 1.00—Principal Species in Uninhibited Flame as a Function of Distance of Quartz Probe from Burner.

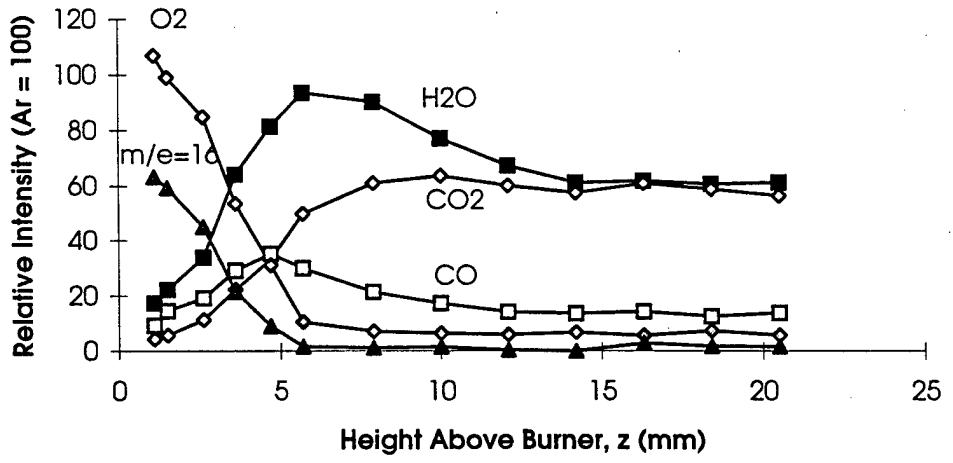

Figure 98. Experiment C143_Z: 40 torr, ϕ = 1.00—Principal Species in Inhibited Flame as a Function of Distance of Quartz Probe from Burner.

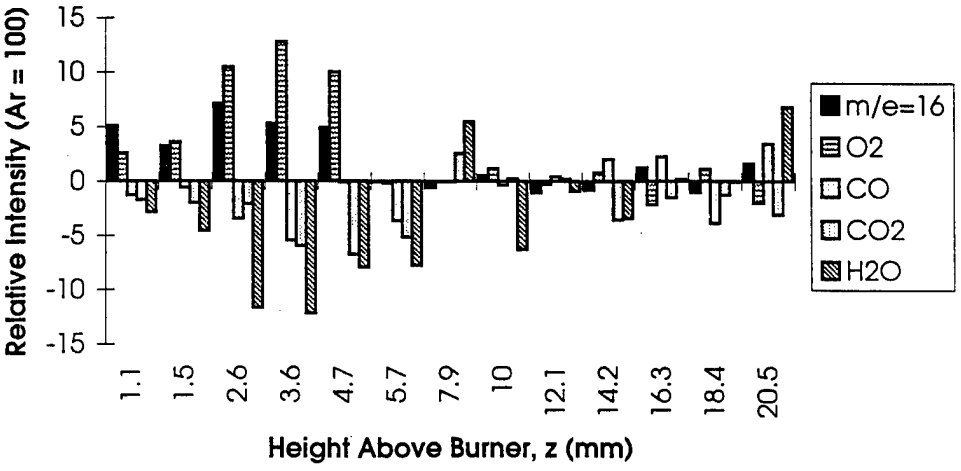

Figure 99. Experiment C143_Z: 40 torr, $\phi = 1.00$—Difference between Intensities of Peaks as a Function of Distance of Quartz Probe from Burner.

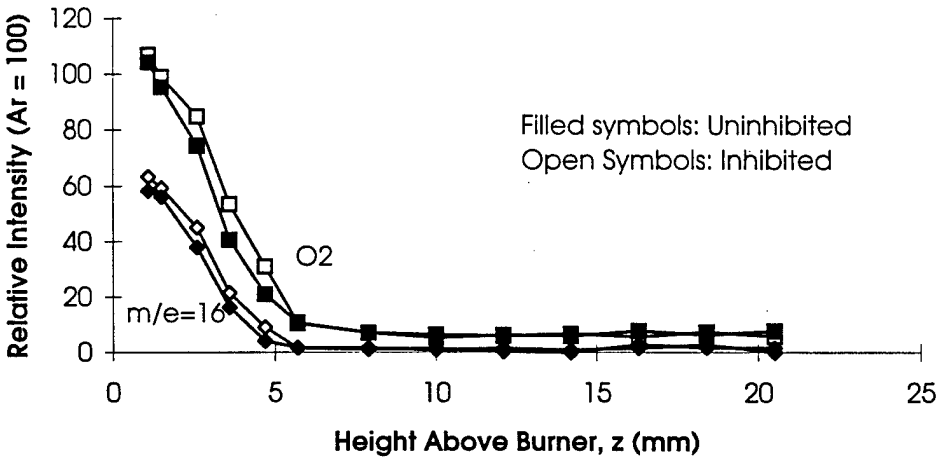

Figure 100. Experiment C143_Z: 40 torr, $\phi = 1.00$—Shift of m/e = 16 and O_2 Peaks as the Result of Inhibition by $Fe(CO)_5$.

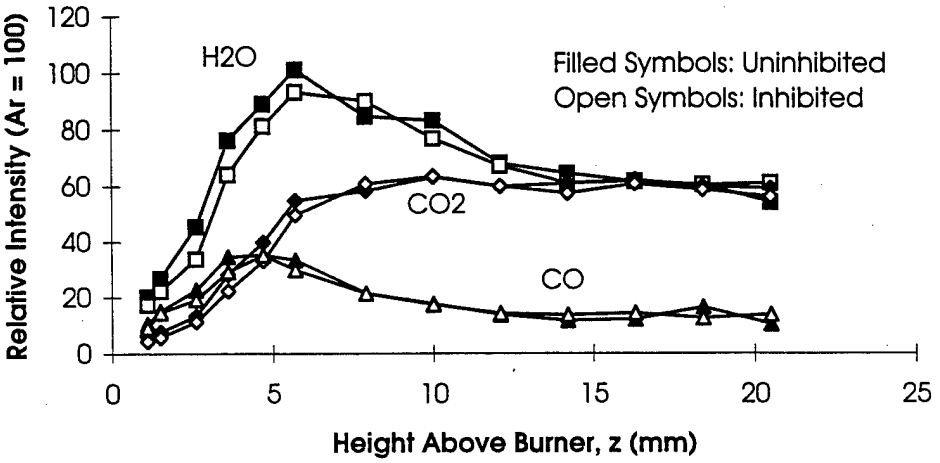

Figure 101. Experiment C143_Z: 40 torr, $\phi = 1.00$—Shift of CO_2, CO, and H_2O Peaks as the Result of Inhibition by $Fe(CO)_5$.

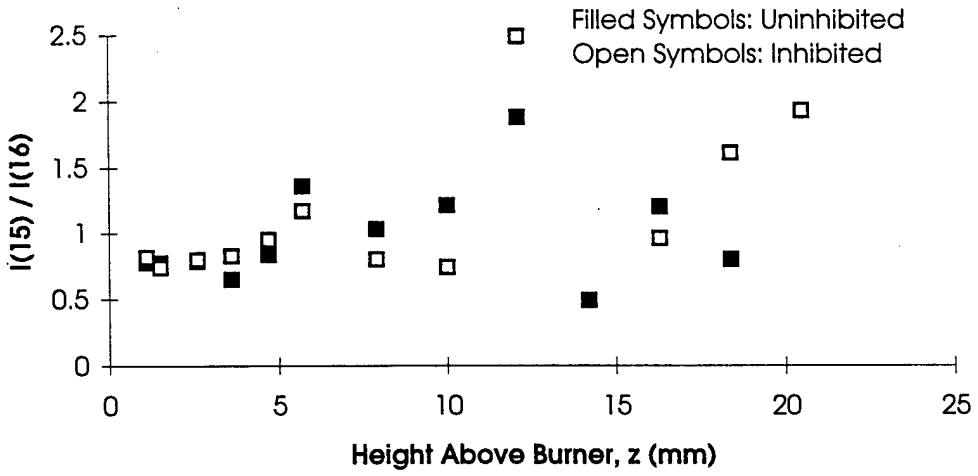

Figure 102. Experiment C143_Z: 40 torr, $\phi = 1.00$—Apparent Fragmentation Ratios (15 amu/16 amu).

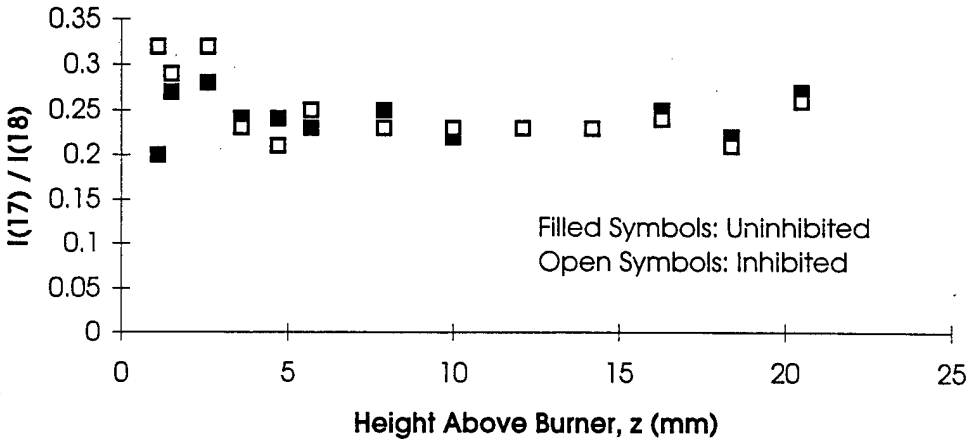

Figure 103. Experiment C143_Z: 40 torr, ϕ = 1.00—Apparent Fragmentation Ratios (17 amu/18 amu).

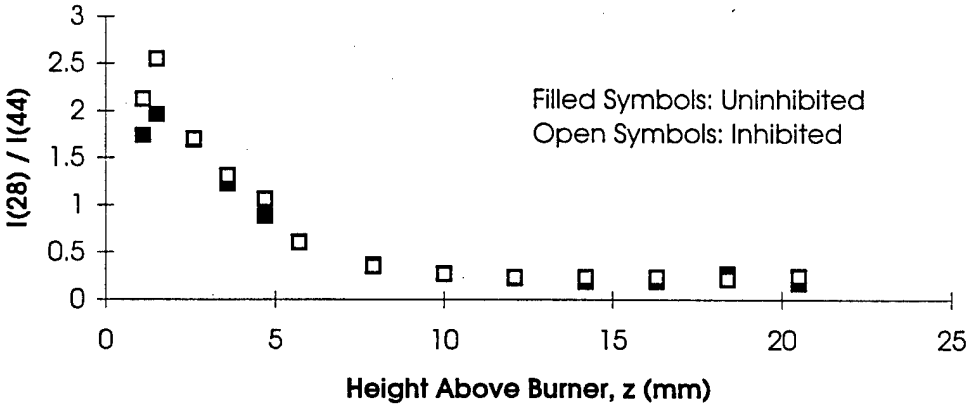

Figure 104. Experiment C143_Z: 40 torr, ϕ = 1.00—Apparent Fragmentation Ratios (28 amu/44 amu).

C. SUMMARY AND IMPLICATIONS

The most striking result of the work to date is the fact that inhibition by $Fe(CO)_5$ parallels in every respect that observed by Biordi et al. with $CBrF_3$ in a similar set of experiments (References 15 and 16). In both cases, the most dramatic changes were observed in the vicinity of the reaction zone. Addition of the inhibiting agent resulted in a significant increase in the concentrations of reactants (CH_4 and O_2) and a corresponding decrease in the concentrations of products (CO, CO_2, and H_2O). In essence the initiation zone was stretched and the first visible evidence of combustion (the luminous zone) was shifted downstream. Even the magnitude of the shifts observed in the present work was similar to those observed by Biordi and coworkers.

The mechanism of flame inhibition in flames seeded with iron appears to involve the catalytic recombination of flame radicals (most likely, H atoms) in the same manner as Br atoms catalyze the recombination of H atoms in flames inhibited by $CBrF_3$. While the results presented here are not conclusive in this regard, the present results permit comparison with detailed models of proposed inhibition mechanisms. This comparison will go a long way toward clarifying current questions concerning the mechanism of inhibition by iron-containing compounds.

It is immediately apparent that the experiments completed to date have added valuable insights into the inhibition of flames by iron-containing compounds, and that much work remains to be done. Recommended additional work includes the following:

(1) Measurement of the concentration of H_2 as a function of z

(2) Measurement of the concentration of OH as a function of z. These data can then be compared with the results published by the Göttingen group in the mid-1950s. This may be possible with the current instrument, or may require an optical technique.

(3) The effect of changing the concentration of $Fe(CO)_5$ should be studied (within the rather narrow range permitted by the limitations imposed by plugging of the nozzle at higher concentrations of $Fe(CO)_5$).

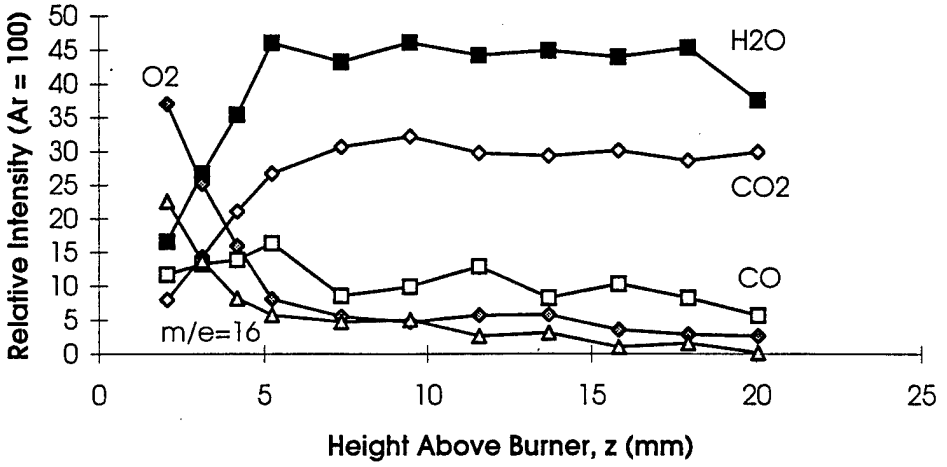

Figure 105. Experiment C148_Z: 35 torr, ϕ = 1.00—Stable Molecules in Uninhibited Flame as a Function of Distance of Quartz Probe from Burner.

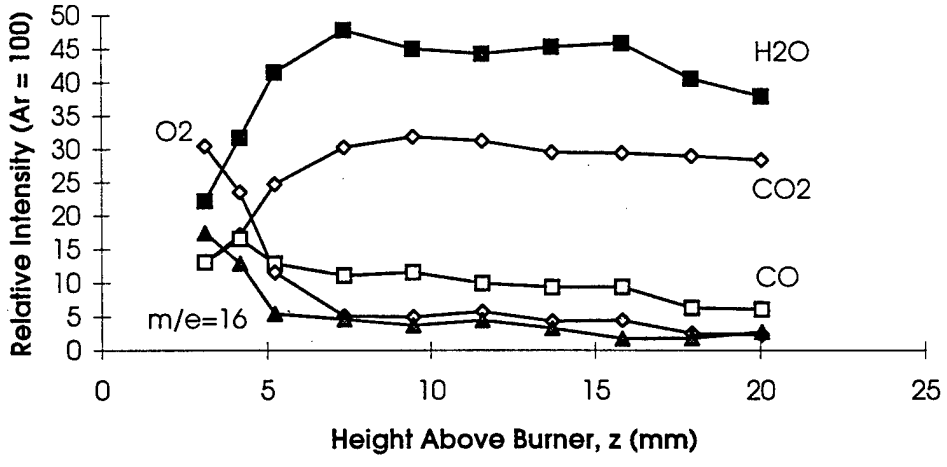

Figure 106. Experiment C148_Z: 35 torr, ϕ = 1.00—Stable Molecules in Inhibited Flame as a Function of Distance of Quartz Probe from Burner.

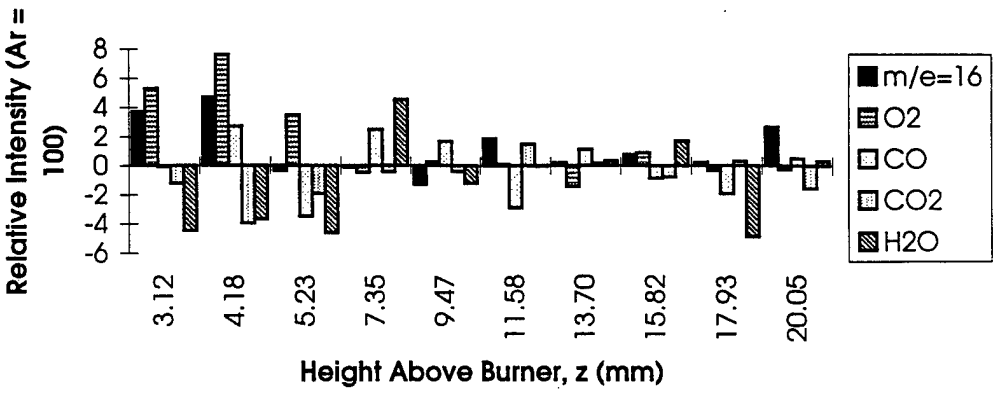

Figure 107. Experiment C148_Z: 35 torr, $\phi = 1.00$—Difference between Intensities of Peaks as a Function of Distance of Quartz Probe from Burner.

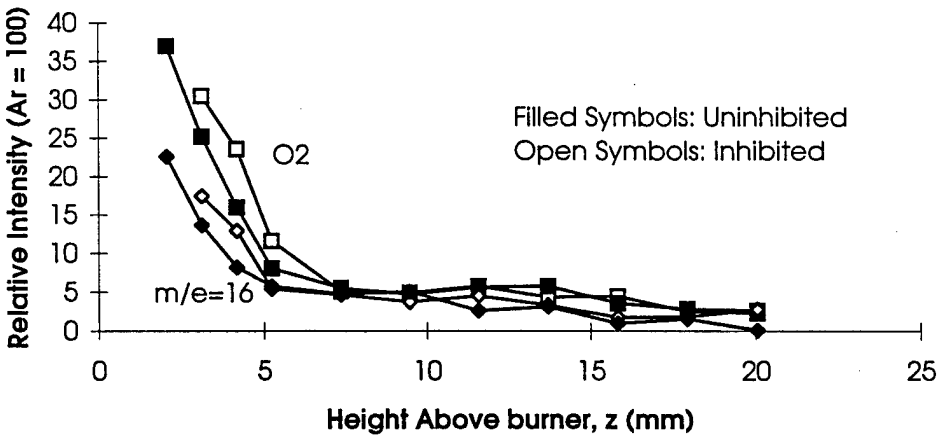

Figure 108. Experiment C148_Z: 35 torr, $\phi = 1.00$—Shift of CH_4 and O_2 Peaks as the Result of Inhibition by $Fe(CO)_5$.

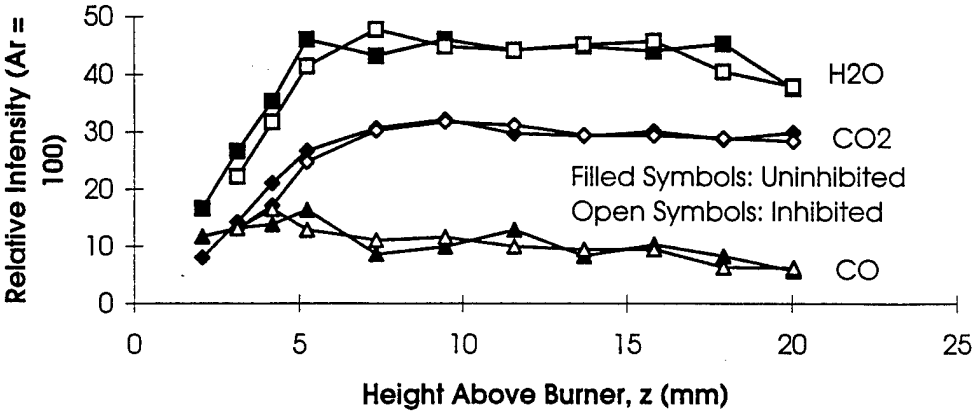

Figure 109. Experiment C148_Z: 35 torr, $\phi = 1.00$—Shift of CO_2, CO, and H_2O Peaks as the Result of Inhibition by $Fe(CO)_5$.

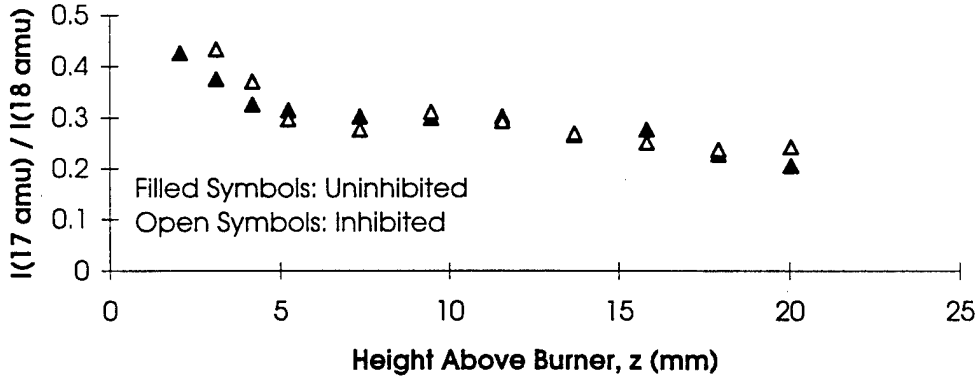

Figure 110. Experiment C148_Z: 35 torr, $\phi = 1.00$—Apparent Fragmentation Ratios (17 amu/18 amu)

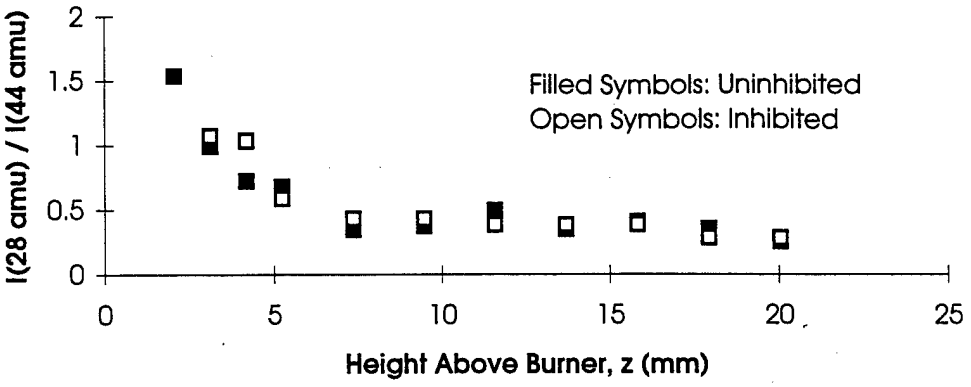

Figure 111. Experiment C148_Z: 35 torr, $\phi = 1.00$—Apparent Fragmentation Ratios (28 amu/44 amu)

(4) Data acquisition must be improved to the degree that concentrations of important radicals can be determined with confidence.

(5) If direct observation of key iron-containing species cannot be achieved, consideration must be given to optical absorption and/or laser-induced fluorescence experiments.

(6) The flames must be studied as a function of ϕ, the fuel/oxygen equivalence ratio.

SECTION VII
IRON COMPOUNDS

A. INTRODUCTION

The 11 September 1961 issue of the *Chemical and Engineering News*, in the article entitled "Iron Carbonyl Found to Be Powerful Flame Inhibitor" (Reference 17), reported the discovery, at the University of Göttingen, Germany, of the flame inhibition properties of iron pentacarbonyl. A flurry of activity in several laboratories over the next decade and a half was followed by a relatively quiet period. However, with the search for replacements for the halons, there has been a resurgence of interest in the transition metal compounds, especially compounds containing iron.

B. REVIEW OF THE LITERATURE ON IRON PENTACARBONYL

1. Work at Göttingen, Started in the Mid-1950s

The papers cited here give some details about the experiments, but dwell mostly on the results (References 9, 10, 17, and 18). Premixed flames were studied at atmospheric pressure with a stainless steel nozzle burner; the height of the tip of the luminous cone was used as a measure of the burning velocity. Flame speeds were measured for several different flames (methane-air, methane-oxygen, hydrogen-air, hydrogen-oxygen, acetylene-oxygen, ethane-oxygen, benzene-air, *n*-hexane-air), both at atmospheric pressure and at reduced pressures. For the most part, stoichiometric flames were investigated, although small excursions were occasionally made to slightly fuel-rich and fuel-lean flames. The influence of pressure was studied in considerable detail, especially for the methane-air flame. The concentrations of Fe atoms and of the OH radicals as a function of location in the flame were measured by absorption spectroscopy. Emission spectroscopy was used to follow •OH, •CH, C_2, FeO, and Fe. Key results from these four papers are listed here.

(1) Iron pentacarbonyl ($Fe(CO)_5$) is much more effective than Br_2 in reducing the burning velocity of typical flames. Addition of 0.03 percent (mol) $Fe(CO)_5$ reduced the flame

speed of a stoichiometric *n*-hexane-air flame by 40 percent. $Fe(CO)_5$ was less effective (though still much more effective than Br_2) in reducing the flame speed of a hydrogen (37 percent)-air flame; for this latter flame, addition of 0.35 percent (mol) $Fe(CO)_5$ resulted in a 60 percent reduction in the flame speed. In sharp contrast, while the $Fe(CO)_5$ was more effective in the *n*-hexane-air flame than in the hydrogen-air flame, the reverse was true for Br_2.

(2) $Fe(CO)_5$ is more effective in stoichiometric methane-air flames than in the hotter stoichiometric methane-oxygen flames. Addition of 0.01 percent (mol) $Fe(CO)_5$ to an atmospheric methane-air flame resulted in a 25 percent reduction in burning velocity, while addition of 0.035 percent (mol) to an atmospheric methane-oxygen flame yielded only an 8 percent reduction in flame speed.

(3) $Fe(CO)_5$ is less effective in low pressure flames than in atmospheric flames. For stoichiometric methane-air flames at one atmosphere, a 25 percent reduction in burning velocity was achieved at 0.01 percent (mol) $Fe(CO)_5$, while a similar reduction in burning velocity required 0.03 percent (mol) $Fe(CO)_5$ at 0.5 atm.

(4) When the [•OH] was measured in a flat, 60-torr, stoichiometric, methane-air flame, it was found that the addition of $Fe(CO)_5$ shifted the point of maximum absorbance (about 0.4 in [1 cm] above the burner) slightly away from the burner and did not change appreciably the value of [•OH] at the point of maximum absorbance. However, as measurements were made further and further from the burner surface, appreciable differences in [•OH] were found; at a distance of 2.4 in (6 cm) above the burner, addition of 0.01 percent $Fe(CO)_5$ resulted in a three-fold reduction in [•OH].

(5) The peak in the Fe emission corresponded to the peaks in •CH and C_2 emissions. However, the [Fe] bore little correspondence to the Fe emission profile; [Fe] peaked just above the reaction zone (about 0.4 in [1 cm] above the burner) and then fell only slowly with increasing distance from the burner.

(6) The intensity of the FeO emission peaked near the top of the reaction zone, fell for a short distance, and then recovered to a second maximum at about 1.3 in (3.3 cm) above the burner (well into the recombination zone).

Although the authors declined to speculate as to the details of the inhibition mechanism, they suggested that the removal of •OH radicals may play an important role.

2. Induction Time of Acetylene-Oxygen Reactions

In this work by Erhard (Reference 19), acetylene-oxygen mixtures were initiated photolytically with amylnitrate as a sensitizer. The induction time (the time between ignition and observation of luminosity, and a measure of the initial rate of buildup of radicals) was measured as a function of the concentrations of three volatile metal compounds: $Ni(CO)_4$, $Cr(CO)_6$, and $Fe(CO)_5$. For the Ni and Cr compounds, it was shown that an increase in the concentration of volatile metal compound resulted in a decrease in induction time (i.e., an increase in the initial rate of radical generation). The situation was more complex for $Fe(CO)_5$.

(1) For strongly initiated (high photon flux) mixtures, the addition of $Fe(CO)_5$ resulted in a decrease in induction time, as in the case of the other metals studied.

(2) For weakly initiated mixtures, the situation was more complicated. At concentrations below about 0.2 percent (mol), $Fe(CO)_5$ behaved like the other volatile metal compounds; an increase in metal concentration resulted in a decrease in induction time.

(3) However, there was a discontinuity in the behavior of weakly initiated mixtures at an $Fe(CO)_5$ concentration of 0.2 percent. As the concentration of $Fe(CO)_5$ was increased above 0.2 percent, the induction period increased, passed through a maximum at about 0.6 percent (mol), and then decreased again. The effect was greater for a fuel-lean mixture than for a fuel-rich mixture.

Erhard suggested that the observed increase in induction time at intermediate concentrations could be attributed to the buildup of FeO. A similar situation was observed in the case of tetraethyl lead, in which PbO appeared to play a key role.

3. Effect of Inhibitors on Hydrogen-Air Flames

In these experiments, D. R. Miller and coworkers (Reference 20) estimated the flame speed from schlieren photographs. The experiments were conducted at a fuel/oxidizer ratio at which the flame speed of the uninhibited flame was maximized. For the uninhibited

flame, the flame speed was 140 in/s (cm/s); addition of 0.51 percent (mol) $Fe(CO)_5$ reduced the speed to 25.6 in/s (65 cm/s).

4. Work at AeroChem Research Laboratories, Inc.

W. J. Miller and coworkers (References 21, 22, and 23) studied two different types of flames. One set of experiments involved a spherical diffusion flame in which methane was introduced into an oxygen-filled chamber kept at 10^{-2} atm, and continuously supplied with oxygen; the inhibitor was added either to the fuel side or to the oxidizer side. In another set of experiments, also at 10^{-2} atm, the inhibitor was introduced into a premixed stoichiometric methane-oxygen flame with a small amount of nitrogen diluent. The following results were mentioned in the abstracts.

(1) The diffusion flame was extinguished at 0.12 percent (mol) $Fe(CO)_5$ added to the fuel; experiments with $Fe(CO)_5$ added to the oxidizer were not reported because of the reactivity of $Fe(CO)_5$ with the oxygen in the lines leading to the apparatus.

(2) In experiments with the majority of the extinguishing agents tested, it was observed that the luminous zone of the flame expanded spherically upon addition of the extinguishing agent, suggesting that the agent was reducing the flame speed. In the case of $Fe(CO)_5$, it was observed that the flame did not expand on addition of the agent.

(3) The concentration of $Fe(CO)_5$ required to extinguish the premixed flame was found to be 0.23 percent (mol); by comparison with CCl_4, $Fe(CO)_5$ was found to be 25 times more effective.

(4) Spectra of $Fe(CO)_5$-inhibited flames showed emissions attributable to Fe, FeO, and hot particles (continuum emission) in the region upstream of the •CH and C_2 bands and well upstream of the temperature maximum.

The authors concluded that the relatively large inhibition efficiency of $Fe(CO)_5$ could be attributed to in situ formation of ultra-fine particles in the relatively cooler, oxygen-rich regions of the flame.

5. Hot-Wire Ignition Experiments

In these experiments, Morrison and Scheller (Reference 18) measured the hot-wire ignition temperature for propane-air mixtures with various inhibitors and compared them with the value for an uninhibited mixture. This paper also presented the results of a 1955 preliminary technical report prepared by H. G. Wagner, in which that author reported the volume percent of inhibiting agent required to reduce the flame speed by 30 percent; the results recorded in this technical report were subsequently published in the open literature (References 9 and 10).

The hypothesis of the work was that there might be a correlation between ignition temperatures and reductions in flame speed. A rather poor correlation was found, suggesting that there are wide differences in mechanisms by which the different inhibiting agents interact with the radicals in the flame. In the case of hot-wire experiments with $Fe(CO)_5$, for example, it was found that the addition of $Fe(CO)_5$ had no effect on the ignition temperature

6. Catalytic Recombination of Flame Radicals

Jensen and Jones (References 24 and 25) measured the hydrogen atom concentrations in atmospheric pressure, premixed, fuel-rich, $H_2/O_2/N_2$ flames at several points in the recombination zone (0.40 to 0.14 in [10 to 40 mm] above the reaction zone), first without addition of any inhibiting agent, and then with 10^{-5} to 10^{-4} mole fraction $Fe(CO)_5$. The experimental data were compared with results computed using equations descriptive of several different mechanistic schemes. The key results are presented here.

(1) From thermodynamic data, it is estimated that the concentrations of the important iron-containing species can be expressed as follows, where $[Fe]_t$ is the total concentration of all iron-containing species.

$[FeOH] \sim 0.6\ [Fe]_t$

$[Fe] \sim 0.4\ [Fe]_t$

$[Fe(OH)_2] \sim 0.02\ [Fe]_t$

$[FeO] \sim 0.01\ [Fe]_t$

(2) It was found experimentally that the number density of H atoms was about the same for uninhibited and inhibited flames at the edge of the reaction zone, and that the number density in the inhibited flame decreased steadily relative to the number density in the uninhibited flame as the distance from the reaction zone increased.

(3) The following set of reactions is the only set found to yield computed results consistent with the experimental data.

$$FeOH + H \leftrightharpoons FeO + H_2 \quad (2)$$

$$FeO + H_2O \leftrightharpoons Fe(OH)_2 \quad (3)$$

$$Fe(OH)_2 + H \leftrightharpoons FeOH + H_2O \quad (4)$$

In addition, it is required that the following reaction be effectively balanced.

$$Fe + H_2O \leftrightharpoons FeOH + H \quad (5)$$

7. High Temperature Vapors

In his monograph with this title Hastie (Reference 14) considers the interaction of metal-containing species with flames (among many, many other topics). Key observations and comments which are particularly relevant to the $Fe(CO)_5$ system are summarized below.

(1) Hastie recast the data published by Lask and Wagner (Reference 10) in terms of the figure of merit, ϕ_v, proposed by Fristrom and Sawyer in 1971:

$$\phi_v = ([O_2]/[\text{Inhibitor}])/(\delta V/V_0) \quad [2]$$

where δV is the change in burning velocity, V_0 is the burning velocity of the uninhibited flame, and the square brackets are used to indicated the concentrations of the O_2 and the inhibitor. Values obtained were $\phi_v = 356$ for $Fe(CO)_5$ in a *n*-hexane-air flame, and $\phi_v = 19$ for $Fe(CO)_5$ in a hydrogen-air flame.

(2) Hastie suggested that the following catalytic cycle (in which X represents a third body to carry off excess energy) could account for the inhibition of flames by transition metals. He noted that the MOH molecule (where M = metal atom) must be stable in the flame

environment while able to react readily with •H or •OH; this places constraints on the bond energies of the species involved.

$$FeO + \bullet H + X \rightleftharpoons FeOH + X^* \quad (6)$$

$$FeOH + \bullet H \text{ (or } \bullet OH) \rightleftharpoons FeO + H_2 \text{ (or } H_2O) \quad (7)$$

(3) Hastie noted that $Fe(CO)_5$ is more effective in fuel-rich systems than in fuel-lean systems; since •H atoms are favored over •O• atoms and •OH radicals as the dominant flame radicals in fuel-rich systems, an inhibition mechanism involving •H-atom recombination appears to be supported.

(4) With respect to the oxidation of CO to CO_2, Hastie noted that Fe, Cr, and Ni accelerate this reaction, while Pb and Te retard this reaction.

(5) Hastie also noted an interesting similarity between $Fe(CO)_5$ and $CBrF_3$: both compounds exhibit reduced effectiveness at low pressures. Conversely, the extinguishing effectiveness of CH_2Cl_2 (in which it is energetically unfavorable for the •Cl atom to participate in a catalytic recombination of •H atoms) does not appear to be affected by changes in pressure. Hastie noted in this regard the importance of the thermolecular reaction in the proposed two-step catalytic cycle, shown above.

8. Counter-Flow Ethanol-Oxidizer Experiments

Vanpee and Shirodkar (Reference 26) studied counter-flow diffusion flames in which the oxidizer stream was flowed down onto a pool of fuel (ethanol). Gaseous inhibitors were premixed with the oxidizer stream. Less volatile inhibitors were introduced as inhibitor-ethanol aerosols in the oxidizer stream; the inhibitor was dissolved in ethanol, and this solution was passed through a sonic nozzle in the oxidizer duct. The "Mole Merit Number" (MOMN) for the inhibitor was defined in terms of experimental observables as follows.

$$MOMN = (OMOF - OMOFP)/AMOF \quad [3]$$

where: OMOF = O_2 mole fraction in oxidizer stream at extinction

OMOFP = O_2 mole fraction in oxidizer stream at extinction of the uninhibited flame.

AMOF = Additive (inhibitor) mole fraction in oxidizer stream

With respect to iron-containing compounds, the following results were reported in this study.

(1) The MOMNs presented were 57-62 for $Fe(CO)_5$ and 180-206 for $Fe(C_5H_7O_2)_3$.

(2) From the data presented in tabular and graphical form, the following concentrations of inhibitor in the oxidizer stream can be estimated: for $Fe(CO)_5$: 0.2 percent (mol); and for $Fe(C_5H_7O_2)_3$: 0.001 percent (mol). While the first of these two estimates seems reasonable, the second seems far too small.

9. Discussion in Terms of Thermal Mechanisms

Ewing and coworkers (References 27 and 28) presented the thesis that, to a very good approximation, the extinguishment effectiveness of a wide spectrum of extinguishing agents can be accounted for by the following endothermic heat sinks: heat capacity, phase changes, and decomposition. It is suggested that this remains true even for those agents which at very low concentrations cause large changes in one or more flame characteristics. Experimental data from a variety of sources are discussed in terms of this thermal model in several papers.

(1) Counter-flow ethanol-oxidizer diffusion flame (Reference 26). The extinguishing concentration predicted by the model was 1.2 percent (mol) (Reference 27) or 88 mg/L (Reference 28). For comparison, the corresponding values calculated by Ewing et al. (References 27 and 28), from the experimental data were 1.7 percent (mol) and 125 mg/L, respectively. On examining the experimental data of Vanpee and Shirodkar (Reference 26), the present author calculates a smaller experimental value, 0.22 percent (mol).

(2) Premixed methane-air flames (Reference 10). The predicted and experimental data were 38 mg/L and 52 mg/L, respectively. It should be noted that Lask and Wagner (Reference 10) reported the concentration required to reduce the flame speed by 30 percent; extrapolation to extinguishment yielded a value of 2.5 mg/L. Ewing et al. correctly

note that this extrapolation is not valid, and that the early part of the inhibition curve is not a good predictor of the amount required for extinguishment. Unfortunately, Ewing and coworkers do not indicate how they estimated a value at extinguishment from the data presented by Lask and Wagner.

10. Burning Rate Measurements

Linteris and coworkers (References 29 and 30)studied the relative burning rates of premixed methane-air, premixed methane-oxygen-nitrogen-argon, and premixed propane-air flames with a nozzle burner. Note that the results presented in Reference 29 differ somewhat from those presented in Reference 30. The results presented in the latter are more recent and, therefore, are given more weight. Here are the key results of these studies.

(1) At $Fe(CO)_5$ concentrations less than 200 ppm (0.02 mol percent) in methane-air flames, stoichiometric and rich ($\phi = 1.1$) flames showed large reductions in burning velocity. Lean ($\phi = 0.9$) flames showed even larger reductions in burning velocity, and could not be stabilized on the burner at concentrations greater than 24 ppm ($Fe(CO)_5$).

(2) A burning rate reduction of 20 percent was found at 24 ppm $Fe(CO)_5$ for stoichiometric methane-air flames; for lean flames at the same inhibitor concentration, the reduction was 30 percent.

(3) For concentrations of $Fe(CO)_5$ greater than about 200 ppm in methane-air flames, the $Fe(CO)_5$ appeared to have almost no further effect on the burning rate.

(4) The premixed propane-air flames were less inhibited than the methane flames, but the general pattern of behavior was similar.

(5) Changes in the concentration of oxygen dramatically affected the observed results. At low oxygen concentrations (e.g., $X_{O2} = 0.175$), small amounts of added $Fe(CO)_5$ dramatically reduced the burning rate, but concentrations of $Fe(CO)_5$ above 100 ppm had little further effect on the burning rate. For flames with larger concentrations of O_2 (up to $X_{O2} = 0.24$), the initial effect of the $Fe(CO)_5$ was smaller, but extended to higher (up to 500 ppm) concentrations of $Fe(CO)_5$.

11. Counter-Flow Diffusion Flames

In the counter-flow diffusion burner, a mixture of methane and nitrogen was introduced through the upper duct, and a mixture of oxygen and nitrogen was introduced through the lower duct. The strain rate at extinction was found by proportionately increasing all flows until the flame abruptly went out. Then an amount of $Fe(CO)_5$ was added to the fuel stream or to the oxidizer stream, and the strain rate at extinction was redetermined. Key results of this work (References 29 and 30) were these.

(1) For an air-methane (no N_2 in the fuel stream) flame, the flame was located on the oxidizer side of the stagnation plane. Addition of $Fe(CO)_5$ to the methane stream promoted the combustion, while addition of the $Fe(CO)_5$ to the oxidizer stream inhibited the flame.

(2) By enriching the O_2 concentration in the oxidizer stream (45 percent O_2/55 percent N_2) and diluting the methane in the fuel stream (13 percent CH_4/87 percent N_2), the reaction zone could be shifted to the fuel side of the reaction zone. In this situation, the addition of $Fe(CO)_5$ to either stream had almost no inhibiting effect.

(3) At an intermediate condition (30 percent O_2/70 percent N_2 *vs.* 20 percent CH_4/80 percent N_2), the reaction zone was on the oxidizer side of the stagnation plane. The results were similar, though not quite as dramatic, as for the air-methane flame.

C. REVIEW OF THE LITERATURE ON OTHER IRON COMPOUNDS

1. Afterburning Experiments

Vanpee and coworkers (Reference 31) ignited a fuel-rich mixture of $C_2H_4 + O_2 + N_2$ in an explosion sphere. Eighty milliseconds after ignition, a quick acting valve allowed the hot, H_2/CO-rich gases to exit into the atmosphere, and the hot gases ignited in the atmosphere, a phenomenon called "afterburning." In inhibited experiments, the powdered inhibiting agent was premixed with the initial explosive mixture; the index of performance was the amount of agent required to reduce the duration of the afterburning by 50 percent. Both iron and $FeCO_3$ were tested, and neither was found to be effective in reducing the afterburning duration.

2. A Study of Alkali-Metal Salts

Birchall (Reference 32) performed two types of experiments. In the first, 70-μm particles of inhibiting agent were introduced into the air stream of a con-flow diffusion town's gas flame; the figure of merit was the mass of agent required to extinguish the flame in 7 of 10 trials. The second type of experiment was similar except that a counter-flowing air stream was used; the sample of agent was introduced with the air stream at the top of the vessel, and the amount of agent needed to cause extinguishment was measured. Four iron compounds were studied (among many other compounds), and found to be markedly better than other compounds. Unlike many of the other compounds, the iron compounds did not appear to be sensitive to fuel/air composition. Important factors in the interpretation of the results included the ability of the particles to penetrate the flame and the rate of thermal decomposition of the particles in the flame.

(1) Con-flow experiment: The minimum mass required for extinguishment was 5 mg for $K_4Fe(CN)_6$; 10 mg for $K_4Fe(CN)_6 \bullet 3\ H_2O$; and 4 mg for $Na_2[Fe(CN)_5NO] \bullet 2\ H_2O$. For reference, $K_2C_2O_4 \bullet H_2O$ required 40 mg.

(2) Counter-flow experiment: Amount of agent expressed in surface area for 70-μ particles: 46 cm^2 for $K_4Fe(CN)_6 \bullet 3\ H_2O$; 596 cm^2 for $Na_2[Fe(CN)_5NO] \bullet 2\ H_2O$; and 350 cm^2 for $Na_4Fe(CN)_6 \bullet 10\ H_2O$.

3. Acetylacetonatoiron(III), $Fe(C_5H7O_2)_3$, in Counter-Flow Ethanol-Oxidizer Experiments

As previously mentioned, the MOMNs were 57-62 for $Fe(CO)_5$ and 180-206 for $Fe(C_5H_7O_2)_3$ (Reference 26).

4. Extinguishment of *n*-Heptane Pan Fires

In these experiments, Ewing and coworkers (Reference 33) introduced existing and candidate dry chemical extinguishing agents into the fire environment using a dry chemical extinguishing system pressurized to 50 psi (345 kPa); data were compared with the thermal model developed by these workers. One iron-containing chemical, potassium ferrocyanide

trihydrate, $K_4Fe(CN)_6 \bullet 3\ H_2O$, was included. In most instances, except for the iron-containing compound, the model was an excellent predictor of performance.

For $K_4Fe(CN)_6 \bullet 3\ H_2O$, the experimental and predicted extinguishing concentrations were 15 mg/L and 46 mg/L, respectively. For this compound, the authors used the following decomposition reaction as one of the important endothermic heat sinks in the model:

$$K_4Fe(CN)_6 \bullet 3\ H_2O \rightarrow 4\ KCN(g) + C_2N_2(g) + Fe(cr,liq) + 3\ H_2O(g) \qquad (8)$$

In discussing their results, the authors suggested two possibilities. On the one hand, this thermal decomposition reaction may not adequately represent the endothermic decomposition mechanisms actually in play. On the other hand, the iron may have a catalytic role in the extinguishment.

D. INTRODUCTION TO EXPERIMENTS WITH IRON-CONTAINING COMPOUNDS IN THE PRESENT WORK

The compounds studied in the present work may be conveniently grouped in three classes:

1. Volatile Organo-iron Compounds

Iron pentacarbonyl, $Fe(CO)_5$, was selected. Although the toxicity of this compound makes it a highly unlikely candidate as a practical fire extinguishing agent, it is introduced easily both into premixed flames and into most counterflow diffusion flames, and, therefore, serves as a convenient surrogate for other iron-containing compounds. The vapor pressure at room temperature is about 25 torr, quite adequate for a wide variety of studies.

2. Slightly Volatile Organo-iron Compounds

Several acetylacetonates of iron can be made quite easily and were included in the project. While these compounds are far less volatile than $Fe(CO)_5$, they can be introduced into flames almost as easily as $Fe(CO)_5$, provided the hardware is heated to prevent condensation.

3. Inorganic Salts of Iron

Iron nitrate was selected here, although other iron-containing inorganic salts have been studied by other workers (Section VII.B). Iron nitrate was introduced as an aerosol, generated from an aqueous solution by an ultrasonic aerosol generator.

The spectroscopic experiments are discussed first. Next, the work with premixed flames is described. This is followed by a short section detailing the results with counterflow diffusion flames. The mass spectrometry of flames seeded with $Fe(CO)_5$ is described in Section VI.

E. SPECTROSCOPY OF IRON-CONTAINING FLAMES

Combustion of $Fe(CO)_5$ yields a distinctive yellow-orange flame. Emission spectra in the visible region of the spectrum were recorded with a Chromex 250FG f/4 Imaging Spectrograph, (Chromex, Inc., Albuquerque, NM) equipped with a Photometrics CH-250 charge coupled device (CCD) camera (Photometrics, Inc., Tucson, AZ). The imaging spectrograph was a 1/4-meter instrument and had a 300 lines/mm grating blazed at 600 nm. The CCD camera was thermo-electrically cooled to -25 °C (-13 °F), and had a range from 400 to 1000 nm. A seven-element optical fiber with a 1/2-in tip lens was used to collect the light and image it on the slit of the spectrograph. No attempt was made to resolve the emission as a function of location in the flame.

Typical spectra are shown in Figures 112 and 113. The emission spectroscopy of flames seeded with $Fe(CO)_5$ demonstrated a distinct change in the character of the flame as a function of the amount of $Fe(CO)_5$ added. For very small amounts of added $Fe(CO)_5$ (mole fraction less than 0.0002, or percent by volume less than 0.02 percent), the flame was observed to be orange and the spectrum was dominated by emission by the FeO molecule (Reference 34; Figure 112). As the amount of $Fe(CO)_5$ was increased, luminous particles began to appear in the flame and the spectrum was increasingly dominated by the broad feature illustrated in Figure 113. With relatively large amounts of added $Fe(CO)_5$, the spectrum was entirely dominated by the broad emission, though the absolute intensity of the FeO emission appeared to remain constant. This broad, intense emission is assigned to chemiluminescence of perturbed FeO molecules on the

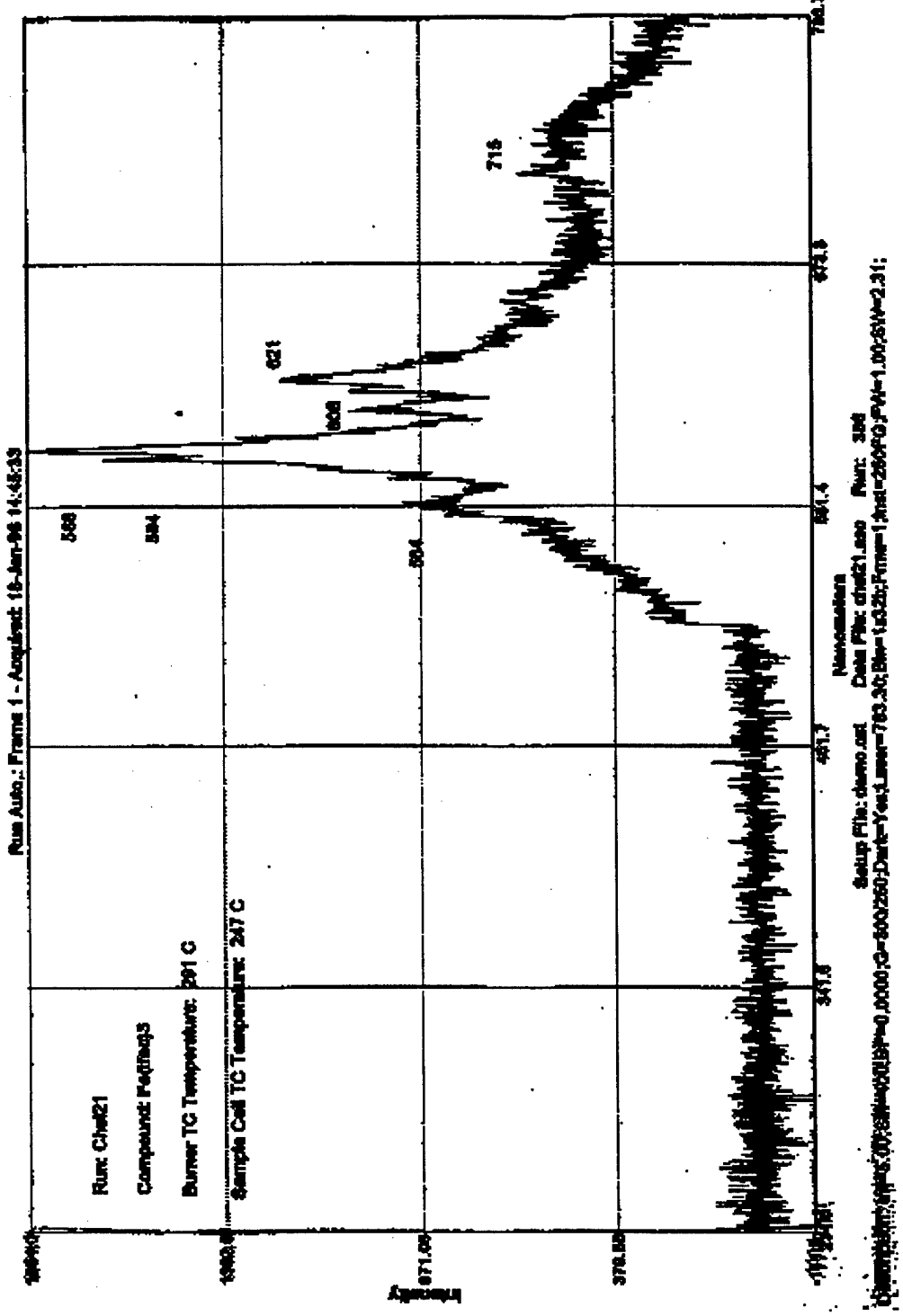

Figure 112. Visible Spectrum of Methane-Air Flame Seeded with a Low Concentration of Fe(CO)5.

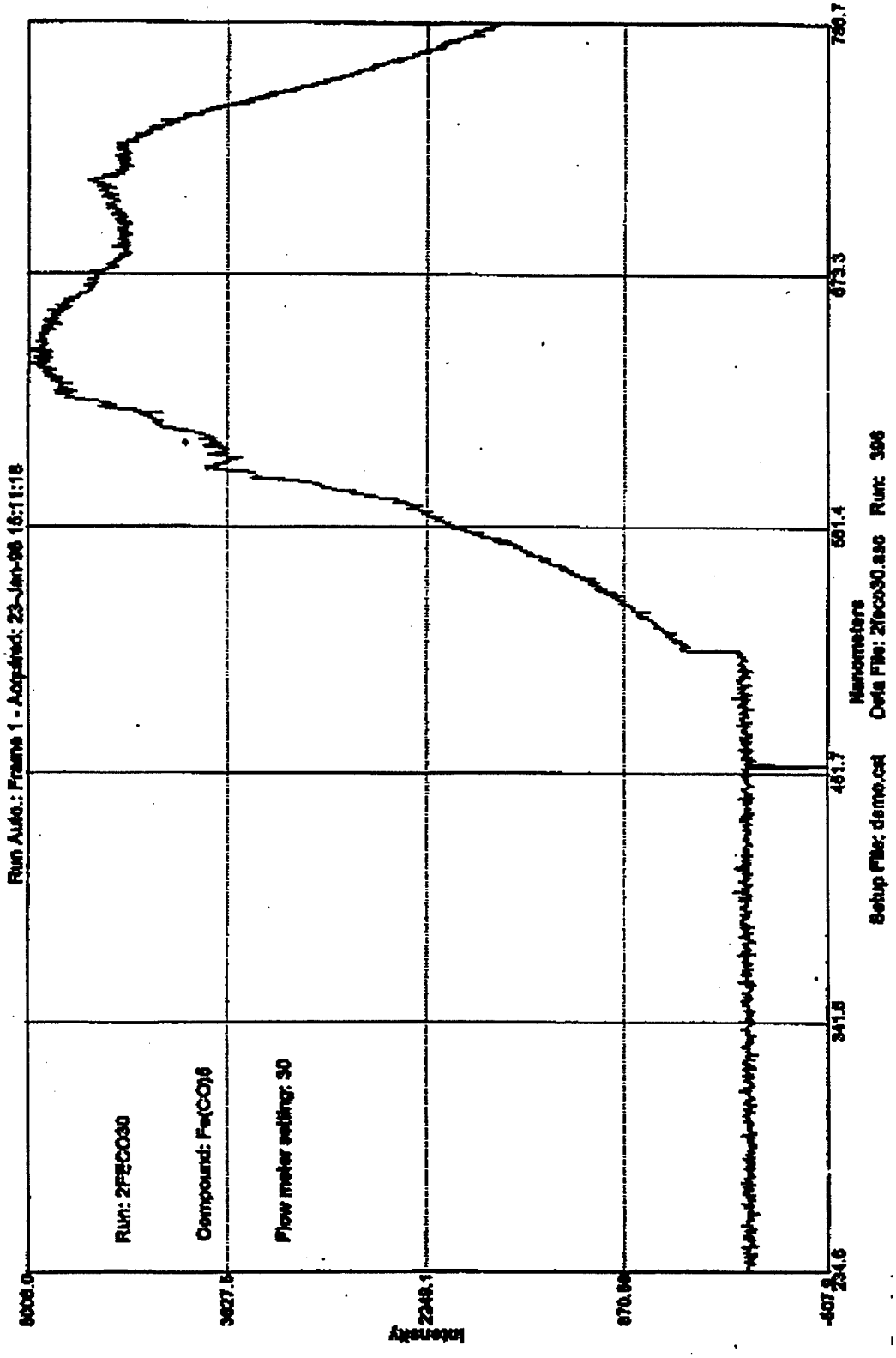

Figure 113. Visible Spectrum of Methane-Air Flame Seeded with a High Concentration of Fe(CO)5.

surfaces of the luminescent particles, based on the observation that the feature was structured (had three maxima) and lay slightly to the red (at longer wavelengths) of the FeO emission bands. The broad feature clearly was not black-body radiation, which would not have been structured and would have had a maximum at a wavelength longer than 1000 nm for flame temperatures typical of those in these experiments. The suggestion that the broad feature should be assigned to perturbed FeO molecules is consistent with the vast literature on the spectroscopy of species trapped in frozen inert gas matrices. Except in rare instances, the features in spectra of molecules trapped in frozen inert gas matrices are broadened and shifted to longer wavelengths as the result of the perturbations by the surrounding environment.

When the atmospheric flames were viewed along a line-of-sight coinciding with the orientation of the flame-holding grid in the burner, the particulates appeared to form thin sheets originating on the elements of the grid. These sheets persisted for a distance of several centimeters in the flames. The fact that the sheets appeared to originate on the elements of the grid is no doubt a reflection of the aerodynamic perturbations caused by the elements of the grid. It also suggests that the particulates were formed very early in the flow, within the first millimeter above the surface of the burner. Aggregation of the FeO molecules to form the luminous particulates evidently is a very facile process. If one pursues this line of thought further, it may be concluded that the observed luminescence was due to reactions with molecules previously deposited on the surface of the particles.

Although the very intense yellow-orange emission dominated the $Fe(CO)_5$-seeded flames, hints of yellow-green were frequently observed as well, especially in dilute (with small mole fractions of $Fe(CO)_5$) flames. This weak yellow-green emission was even more evident in the low-pressure flames with the Sapphire 2 instrument and was most evident in the recombination region of the flame. Spectra of this emission were not of good quality, owing principally to the weakness of the emission. Nevertheless, the yellow-green emission did appear to be molecular in origin. West and Broida (Reference 34) also reported molecular bands in the green, but the bands reported by those workers seem to be qualitatively different from the bands observed in the present work. Obviously, one must be very careful when observing bands in the green with a

system such as the Sapphire burner in which silver solder, brass, or another copper-containing alloy has been used. It is recommended that this emission be looked at again.

Additional emission experiments with $Fe(CO)_5$-seeded flames were conducted with an ISA spectrophotometer (Instruments SA, Inc., Metuchen, NJ). A typical low-resolution result is displayed in Figure 114. Here, the easily observed iron atom emission in the UV portion of the spectrum was particularly evident.

The ISA spectrophotometer was also used to record the emission spectrum of atmospheric flames seeded with aqueous $Fe(NO_3)_3$ aerosols. A typical spectrum is shown in Figure 115. The similarities between the spectra of the two different iron-containing compounds are evident. In the spectrum of the iron nitrate aerosol, there is an even more compelling reason to ignore the bands in the green portion of the spectrum; the iron nitrate reacted with the brass parts in the ultrasonic aerosol generator during the course of the experiment, thus adding soluble copper compounds to the aerosol.

The f/4 Chromex 250FG Imaging Spectrograph was also used to record the emission of tris-1,1,1-trifluoroacetylacetonatoiron(III), $Fe(C_5H_4F_3O_2)_3$. The visible spectrum of this compound was identical in every respect to that observed for $Fe(CO)_5$.

F. AQUEOUS IRON NITRATE AEROSOL EXPERIMENTS

Both dry and wet aerosols were studied; for the latter, the hot tube and condenser were removed (Figure 10), and the ultrasonic aerosol generator was connected directly to the bottom of the burner. The solutions used in these experiments were 1.0 M in $Fe(NO_3)_3$. Although the principal interest was in the spectroscopy of the inhibited flame, some data relating to the extinguishing efficiency were recorded. The temperature at the center of the burner dropped significantly upon introduction of the aerosol; typical decreases were on the order of -20 °C (-36 °F). In one representative experiment, the addition of dry $Fe(NO_3)_3$ aerosol resulted in a 16 °C (29 °F) drop in temperature at the center of the burner and in a 12 percent decrease in heat extracted by the burner. Considerable care must be used in interpreting these data, however, in

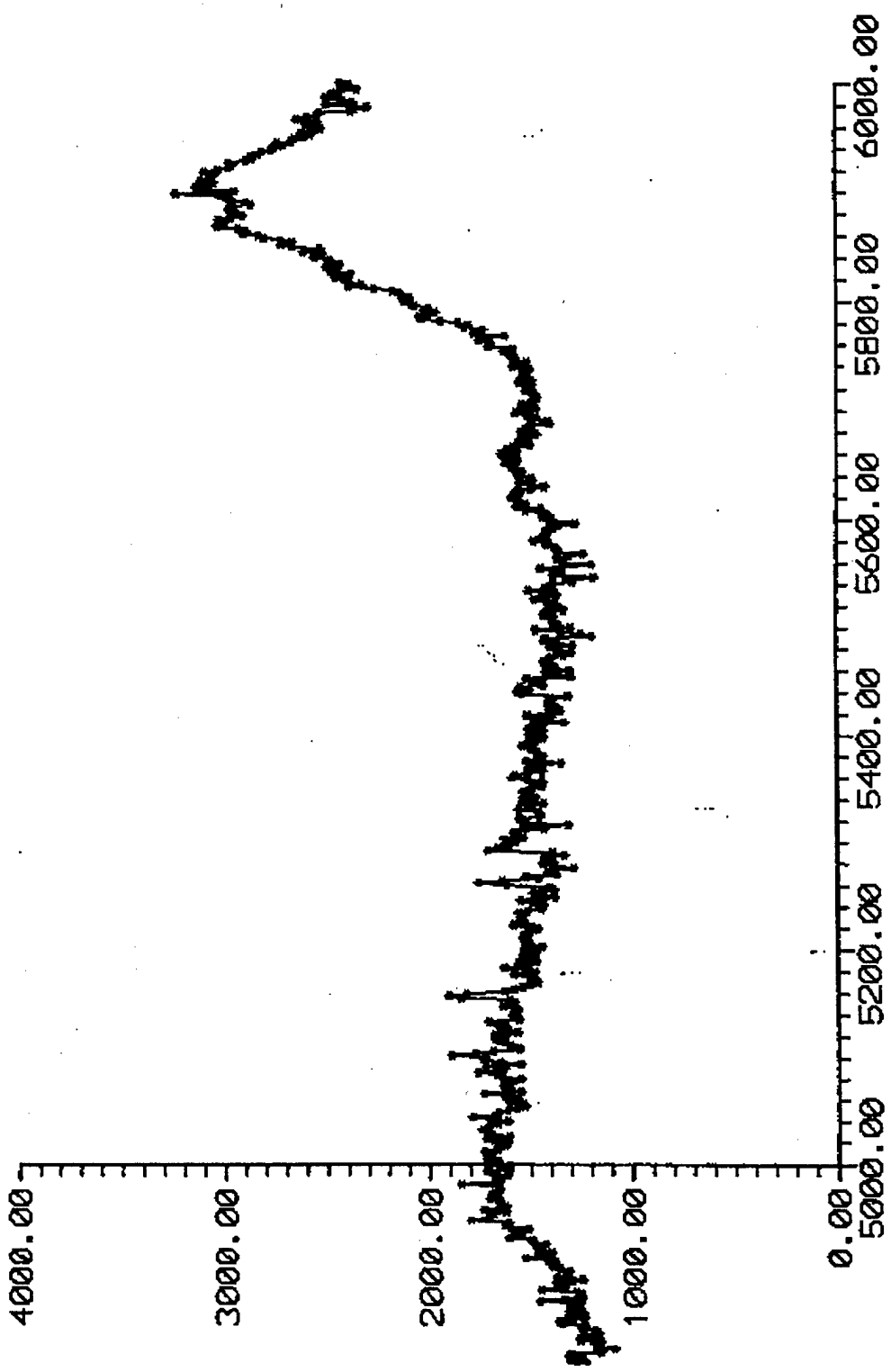

Figure 114. UV-Visible Spectrum of Methane-Air Flame Seeded with Fe(CO)5.

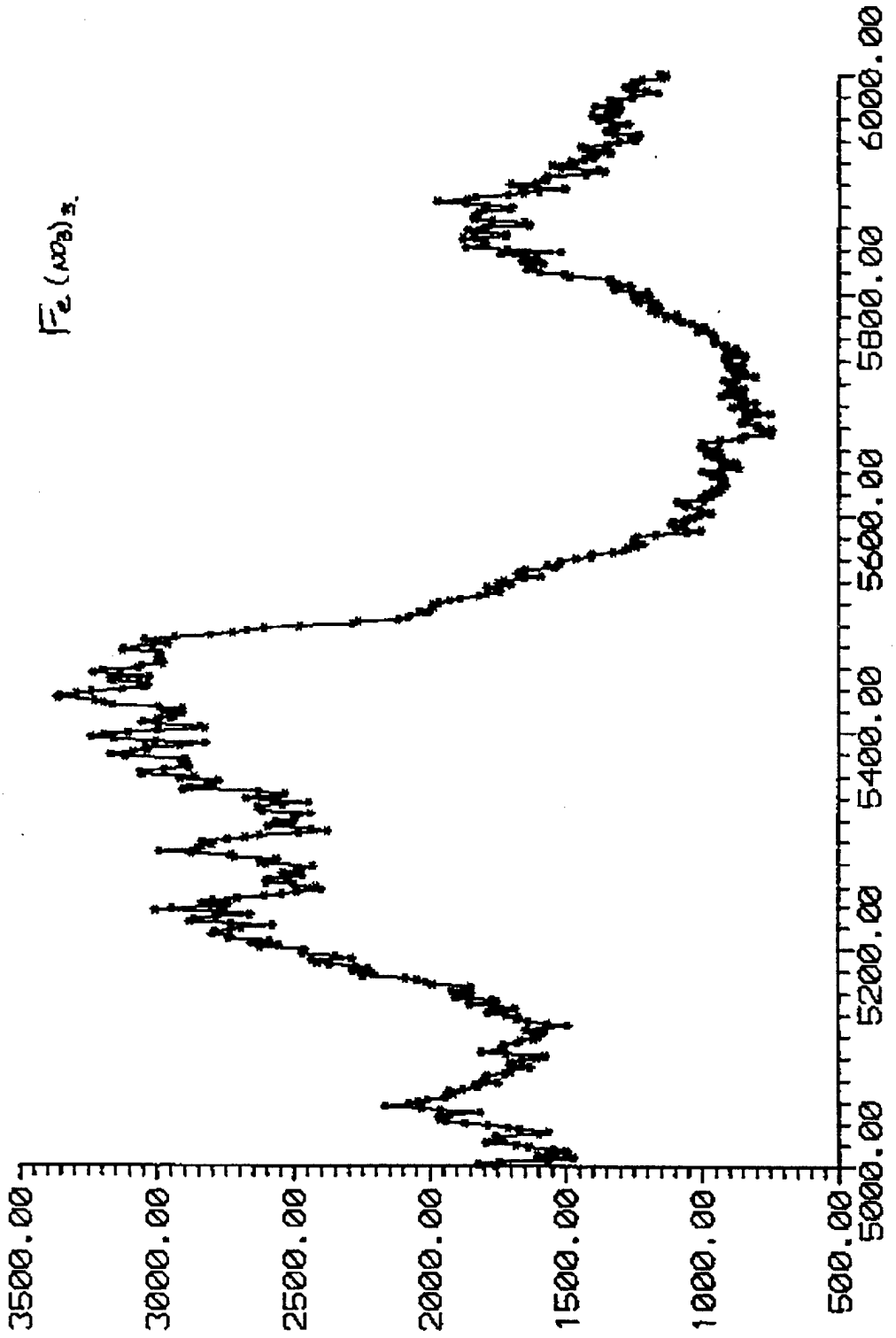

Figure 115. UV-Visible Spectrum of Methane-Air Flame Seeded with Fe(NO3)3.

view of the problems associated with reaction of the aqueous $Fe(NO_3)_3$ with the ultrasonic aerosol generator components, mentioned in the previous paragraph. There is a clear need to remanufacture the ultrasonic aerosol generator (using chemically inert materials) and reexamine the inhibiting efficiency of these aerosols.

G. HEAT EXTRACTED EXPERIMENTS WITH IRON PENTACARBONYL

1. Introduction of $Fe(CO)_5$ into the Flame

In most of the experiments reported here, the $Fe(CO)_5$ was introduced into the flame by passing a small fraction of the diluent (nitrogen) through a bubbler containing liquid $Fe(CO)_5$ at room temperature. The flow rate of the diluent passing through the bubbler was measured with a variable area flow meter, and the concentration of $Fe(CO)_5$ in this stream was calculated from the available vapor pressure data. Based on data published in the *CRC Handbook of Chemistry and Physics* (Reference 3), the vapor pressure of $Fe(CO)_5$ was estimated to be 27.6 torr at 23 °C (73 °F). Assuming saturation of the carrier gas, the mole fraction in the carrier gas stream was 0.046. To the degree that saturation of the carrier gas was not achieved, the concentrations of $Fe(CO)_5$ reported in this work are overstated. Thus, even at the very highest flow rates of $Fe(CO)_5$ employed in these studies, the incremental increase in the flow rate of diluent was less than 5 percent.

2. Heat Extracted *vs.* Flow Rate Experiments

The experiment that most convincingly demonstrated the fact that the iron-containing extinguishants catalytically inhibited the flame was the experiment in which the heat removed by the burner was studied as a function of the amount of extinguishing agent added to the premixed gases. A typical result is shown in Figure 116. In a typical data set (and this set is representative), the heat extracted by the burner showed a precipitous drop for the first few incremental additions of agent, followed by a linear decrease, and finally by extinguishment (flameout). In the data set represented by Figure 116, extinguishment was not observed; a limitation on the flow rate of the carrier gas for the $Fe(CO)_5$ prevented any further increases in the amount of agent added.

The results were easily treated by first fitting the data for relatively large flow rates to a linear equation, and then fitting the residual data for small flow rates to an exponential equation of the form $y = a + b\, e^{-cx}$. The exponential form of the behavior at small flow rates is characteristic of catalytic quenching. For comparison with data for other catalytic quenching agents, such as $CBrF_3$ and CF_3I, the reader is referred to Section V.

The slope of the curve at any point is a measure of the effectiveness of the agent at that point. The following, essentially meaningless, calculation illustrates the dramatic effect that small amounts of $Fe(CO)_5$ have on the flame. From the initial slope, and the fact that about 20 percent of the total heat in the flame was removed by the Sapphire 0-7 burner, it can be estimated that the impact on the reduction of the heat in the flame was on the order of 4×10^5 kJ/mol $Fe(CO)_5$. (For comparison, the heat of complete atomization of $Fe(CO)_5$ is only 6.0×10^4 kJ/mol.) Even with the final slope of -29 cal/cc, the effectiveness of this iron-containing compound is quite significant. For comparison, if one dissociates the $Fe(CO)_5$ into Fe(g) and CO(g) and adds the energy required to bring these gas-phase species to a temperature near that of the flame, one would expect to observe a slope of about -6 cal/cc.

In the experiment illustrated by Figure 116, the higher flow rates of $Fe(CO)_5$ resulted in significant buildup of deposits on the surface of the burner; these deposits insulated the burner and caused the heat removed by the burner to be smaller than it would have been in the absence of these deposits. This information is offered as a plausible, though not conclusive, explanation for the "tail-off," beginning with a flow rate of $Fe(CO)_5$ near 2 cc/min.

Although flameout was not observed in the experiment illustrated here, extinguishment was observed in some $Fe(CO)_5$ experiments. Typical $Fe(CO)_5$ volume percentages at which extinguishment was observed ranged from 0.05 percent to 0.08 percent. Table 16 summarizes the data for all of the experiments of this type, and Figures 117 and 118 present these results in graphical formats. The predicted mole fraction at flameout in Figure 117 was obtained by extending the straight-line portion of the Heat Extracted curve to the x-axis. It is important to note that, while the data points in Figure 117 appear to represent the pattern of a shotgun blast, flameout was predicted at very respectable concentrations of $Fe(CO)_5$, even in the worst cases. The data also faintly suggest that fuel-rich and fuel-lean flames may be easier to

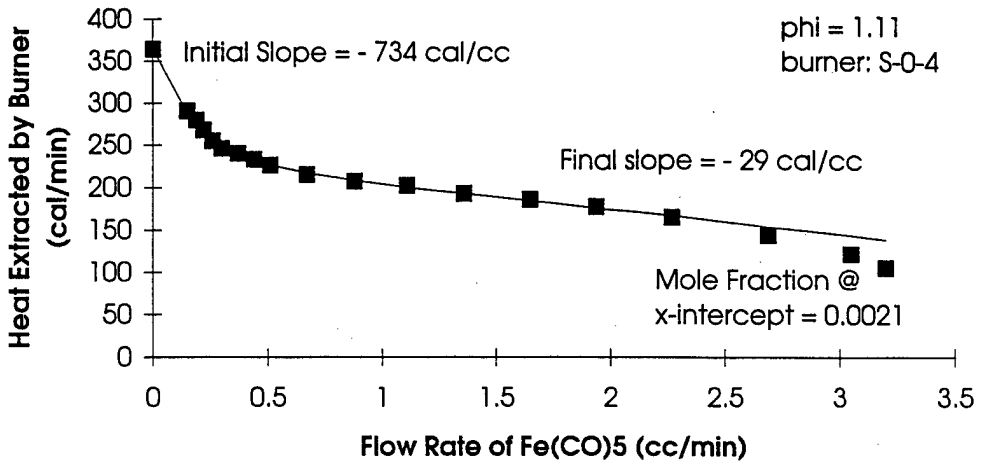

Figure 116. Inhibition by $Fe(CO)_5$: Heat Extracted as a Function of Flow Rate.

extinguish than stoichiometric flames. With this thought in mind, the experiments described in the next paragraph were undertaken.

3. Heat Extracted *vs.* Fuel/Oxygen Equivalence Ratio Experiments

To explore the importance of fuel/oxidizer equivalence ratio on the overall extinguishment effectiveness of $Fe(CO)_5$, the concentrations of all the gases except methane were fixed, and the fuel/oxygen equivalence ratio, ϕ, was "scanned" by varying the flow rate of methane from the lean inflammability limit to the rich inflammability limit. The results of a typical experiment are shown in Figures 119 and 120. The Heat Extracted by the burner (Figure 119) has the units of calories per cc of methane per minute. To provide a baseline for the experiment, an uninhibited flame was "scanned" first; these data are represented by the filled squares in Figure 119. As expected, the Heat Extracted by the burner for the uninhibited flame had its maximum at the stoichiometric ratio.

Next, a fixed amount of $Fe(CO)_5$ was added to the flame and the "scan" was repeated; the data for this "scan" are represented by the open squares. By contrast with the results for the uninhibited flame, the peak for the inhibited flame was on the fuel-lean side. The Difference curve (represented by the open triangles) was calculated by subtracting the data for

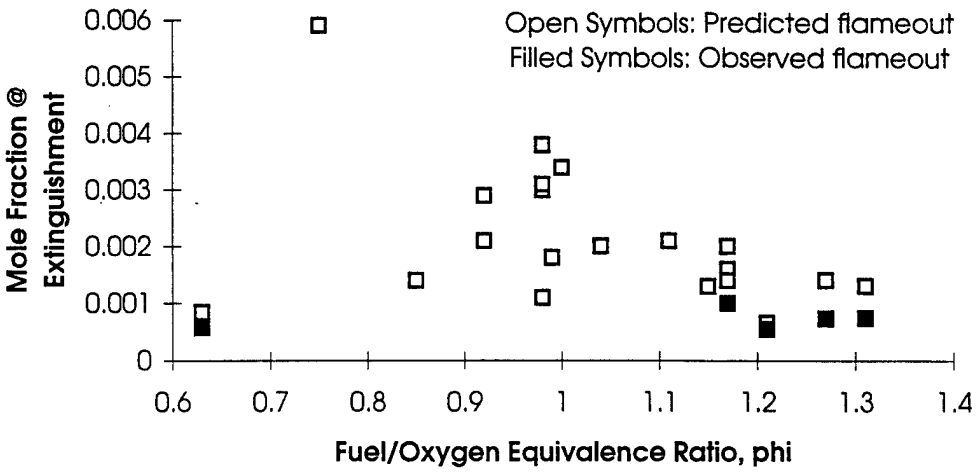

Figure 117. Extinguishment by $Fe(CO)_5$: Mole Fraction at Extinguishment as a Function of Fuel/Oxygen Equivalence Ratio.

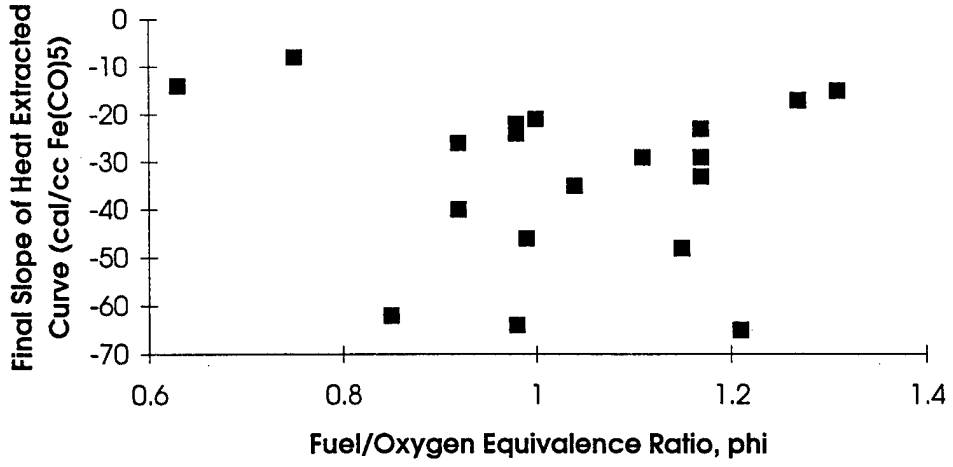

Figure 118. Extinguishment by $Fe(CO)_5$: Final Slope of the Heat Extracted Curve as a Function of Fuel/Oxygen Equivalence Ratio.

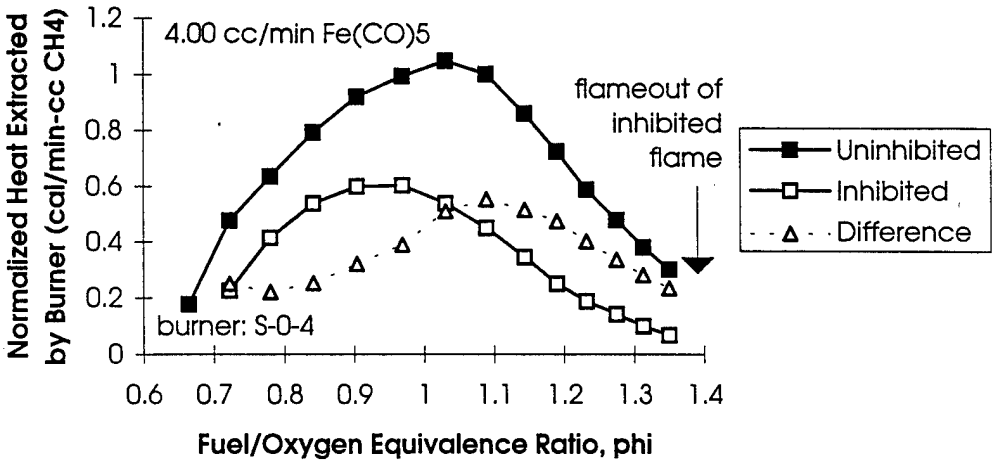

Figure 119. Inhibition by $Fe(CO)_5$: Heat Extracted by Burner.

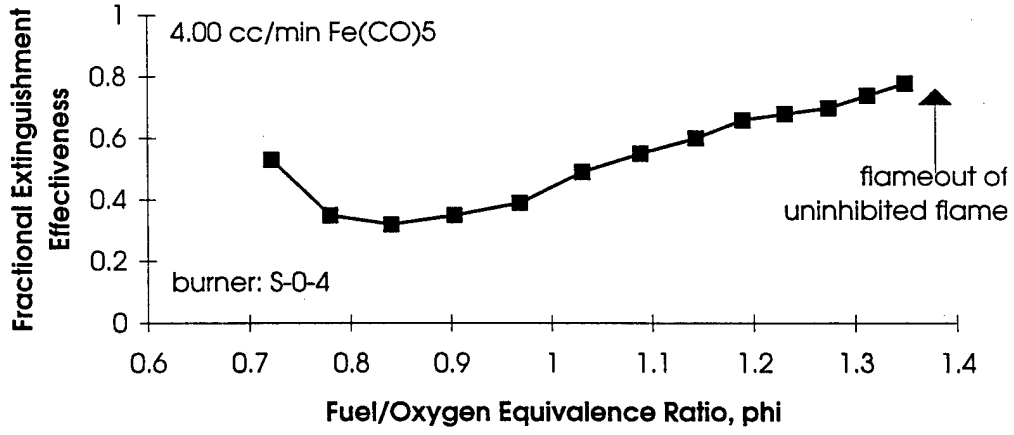

Figure 120. Inhibition by $Fe(CO)_5$: Fractional Extinguishment Effectiveness.

TABLE 16. HEAT EXTRACTED *vs.* FLOW RATE OF $FE(CO)_5$ EXPERIMENTS.

Experiment	ϕ	Slope (cal/cc)		Mole fraction @ flameout	
		Initial	Final	Predicted	Observed
FECO5_V	0.63	- 75	- 14	0.00084	0.00058
FECO5_U	0.75	- 45	- 8	0.0059	
FECO5_H	0.78				
FECO5_W	0.81	- 53			
FECO5_F	0.85[a]	- 491	- 62	0.0014	
FECO5_C	0.92[a]	- 266	- 26	0.0029	
FECO5_X	0.92	- 242	- 40	0.0021	
FECO5_S	0.98	- 307	- 64	0.0011	
FECO5_R	0.98	- 95	- 24	0.003	
FECO5_O	0.98	- 74	- 22	0.0031	
FECO5_N	0.98	- 281	- 22	0.0038	
FECO5_T	0.99	- 359	- 46	0.0018	
FECO5_P	1.00	- 94	- 21	0.0034	
FECO5_AN	1.04	- 860	- 35	0.002	
FECO5_D	1.07[a]	- 199			
FECO5_Y	1.11	- 734	- 29	0.0021	
FECO5_B	1.14[a]	- 163			
FECO5_E	1.15[a]	- 445	- 48	0.0013	
FECO5_L	1.17	- 132	- 29	0.0016	
FECO5_K	1.17	- 281	- 33	0.0014	
FECO5_M	1.17	- 193	- 23	0.002	0.001
FECO5_AA	1.21	- 476	- 65	0.00066	0.00055
FECO5_A	1.22[a]	- 156			
FECO5_AB	1.27	- 251	- 17	0.0014	0.00073
FECO5_AC	1.31	- 259	- 15	0.0013	0.00074
FECO5_G	1.34[a]	- 69			

[a] ϕ Unreliable

the inhibited "scan" from the data for the uninhibited "scan." Thus the Difference curve represents the amount of heat that did not have to be removed by the burner because of the addition of the $Fe(CO)_5$ to the flame. Putting it another way, the Difference curve is a measure of the degree to which the $Fe(CO)_5$ reduced the total heat in the flame. It is apparent that, while the $Fe(CO)_5$ contributed to the net inhibition of the flame at all values of ϕ, fuel-rich flames were inhibited more effectively than fuel-lean flames.

The results of this experiment are reminiscent of experiments in which extinguishment by CF_4 was compared with extinguishment by CHF_3 (Section III). In the CF_4/CHF_3 experiments, it was concluded that the CHF_3 has some fuel value; when ϕ was adjusted for the amount of O_2 required to react with the H in the HCF_3, it was found that the Heat Extracted by the Burner curves for the two compounds were nearly superimposeable, lending credence to the hypothesis concerning the fuel value of the CHF_3. In the same vein, it is tempting to attribute the observations in the $Fe(CO)_5$ experiments to the "fuel value" of the CO molecules. A difficulty arises, however, when one realizes that the shift in the peak of the Heat Extracted curve is quite significant and is not commensurate with the very small amounts of CO and Fe (both of which consume O_2) actually contributed to the flame by the added $Fe(CO)_5$. Thus, the most that can be said is that, while contributing to the overall extinguishment of the flame, the $Fe(CO)_5$ is less effective in the fuel-lean regime.

The fractional extinguishment effectiveness (FEE) curve in Figure 120 yielded the same message. The FEE is defined as follows.

$$FEE = \frac{\Delta Q(uninhibited) - \Delta Q(inhibited)}{\Delta Q(uninhibited)} \qquad [4]$$

Here again, it was evident that the fuel-lean flame was the least affected by the presence of the $Fe(CO)_5$; the $Fe(CO)_5$ was about twice as effective in fuel-rich flames as in fuel-lean flames.

Figure 121 presents Difference data for seven different experiments, and Figure 122 shows the FEE data for the same experiments. It is important to observe that, at small concentrations of $Fe(CO)_5$, the FEE was a very non-linear function of the mole fraction of $Fe(CO)_5$ added to the flame. Note that a 17-fold increase in the mole fraction of $Fe(CO)_5$ resulted

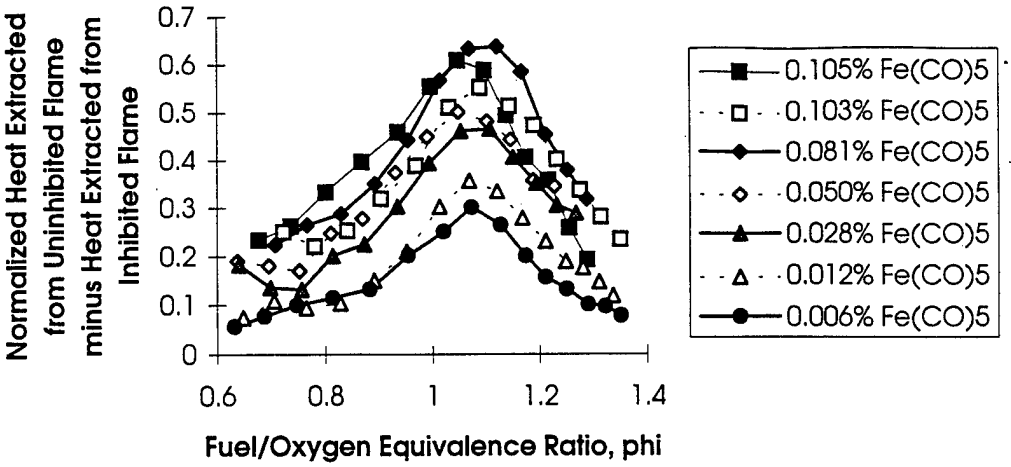

Figure 121. Effect of Various Amounts of $Fe(CO)_5$ on the Heat Extracted by the Burner.

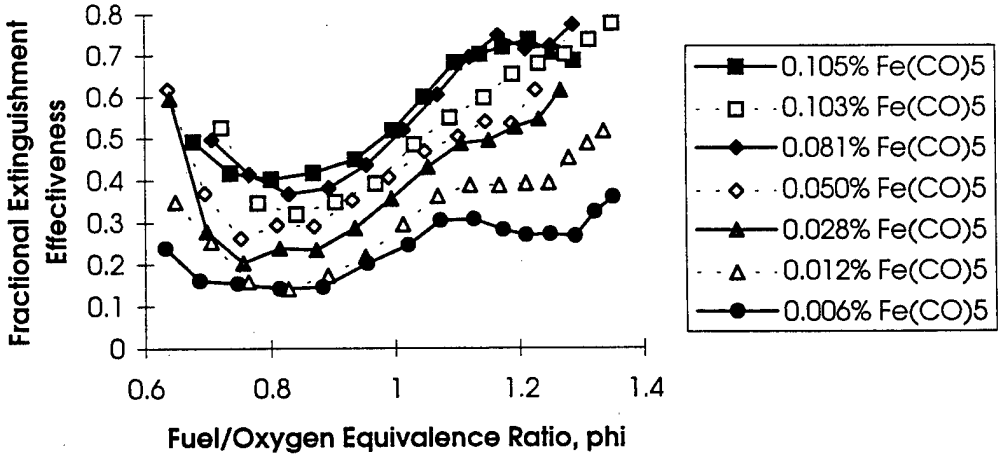

Figure 122. Effect of Various Amounts of $Fe(CO)_5$ on the Fractional Extinguishment Effectiveness.

in less than a two-fold increase in FEE. This observation is, of course, entirely consistent with the results of the Heat Extracted *vs.* Flow Rate of $Fe(CO)_5$ experiments, discussed above.

It is especially instructive to compare the data offered in Figures 121 and 122 with a similar set of results for a typical physical extinguishing agent such as CF_4 (see Section III for representative CF_4 data). While the decrease in heat absorbed by the burner was essentially independent of ϕ for CF_4, the distinct maximum near $\phi = 1.1$ for the $Fe(CO)_5$ in Figure 121was clearly indicative of the catalytic quenching mechanism at work for this compound.

It may be necessary to obtain detailed concentration profiles by mass spectrometry and other techniques and model the system with a complete kinetics code to elucidate completely the implications of these findings. However, it is interesting to observe that $CBrF_3$ (which catalytically recombines •H atoms, as noted earlier) displays a similar, though not as marked, maximum near the same value of ϕ (see Section III for representative results).

Since analysis of several Heat Extracted *vs.* Fuel/Oxidizer Equivalence Ratio experiments showed that the extinguishing effectiveness of $Fe(CO)_5$ was smallest at $\phi = 0.85$ (fuel-lean, as mentioned above), data for this particular value of the fuel/oxygen equivalence ratio have been collected in Table 17, and plotted in Figure 123. The result was a straight line, with some scatter, and two important features. First, the line does not go through the origin. This fact is consistent with the observation that, in Heat Extracted *vs.* Flow Rate of $Fe(CO)_5$ experiments, the initial slope was very steep but not indicative of the final concentration required to extinguish the flame. Second, the extrapolated value at which $Fe(CO)_5$ is predicted to extinguish a $\phi = 0.85$ flame is 0.35 percent (v/v). Admittedly, the extrapolation is quite long: from 40 to 100 percent extinguishment. However, this result is consistent with all other available data; note especially the data presented in Table 17.

H. A SYNERGISTIC EXPERIMENT

1. Rationale

A single experiment was performed in which both $Fe(CO)_5$ and N_2 were added to a fuel-lean flame. The motivation for this experiment stemmed in part from the report by

TABLE 17. FRACTIONAL EXTINGUISHMENT EFFECTIVENESS AS A FUNCTION OF MOLE FRACTION.

Experiment	$Fe(CO)_5$ flow rate (cc/min)	Mole fraction $Fe(CO)_5$ (X)	FEE @ $\phi = 0.85$
FECO5_AI	0.25	0.000063	0.15
FECO5_AD	0.25	0.000065	0.18
FECO5_AJ	0.50	0.00012	0.15
FECO5_AE	0.87	0.00022	0.26
FECO5_AH	1.04	0.00026	0.27
FECO5_AL	1.08	0.00028	0.23
FECO5_AM	1.96	0.00050	0.28
FECO5_AG	3.07	0.00077	0.38
FECO5_AF	3.15	0.00079	0.46
FECO5_AK	3.17	0.00081	0.37
FECO5_AP	4.00	0.0010	0.32
FECO5_AO	4.13	0.0010	0.40

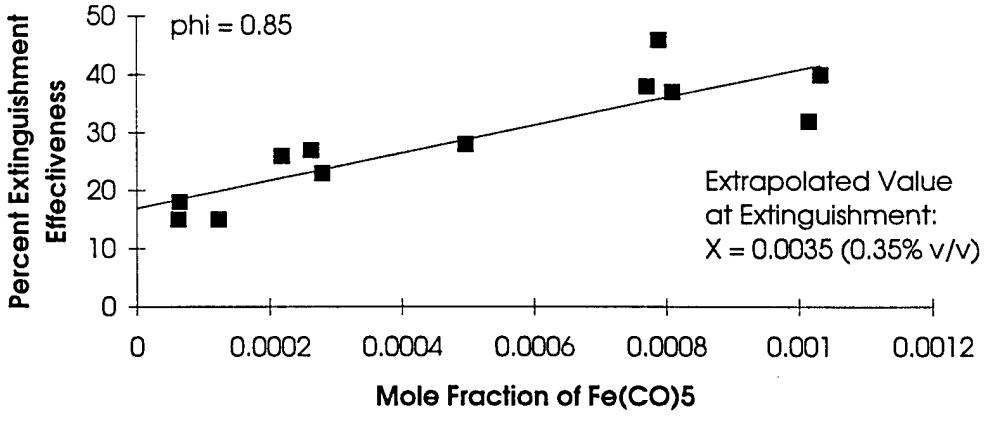

Figure 123. Percent Extinguishment Effectiveness as a Function of Amount of $Fe(CO)_5$ Added to Fuel-Lean Methane-Air Flames.

Göttingen group that methane-air flames were inhibited more effectively than methane-oxygen flames by equivalent amounts of $Fe(CO)_5$. In addition, there was the tantalizing thought that there might be some synergism between the two agents if each had a different dominant mechanism of inhibition.

2. Experimental Results

The results of the experiment are displayed in Figure 124. A fuel-lean flame, ϕ = 0.78, was selected, because a flame of about this stoichiometry has been shown to be the most difficult for $Fe(CO)_5$ to extinguish. The Heat Extracted by the Burner was measured for the uninhibited flame; $Fe(CO)_5$ was then added at a rate sufficient to reduce the Heat Extracted by about one-third. At this point, N_2 was added, with all other flow rates being held constant. Successively larger amounts of N_2 were introduced until flameout was achieved. Both the Heat Extracted by the Burner and the Temperature at the Center of the Burner were measured at each point. There were several key observations:

(1) The heat extracted was a linear function of the flow rate of N_2. In this respect, the experiment was identical with all other experiments with N_2 as the inhibiting agent.

(2) The slope of the Heat Extracted curve, - 0.095 cal/cc, was half of that observed in Experiment N2_A, - 0.21 cal/cc (Table 3), which was a "pure N_2" experiment with the same stoichiometry.

(3) The mole fraction of N_2 at extinguishment was similar to that of Experiment N2_A. In the "pure N_2" experiment, extinguishment was observed at a nitrogen mole fraction of 0.20 and the predicted mole fraction at extinguishment (obtained by extrapolating the straight line to the x-axis) was 0.21. In this "synergistic" experiment, the observed mole fraction at flameout was 0.17, while the extrapolated value was 0.23.

(4) The intercept of the straight line with the y-axis (N_2 flow rate equal to 0 cc/min) was significantly below the experimental data point.

3. Assessment

The first incremental addition of N_2, 300 cc/min, reduced the heat extracted by far more than the expected amount; otherwise, the linear curve would have intercepted the y-axis at the observed data point, indicated by "$Fe(CO)_5$ added" (Figure 124). This observation is consistent with the notion that $Fe(CO)_5$ is more effective in cool flames than in hot flames.

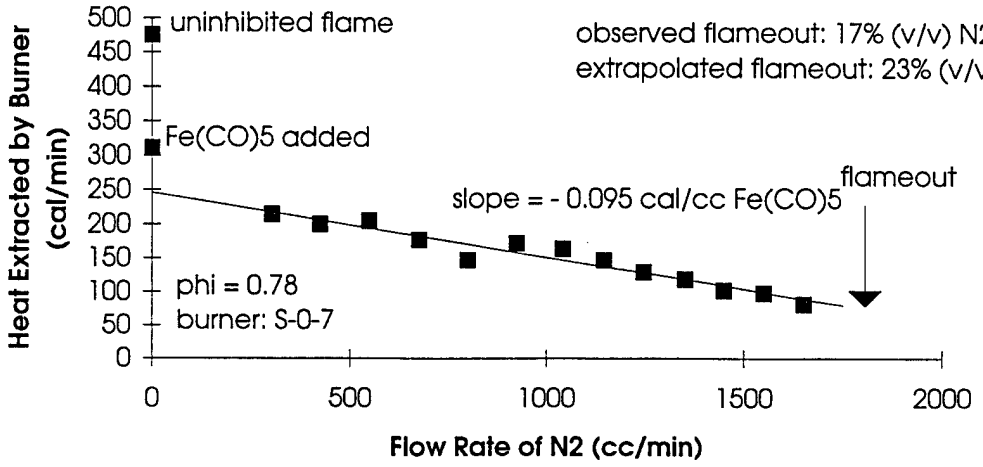

Figure 124. Inhibition of a Fuel-Lean Methane-Air Flame by a Mixture of $Fe(CO)_5 + N_2$.

The fact that the slope of the Heat Extracted curve was significantly less in the "synergistic" experiment than in the "pure" experiment was contrary to expectation. Similar slopes were expected. Indeed, given the hypothesis that $Fe(CO)_5$ becomes more effective as the temperature of the flame is lowered, one might have expected that the slope of the Heat Extracted line would have been steeper in the "synergistic" experiment than in the "pure" experiment. Given the fact that the flame was approximately 35 percent extinguished before the N_2 was added, one might have anticipated that an N_2 mole fraction of about 0.14 would have been required for extinguishment.

All told, this experiment probably raised more questions than it answered. At best it would appear that the effects of the two agents were additive. While evidence for an "interesting" effect was present; convincing evidence for a "synergistic" effect was lacking. A complete understanding of the results of this experiment will shed more light on the nature of the

interaction of $Fe(CO)_5$ with a flame. Whether there is a synergistic effect is an open question. The experimental region between 0 cc N_2/min and 300 cc N_2/min should be mapped. It appears very likely that the Heat Extracted curve for N_2 added to a $Fe(CO)_5$-seeded flame will have an initial exponential decrease followed by a straight line with a lesser slope, which is, of course, the shape that is expected for flames inhibited by successively larger additions of catalytic agents such as $Fe(CO)_5$ and $CBrF_3$. Since this shape is not expected for thermal agents such as N_2, the understanding of the "synergistic" experiment should provide important insights into the interactions of catalytic agents with flames.

I. HEAT EXTRACTED EXPERIMENTS WITH IRON ACETYLACETONATES

1. Introduction

Inasmuch as the toxicity of $Fe(CO)_5$ rules it out as a practical extinguishing agent, attention was given to other iron compounds that might be sufficiently volatile to be conveniently introduced into preheated gas streams. The iron acetylacetonates constitute such a class of compounds. Of these, three were easily made from readily available starting materials: (1) the parent compound, tris(acetylacetonato)iron(III), $Fe(C_5H_7O_2)_3$, "Fe(acac)"; (2) tris-1,1,1-trifluoro-acetylacetonatoiron(III), $Fe(C_5H_4F_3O_2)_3$, "Fe(tfac)"; and (3) tris-1,1,1,5,5,5-hexafluoroacetyl-acetonatoiron(III), $Fe(C_5HF_6O_2)_3$, "Fe(hfac)." Although all three compounds are of interest, and all three were prepared in the laboratory, most of the attention was given to the most volatile of the three—Fe(hfac).

2. Preparation of the Iron Acetylacetonates

The iron acetylacetonates were prepared by the method described by Chaudhuri and Ghosh (Reference 35). $Fe(OH)_3$ was precipitated from a warm aqueous solution of $FeCl_3 \cdot 6H_2O$ with concentrated NH_4OH, and the precipitate was digested on a steam bath. Following filtration and washing with water to remove residual chloride ions, the moist $Fe(OH)_3$ was added to the appropriate acetylacetone and digested on the steam bath. On cooling, large red crystals were recovered, washed with water and dried. The product was not recrystallized for the experiments discussed here.

3. Vapor Pressure of Fe(hfac)

Because all three iron acetylacetonates are very highly colored, a photometric technique was adopted for assaying the amount of the acetylacetonate in the premixed gas stream, and the Sapphire 0-7 burner, was designed and constructed specifically to use this technique (Section II). However, before this technique could be applied, it was necessary to know the relationship between the optical absorbance and the vapor pressure. A review of the literature failed to locate the necessary information; the development of this relationship then became one of the first tasks.

The vapor pressure of liquid phase $Fe(C_5HF_6O_2)_3$ has been measured from 343 K to 388 K (70 to 115 °C [158 to 239 °F]) (Reference 36). The results have been reported in the usual form, which tacitly assumes that the heat of vaporization is constant over the short range of the measurements.

$$\ln(p) = - \alpha/T + \beta \qquad [5]$$

$$\alpha = H_v/R \qquad [6]$$

Here, p is the pressure in atmospheres, ΔH_v is the heat of vaporization (J/mol), R is the gas constant (= 8.314 J/mol-K), T is the absolute temperature (K), and β is the intercept of the linear relationship. The reported values were 7199 K for α and 14.99 for β, respectively.

The observed partial pressure is conveniently related to the absorbance through the ideal gas equation and Beer's law.

$$\ln(p) = \ln(nRT/V) = \ln(RTC) = \ln(RTA/b\varepsilon) = - \alpha/T + \beta \qquad [7]$$

Here, n is the number of moles, R is the gas constant (= 0.08206 atm-L/mol-K), V is the volume in liters, C is the concentration expressed in moles/liter, A is the absorbance, b is the optical path length in cm, and ε is the molar absorptivity (molar extinction coefficient, in M^{-1}-cm^{-1}). Two useful forms can now be written.

$$\ln(AT) = \ln(b\varepsilon/R) + \beta - \alpha/T \qquad [8]$$

$$AT = p(b\varepsilon/R) \qquad [9]$$

From the first of these equations, it follows that a plot of ln(AT) as a function of 1/T should yield a straight line with a slope equal to - α, and an intercept from which the molar extinction coefficient, ε, can calculated (assuming that the value of β is known, as it is in this case). From the second of these equations, provided ε can be found, the pressure can be calculated from the observed value of the absorbance (A) at any temperature. Needless to say, ε can be calculated from the data of any experiment in which both the Absorbance (A) and the pressure (p) have been measured simultaneously.

In our first experiment, the Fe(hfac) was contained in a 1.97 in (5-cm) optical cell with Pyrex windows. A blue light-emitting diode (LED) was used as the source, and a 1P28 photomultiplier tube (PMT) with a cobalt-blue glass filter was used as the detector. A electrometer (Kiethly) was used to sense the output from the PMT; the output from the electrometer was transmitted directly to a strip chart recorder. The absorbance was calculated in the usual manner from the relative radiant power values recorded. With very little effort, it was possible to select a set of operating parameters such that the optical system was virtually insensitive to changes in ambient light in the room.

Figure 125 displays the experimental data. The data from Reference 36 were used to calculate the vapor pressure at each temperature. It must be noted that the data in Reference 36 apply only to temperatures above the melting point of the sample, reported to be 47 °C (117 °F) (Reference 37). These are the 6 highest temperature points in the data reported here. Accordingly, the data for these 6 points were fitted to a linear equation of the form described above, and the value of the molar extinction coefficient (ε) obtained from the slope was 3600 M^{-1} cm^{-1}. It is observed that the least-squares line did not pass through the origin, although it should do so. This suggests that the true value of ε is most likely somewhat larger than 3600 and probably closer to 4000 M^{-1} cm^{-1}. Nevertheless, a reasonably good value of ε was now in hand, and could be used to calculate the partial pressure of Fe(hfac) at any temperature, regardless of the physical state (solid or liquid) of the sample with which the vapor was in equilibrium.

Figure 126 displays the data plotted in a different manner. Here, the slopes of the two lines are the heat of vaporization of the liquid (higher temperature data) and the heat of sublimation of the solid (lower temperature data). The intersection of the two lines is the melting point. Comparison of these data with the literature values gives considerable insight into the experiment. The heat of vaporization of the liquid was about 13 percent lower than the literature value, and the melting point of the sample was about 5 °C (9 °F) below the reported value. These differences were not surprising in view of the scatter of the experimental data. However, the essential correctness of the results was strong confirmation of the validity of the experiment

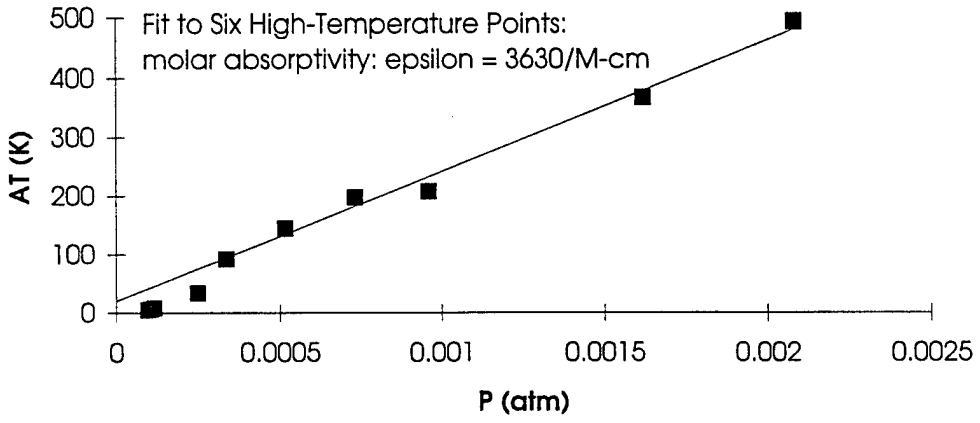

Figure 125. Absorbance of tris(Hexafluoroacetylacetonato)iron(III) as a Function of Vapor Pressure.

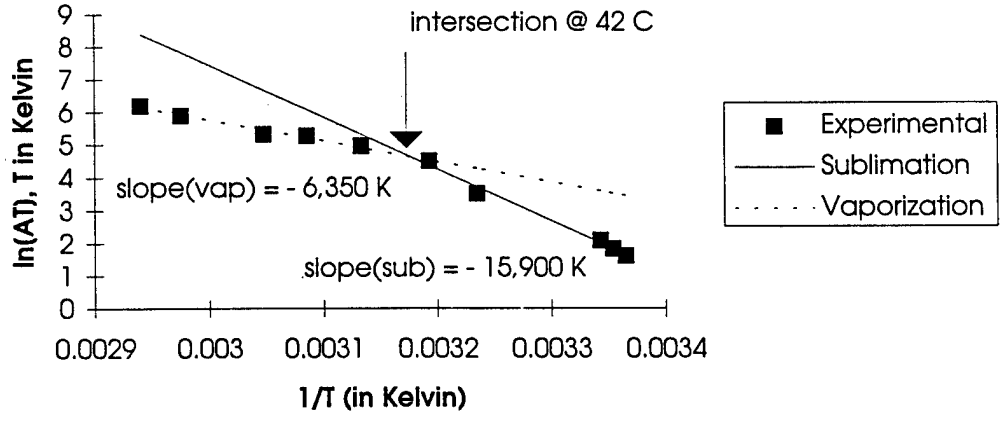

Figure 126. Determination of the Heats of Sublimation and Vaporization of tris(Hexafluoroacetylacetonato)iron(III).

and enabled the vapor pressure data to be obtained for the entire region of interest. It was estimated that the accuracy of the data obtained by this optical technique was ± 20 percent.

4. Heat Extracted Experiments with Iron tris-Hexafluoroacetylacetonate

With the molar absorptivity in hand, it was now possible to use the Sapphire 0-7 burner to perform Heat Extracted *vs.* Flow Rate of Fe(hfac) experiments. Figure 127 illustrates the results, and data for the entire set of experiments are collected in Table 18. The results were very similar to the corresponding results for $Fe(CO)_5$. The curves displayed the same initial exponential shape and had linear segments (with negative slopes) at higher Fe(hfac) flow rates. By comparison with data for $Fe(CO)_5$, the slopes of the Fe(hfac) curves appeared to be about a factor of 2 greater. However, the reader must be alerted to the fact that small experimental uncertainties can lead to large uncertainties in these slopes; undue emphasis must not be placed on these apparent differences at this point.

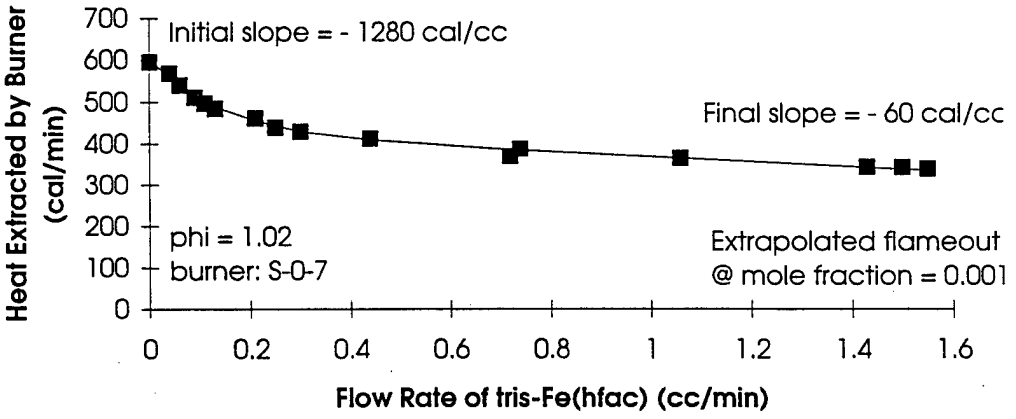

Figure 127. Inhibition by tris(Hexafluoroacetylacetonato)iron(III). Heat Extracted as a Function of Flow Rate.

The complexity and associated uncertainties in these experiments is apparent. A measure of this uncertainty is evident from an examination of the apparent disparities in the tabulated data. One experimental difficulty in particular should be noted. It was not possible to take the experiments to flameout. This appeared to be a consequence of thermal decomposition

TABLE 18. HEAT EXTRACTED *vs.* FLOW RATE OF Fe(HFAC) EXPERIMENTS.

Experiment	ϕ	Initial slope, cal/cc	Slope @ 1.0 cc Fe(hfac)/min, cal/cc	Mole fraction predicted @ f/o
FEHFA_B	1.04	-650	-130	0.0027
FEHFA_C	1.04	-880	-37	---
FEHFA_D	1.03	-500	----	0.0038
FEHFA_E	1.03	-730	55	0.0033
FEHFA_F	1.02	-1280	-60	0.0017

of the Fe(hfac) at the higher effusion cell temperatures required to achieve the higher flow rates of Fe(hfac).

Perhaps the most important conclusion from these measurements is that the Fe(hfac) is equally as good as, or perhaps slightly better than, $Fe(CO)_5$ as far as extinguishment effectiveness is concerned, and that the extinguishment mechanism is the same for both.

5. $Fe(CO)_5$ Experiments with the Sapphire 0-10 Counterflow Diffusion Burner

The first extinguishing agent introduced into the Sapphire 0-10 burner was $Fe(CO)_5$. Preliminary experiments verified the results published by Linteris and coworkers at NIST (References 29 and 30). Most of the emphasis was placed on counterflow flames of pure methane and air. As reported by Linteris and coworkers, no color was observed when the $Fe(CO)_5$ was introduced with the fuel, and no inhibition was observed. This finding raises important questions as to how the iron-containing compound interacts with the flame. It may be asked, for example, whether it is important for the $Fe(CO)_5$ to react with O_2 to form FeO before the agent actually reaches the flame front.

An important experiment is illustrated by Figure 128. Because of limitations imposed by the lack of high-rate flow meters, the maximum strain rate achieved in this experiment was about one-quarter that typically used by other workers in the field. As a consequence, the flame was to some degree stabilized by the cooled burner. In this experiment,

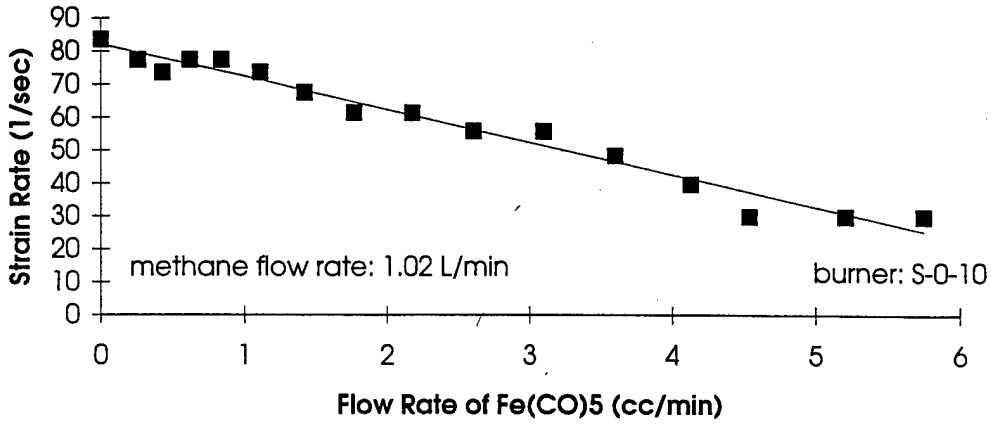

Figure 128. Inhibition by $Fe(CO)_5$ in a Counter-Flow Diffusion Flame.

the $Fe(CO)_5$ was added to the air stream, with the flow rate of the CH_4 stream being set at 1.025 L/min. For a fixed flow rate of $Fe(CO)_5$, the air flow rate was then increased until flameout was observed, and the corresponding strain rate was calculated. It was found that strain rate decreased linearly with increased flow of $Fe(CO)_5$. Extrapolation of this linear curve to zero strain rate (a relatively short extrapolation) yielded a flow rate of $Fe(CO)_5$ equal to 8.31 cc/min. The conversion of this flow rate into a mole fraction presented an interesting problem: The extrapolation to SR = 0.0 s^{-1} implied a 0.0 L/min flow rate for the air. To estimate a mole fraction, it was assumed that the flame was stoichiometric (ϕ = 1.00) with a methane flow rate of 1.025 L/min and a $Fe(CO)_5$ flow of 8.31 cc/min; the corresponding mole fraction of $Fe(CO)_5$ was 0.00077 (corresponding to 0.077 percent (v/v)). This value is of the same magnitude as that observed in Heat Extracted *vs.* Flow Rate of $Fe(CO)_5$ experiments. It is interesting to note that the curve was linear, and did not have an initial, much steeper slope. However, in a later experiment, a sharp drop in strain rate was observed for the first increment of $Fe(CO)_5$ added.

We also report a particularly interesting observation with flames in which the $Fe(CO)_5$ was added to the CH_4 stream. For relatively small flow rates of air (far from extinction) two flame zones were observed, one orange and the other blue. By careful measurements of the locations, it was determined that the orange zone (FeO emission) was at the stagnation plane and the blue zone (CH and C_2 emission) was about 0.08 in (2 mm) on the air side of the stagnation plane. To the best of our knowledge, this was the first observation of a separate zone in which

the $Fe(CO)_5$ was being decomposed and FeO was being generated. This finding is consistent with all the other anecdotal evidence which indicates that the $Fe(CO)_5$ is very easily (and completely) reacted very early in the flame.

J. PROPOSED MECHANISMS FOR INHIBITION BY IRON SPECIES

1. Proposed Mechanisms

In their paper on the catalysis of radical recombination in flames by iron-containing species, Jensen and Jones proposed 17 possible catalytic cycles by which the observed reduction in H-atom concentrations might be explained (Reference 24). All of the experiments were conducted with fuel-rich mixtures of H_2 and O_2, and the amount of N_2 diluent was adjusted so that the temperature was the same for each experiment in the set. The proposed cycles and their reactions are listed in Table 19. Of these cycles, only Cycle III was found to be consistent with the experimental data; the ratio of Fe to FeOH was established by the following, effectively balanced, reaction.

$$Fe + H_2O \leftrightharpoons FeOH + H \qquad (9)$$

Although a third body was indicated in Reaction 14 (Table 19), the authors believe that this reaction was more likely bimolecular than termolecular.

Jensen and Jones noted that, although rates were not known for Reactions 6 and 13 (Table 19), they were most likely termolecular. When reasonable estimates were made for thermolecular rate constants, Cycles VI through XVII failed to account for the observed rate of removal of H atoms. Based on this finding, the authors ruled out Cycles VI through XVII.

Table 19 is presented to the reader as a useful starting point in the evaluation of possible mechanisms of inhibition. The energies explicitly included in each reaction are the standard zero point enthalpies at 0 K. The data from which these energies were calculated are included in Table 20. With the exception of the enthalpy for FeOH, the JANAF values were used for these calculations. In a companion paper to their report on catalysis of radical recombination in flames by iron, Jensen and Jones experimentally determined values for the enthalpies of formation of FeO and FeOH (Reference 25). These data are included in Table 20;

TABLE 19. MECHANISMS EVALUATED BY JENSEN AND JONES.

Mechanism	Reaction no.[a]	Reaction
I	(-7)	$FeOH + H \rightarrow Fe + H_2O + 111$ kJ
	(-12)	$Fe(OH)_2 + H \rightarrow H_2O + FeOH + 63$ kJ
	(8)	$Fe + H_2O \rightarrow H_2 + FeO - 77$ kJ
	(14)	$FeO + H_2O + M \rightarrow Fe(OH)_2 + M^* + 335$ kJ
II	(-7)	$FeOH + H \rightarrow Fe + H_2O + 111$ kJ
	(-12)	$Fe(OH)_2 + H \rightarrow H_2O + FeOH + 63$ kJ
	(5)	$Fe + OH \rightarrow FeO + H - 16$ kJ
	(14)	$FeO + H_2O + M \rightarrow Fe(OH)_2 + M^* + 335$ kJ
III	(9)	$FeOH + H \rightarrow FeO + H_2 + 34$ kJ
	(-12)	$Fe(OH)_2 + H \rightarrow H_2O + FeOH + 63$ kJ
	(14)	$FeO + H_2O + M \rightarrow Fe(OH)_2 + M^* + 335$ kJ
IV	(11)	$FeOH + OH \rightarrow FeO + H_2O + 95$ kJ
	(-12)	$Fe(OH)_2 + H \rightarrow H_2O + FeOH + 63$ kJ
	(14)	$FeO + H_2O + M \rightarrow Fe(OH)_2 + M^* + 335$ kJ
V	(10)	$FeOH + OH + M \rightarrow Fe(OH)_2 + M^* + 430$ kJ
	(-12)	$Fe(OH)_2 + H \rightarrow H_2O + FeOH + 63$ kJ
VI	(6)	$Fe + OH + M \rightarrow FeOH + M^* + 382$ kJ
	(-7)	$FeOH + H \rightarrow Fe + H_2O + 111$ kJ
VII	(6)	$Fe + OH + M \rightarrow FeOH + M^* + 382$ kJ
	(9)	$FeOH + H \rightarrow FeO + H_2 + 34$ kJ
	(-8)	$FeO + H_2 \rightarrow Fe + H_2O + 77$ kJ
VIII	(6)	$Fe + OH + M \rightarrow FeOH + M^* + 382$ kJ
	(9)	$FeOH + H \rightarrow FeO + H_2 + 34$ kJ
	(-5)	$FeO + H \rightarrow Fe + OH + 16$ kJ

[a]Derived from Reference 25.

TABLE 19. MECHANISMS EVALUATED BY JENSEN AND JONES (CONCLUDED).

Mechanism	Reaction no.[a]	Reaction
IX	(6)	$Fe + OH + M \rightarrow FeOH + M^* + 382$ kJ
	(10)	$FeOH + OH + M \rightarrow Fe(OH)_2 + M^* + 430$ kJ
	(-14)	$Fe(OH)_2 + M \rightarrow FeO + H_2O + M^* - 335$ kJ
	(-8)	$FeO + H_2 \rightarrow Fe + H_2O + 77$ kJ
X	(6)	$Fe + OH + M \rightarrow FeOH + M^* + 382$ kJ
	(10)	$FeOH + OH + M \rightarrow Fe(OH)_2 + M^* + 430$ kJ
	(-14)	$Fe(OH)_2 + M \rightarrow FeO + H_2O + M^* - 335$ kJ
	(-5)	$FeO + H \rightarrow Fe + OH + 16$ kJ
XI	(6)	$Fe + OH + M \rightarrow FeOH + M^* + 382$ kJ
	(11)	$FeOH + OH \rightarrow FeO + H_2O + 95$ kJ
	(-5)	$FeO + H \rightarrow Fe + OH + 16$ kJ
XII	(6)	$Fe + OH + M \rightarrow FeOH + M^* + 382$ kJ
	(11)	$FeOH + OH \rightarrow FeO + H_2O + 95$ kJ
	(-8)	$FeO + H_2 \rightarrow Fe + H_2O + 77$ kJ
XIII	(-7)	$FeOH + H \rightarrow Fe + H_2O + 111$ kJ
	(13)	$FeO + H + M \rightarrow FeOH + M^* + 398$ kJ
	(5)	$Fe + OH \rightarrow FeO + H - 16$ kJ
XIV	(-7)	$FeOH + H \rightarrow Fe + H_2O + 111$ kJ
	(13)	$FeO + H + M \rightarrow FeOH + M^* + 398$ kJ
	(8)	$Fe + H_2O \rightarrow H_2 + FeO - 77$ kJ
XV	(9)	$FeOH + H \rightarrow FeO + H_2 + 34$ kJ
	(13)	$FeO + H + M \rightarrow FeOH + M^* + 398$ kJ
XVI	(10)	$FeOH + OH + M \rightarrow Fe(OH)_2 + M^* + 430$ kJ
	(13)	$FeO + H + M \rightarrow FeOH + M^* + 398$ kJ
	(-14)	$Fe(OH)_2 + M \rightarrow FeO + H_2O + M^* - 335$ kJ
XVII	(11)	$FeOH + OH \rightarrow FeO + H_2O + 95$ kJ
	(13)	$FeO + H + M \rightarrow FeOH + M^* + 398$ kJ

[a]Derived from Reference 25.

TABLE 20. STANDARD HEATS OF FORMATION.

Species	Reference Number	$\Delta_f H^\circ$(0 K) (kJ/mol)	$\Delta_f H^\circ$(298.15 K) (kJ/mol)
Fe(g)	6	413.1	415.5
FeO(g)	6	251.05	251.04
FeO(g)	25	259	---
FeOH(g)	6	69	---
$Fe(OH)_2$(g)	---	- 323.09	- 330.54
H(g)	6	216.035	217.999
O(g)	6	246.79	249.17
OH(g)	6	38.39	38.987
H_2O(g)	6	- 238.921	- 241.826
$Fe(CO)_5$(l)	6	---	- 766.09
$Fe(CO)_5$(g)	6	- 729.52	- 727.85
CO(g)	6	- 113.81	- 110.53
CO_2(g)	6	- 393.151	- 393.522

the enthalpy of formation of FeOH obtained by Jensen and Jones was needed for the data reported in Table 19.

Cycle III (other examples of this cycle). Cycle III has been invoked in several other cases. In each case, the cycle was written in terms of the equivalent metal species.

- Cobalt (Reference 38).
- Calcium, strontium, and barium (References 39 and 40)

Cycle XV. Several workers have invoked Cycle XV.

- Lead compounds (Reference 26)
- Chromium compounds (Reference 41)

Cycle XVII. Workers who invoked Cycle XV often invoked Cycle XVII as well, by simply replacing the "H" with an "OH" to yield water.

- Lead compounds (Reference 26)

Cycle XVIII. Erhard and Norrish proposed the following cycle, in which R is a hydrocarbon radical, to account for the lengthening of the induction period in combustion inhibition experiments with tetraethyl lead (References 42 and 43).

XVIII: $PbO + OH \rightarrow PbO(OH)$ (10)

$PbO(OH) + OH \rightarrow PbO_2 + H_2O$ (11)

$PbO_2 + R \rightarrow PbO + RO$ (12)

It is interesting to note in passing that the analogous iron oxide hydroxide, FeO(OH) is well known.

Cycles XIX and XX. Padley and Sugden suggest the direct homogeneous three-body recombination of radicals by the alkali metal atoms, followed by chemiluminescent radiation of the acquired energy (References 44 and 45).

XIX: $H + H + Na \rightarrow H_2 + Na^*, \Delta E = - 436$ kJ/mol (13)

$Na^* \rightarrow Na + h\nu$ (14)

XX: $H + OH + Na \rightarrow H_2O + Na^*, \Delta E = - 493$ kJ/mol (15)

$Na^* \rightarrow Na + h\nu$ (16)

Although these authors focused mainly on the alkali metals, they suggested that the same cycles may be important for Mn, Fe, and other metals. Of particular interest is the comment by these authors that thermally excited emission of atomic Mn dominates the hotter flames, while the chemiluminescent emission is more important in cooler flames. The authors noted that, for chemiluminescent emission by Fe, an energy of 122 kcal/mol (510 kJ/mol) would be required, but that for other metals, the energy requirement would be less. The Mn atom experiments were done by introducing aqueous $MnCl_2$ as an aerosol. Both MnO and MnOH bands were observed, in addition to the Mn-atom luminescence.

Other Cycles for the Alkali Metals. Several authors have invoked Cycle VI for the alkali metals. Schofield wrote a comprehensive review in the context of his own work in 1992 (Reference 46). He noted that flame stoichiometry plays a vital role. In fuel-rich flames, the hydrogen atom concentration suppresses the concentrations of oxides and hydroxides, and the metal atoms are the dominant species. Cycle VI is preferred under these conditions.

In fuel-lean flames, on the other hand, Schofield noted that there is a more complex chemistry involving hydroxides, oxides and superoxides. He wrote the following cycle for these conditions.

XXI: $K + O_2 + M \rightarrow KO_2 + M^*$ (17)

$KO_2 + OH \rightarrow KOH + O_2$ (18)

$KOH + H \rightarrow K + H_2O$ (19)

It may be important to note that, having arrived at definitive ideas concerning the inhibition by alkali metal atoms, Schofield declined to suggest that the same cycles might apply to alkaline earth or other metal compounds.

2. Implications of Other Experimental Observations

Pressure Dependence. It has been observed that $Fe(CO)_5$ is less effective at lower pressures, which suggests the importance of at least one termolecular step in the catalytic cycle. This appears, on the surface at least, to be at variance with the findings of Jensen and Jones (cited above) and certainly must be reconciled with these findings. There remains the interesting possibility that Reaction 14 (Table 19) may be termolecular, in spite of the arguments by Jensen and Jones to the contrary.

Temperature Dependence. It has been observed that $Fe(CO)_5$ is more effective in hexane/air flames than in hydrogen/air flames, and more effective in methane/air flames than in methane/oxygen flames. Although other possibilities must be considered, this may very well represent a response to differences in temperature; the hydrogen/air flame is hotter than the hexane/air flame, and the methane/oxygen flame is hotter than the methane/air flame.

The following equilibrium has been studied by Jensen and Jones (Reference 24).

$$Fe + H_2O \rightarrow FeOH + H,\ K = 66\ e^{(-16{,}100/T)} \qquad (20)$$

Using the data published by Jensen and Jones for flames at 1800 K and 2150 K, it is found that the ratio of FeOH to Fe decreases with increasing temperature. At 1800 K, [FeOH]/[Fe] = 13, while at 2150 K, [FeOH]/[Fe] = 6. This is consistent with expectations based on the entropies of the species involved. A similar result was noted by Friedman and Levy in flames seeded with Na and K. Calculations show that, at 2222 K, [KOH]/[K] = 2.6, while at 2000 K, [KOH]/[K] > 6 (Reference 47). For the alkali metal flames, this finding was used to support the conclusion that the metal atom was the important species (rather than the metal hydroxide); this was reasonable in that these two species are the only important species in fuel-rich alkali-metal-seeded flames. Inasmuch as FeO is very evident in the iron-seeded flames, this analysis is not sufficient for the iron system, and it is clearly necessary to consider the temperature coefficients of other reactions in the iron system. Note, however, that, as in the alkali metal systems, FeOH and Fe are the dominant species in Fe-seeded flames, especially in the fuel/rich flames.

Another piece of evidence may be important here. In the experiment in which a synergistic effect between $Fe(CO)_5$ and N_2 was investigated, the initial increment of added N_2 resulted in a larger than expected decrease in heat extracted by the burner. This is entirely consistent with the notion that the catalytic iron species is more effective in a cooler flame.

Similarly, it has been found that the initial effect of $Fe(CO)_5$ is greater in the flames with the more dilute (with N_2) oxidizer streams.

Luminescence by FeO. The observed intense luminescence by FeO has been assigned to chemiluminescence based on the characteristics of the observed spectrum. For FeO, the origin of the orange band system is at about 5880Å, which corresponds to 17,000 cm^{-1}, or 203 kJ/mol. While two of the reactions in Table 19 that yield FeO are exothermic (Reaction 9, ΔH = -34 kJ/mol, and Reaction 11, ΔH = - 95 kJ/mol), neither is sufficiently exothermic to account for the FeO emission. One should at least ask whether there is enough thermal energy to make up the required difference; at 2000 K, the average kinetic energy = 25 kJ/mol [= (3/2)RT].

The FeO band emission associated with the initial formation of FeO is another matter. It is quite apparent that $Fe(CO)_5$ is easily decomposed in the flame. In the counter-flow diffusion burner, the FeO emission was observed at the stagnation plane, several millimeters from the reaction zone. The following reactions suggest that there is ample energy to excite the FeO emission, even from partial combustion of the iron pentacarbonyl.

$$Fe(CO)_5(g) + O_2(g) \rightarrow FeO(g) + CO_2(g) + 4\ CO(g),\ \Delta H = +\ 157\ kJ \qquad (21)$$

But,

$$Fe(CO)_5(g) + 2\ O_2(g) \rightarrow FeO(g) + 3\ CO_2 + 2\ CO(g),\ \Delta H = -\ 409\ kJ \qquad (22)$$

Luminescence by other species. The luminescence by iron atoms is most likely thermal. However, in view of the results reported by Padley and Sugden for Mn-seeded flames, this luminescence certainly should be studied, especially as a function of flame temperature and fuel/oxygen equivalence ratio (References 44 and 45).

One reaction that yields FeOH (Reaction 13; Table 19), $\Delta H = -398$ kJ) is quite exothermic. A search through *Chemical Abstracts* failed to yield any information about the visible spectroscopy of this molecule.

Dependence on Fuel/Oxygen Equivalence Ratio. The strong dependence of FEE on fuel/oxygen equivalence ratio immediately highlights the probable role of hydrogen atoms in suppressing the concentrations of oxides and hydroxides. Initially, this would seem to suggest that FeO cannot be the principal inhibiting species (contrary to conventional wisdom). However, potential roles for FeO_2 and $Fe(OH)_2$ must also be considered; these may be the key species in determining the overall concentrations of iron-bearing species in the flames.

Counter-Flow Diffusion Flames. There is a very interesting apparent anomaly here. When added to the methane stream, the $Fe(CO)_5$ promoted combustion; when added to the air stream, the $Fe(CO)_5$ inhibited combustion. This would seem to be at odds with the finding that $Fe(CO)_5$ inhibits fuel-rich flames more effectively than fuel-lean flames. And yet, it may simply indicate that no iron oxides are formed initially when the $Fe(CO)_5$ is added to the methane

stream; this would be consistent with the conventional view that an oxide (or perhaps hydroxide) is the inhibiting species and not the Fe atom.

Delayed Combustion. The fact that $Fe(CO)_5$ shifts combustion downstream in premixed flames is almost universally accepted. This fact is clearly evident in the mass spectrometric data for low-pressure flames. It indicates that the $Fe(CO)_5$ has reduced the rate of the reactions leading to growth of the hydroxyl radical concentrations. However, it must be brought into consonance with the observation by Erhard that, for similarly small concentrations of $Fe(CO)_5$ in oxygen-acetylene mixtures, the effect is to accelerate the reactions leading to growth of the concentration of •OH radicals and thus shortening the induction time (Reference 19).

SECTION VIII
PRINCIPAL FINDINGS AND RECOMMENDATIONS

A. HEAT EXTRACTED AS A MEASURE OF DEGREE OF INHIBITION

1. Overview

The heat extracted from the premixed flame by the cooled burner was found to be an excellent measure of the degree of inhibition by the candidate extinguishing agent. This technique was equally suitable for atmospheric-pressure flames and for low-pressure flames, and did not disturb or interfere with other measurements. The only drawback of this technique was the equilibration time required for the temperature to stabilize following a change in parameters. Typically, an equilibration time of 6 minutes was required for each data point.

As a useful adjunct to the measurement of the heat extracted by the burner, the temperature at the center of the flame holder was also measured. This measurement was characterized by a large dynamic range (as much as 300 °C (540 °F)) and a somewhat faster response time than that of the Heat Extracted measurement. The relationship between the temperature at the center of the burner and the heat extracted by the burner was reproducible, although not linear. For most purposes, the Heat Extracted measurement was preferred.

Two different types of experiments were performed; the following paragraphs give additional details.

2. Heat Extracted *vs.* Flow Rate

Experiments in which the heat extracted by the burner was measured as a function of the flow rate of agent added to the flame proved to provide important insights into the mechanisms of inhibition. Three uniquely different behaviors were observed and assigned to characteristics of the inhibiting agents.

Very steep initial slope. Compounds such as $CBrF_3$ and CH_3Br, which are known to recombine flame radicals catalytically, were found to yield Heat Extracted *vs.* Flow Rate curves with very steep initial slopes. The initial part of the curves, for the first few incremental

additions of agent to the flame, were best fitted by an exponential equation of the form $y = a+be^{-cx}$. The remaining data formed a straight line, with a negative slope, which intercepted the x-axis (within experimental uncertainty) at the point at which flameout was actually observed.

Lesser initial (or even positive) slope. Some compounds were found to promote fuel-lean flames. These compounds, such as C_2HF_5, included one or more hydrogen atoms. In fuel-rich flames, these compounds were found to yield linear Heat Extracted *vs.* Flow Rate curves with negative slopes. Here again, the intercepts with the x-axis were, within experimental uncertainty, the same as the points at which flameout was observed. In fuel-lean flames (and to a lesser extent in flames near $\phi = 1.0$), the initial slopes of the Heat Extracted *vs.* Flow Rate curves were less than the final slopes; in some cases, the initial slopes were positive, indicating that the compound combined with the excess oxygen in these fuel-lean flames to increase the total amount of heat in the flame. Compounds in this group had the additional characteristic that they shifted the effective fuel/oxygen equivalence ratio. A plot of heat extracted by the burner as a function of ϕ resulted in a curve with a maximum at a value of $\phi < 1.0$, thus implying that an oxygen-rich flame was the most difficult for a compound in this group to extinguish.

Constant slope. The last group of compounds exhibited linear curves throughout the entire range of amount of agent added, which was true for all flames, regardless of the fuel/oxygen equivalence ratio. Compounds in this group included the typical thermal agents such as Ar and N_2. However, this group also included other compounds in which an additional linear inhibition mechanism was operative. Perhaps the most important example is the scavenging mechanism, in which one atom generated by reaction of the agent molecule reacts with and permanently removes a flame radical. As in the other two cases, the intercepts with the x-axis were, within experimental uncertainty, the same as the points at which flameout was observed.

The value of the Heat Extracted *vs.* Flow Rate data was not limited to an assessment of the significance of the shape of the curve. Additional information was provided by the slope of the curve. Since the slope of the Heat Extracted curve had units of energy/volume of agent (cal/cc), the slope of the curve was a measure of the effectiveness of the agent in removing energy from the flame (energy that, otherwise, would have been extracted by the burner).

3. Heat Extracted *vs.* Fuel/Oxygen Equivalence Ratio Experiments

Experiments in which the heat extracted by the burner was studied as a function of ϕ, the fuel/oxygen equivalence ratio, complemented the experiments in which the measurements were made as a function of the amount of agent added to the flame. In essence, the two types of experiments were complementary; however, since the uninhibited flame was compared with the inhibited flame at each data point in the Heat Extracted *vs.* Fuel/Oxygen Equivalence Ratio experiment, this experiment also yielded a direct measure of the extinguishment effectiveness of the agent at each value of ϕ. Two distinguishable types of behavior were observed.

Similar extinguishment effectiveness at all values of ϕ. It was not surprising to discover that the thermal agents such as N_2 displayed this behavior. The real surprise was that the extinguishment effectiveness curve for Halon 1301, $CBrF_3$, was nearly as flat as those for the purely thermal agents. The significance of this observation has not yet been fully worked out.

Minimum extinguishment effectiveness for fuel-lean flames. The agents with "fuel-content" were expected, and found, to be characterized by this type of behavior. The surprise here was that $Fe(CO)_5$ displayed the same behavior. Although it was tempting to attribute this observation to combustion of the $Fe(CO)_5$, there was far too little of this compound in the flame to account for the observed effect. Herein lies one of the keys to the understanding the chemistry of this compound, and it is necessary to consider other explanations for the fact that the Heat Extracted *vs.* Fuel/Oxygen Equivalence Ratio curves for the $Fe(CO)_5$ experiments displayed distinct minima.

4. Heat Extracted Measurements in Low-Pressure Systems

The measurements of heat extracted by the burner were equally easy in atmospheric and low-pressure experiments. However, a complication arose in the low pressure experiments due to the fact that the flame was propagated into an atmosphere of burned gases. As a consequence, the hot combustion products recirculated in the vicinity of the burner, both perturbing the flame and adding energy to the burner as flameout was approached. This difficulty was obviated in the atmospheric pressure experiments by provision of a sheath of nitrogen gas.

B. TECHNIQUES FOR INTRODUCING AGENTS

1. Overview

For compounds that could be handled as gases, the agent was simply premixed with the fuel, oxidant, and diluent; the flow was controlled by a needle valve and measured with a variable area flow meter. However, for metal-containing compounds and for the phosphorous nitrides, most of which had relatively low or negligible vapor pressures, the alternate techniques described elsewhere in this report were found to be effective.

2. Effusion Cell

Three different iron acetylacetonates and three different phosphorous nitrides were conveniently introduced into the flames from effusion cells located immediately below the burners. The vapors from the effusion cell were swept into the burner by the premixed gases moving past the orifice of the effusion cell. As a precaution against condensation of the compounds in the burner, the entire burner was resistively heated by electrically insulated resistance wire wrapped around the body of the burner. The heat introduced into the cooling loop by the heated burner proved to be only a minor inconvenience; once a baseline had been established for a burner with no flame, the Heat Extracted experiments were conducted in the usual manner.

Since the iron acetylacetonates are highly colored (orange), it was possible to measure the concentrations of these compounds in the premixed gases using a very simple photometric technique. The optical elements leading to the light source and detector were located on either side of the burner tube, below the flame holder. The diameter of the burner tube (1 in [2.5 cm]) proved to be essentially ideal for these absorbance measurements.

3. Ultrasonic Aerosol Generator

An ultrasonic nebulizer was used successfully to introduce aerosols of inorganic salts both into atmospheric and into subatmospheric flames. Both wet and dry aerosols were introduced into the flames. However, experiments to quantify the differences between wet and dry aerosols were not completed.

There were two principal shortcomings with the system. First, the aerosol densities were not sufficient to extinguish the flames. This was attributed to inadequate aerosol generation capacity. Second, it was not possible to maintain aerosols with constant compositions. Even over short runs, the intensity of the light emitted by the flame (an easy diagnostic for the amount of aerosol introduced into the flame) decreased noticeably, which made quantitative studies very difficult. It has been learned subsequently that the efficiency of aerosol generation is highly dependent on the height of the liquid level above the ultrasonic crystal. Especially in the sub-atmospheric experiments, the initial charge of solution in the generator lost water at a measurable rate due to evaporation. This resulted both in a lower liquid level and in a more concentrated solution. It is possible, but cannot be verified without additional experiments, that the observed reductions in efficiency of aerosol generation were due to lowered liquid levels rather than (or, perhaps, in addition to) formation of saturated solutions.

In spite of these shortcomings, quite bright flames were achieved, and spectra due to emission by metal atoms and metal oxides were easily recorded.

4. Pulsed Valve

The use of a pulsed valve was limited to a set of experiments with a cup-burner (diffusion flame) apparatus. These experiments showed considerable promise. In experiments with HCFC-22 ($CHClF_2$), for example, it was found that results could be obtained that were comparable with the results obtained with conventional (gas-phase) techniques for introduction of the agent into the flame.

A limitation in the use of a pulsed valve with relatively volatile materials such as HCFC-22 resulted from the flash evaporation of the pulse of vapor; the flash evaporation generated a pressure pulse that disturbed the flame. This phenomenon was not observed for lower vapor pressure solvents such as water.

Planned experiments with aqueous solutions were sidetracked by failure of the first pulsed valve. Other priorities prevented a return to these experiments.

C. FLAME-MOLECULAR BEAM-MASS SPECTROMETRY EXPERIMENTS—SAPPHIRE 2

Experiments with $Fe(CO)_5$-doped flames yielded immediate results. It was known from experiments with atmospheric-pressure flames (Sapphire 0 experiments) that, even with relatively small amounts of this compound added to the flame, iron-oxide aerosol particles were generated. For this reason, the amounts of $Fe(CO)_5$ added were very small, sufficient only to give good color to the flame. Even with such small amounts of material added, significant changes in the concentrations of stable species (CH_4, O_2, H_2O, CO_2, and CO) were observed when the $Fe(CO)_5$ was added. Additional details and implications are given in the following text. When larger amounts of $Fe(CO)_5$ were added to the flame, the sampling nozzle became plugged with the iron oxide particles. As a consequence, the results obtained in these experiments probably reflect mainly the homogeneous interactions of the $Fe(CO)_5$ with the flame. Note, however, that particles smaller than about 5000Å would not have been easily observed (and would not have plugged the nozzle) and yet could have been important.

The amount of $Fe(CO)_5$ in the premixed gas stream was estimated photometrically by passing the premixed gases through a long-path absorption cell.

Attempts to observe directly the iron-containing species (FeO, FeOH, and $Fe(OH)_2$) did not meet with success. While the m/e = 17 (OH^+) peak was measured, experiments were not performed that would have differentiated between •OH radicals generated by the flame and OH^+ ions due to fragmentation of H_2O; the latter was the principal contributor to the observed peak.

The sensitivity of the Sapphire 2 experiments was limited by the background pressure (and, hence, the mean free path) in the differential pressure chamber; this was, in turn, a function both of the diameter of the orifice in the quartz sampling nozzle and of the pumping speed in the differential pressure chamber. Extensive measures were taken to maximize the pumping speed for this chamber. From a practical point of view, there remained little else, short of complete redesign and addition of a second stage of differential pumping, that could be done to improve pumping speed. Nevertheless, it was evident that signal-to-noise improvements of more than a factor of 10 could be achieved if the throughput into the differential pressure chamber were

reduced by reducing the size of the orifice in the sampling nozzle. Unfortunately, the quartz sampling nozzle could not be easily changed out; this problem can be obviated with minor design changes.

D. INHIBITION BY IRON-CONTAINING COMPOUNDS

1. Comparison of $Fe(CO)_5$ with Halon 1301

The similarities between $Fe(CO)_5$ and Halon 1301 ($CBrF_3$) are indeed striking, and the difference is equally important. It is noted, but not stressed at this time, that $Fe(CO)_5$ is on the order of 10 times more effective on a molar (volume) basis than $CBrF_3$. The following similarities between the two compounds were found.

In the Heat Extracted *vs.* Flow Rate of agent experiments, both compounds had large, negative initial slopes. The initial data points were best fit by exponential equations in both cases. This behavior is uniquely characteristic of agents that catalytically recombine flame radicals.

In the low pressure flame-molecular beam-mass spectrometer experiments, both compounds shifted the combustion downstream. If concentrations of stable molecules at the downstream edge of the reaction zone are examined, addition of either compound decreased the concentrations of products (H_2O and CO_2) and increased the concentrations of reactants (CH_4 and O_2). This delay is characteristic of compounds that reduce the rate of multiplication of flame radicals.

A major difference between the two compounds was also found.

In both the Heat Extracted *vs.* Flow Rate of Inhibitor experiments and in the Heat Extracted *vs.* Fuel/Oxygen Equivalence Ratio experiments, it was found that the $Fe(CO)_5$ was least effective in the inhibition of flames with $\phi = 0.85$. In sharp contrast, $CBrF_3$ displayed only a slight asymmetry; this compound was nearly equally effective at all values of the fuel/oxidizer equivalence ratio.

The two similarities strongly suggest that both compounds interfere with flame chemistry by the same mechanism—recombination of flame radicals. The difference suggests

that the concentration of the active catalytic species in the flame is dependent on the concentration of a key flame radical, most likely the H atoms.

2. Dependence on Flame Temperature

The weight of evidence, from experiments in both these and other laboratories, leads to the conclusion that inhibition by iron-containing species is temperature dependent. It has been reported that methane-air flames are more effectively inhibited than methane-oxygen flames, and that methane-air flames are more effectively inhibited than hydrogen-air flames. It has also been shown that addition of N_2 to a flame inhibited by $Fe(CO)_5$ results in an unexpectedly large increase in inhibition. It seems very likely that these findings are a result of the fact that the balance of a key reaction involving the catalytically active species is temperature dependent.

3. Heterogeneous Recombination of Flame Radicals

Based on spectroscopic evidence, it seems certain that, at least at higher concentrations of iron, the heterogeneous recombination of flame radicals is important. Iron oxide aerosol particles are implicated in this process.

4. Dependence on Pressure

The dependence of the effectiveness of $Fe(CO)_5$ on pressure has been reported in the literature but not evaluated in detail in these laboratories. However, taken at face value, this information makes it necessary to consider a mechanism involving a termolecular elementary step. The situation is complicated by the fact that heterogeneous recombination of flame radicals is important, at least at higher concentrations of iron. If heterogeneous recombination is important for flames in which the particles are large enough to be observed visually, the question of whether the same process is important for smaller particles may be asked. Indeed, how small is too small for heterogeneous reactions? Since the growth rate of the particles depends on number density, it is conceivable that the observed pressure dependence reflects this growth rate rather than a true termolecular reaction pathway.

5. Homogeneous and Heterogeneous Inhibition

The observation (albeit at low resolution) of an apparently unperturbed molecular band system for FeO at low concentrations of iron in the flame suggests that the inhibition at low concentrations is homogeneous. However, it must be noted that the initial combustion of the $Fe(CO)_5$ would also be expected to yield an unperturbed molecular band system. Thus this observation cannot be taken as incontrovertible proof of a homogeneous contribution. Nor, on the other hand, can a homogeneous contribution be ruled out.

6. Thermodynamics

More than 20 homogeneous catalytic cycles have been evaluated, and available thermodynamic data have been used to estimate the energies associated with each of the elementary steps. Of the elementary steps in which FeO is produced, the most exothermic yields an estimated 95 kJ/mol, far short of the 203 kJ/mol needed for excitation of the FeO molecular band system. On the other hand, the termolecular recombination of flame radicals, to form either H_2 or H_2O, is more than sufficient to generate the observed emission. Moreover, a "pseudo termolecular" process involving a small aerosol particle (nano-particle?) would have somewhat reduced coincidence requirements and be more probable than a strictly termolecular process.

7. Primary Role of Aerosol Particles of Iron Oxide

With all of the foregoing considerations in mind, current thought favors the primary role of aerosol particles of iron oxide. Whether there is a regime where homogeneous catalytic recombination is important must be considered an open question.

E. RECOMMENDATIONS

1. Aerosol Generation and Delivery Techniques

Both the pulsed valve and the ultrasonic aerosol generator should be pursued. Work with the pulsed valve should focus mainly on delivery of metal-containing compounds dissolved in solvents with relatively low volatilities, including, but not limited to, water. Efforts

with the ultrasonic aerosol generator should be directed toward achieving higher and steadier delivery rates.

2. Possible Synergistic Effects

The possibility that two agents, which interact with the flame by different mechanisms, may exhibit synergistic effects should be explored. Whether or not a synergism is found, there is evidence that this work will yield important new information about the interactions of catalytic agents with flames.

3. Flame-Molecular Beam-Mass Spectrometer Experiment

The Sapphire 2 instrument has been shown to be a particularly effective instrument for studying inhibition chemistry. Moreover, it is apparent that quite modest improvements in the hardware can make very large improvements in the capabilities of this instrument. These improvements should be pursued.

4. Inhibition by Iron-Containing Compounds

The chemistry of inhibition by iron-containing compounds should be pursued on several fronts; for example, additional experiments should be conducted with the Sapphire 2 instrument. These experiments should measure the concentrations of H_2, •OH, and iron-containing species, in addition to the stable species already measured. Furthermore, work with the Sapphire 2 instrument should be extended to examine the behaviors of other iron-containing compounds. The best techniques for introducing these compounds may evolve from efforts to improve the currently available techniques for delivering aerosols—the pulsed nozzle and the ultrasonic aerosol generator.

5. The Heterogeneous-Homogeneous Question

The question of whether the dominant mechanism of inhibition by metal-containing compounds is homogeneous or heterogeneous should be resolved. The iron-containing compounds seem to be quite suitable for an initial exploration of this question. However, it may be necessary to examine other compounds (with different propensities for forming aerosols) to find a satisfactory answer to this question.

6. Manganese Compounds

Manganese compounds should be thoroughly explored to the same degree that iron-containing compounds have been investigated. The contrasts and similarities between iron and manganese compounds should provide additional insights into the mechanisms of interactions of metals with flames. It seems likely, at this juncture, that in some scenarios manganese compounds have considerable promise as potential inhibiting agents.

7. Sapphire 2

It is immediately apparent that the experiments completed to date have added invaluable insights into the homogeneous inhibition of flames by iron-containing compounds, and that much work remains to be done in addition to the simple determination of the absolute amount of $Fe(CO)_5$ in the premixed gases. The following are recommendations for future work using the Sapphire 2 burner:

a. The concentration of H_2 must be measured in the same manner as the concentration of the other stable species.
b. The concentration of •OH must be measured as a function of z, and compared with the results published by the Göttingen group in the mid-1950s. This may be possible with the current instrument, or may require an optical technique.
c. The effect of changing the concentration of $Fe(CO)_5$ should be studied within the rather narrow range permitted by the limitations imposed by plugging of the nozzle at higher concentrations of $Fe(CO)_5$.
d. Data acquisition must be improved to the degree that concentrations of important radicals can be determined with confidence.
e. If direct observation of key iron-containing species cannot be achieved, consideration must be given to optical absorption and/or laser-induced fluorescence experiments.
f. The flames must be studied as a function of f, the fuel/oxygen equivalence ratio.

(The reverse of this page is intentionally blank.)

REFERENCES

1. Patterson, R. A., Gobeli, G. W., Brabson, G. D., and Tapscott, R. E., *Advanced Streaming Agent Development, Volume II: Metal Compounds*, Vol. 2 of 5, Wright Laboratory (WL/FIVCF) and Applied Research Associates, Inc., Tyndall Air Force Base, Florida, June 1996. NMERI 96/3/32540

2. Biordi, Joan C., Lazzara, Charles P, and Papp, John F., "The Effect [of] CF_3Br on Radical Concentration Profiles in Methane Flames," *Halogenated Fire Suppressants,* Richard G. Gann, Editor, ACS Symposium Series 16, American Chemical Society, Washington, DC, pp. 256-291, 1975.

3. *CRC Handbook of Chemistry and Physics,* 71st Ed., D. R. Lide, Editor, CRC Press, Boca Raton, FL, Section 6, pp. 158-159, 1990.

4. Moore, T. A., Weitz, C., and Tapscott, R. E., "An Update on NMERI Cup-Burner Test Results," *Proceedings of the Halon Options Technical Working Conference,* Albuquerque, NM, pp. 551-564, 7-9 May 1996.

5. Botha, J. P., and Spalding, D. B., "The Laminar Flame Speed of Propane/Air Mixtures with Heat Extraction from the Flame," *Proceedings of the Royal Society of London, Series A,* Vol. 225, pp. 71-96, 1954.

6. Chase, M. W., Jr., Davies, C. A., Downey, J. R., Jr., Frurip, D. J., McDonald, R. A., and Syverud, A. N., "JANAF Thermochemical Tables," 3rd ed., *Journal of Physical and Chemical Reference Data,* Supplement #1, Vol. 14, 1985.

7. Fristrom, R. M., *Flame Structure and Processes,* Oxford University Press, New York, p. 412, 1995.

8. Safieh, H. Y., Vandooren, J., and Van Tiggelen, P. J., *Nineteenth Symposium (International) on Combustion,* The Combustion Institute, pp. 117-126, 1982.

9. Bonne, U., Jost, W., and Wagner, H. G., "Iron Pentacarbonyl in Methane-Oxygen (or Air) Flames," *Fire Research Abstracts and Reviews,* Vol. 4, pp. 6-18, 1962.

10. Lask, G., and Wagner, H. G., "Influence of Additives on the Velocity of Laminar Flames," *Eighth Symposium (International) on Combustion,* Williams and Wilkins, Baltimore, pp. 432-438, 1962.

11. Fassel, V. A., and Bear, B. R., "Ultrasonic Nebulization of Liquid Samples for Inductively Coupled Plasma-atomic Spectroscopy: An Update," *Spectrochimica Acta,* Vol. 41B(10), pp. 1089-1113, 1986.

12. Gaydon, A. G., and Wolfhard, H. G., *Flames. Their Structure, Radiation, and Temperature,* 2nd ed, Chapman & Hall, London, 1960.

13. Cornu, A., and Massot, R., *Compilation of Mass Spectral Data,* Heyden & Son, Ltd., London, 1966.

14. Hastie, J. W., *High Temperature Vapors*, Academic Press, NY, pp. 332-337, 344-357, 1975.

15. Biordi, J. C., Lazzara, C. P., and Papp, J. F., "Flame Structure Studies of CF_3Br-Inhibited Methane Flames. II. Kinetics and Mechanisms," *Fifteenth Symposium (International) on Combustion*, The Combustion Institute, Pittsburgh, pp. 917-931, 1975.

16. Biordi, J. C., Lazzara, C. P., and Papp, J. F., "Flame Structure Studies of CF_3Br-Inhibited Methane Flames," *Fourteenth Symposium (International) on Combustion*, The Combustion Institute, Pittsburgh, pp. 367-381, 1973.

17. Jost, W., Bonne, V., and Wagner, H. G., "Iron Carbonyl Found to Be Powerful Flame Inhibitor," *Chemical and Engineering News,* Vol. 39, p. 76, 11 September 1961.

18. Morrison, M. E., and Scheller, K., "The Effect of Burning Velocity Inhibitors on the Ignition of Hydrocarbon-Oxygen-Nitrogen Mixtures," *Combustion and Flame,* Vol. 18, pp. 3-12, 1972.

19. Erhard, K., "Die Beschleunigung der Acetylen-Sauerstoff-Verbrennung durch Metallcarbonyle," *Zeitschrift fur Physikalische Chemie,* Vol. 36, pp. 126-132, 1963.

20. Miller, D. R., Evers, R. L., and Skinner, G. B., "Effects of Various Inhibitors on Hydrogen-Air Flame Speeds," *Combustion and Flame,* Vol. 7, pp. 137-142, 1963.

21. Miller, W. J., and Vree, P. H., "Flame Ionization and Combustion Reactions," *Fire Research Abstracts and Reviews,* Vol. 10, pp. 190-191, 1968.

22. Miller, W. J., "Inhibition of Low-Pressure Flames," *Combustion and Flame,* Vol. 13(2), pp. 210-212, 1969.

23. Miller, W. J., "Flame Ionization and Combustion Reactions," *Fire Research Abstracts and Reviews*, Vol. 10, p. 191, 1968.

24. Jensen, D. E., and Jones, G. A., "Catalysis of Radical Recombination in Flames by Iron," *Journal of Chemical Physics,* vol. 60, pp. 3421-3425, 1974.

25. Jensen, D. E., and Jones, G. A., "Iron Compounds in Flames. Relative Stabilities of Fe, FeO, FeOH and $Fe(OH)_2$," *Journal of the Chemical Society.* Faraday I, Vol. 69, pp 1448-1454, 1973.

26. Vanpee, M., and Shirodkar, P. P., "A Study of Flame Inhibition by Metal Compounds," *Seventeenth Symposium (International) on Combustion,* The Combustion Institute, Pittsburgh, PA, pp. 787-795, 1978.

27. Ewing, C. T., Hughes, J. T., and Carhart, H. W., "The Extinction of Hydrocarbon Flames Based on the Heat-Absorption Processes Which Occur in Them," *Fire and Materials,* Vol. 8, pp. 148-156, 1984.

28. Ewing, C. T., Faith, F. R., Hughes, J. T, and Carhart, H. W., "Evidence for Flame Extinguishment by Thermal Mechanisms," *Fire Technology,* Vol. 25, pp. 195-212, 1989.

29. Linteris, G. T., Gmurczyk, G., "Inhibition of Premixed Methane-Air Flames by Iron Pentacarbonyl," *15th International Colloquium on the Dynamics of Explosions and Reactive Systems*, 30 July - 4 August 1995, Boulder, CO, p. 298.

30. Linteris, G. T., Reinelt, D., "Inhibition of Flames by Condensed-Phase Agents," in *Interflam '96,* Seventh International Fire Science and Engineering Conference, March 26-28, 1996, Cambridge, England, Interscience, London, 1996, pp. 477-86.

31. Vanpee, M., Tromans, R. H., Burgess, D., "Inhibition of Afterburning by Metal Compounds," *Progress in Astronautics and Aeronautics,* Vol. 15, pp. 419-448, 1964.

32. Birchall, J. D., "On the Mechanism of Flame Inhibition by Alkali Metal Salts," *Combustion and Flame,* Vol. 14, pp. 85-96, 1970.

33. Ewing, C. T., Faith, F. R., Romans, J. B., and Carhart, H. W., "Flame Extinguishment Properties of Dry Chemicals: Extinction Weights for Small Diffusion Pan Fires and Additional Evidence for Flame Extinguishment by Thermal Mechanisms," *Journal of Fire Protection Engineering*, Vol. 4(2), pp. 35-52, 1992.

34. West, J. B., and Broida, H. P., "Chemiluminescence and photoluminescence of diatomic iron oxide," *Journal of Chemical Physics,* Vol. 62(7), pp. 2566-2574, 1975.

35. Chaudhuri, M. K., and Ghosh, S. K., "Novel Synthesis of Tris(acetylacetonato)-iron(III)," *Journal of the Chemical Society, Dalton Transactions*, Vol. 1983, pp. 839-840, 1983.

36. Igumenov, I. K., Gerasimenko, T. Yu., Morozova, N. B., "Saturated Vapour Pressure of tris-Hexafluoroacetylacetonates of Metals of the First Transition Row," *Izv. Sib. Otd. Akad. Nauk SSSR, Ser. Khim. Nauk,* 1986, (2), 54-7.

37. Gafney, H. D., Lintveldt, R. L., and Jaworiwsky, I. S., "Photoinduced Reduction of Tris-(1,1,1,5,5,5-hexafluoro-2,4-pentanedionato)iron(III)," Inorganic Chemistry, Vol. 9(7), 1728-33, 1970.

38. Jensen, D. E., and Jones, G. A., "Aspects of the Flame Chemistry of Cobalt," *Journal of the Chemical Society, Faraday Transactions 1,* Vol. 72(11). pp. 2618-2630, 1976.

39. Cotton, D. H., and Jenkins, D. R., "Catalysis of Radical-Recombination Reactions in Flames by Alkaline Earth Metals," *Transactions of the Faraday Society,* Vol. 67, pp. 730-739, 1971.

40. Bulewicz, E. M., Padley, P. J., Cotton, D. H., and Jenkins, D. R., "Metal-Additive-Catalyzed-Recombination Rates in Flames," *Chemical Physics Letters,* Vol. 9(5), pp. 467-468, 1971.

41. Bulewicz, E. M., and Padley, P. J., "Temperature of Metal Oxide Particles in Flames," *Combustion and Flame,* Vol. 13, pp. 409-412, 1969.

42. Erhard, K. H. L., and Norrish, R. G. W., "Studies of Knock and Antiknock by Kinetic Spectroscopy," *Proceedings of the Royal Society of London,* Series A, Vol. 234, pp. 178-191, 1956.

43. Erhard, K. H. L., and Norrish, R. G. W., "Studies of Knock and Antiknock by Kinetic Spectroscopy II," *Proceedings of the Royal Society of London,* Series A, Vol. 259, pp. 297-303, 1960.

44. Padley, P. J., and Sugden, T. M., "Chemiluminescence and Radical Recombination in Hydrogen Flames," *Seventh Symposium (International) on Combustion,* Butterworths, London, pp. 235-244, 1959.

45. Padley, P. J., and Sugden, T. M., "Determination of the dissociation constants and heats of formation of molecules by flame photometry. Part 6. Stabilization of MnO and MnOH and their mechanisms of formation," *Transactions of the Faraday Society,* Vol. 55, pp. 2054-2061, 1959.

46. Schofield, K., "Flame Chemistry of Alkali and Alkaline Earth Metals," in *Gas-Phase Metal Reactions,* Fontijn, A., Editor, North-Holland, Amsterdam, pp. 529-571, 1992.

47. Friedman, R., and Levy, J. B., "Inhibition of Opposed-Jet Methane-Air Diffusion Flames. The Effects of Alkali Metal Vapors and Organic Halides," *Combustion and Flame,* Vol. 7, pp. 195-201, 1963.